Intracellular Ion-Sensitive Microelectrode Studies on Fish Retinal Neurones

by

Peter James Laming

Thesis submitted for the degree of Doctor of Philosophy

1982

University of London

Imperial College of Science and Technology

Department of Physics
Biophysics Section

&

Department of Pure and Applied Biology
Neurobiology Section

ABSTRACT

This thesis describes an experimental investigation of the ionic bases of electrical properties of horizontal cells in the retina of the roach (Rutilus rutilus), using intracellular ion-sensitive microelectrodes.

The introduction reviews both retinal neuronal organisation and ion-sensitive microelectrodes, and concludes by stating the aims and scope of the present study. The second chapter describes the technique developed to manufacture double-barrelled ion-sensitive microelectrodes, and the apparatus used to record intracellularly with them from retinal neurones. The experimental results reported here are novel in that direct quantitative measurements of ionic activity in fish retinal neurones made with ion-sensitive microelectrodes are reported for the first time.

Measurements of potassium and chloride activities were made in L_1-type and C_b-type horizontal cells. The potassium equilibrium potential (E_K) was always significantly more negative than the dark resting membrane potential (E_m), and corresponded closely to the maximal hyperpolarisation attained during interruption of photoreceptor input resulting from saturating light stimulation or application of Co^{2+} to the retina. The chloride equilibrium potential (E_{Cl}) was always significantly more positive than E_m thereby suggesting that a chloride conductance mechanism might contribute to the relatively depolarised level of E_m. When dopamine was sprayed onto the retina, the difference between E_{Cl} and E_m was abolished, and it is suggested that Cl^- is involved at the interplexiform cell - horizontal cell synapse.

In the final chapter the results are discussed, and an electrophysiological model of the horizontal cell is proposed. It is concluded that the techniques used in this study provide new and sometimes unexpected results concerning the electrophysiological properties of fish retinal horizontal cells.

CONTENTS

LIST OF TABLES

CHAPTER I

INTRODUCTION

PART A: THE FUNCTIONAL ORGANISATION OF THE VERTEBRATE (FISH) RETINA

I.1 Retinal Cells and their Connectivity

The retina is the light-sensitive tissue of the eye, and is derived from the forebrain during the development of the nervous system. The retina is made up of six types of neurone, which connect via synapses in the outer and inner plexiform layers, and glial (Müller) cells (figs. 1-3). The six types of neurone, which are found in well-defined layers are:

1. Photoreceptor Cells: (Rods and Red-, Green-, Blue-sensitive Cones): the transducer elements, which absorb and convert light energy into electrical signals;
2. Horizontal Cells: interneurones, which connect laterally across the outer retina;
3. Bipolar Cells: second-order neurones, which transmit the visual signals deeper into the retina;
4. Amacrine Cells: axonless interneurones, which connect laterally in the inner retina;
5. Interplexiform Cells: located amongst the amacrine cells; feed signals from the inner plexiform back to the outer plexiform layer;
6. Ganglion Cells: the output neurones of the retina whose axons form the optic nerve.

Müller cells are the glial cells of the vertebrate retina. They are thought to provide physical and chemical support for the neurones of the retina (Magalhaes, 1976) e.g. Müller cells have been shown to regulate light-evoked changes in the extracellular potassium activity (Karwoski & Proenza, 1977) and take up neurotransmitters (Neal & Iversen, 1972).

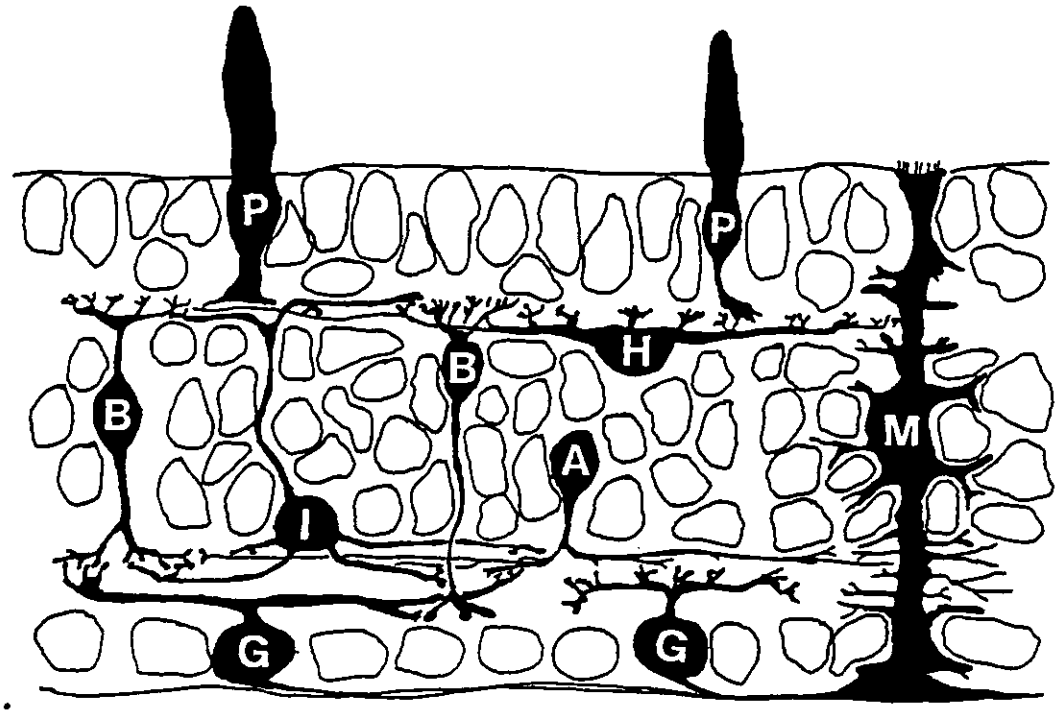

Fig. 1.

Principal cell types found in the (vertebrate) sensory retina. P, photoreceptors; H, horizontal cell; B, bipolar cells; A, amacrine cell; I, interplexiform cell; G, ganglion cells; M, Muller (glial) cell. (modified & redrawn from Dowling 1974 by J.E.G. Downing).

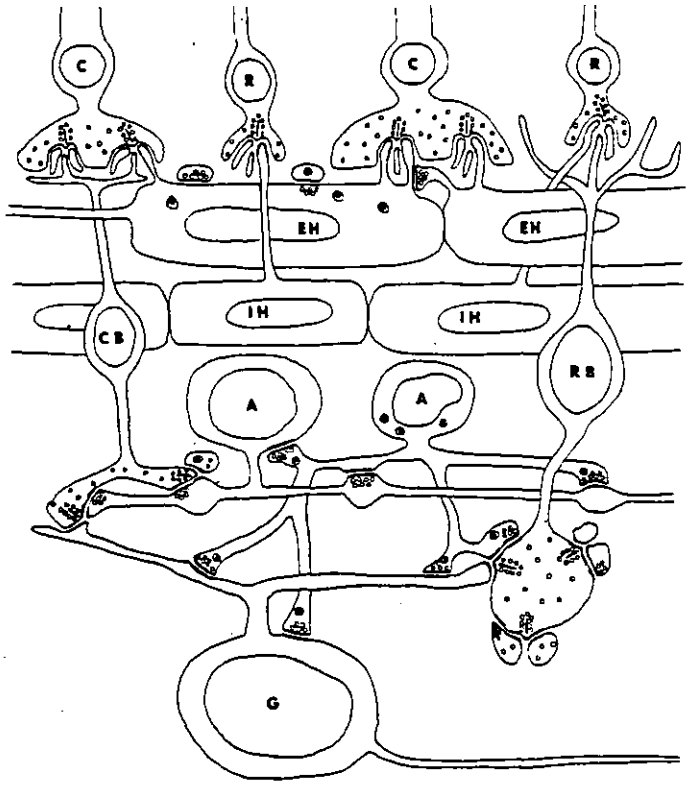

Fig. 2.

Diagram summarizing the synapses found in carp retina. In the outer plexiform layer, bipolar and external horizontal cell processes enter cone pedicles, bipolar and intermediate horizontal cell processes enter rod spherules. Conventional synapses are found between horizontal cell bodies and processes. In the inner plexiform layer, bipolar cell terminals contain synaptic ribbons. Opposite the ribbon lie either two amacrine processes, or one amacrine process, one ganglion cell dendrite. Amacrine processes make conventional synapses onto bipolar terminals, amacrine cell bodies, other amacrine processes, ganglion cell dendrites and ganglion cell bodies. See text for further discussion. The diagram is not to scale

(from Witkovsky & Dowling 1969)

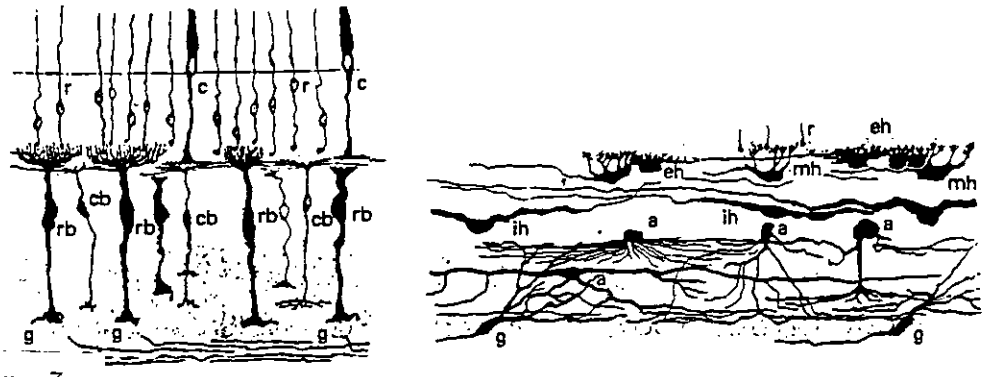

Fig. 3. Vertical section of the teleost fish retina stained by the Golgi technique. Vertical elements (left section) and horizontal elements (right section) shown separately; for a complete model both groups must be superimposed. c, cones; r, rods, cb, small bipolar cells; rb, large bipolar cells; eh, external horizontal cells; mh, intermediate horizontal cells: ih, internal horizontal cells; a, amacrine cells; g, ganglion cells. (Reproduced from Ramón y Cajal, 1893.)

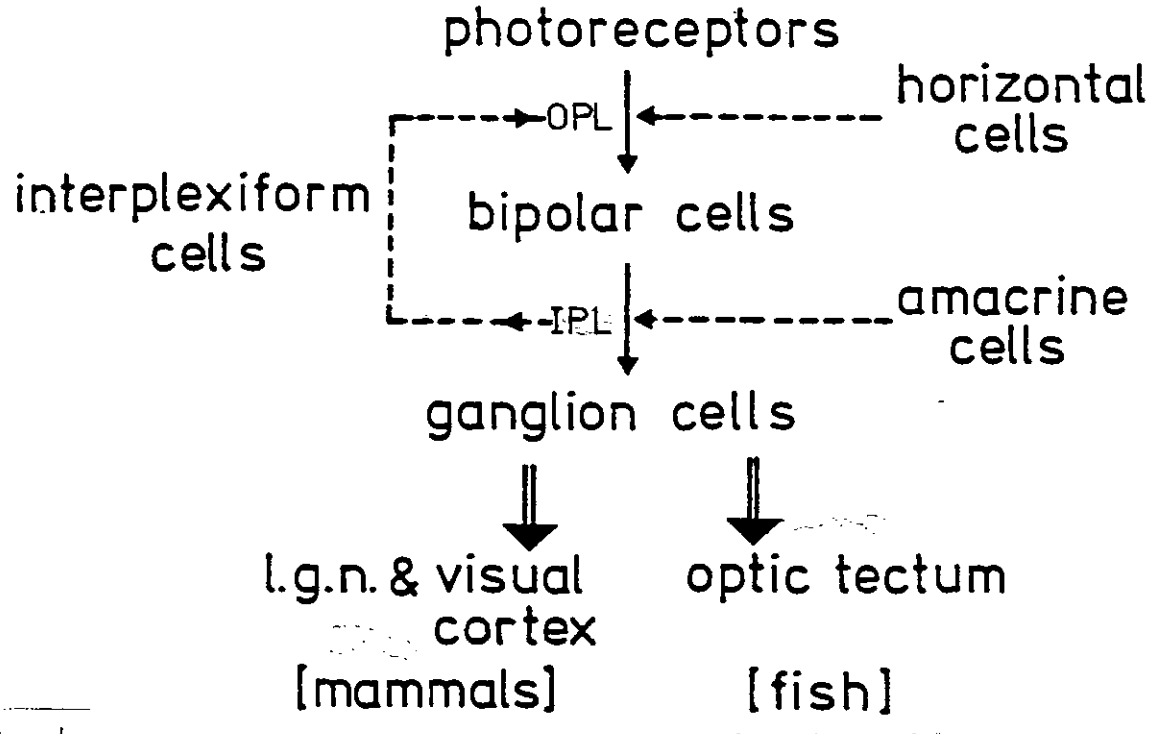

Fig. 4.

Schematic diagram showing the levels of interneuronal interactions in the vertebrate retina, and the neuronal stages in transmission of the electrical signals beyond the photoreceptors. O.P.L., outer plexiform layer; I.P.L., inner plexiform layer. (from M.B.A. Djamgoz 1978)

I.2 Functional Aspects of Neuronal Connectivity

Light in the retinal image is absorbed and transduced to electrical signals by the photoreceptors. These signals are transmitted to the bipolar cells, then to the ganglion cells through chemical synapses in the outer and the inner plexiform layers, respectively. Electrical signals encoding the visual information are carried out of the retina to central visual areas via the ganglion cell axons which form the optic nerve. The horizontal cells which are synaptically driven by the photoreceptors exert interneuronal influences on the photoreceptor-bipolar cell transmission in the outer plexiform layer. The horizontal cells themselves are coupled through electrical junctions (Naka & Rushton, 1967; Kaneko, 1971; Djamgoz & Ruddock, 1978). Amacrine cells play a similar interneuronal role at the inner plexiform layer where bipolar cells synapse onto ganglion cells and also onto amacrine cells themselves (Stell, 1972; Dowling, 1975). Interplexiform cells effect feedback from the inner to the outer plexiform layer.

Thus there exists in the retina a vertical chain of neurones consisting of photoreceptors, bipolar cells and ganglion cells whereby the signals are carried through the retina. This vertical neuronal chain comes under the influence of interneurones at two levels: horizontal cells at the outer plexiform layer and amacrine cells at the inner plexiform layer, with interplexiform cells performing feedback between these layers (fig. 4). The interneurones, by modifying the direct propagation of signals, contribute to the control of sensitivity in the retina.

I.3 Light-evoked Electrical Response Characteristics of Retinal Neurones

I.3.i Photoreceptors

Intracellular recordings from vertebrate photoreceptors (e.g. Tomita et al, 1967; Kaneko & Hashimoto, 1967; Dowling et al, 1976; Burkhardt, 1977) show a transmembrane potential of -10 to -40 mV in the dark, depending on the species. Illumination causes a hyperpolarisation response which is maintained for the duration of the stimulus (fig. 5A). The response amplitude increases with the intensity of the light stimulus (i.e. the response is graded) up to a saturating value of 5 to 30 mV depending on the species (fig. 5A,B). Responses from rods are slower and are about 3 log units more sensitive to light than those from cones. The response amplitude (V) as a function of light intensity (I) follows a template function proposed by Naka and Rushton (1966a):

$$\frac{V}{V_m} = \frac{I}{I+I_{\frac{1}{2}}} \qquad (1)$$

where V_m = maximum (saturation) response; $I_{\frac{1}{2}}$ = value of I for which $V = \frac{V_m}{2}$. When $I \sim I_{\frac{1}{2}}$ the relationship is approximately logarithmic. Figure 5B shows this relation for turtle cones.

Rods subserve scotopic (dim light) vision while cones subserve photopic (bright light) vision (Schultze 1866). The loss of colour vision in dim light suggested that cones also mediate colour vision. Microspectrophotometry of single cones of a cyprinid fish (goldfish) revealed three spectral classes of cone sensitive in the red ($\lambda max \sim 625$ nm), the green ($\lambda max \sim 530$ nm) and the blue ($\lambda max \sim 455$ nm) regions of the visible spectrum (Marks, 1965; fig. 6). Intracellular recordings from single cones confirmed the existence of three spectral classes of cone in the carp (Tomita et al, 1967). It has been shown in the cyprinid fish retina that different spectral classes of pigment are confined to structurally distinct cones (Scholes, 1975; Scholes & Morris, 1973;

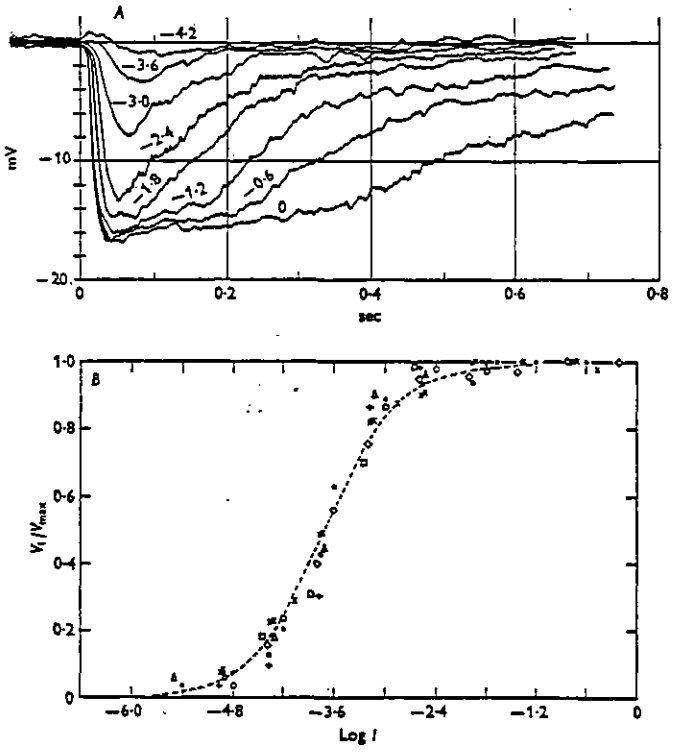

Fig. 5.

Text-fig. 1. Cone response to flashes of different intensities. *A*. Superimposed tracings of responses to 10 msec flashes of increasing intensity, as indicated (log units), applied at time zero. Brightest flash delivered about $8{\cdot}5 \times 10^6$ absorbable photons to the cone. Potential drop on penetration of cell was 22 mV. Downward deflexion represents hyperpolarization.

B. Peak height of response plotted as a function of light intensity. The symbols plot normalized voltages obtained from ten different cells. As different cells had different sensitivities to light, some shift along the abscissa was necessary to superimpose all points. The largest shift was about 0·6 log unit. The interrupted line plots eqn. (1) in the text.

(from Baylor & Fuortes 1970)

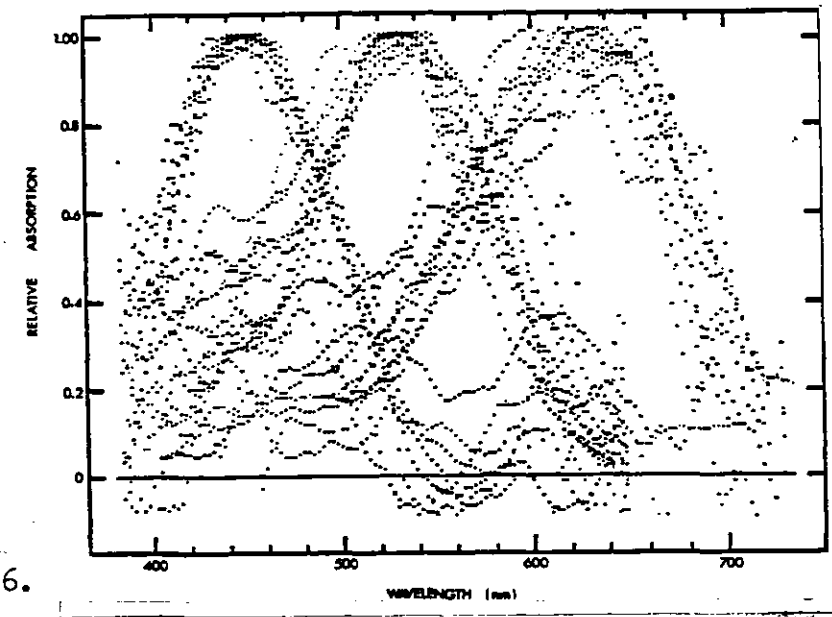

Fig. 6.

Difference spectra of single goldfish cones, determined by microspectrophotometry. The spectra clearly fall into three groups. Within each group the scatter is thought to be due to photon noise fluctuations of the original and bleached scans, inaccuracies in estimating the amount of bleaching per scan, and interference fringes due to reflections within the cover slips. [After Marks (1965).]

Marc & Sperling, 1976a,b; Stell & Harosi, 1976).

In the turtle retina, light-evoked responses of cones depend not only on the light incident on the cone itself but also on the illumination of the surround (Baylor & Fuortes, 1970; Baylor et al, 1971). The direct response of each cone is modified by two interactions: enhancement only from nearby cones of the same spectral sensitivity, and depression controlled by all spectral classes of cone via negative feedback through L-type horizontal cells (Fuortes et al, 1973; O'Bryan, 1973; Baylor & Hodgkin, 1973). In the perch retina, cones summate their signals over a 250 μm diameter; surround illumination depolarises them, although this surround antagonism is fragile and not always effective (Burkhardt, 1977). Thus the receptive field* of the photoreceptors is basically summative, but very small: for a spot stimulus centred on the receptor, the response increases with increasing spot diameter (for constant illumination level) up to some 250 μm.

I.3.ii Horizontal Cells

Svaetichin (1953) was the first to record intracellular responses from the vertebrate retina, and so the responses he found were called "S-potentials" (fig. 7). It has since been shown that S-potentials are generated by horizontal cells (Kaneko, 1970; Werblin & Dowling, 1969; Steinberg & Schmidt, 1970). S-potentials are maintained, graded responses to retinal illumination whose amplitude as a function of the light intensity follows the same template function as that for the photoreceptors (equation 1). Two types of S-potential may be distinguished:

i) L-type, which yield hyperpolarising responses to all light stimuli;

ii) C-type, which hyperpolarise to certain wavelengths of stimulus and depolarise to others.

* The receptive field of a neurone may be defined as the area of the retina over which light stimulation is able to elicit a response from that neurone.

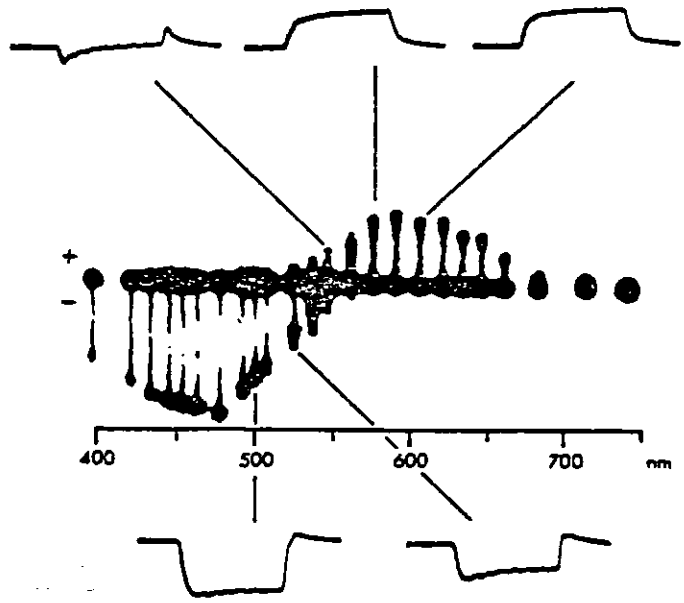

Fig. 7.

S-potentials recorded in a mullet. The central record shows the response to a sequence of monochromatic lights, as a function of the wavelengths of these lights. Certain records are shown on an expanded time scale, the flash duration for each being about 300 ms. [After Svaetichin and MacNichol (1958).]

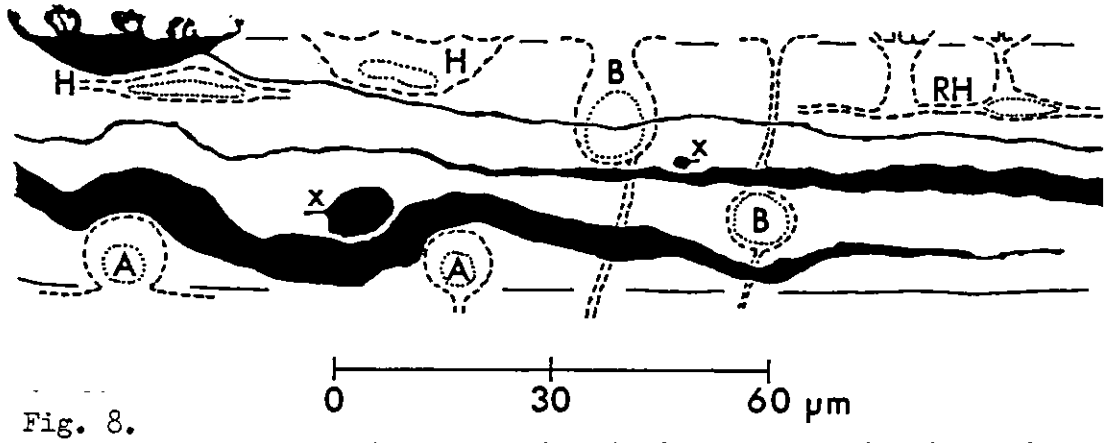

Fig. 8.

Scale drawing which summarizes relationships between structure of cone horizontal cell axon and its level in the inner nuclear layer. In this idealized vertical section, the axon of one *H1* cell is represented in three segments: cell body and initial portion (above), intermediate thin and expanding portions (middle), and thick and terminal portions (below). Also shown are cross-sections of axons with horizontally-projecting appendages (x); and horizontal (H), bipolar (B), and amacrine (A) cells. The area drawn is delimited above by the outer synaptic layer, and below by the inner synaptic layer. The vitread limit of the layer of horizontal cell bodies is at the level of the soma of a rod horizontal cell (RH). (from Stell 1975)

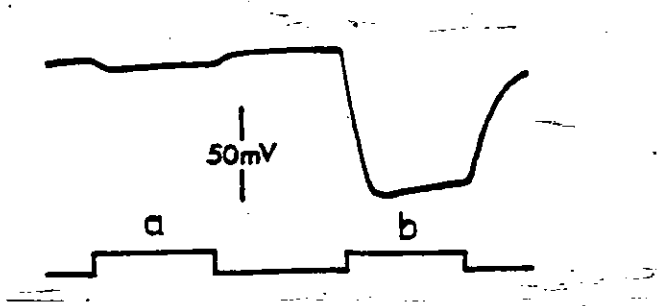

Fig. 9.

Intracellularly recorded responses of a horizontal cell in the carp retina. a. response to a 0.2mm diameter light spot. b. response to diffuse illumination. (from Tomita 1965)

It was proposed that the function of L-type responses is to encode luminosity information while C-type responses encode colour information (MacNichol & Svaetichin, 1958; Svaetichin & MacNichol, 1958). Several workers have classified the different types of S-potentials which they recorded from various species. Two kinds of C-type response have been found: biphasic - hyperpolarising to short wavelengths (λ), and depolarising to long λ; triphasic - hyperpolarising to short and long λ, and depolarising to medial λ. The latter is by far the rarer of the two (Tamura & Niwa, 1967; Spekreijse & Norton, 1970; Mitarai et al, 1974). An extensive study of S-potentials in the retinae of cyprinid fish (tench, bream and rudd) was made by Naka & Rushton (1966a,b,c) who found three L-type and two C-type responses. In the goldfish and carp retina, Tamura & Niwa (1967) found, under photopic conditions, three L-type and two C-type responses. Mitarai et al (1974) found one L-type and three C-type responses in the carp retina. The spectral sensitivities of all these responses were measured by an equal energy criterion (Naka & Rushton, 1966a).

Under scotopic conditions, Kaneko & Yamada (1972) and Mitarai et al, (1974) found a rod-driven S-potential in the carp retina. The spectral sensitivity peaked at about 520 nm and followed closely the absorption spectrum of the rod photopigment porphyropsin. The rod horizontal cell in fish receives no cone input.

In some fish retinae a number of distinct layers of horizontal cells are found which are associated with specific classes of response (Parthe, 1972). Cajal (1893) distinguished three types of horizontal cells in cyprinid fish retinae: "external", "intermediate", and "internal", in order of increasing distance from the outer plexiform layer (fig. 3). Mitarai et al, (1974) marked the recording sites of the observed responses by intracellular injection of Procion Yellow dye.

The L- and C-type responses originated in either the external or the internal horizontal cells; in the external layer C-units seemed to be below the L-units. Hashimoto et al, (1976) injected Procion Yellow into horizontal cells of the carp retina and found four layers containing cells with the following types of responses:

Layer I : L-type responses (external)

Layer II : C-type responses (medial)

Layer III : rod-driven responses (intermediate)

Layer IV : L- and C-type responses (internal)

Kaneko (1970) and Kaneko & Yamada (1972) found in the carp and goldfish retinae that both L-type and C-type units existed in the external and internal horizontal cell layers. The internal horizontal cells appeared to send no dendrites to the outer plexiform layer and had no nuclei (Cajal, 1893). These cells were later identified by electron microscopy of serial sections as terminal expansions of the axons of the external horizontal cells (Stell, 1975; fig. 8).

Djamgoz & Ruddock (1979) performed a spectral analysis of S-potentials recorded from the roach retina by using laser irradiation to selectively suppress cone input mechanisms. They discovered four classes of cone S-potential: two L-type, one biphasic C-type and one triphasic C-type. The biphasic C-type response depolarised to red light and hyperpolarised to blue-green. The triphasic C-type depolarised for green and hyperpolarised for red and blue stimuli, but only few of these units were observed. The L-type responses were designated L_1 and L_2; the L_1-type was red sensitive (peak sensitivity at 620 nm) and the L_2 type was blue-green sensitive.

Horizontal cells have large receptive fields, especially in fish retinae. A horizontal cell responds to increased area of illumination with increased response amplitude to an extent much greater than its

individual dendritic spread (fig. 9). In the fish retina this was attributed to the electrical coupling of horizontal cells such that a layer of these cells is electrically equivalent to a laminar conducting medium bound by two parallel high resistance membranes (Naka & Rushton, 1967). This structure which extends over the entire retina was termed the "S-space". In the carp retina it was shown that potential summation occurs over a large portion of the retina in accordance with Ricco's Law, i.e. for a constant threshold response the relationship "intensity x area = constant" holds for an area nearly equal to that of the entire retina (Norton et al, 1968). Any potential change arising in the S-space propagates passively with a given space constant, a. If a response, V_o, is elicited from a spot stimulus, an electrode x mm away from the spot will record a potential change V given by:

$$V = V_o e^{-x/a} \qquad (2)$$

In the tench retina, the space constant, a = 0.25 mm, and it was shown that the potential arising at several points in the S-space sum linearly (Naka & Rushton, 1967). Therefore, the response potential, V_r, for a circular field of radius r is given by the empirical equation:

$$V_r = 2k\pi \int_o^r \frac{I}{I+I_{\frac{1}{2}}} .x.e^{-x/a} dx \qquad (3)$$

when k is a constant and I, $I_{\frac{1}{2}}$ are as in eqn. (1) (Naka, 1972). Kaneko (1971) showed by current and Procion Yellow dye injection that the external horizontal cells of the dogfish retina are electrically coupled. Gap junctions that make such connections possible have been observed in fish and other lower vertebrates by electron microscopy (Yamada & Ishikawa, 1965; Witkowsky & Dowling, 1969; La sansky, 1973).

I.3.iii Bipolar Cells

Intracellular responses from bipolar cells are difficult to obtain because of the small size of these cells (fig. 10). The variation of response amplitude with illumination level follows the photoreceptor template function (equation 1). Werblin & Dowling (1969) showed that in the mudpuppy retina there are two types of bipolar cell:

1. ON-CENTRE bipolar cells - depolarise in response to a small central light spot; hyperpolarise to an annular (surround) stimulus presented simultaneously with the central spot;
2. OFF-CENTRE bipolar cells - hyperpolarise to a central stimulus; depolarise to central and surround stimuli presented together.

Kaneko (1970; 1973) also found these two types of bipolar cell in the goldfish retina; however fish bipolar cells respond to surround illumination in the absence of central illumination (fig. 11). The receptive field of the bipolar cell is described as being "centre-surround antagonistic" as the responses to centre and surround stimuli are of opposite polarity. The receptive field centre was estimated as 100-200 μm in diameter and the surround as 1-1.5 mm.

According to Kaneko's results, there are three spectral types of bipolar cell in cyprinid fish retinae (Kaneko, 1973; Kaneko & Tachibana, 1981):

1. Non Colour Coded Cells - red-sensitive both in the centre and surround. In these cells the centre and surround are well balanced.
2. Opponent Colour Cells - driven by red- and green-sensitive cones:
   i) red-on centre; red- and green-off surround.
   ii) red-off centre; red- and green-on surround.

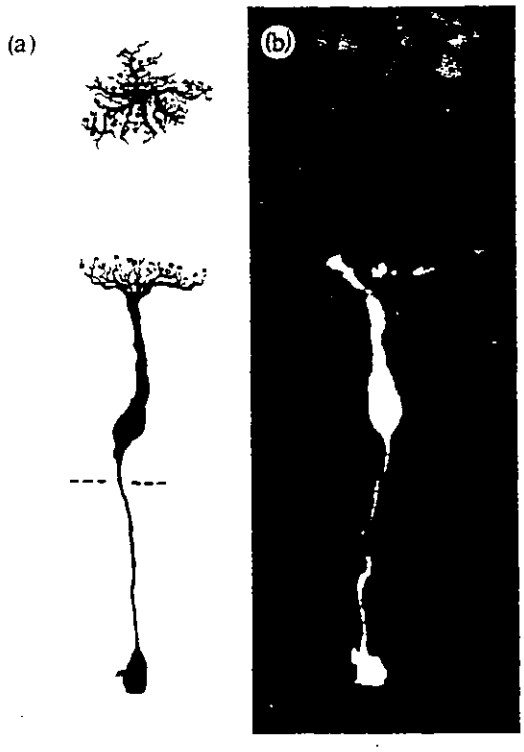

Fig. 10.

A) Camera lucida sketch of a small field rod bipolar from the rudd retina (Scholes, 1975; reproduced by permission of the Roy. Soc. London). It is suggested that these cells are morphologically and functionally homologous in the two closely related fish. That identity enables a characterisation of the detailed synaptic structures which mediate their depolarising responses to illumination of their receptive field-centres.
B) Procion injected on-centre bipolar cell from goldfish retina (Kaneko, 1970; reproduced by permission of the J. Physiol.). Golgi-impregnated

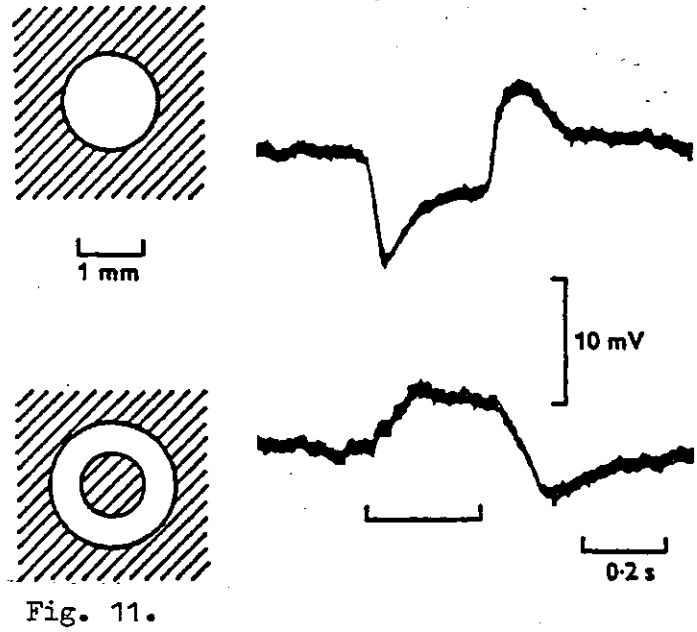

Fig. 11.

Intracellular recordings from a bipolar cell in the goldfish retina; positive upwards. The cell was hyperpolarized by a spot (upper) and depolarized by an annulus (lower). Horizontal line below the response traces indicates roughly the period of illumination. Both types of illumination were white lights of about equal intensity. [From Kaneko (1970).]

3. Double Colour-Opponent Cells - show colour opponency in each of the two spatially antagonistic parts of their receptive fields (Kaneko & Tachibana, 1981). This type of cell is thought to play a major role in the analysis of coloured images by enhancing simultaneous colour contrast (Daw, 1968).

Thus the bipolar cell displays a complex response pattern. The receptive field shows a distinct spatial organisation in which spectral information may also be encoded.

I.3.iv Amacrine Cells

Cajal (1893) described two types of amacrine cell found in all vertebrate retinae that he studied (fig. 3):-

1. Diffuse amacrine cells - processes ramify and terminate throughout the vertical extent of the inner plexiform layer;
2. Stratified amacrine cells - dendrites are confined to one (monostratified) or two (bistratified) distinct levels.

In the goldfish (Kaneko, 1973) and carp (Murakami & Shimoda, 1977), two types of amacrine cell responses were found:

1. "Sustained" amacrine cells - respond to light stimuli with steady potential changes and are colour coded. They hyperpolarise to red and depolarise to green light (Kaneko, 1973). Dye injection showed that this type of response arises in monostratified amacrine cells (Murakami & Shimoda, 1977). Sustained amacrine cells have also been classified according to their responses to white light as those responding with depolarisation (ON-type) and those showing hyperpolarisation (OFF-type) (fig. 12a,b).
2. "Transient" amacrine cells - respond with transient depolarisations at "on" and "off" of light flashes plus a maintained

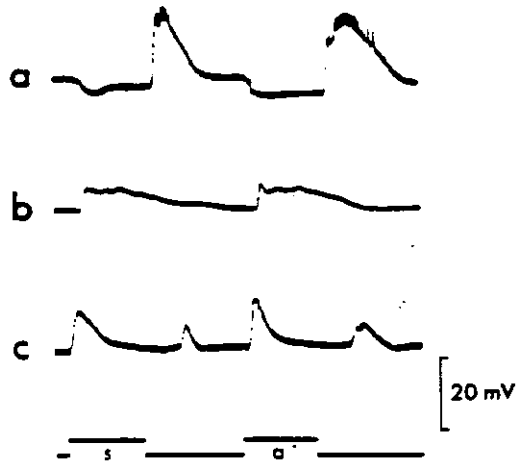

Fig. 12.

Responses of OFF, (a), ON, (b), and ON-OFF, (c), amacrine cells. A spot (0.1 mm in diameter) and an annulus (0.5mm i.d., 3.5mm o.d.) of 400ms white light flashes were projected successively on the light adapted retina. (from Kaneko et. al. 1979)

Fig. 13.

Intracellularly recorded amacrine cell response evoked by diffuse light stimulation (duration indicated by dark bar). Slow potential consists of early transient and later sustained components. Impulses consist of two early large amplitude spikes followed by a low frequency train of small spikes. Termination of the light stimulus evoked a large amplitude spike associated with a slow potential.(from Miller & Dacheux 1976c)

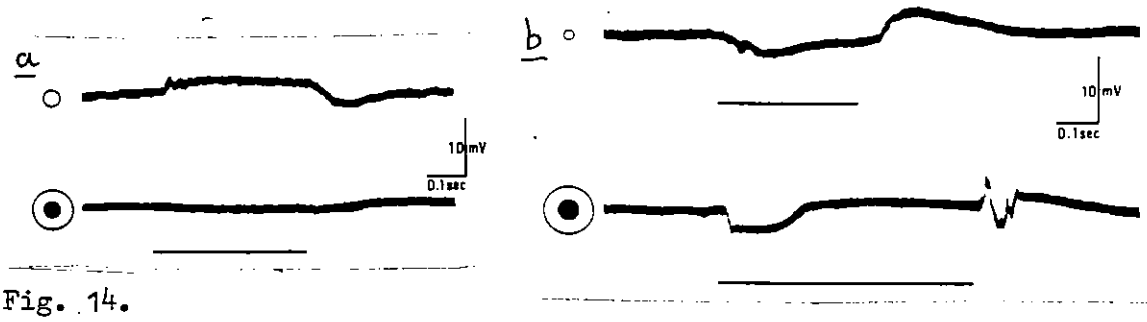

Fig. 14.

Interplexiform cell responses in dace retina.

a. On-center response. Upper record shows the response to a small spot (1.0mm in diameter). Lower record shows the response to an annulus (i.d., 1.0mm, o.d., 2.5mm). Stimulus wavelength is 400nm. Horizontal bar indicates light duration.

b. Off-center cell. Upper record shows the response to 410nm spot (0.5mm in diameter). Lower record shows the response to 680nm large annulus. Horizontal bar on the bottom of each record indicates light duration. (from Hashimoto et.al. 1980)

potential of either polarity (which could also be zero) in between (fig. 12c). These "ON-OFF" type cells are not colour coded (Kaneko, 1973). They were identified as bistratified amacrine cells by dye injection (Murakami & Shimoda, 1977). In the mudpuppy retina, this type of amacrine cell was found also to generate TTX-sensitive somatic and dendritic action potentials (fig. 13; Miller & Dacheux, 1976c).

Both types of amacrine cells show a large spatial summation in an area over 2.5 mm in diameter. Neither type show centre-surround antagonism (Kaneko, 1973; Murakami & Shimoda, 1977). However, Toyoda et al, (1973) found that 50% of the sustained amacrine cells in the carp retina had antagonistic centre-surround organisation as determined using white-light stimuli.

1.3.v Interplexiform Cells

There is so far only one report describing the light-evoked responses of interplexiform cells in the vertebrate retina. Hashimoto et al (1980) used the method of dye injection to identify morphologically and record intracellularly from interplexiform cells in the dace retina. Two types of responses were found: "on-centre" type and "off-centre" type (fig. 14). The responses were all slow potentials. They were similar to the responses of bipolar and amacrine cells so they could only be attributed to interplexiform cells after histological identification of the cells. These responses had a slightly longer latency than those of bipolar cells but the latency was similar to that of amacrine cell responses. The responses of interplexiform cells have been characterised by Hashimoto et al (1980) but it still remains uncertain what function they serve in signal processing in the retina.

I.3.vi Ganglion Cells

The responses of ganglion cells are based on the action potential. Visual information (spectral, spatial, motion, etc.) is encoded in the ganglion cell response as different patterns of spike activity. The response can be described entirely in terms of frequency of spike production. It is at this stage in the processing of visual information that the signal is converted from amplitude-modulated analogue form (slow potentials) to frequency-modulated digital form (action potentials).

The responses of ganglion cells can be classified into 3 main types: (1) ON and (2) OFF type responses consisting of a burst of spike activity at the onset or termination of a centrally presented light stimulus respectively. Such responses can, in turn, be 'sustained' or 'transient'; (3) ON-OFF type response comprising transient bursts of spikes at the onset and offset of the stimulus. Ganglion cells' responses are characteristically organised into concentric centre-surround antagonistic receptive field zones; an ON-centre cell will give an OFF response to surround illumination, etc.

Daw (1968) classified goldfish ganglion cells according to their spectral properties into four types:

(i) Non Colour Coded Units - had similar organisation to the cat ganglion cells described by Kuffler (1953) which were spatially organised with an "ON" or "OFF" roughly annular antagonistic surround. These units give an "ON" response to all wavelengths in the centre and an "OFF" response to all wavelengths in the periphery of the receptive field or vice-versa (fig. 15i). Most of these units were driven by red-sensitive cones.

(ii) Type P Units - found by Wagner et al, (1963). Their spatial and spectral organisation is summarised in Fig. 15ii. These units comprised only about 5% of the ganglion cell population.

Goldfish Ganglion Cells
[Daw 1968]

(i) Non-colour coded

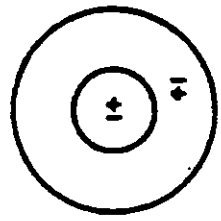

6%

mainly red-driven

(ii) Type P

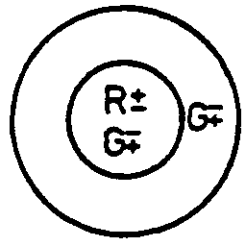

5%

(iii) Type O

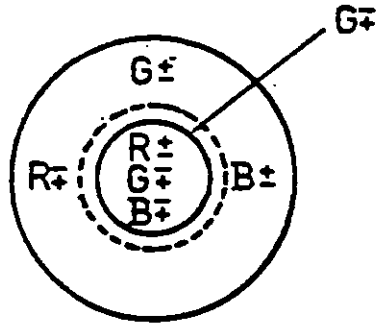

49%

(iv) Type Q

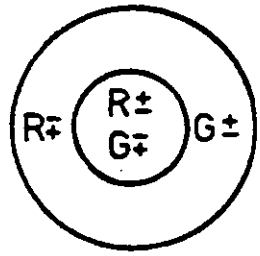

14%

green input masked by red

26% unclassified

Fig. 15. (from Daw 1968)

(iii) Type O Units - comprised about 50% of the ganglion cell population and were organised for simultaneous colour contrast being double colour-opponent. Some type O units possess a narrow annular region surrounding the centre in which the central response to green is unopposed by red due to a slightly larger central field for green (fig. 15iii).

(iv) Type Q Units - in these units the response to green was masked by the red-sensitive component of the response. The "hidden" green-sensitive response was isolated using high intensity stimulation or chromatic adaptation with red bleaching lights. The receptive field organisation discovered is shown in fig. 15 iv.

Beauchamp & Daw (1972) found that ganglion cells in goldfish also received an input from blue cones which was always found in the same part of the receptive field as the green-sensitive component and to have the same response polarity as this component. Further, Adams & Afandor (1971) found that all double-opponent cells had an input from rods with the same 'sign' as that of the red-sensitive response in the same part of the receptive field.

I.4 Synaptic Interactions

The synapses made by the retinal neurones are arranged in two layers: the outer and inner plexiform layers, in which both chemical and electrical synapses have been observed (Stell, 1972; Witkovsky & Dowling, 1969; Dowling & Werblin, 1969).

I.4.i The Outer Plexiform Layer

In the outer plexiform layer (O.P.L) the photoreceptors make synaptic connections to provide input for other photoreceptors, horizontal cells and bipolar cells. Horizontal cells effect feedback onto cones

(Stell et al, 1975; Fuortes & Simon, 1974) and also provide input for bipolar cells. Interplexiform cells are pre-synaptic to bipolar and horizontal cells in the O.P.L. (Dowling & Ehinger, 1975; Dowling et al, 1976).

Photoreceptor-photoreceptor interactions

Photoreceptors make gap (electrical) junction contacts with each other. The synaptic terminations of like and dissimilar cones contact one another in this way, and those of rods contact each other and cones as well, with no evident regard for type (Sjöstrand, 1969; Cohen, 1965; Missotten, 1966). Cones also make invaginating connections with each other (Lasansky, 1971; Scholes, 1975). In the fish (rudd) retina, the cone basal processes make their invaginating contacts with strict selectivity according to type (Scholes, 1975; 1976). Each red cone is connected to 3-5 green cones and vice-versa; blue cones effect a unidirectional invagination of the terminals of green cones (fig. 16).

Synaptic transmission from photoreceptors to horizontal cells

Horizontal cells receive direct synatpic input from the photoreceptors. The photoreceptor-horizontal cell synapse is an excitatory synapse which is active in the dark. The receptor terminals are then depolarised and release an excitatory neurotransmitter which depolarises the L-type horizontal cells. Light hyperpolarises the photoreceptor (fig. 5), reducing transmitter release and thereby hyperpolarising the L-unit giving rise to its light-evoked response. This model of the synaptic action of the photoreceptors was first suggested by Trifonov (1968). Evidence for Trifonov's hypothesis has been presented by various workers and can be summarised as follows:

(i) Depolarisation of receptor terminals in fish retinae by

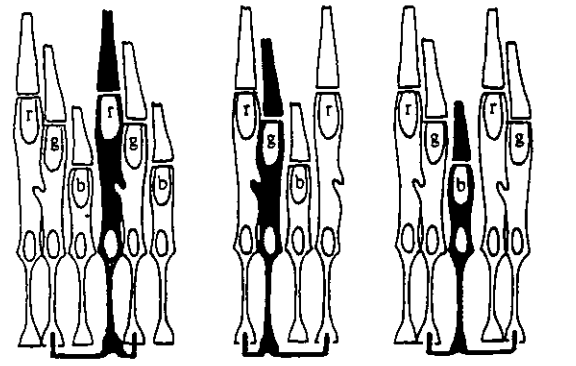

Fig. 16.

Summary diagram of colour coding of invaginating basal processes in the rudd retina. Basal processes ramify from their cone of origin over a field up to 10 μ in diameter, and invaginate other pedicles either en passant with small side branches, or with their terminal ends. Usually only one ending enters a given cone pedicle invagination, and that does not approach the synaptic ribbons there. Only a fraction of cone basal processes make invaginating connection with other cones; the remainder are restricted to the outer plexiform layer, and their connections are not yet known. Rod basal processes ramify at their own more sclerad level, and connect to one another with apposition junctions without invaginating any type of receptor terminal. Connection of oblique cone basal processes are not known

(from Scholes 1976)

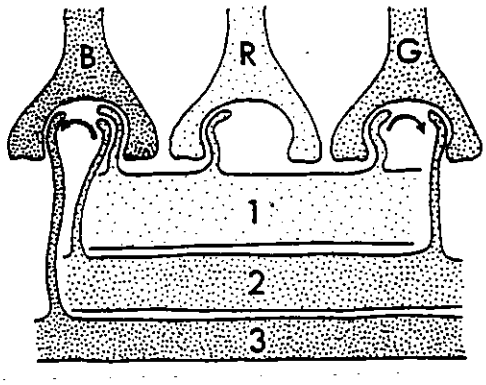

Fig. 17.

Stell and Lightfoot's summary diagram (1975) of the colour coding of horizontal cell connections with the cones in the goldfish retina. Only one type of horizontal cell is selective for just one colour channel; the vitread cells connect to short and miniature single cones, both of which are thought to contain blue sensitive pigment. Two more sclerad layers of cells connect to combinations of colour cones; the intermediate one synapses with green and blue cones, and the outer one connects to all three types of cones. The arrows indicate the direction of synaptic traffic between horizontal cells which Stell and Lightfoot (1975) suggest could explain the origin of chromatic S-potential responses in these cells. According to their scheme, H1 cells would have luminosity responses, while H2 and H3 cells would have chromatic S-potentials, biphasic and triphasic respectively. This model remains to be tested by recording and Procion marking, but it is not inconsistent with findings by those means in the turtle retina. All of these horizontal cells have axons which terminate in large sinuous swellings at the outer margin of the inner nuclear layer, but a fourth class of cells, connected exclusively to rods, apparently does not. Reproduced with the permission of the Journal of Comparative Neurology

(from Stell & Lightfoot 1975)

extrinsic transretinal current depolarises horizontal cells in a graded manner. The response to electrical stimulation is increased during the light evoked hyperpolarisation (Byzov & Trifonov, 1968; Kaneko & Shimazaki, 1976).

(ii) Blocking synaptic transmission from receptors to horizontal cells using Co^{++} or Mg^{++} caused a hyperpolarisation of the horizontal cell membrane and suppression of the light evoked responses (Kaneko & Shimazaki, 1975a ; 1976; Dowling, 1975).

(iii) The L-type S-potential can be reversed in polarity by extracellular depolarisation of the cell membrane up to about zero level implying that the postsynaptic event is an EPSP (excitatory post-synaptic potential) developed in the dark (Trifonov et al, 1974).

(iv) La^{+++} which has been shown to facilitate transmitter release, and putative excitatory amino acid transmitters L-glutamate and L-aspartate depolarise the horizontal cell membrane (Kaneko & Shimazaki, 1975a,b; Murakami et al, 1972).

Synaptic organisation of horizontal cells

In the goldfish retina, Stell & Lightfoot (1975) classified cone-driven (external) horizontal cells into three classes: H1; H2; H3 - in order of increasing dendritic spread, increasing separation from the outer plexiform layer, decreasing size of cell body and decreasing density of cone contacts. These cells all have slender axons which descend to the inner nuclear layer (a layer of cell bodies in the inner retina) where they terminate as Cajal's "internal horizontal cells". The patterns of cone inputs to these cells were as follows (fig. 17):

H1 : red + green + blue

H2 : green + blue

H3 : blue

The H1 cell is associated with the red-sensitive L-type response, the H2 cell with the biphasic C-type (C_b-type) response, and the H3 cell with the triphasic C-type (C_t-type) response (Stell and Lightfoot, 1975). In the roach retina, Djamgoz & Ruddock (1979) found that their (red-sensitive) L_1-units received input from red cones only while L_2 cells received input from blue and green cones with possibly a small amount of negative feedback from red cones.

In a number of species, horizontal cell processes contain synaptic vesicles and appear to make conventional synapses with bipolar cell dendrites, dendrites of other horizontal cells and sometimes even with the soma of an external horizontal cell (Dowling et al, 1966; Dowling, 1968; Dowling & Werblin, 1969; Lasansky, 1973; Witkovsky & Dowling, 1969). In some species (fish, mudpuppy, turtle) horizontal cell processes also make gap junction contacts with one another (Witkovsky & Dowling, 1969; Lasansky, 1973; Dowling & Werblin, 1969). For example in the carp retina, between adjacent horizontal cells of the same layer there are regions where the plasma membranes are closely apposed to form gap junctions (Yamada & Ishikawa, 1965; Witkovsky & Dowling, 1969). Gap junctions such as these would permit electrical coupling between neurones (Bennett, 1973). Electrical coupling between horizontal cells in the roach retina has been shown by Djamgoz & Ruddock (1978).

Whilst the generation of <u>hyperpolarising</u> S-potentials can be explained by Trifonov's (1968) hypothesis, it has been proposed that the <u>depolarising</u> component of the biphasic C-type responses arises as a result of negative feedback from L-units onto cones (Fuortes & Simon, 1974; Stell et al, 1975; Djamgoz & Ruddock, 1980):

a) A structural model based on electron microscopic observation of dendrites of cone horizontal cells at the cone ribbon synapses in the goldfish

retina has been proposed by Stell (Stell et al, 1975; Stell, 1976). It was observed that the dendritic processes of a given type of cone horizontal cell occupy a central or lateral position at the ribbon synapse depending on the cone type. From the patterns of connectivity of the three cone horizontal cells (H1, H2, H3) with the three cone types and the positioning of the dendrites at the ribbon synapses, Stell et al, (1975) proposed that horizontal cells receive excitatory input from cones through their central processes, but inhibit cones through their lateral processes (fig. 18). This model explains how the depolarising response components are generated by a light-mediated reduction of the inhibitory feedback from horizontal cells onto cones causing a depolarisation of the cone terminal and release of excitatory transmitter. The model also shows how the three types of horizontal cell give rise respectively to the three types of response. Some observed properties of S-potentials cannot be explained by this model e.g. in the goldfish retina the red-driven hyperpolarisation in the triphasic response is enhanced both by a depolarising green background and by a hyperpolarising blue background (Tomita, 1965). However the involvement of two synapses in the generation of the depolarising C-type responses is consistent with their longer latency.

b) A functional model based on observation of the depolarisation of cones caused by surround stimuli in the turtle retina was proposed by O'Bryan (1973), Fuortes & Simon (1974) and Fuortes (1976). The depolarising effect of surround illumination was attributed to a negative (inhibitory) synaptic pathway from L-type horizontal cells to cones. This model of cone-horizontal cell interactions in the turtle retina is summarised in figure 19.

c) A model in which the transmitter responsible for the inhibitory feedback was identified by the action of a specific antagonist

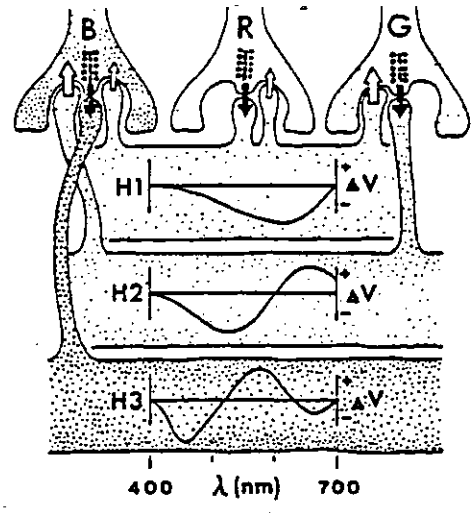

Fig. 18.

Schematic representation of cone horizontal cell pathways in goldfish retina. Cone types are labeled *R*, *G*, and *B* (*6*). The H1, H2, and H3 cells generate monophasic, biphasic, and triphasic spectral response functions (*10*), respectively, by the pathways shown. Synapses where presynaptic and postsynaptic responses have the same polarity are shown by heavy arrows; probable minor synapses from cones to lateral processes, which contact the ribbon synapse in passing, are not indicated. Synapses where presynaptic and postsynaptic responses have the opposite polarities are shown by large and small outlined arrows; the synapses that are most instrumental in generating the spectral response functions (illustrated in the cell bodies) are indicated by the larger arrows.

(from Stell et al 1975)

Fig. 19.

Diagram of connections between cones and horizontal cells. Main connection: solid arrows; additional (and more tentative): dashed arrows. + and - denote transmission without or with inversion of polarity. Both cones and horizontal cells probably have additional output to bipolar cells. Other connection may also exist.
(From Fuortes and Simon, 1974)

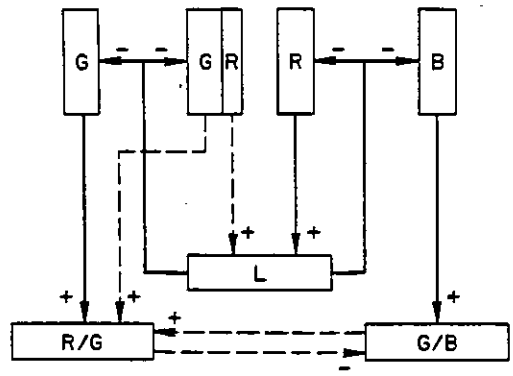

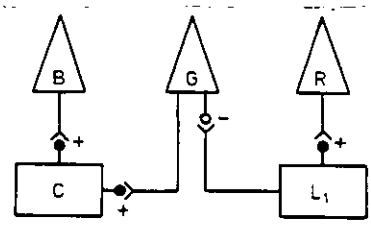

Fig. 20.

Connections between red (R), green (G) and blue (B) sensitive cones and the horizontal cells which generate L_1- and C-type S-potentials, denoted L_1 and C respectively. Plus signs denote excitatory synapses, the minus sign an inhibitory synapse. Pre- and post-synaptic sites are denoted by reverse arrow heads and spots, respectively. (from Djamgoz & Ruddock 1980)

was proposed by Djamgoz & Ruddock (1980). They found evidence in the roach retina for an inhibitory GABA-ergic feedback mechanism in the O.P.L. which was associated with the depolarising component of the C-type response. The proposed model (fig. 20) was similar to that of Stell et al, (1975).

The feedback mechanism from horizontal cells onto cones, therefore, explains the depolarising influence of annular (surround) illumination presented to cones and this pathway, in turn, causes depolarisation in C-type horizontal cells.

Electrical properties of the horizontal cell membrane

In fish (Trifonov et al, 1974) and mudpuppy (Werblin, 1975), the horizontal cell membrane yields a non-linear V-I function, with a slope resistance of 20-30 MΩ at the dark potential level for the mudpuppy. The slope resistance increased by about 15% for each 10 mV depolarisation and decreased similarly for hyperpolarisation (Werblin, 1975a). From a study involving the voltage clamp method, Werblin (1975a) suggested that the horizontal cell response is mediated by a light-elicited resistance increase in the sub-synaptic membrane which is obscured by a potential- and time-dependent resistance decrease at another part of the (non-synaptic) membrane. Byzov et al (1977) proposed an equivalent circuit for the horizontal cell membrane composed of a synaptic and a non-synaptic component as shown in fig. 21. This simple model reflects the essential electrical properties of the horizontal cell membrane. Analysis of the model and of experimental data showed that in horizontal cells, the nonlinearity of the non-synaptic membrane serves to amplify the graded potentials (responses) generated by the sub-synaptic membrane.

On the other hand, Nelson (1973), working on the mudpuppy retina, concluded that the reversal potential for the L-type S-potential is well outside the physiological range (fig. 22). He suggested that the horizontal

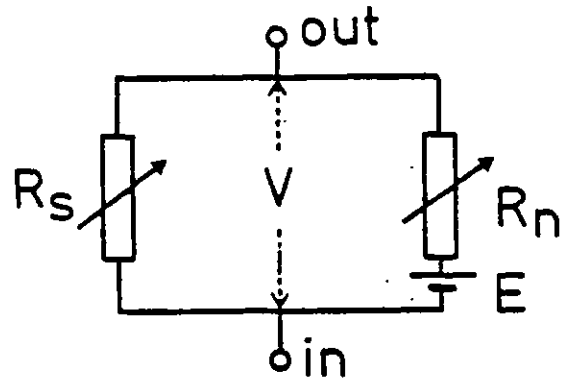

Fig. 21.

The Equivalent Electrical Circuit Model of the Horizontal Cell Membrane

R_s : resistance of the sub-synaptic membrane; low in dark, high in light

R_n : voltage-dependent resistance of the non-synaptic membrane; $R_n = f(V)$

E : resting potential

(from Byzov et al., 1977)

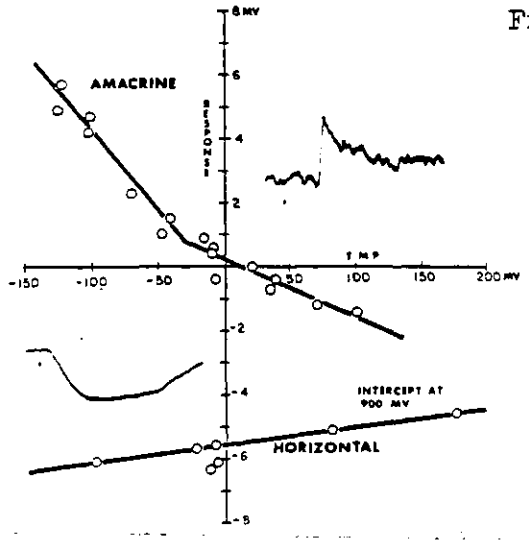

Fig. 22.

Effects of membrane polarizations on responses from amacrine and horizontal cells. TMP is an abbreviation for transmembrane potential. The unpolarized membrane potential of the amacrine cell was −5 to −10 mv; that of the horizontal cell was −15 to −20 mv. The point in the lower left-hand quadrant near the origin was the initial negative response of the amacrine cell. After hyperpolarizing the cell with a potassium chloride-filled electrode (chloride injection), the unpolarized response became slightly positive (see text). An electrode filled with potassium chloride was also used for the horizontal cell. On the right the response of the amacrine cell under hyperpolarized conditions is shown; on the left is that of the unpolarized horizontal cell. The small dot below the beginning of each trace is a 2-mv calibration pulse which also signals the beginning of a 1.1-sec light flash. The amacrine trace is about 1.2 sec long and the horizontal cell trace is about 1.7 sec long.

(from Nelson 1973)

cell might function in a glia-like manner, and respond to light-modulated changes in extracellular potassium concentration brought about by neuronal activity.

Johnston & Lam (1981) investigated the membrane properties of fish horizontal cells which had been dissociated from the retina and electrically uncoupled from each other. They found the specific membrane capacity of these cells to be $\sim 1 \mu F\ cm^{-2}$ and specific membrane resistivity to range from 5,000 to 20,000 $\Omega\ cm^2$. The horizontal cells in isolation showed Ca^{++}-dependent regenerative voltage responses to steps of intracellularly applied currents.

Influence of interplexiform cells in the OPL

Interplexiform cells synapse onto horizontal and bipolar cells in the OPL and appear to use dopamine as the transmitter (Dowling & Ehinger, 1975, 1978; Dowling et al, 1976). Djamgoz & Ruddock (1979) found a difference in adaptation to laser irradiation between cone- and rod-driven L-type horizontal cells in the roach retina. This was later proposed to be due to an excitatory input from the interplexiform cells to L_1 cells but not to L_r (rod-driven), L_2 and C-type cells. Dowling et al (1976) investigated the function of the interplexiform cell in the OPL by studying the differential effects of dopamine on cones, horizontal cells and on-centre bipolar cells. At concentrations which little affected the cone response, dopamine depolarised the L-type (red-sensitive) horizontal cell and suppressed its light-evoked response. The on-centre bipolar cell was slightly hyperpolarised, the hyperpolarising surround response reduced, whilst the depolarising central response was enhanced. From these observations, Dowling et al, (1976) suggested that interplexiform cells in goldfish may regulate centre-surround antagonism in the OPL of the retina.

Bipolar cell synaptic inputs

Bipolar cells receive input from photoreceptors, horizontal cells (Stell, 1972) and from interplexiform cells (Dowling et al, 1976) in the OPL. In the cyprinid fish retina, Cajal (1893) classified bipolar cells into two morphological types: 'giant bipolars' which connect only to rods and 'small bipolars' which connect only with cones. In the goldfish retina, Stell (1967) distinguished two types of bipolar cell: a giant bipolar cell that receives input from both rods and cones and a small bipolar that connects to cones only. Thus Stell showed that Cajal's giant bipolars in fact connect with both rods and cones, so he renamed the giant bipolar a 'mixed' bipolar and the small bipolar a 'cone' bipolar.

Scholes (1976) divided fish (rudd) bipolar cells into three functional classes:

i) Rod bipolar cells (Cajal's giant bipolars) - receive input from rods and red cones; these are of two morphological subtypes (fig. 23).

ii) Selective cone bipolars (Cajal's small bipolars) - receive input exclusively from either blue or green cones (fig. 23).

iii) Mixed cone bipolar cells - predominant input is from cones, although some is from rods. They connect to combinations of different colour cones. The most common type synapsed with red and green cones and with rods (fig. 23).

The input to bipolar cells must be spatially organised to give the centre-surround antagonistic response. The size of the receptive field centre agrees well with the dendritic spread of the bipolar cell whilst the antagonistic surround has been proposed to be mediated by horizontal cells (Werblin & Dowling, 1969). Studies with specific blocking agents, however, showed that, in the turtle retina, bipolar cells retain their antagonistic surround field after the horizontal

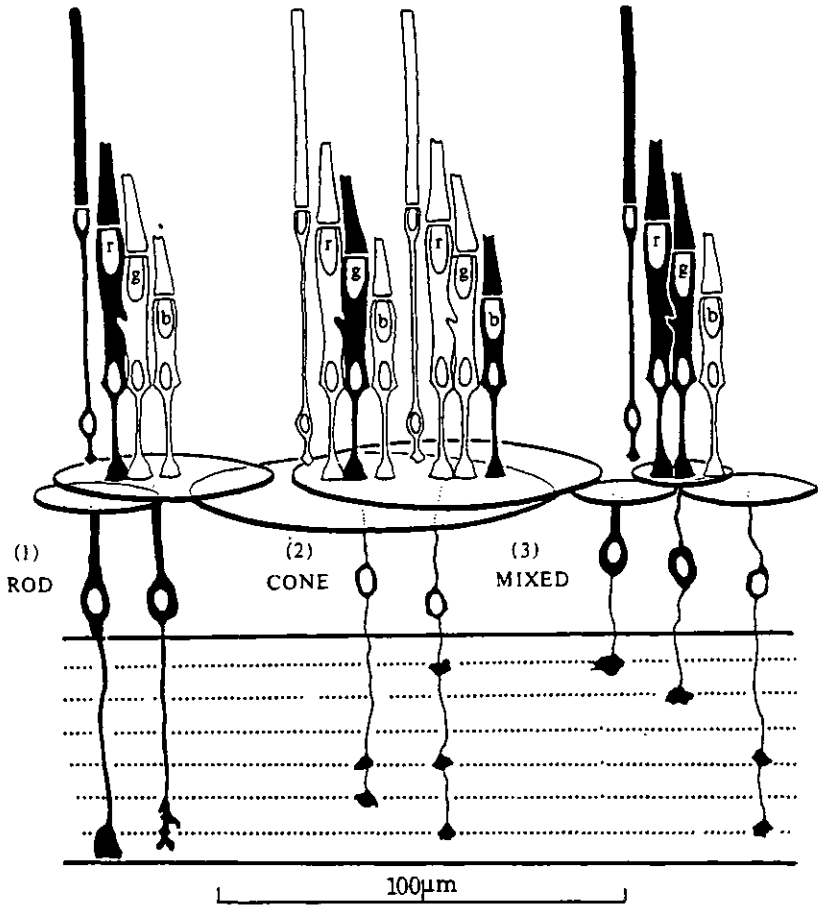

Fig. 23.

Summary diagram (from Scholes, 1975, reproduced by permission of the Roy. Soc. London) of the colour coding of connections between bipolar cells and different receptors in the rudd retina. Some bipolars, filamentous cells with wide dendritic trees (centre group), connect selectively with different types of cones (though a red coded type has not been found). Other cell types, with smaller, more densely branched fields, connect to combinations of receptors. One class, particularly easily identified by light microscopy on account of their massive processes and vitread axon terminals in the inner plexiform layer (Cajal, 1892; Stell, 1967; Parthe, 1972), synapse with rods and with red cones only (left-hand group). Another more varied class of bipolars (right-hand group) connect to combinations of colour cones (e.g. red and green; blue and green) and some of them connect with rods as well. These cells generally have the smallest outer plexiform dendritic fields, their axons predominantly address the more sclerad strata of the inner plexiform layer.

The grouping suggested by the diagram is somewhat arbitrary, but designed to respect the light microscopic nomenclature (Cajal, 1892) for fish bipolars. Likewise, no account is taken of the detailed ultrastructure of the connections involved

(from Scholes 1976)

cells have been selectively inactivated (Piccolino & Gerschenfeld, 1977).

Action of synaptic transmitter at the bipolar cell membrane

Evidence similar to that for L-type horizontal cells (i.e. blockage of synaptic transmission from photoreceptors with Co^{++} causing a hyperpolarisation) indicates that OFF-centre bipolar cell responses are generated in the same way as L-type S-potentials (Toyoda, 1973; Kaneko & Shimazaki, 1976; Murakami et al, 1975). However, different neurotransmitters may be involved in the generation of the bipolar cell response (Gerschenfeld & Piccolino, 1977).

Kaneko & Shimazaki (1975a) and Dacheux & Miller (1976) investigated the synaptic transmission from photoreceptors to bipolar cells and both found evidence to support Trifonov's (1968) hypothesis. Kaneko & Shimazaki (1975a) suggested that the same transmitter produced responses of opposite polarities (ON and OFF responses) by decreasing or increasing respectively the membrane ionic conductance in the dark. This was due to different properties of the respective subsynaptic membranes. Thus for the ON-centre bipolar cell, the excitatory transmitter released from the photoreceptor terminals appears to close the ionic channels in the cell membrane, such that a reduction of transmitter flow by light depolarises the bipolar cell (Kaneko & Shimazaki, 1975a; 1976; Dacheux & Miller, 1976). The identity of the neurotransmitter is at present unknown, but it has been shown that glutamate and aspartate produce potential changes in horizontal and bipolar cells similar to those expected of the endogenous transmitter (Murakami et al, 1972; 1975).

I.4.ii The Inner Plexiform Layer

In the inner plexiform layer (I.P.L.) bipolar cells synapse onto amacrine and ganglion cells; amacrine cells connect with other amacrine cells and provide input for ganglion cells, as well as effecting synaptic

feedback onto bipolar cells (Stell, 1972). Interplexiform cells are pre- and postsynaptic to amacrine cells in the IPL of the goldfish retina (Dowling & Ehinger, 1975, 1978; Dowling et al, 1976). Thus, interplexiform cells appeared to provide a centrifugal pathway from the IPL to the OPL. The synaptic connections of interplexiform cells are shown in figure 24 which also serves as a summary diagram of synaptic interactions in the fish retina.

IPL functional organisation: sublaminae a and b

In Golgi-stained preparations it has been clearly demonstrated that the IPL of various vertebrates consists of several sub-strata (Cajal, 1893), but their functional significance has long been a matter of discussion. Cajal (1893) suggested that the IPL was stratified to permit synaptic contact between certain kinds of (stratified) amacrines and corresponding types of (stratified) ganglion cells. Nelson et al (1978), by intracellular staining of ganglion cells in the cat retina found that the OFF-centre cells terminated in the distal half of the IPL, which they denoted sublamina a, while ON-centre cells terminated in the proximal half, denoted sublamina b. From these results they proposed that the two sublaminae of the IPL provide two separate sites of synaptic interaction for ON- and OFF-pathways respectively.

Famiglietti et al,(1977) investigated the validity of this hypothesis with respect to ganglion, amacrine and bipolar cells in the carp retina. The IPL of the carp retina can be clearly divided into the five-tiered strata described by Cajal (1893) under the fluorescence microscope. Famiglietti et al (1977) discovered that the most striking difference in the morphology of ON- and OFF-bipolar cells was found in the location of their axon terminals: OFF-bipolars at Cajal's strata (S) 1,2,3, and ON-bipolars at S4 and S5. Thus it was proposed to divide the five strata into two major groups:

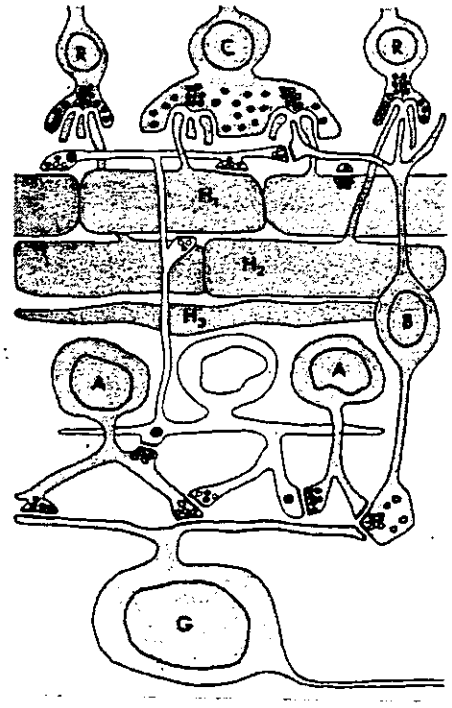

Fig. 24.

A summary diagram of the synaptic connections of amine-containing interplexiform cells of the goldfish retina. The input to these neurons is in the inner plexiform layer via conventional synapses of amacrine cells (*A*). The interplexiform cell processes have been observed to make conventional synapses onto amacrine cell processes in the inner plexiform layer, but never do they contact the ganglion cells (*G*) or their dendrites. In the outer plexiform layer, the processes of the interplexiform cells make synapses on the perikarya of the external horizontal cells (H_1) and onto bipolar cell (*B*) dendrites. The interplexiform cell processes have never been observed as postsynaptic elements in the outer plexiform layer at either rod (*R*) or cone (*C*) receptor terminal synapses or at the occasional external horizontal cell synapse. No synapses have yet been seen between interplexiform cell processes and elements in the intermediate (H_2) or internal (H_3) horizontal cell layers.

(from Dowling & Ehinger 1975)

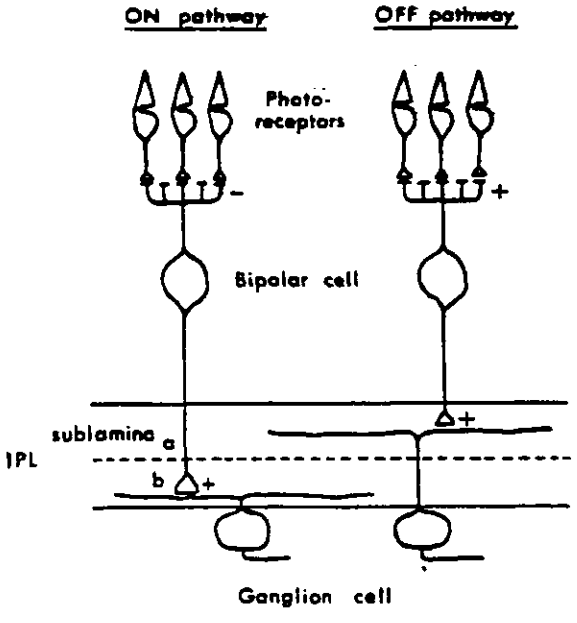

Fig. 25.

Schematic diagram showing the connections of photoreceptors, bipolar and ganglion cells. Plus sign indicates an excitatory synapse or the synapse where the response polarity of the presynaptic cell is preserved in the postsynaptic cell. Minus sign indicates an inhibitory synapse or the synapse where the response polarity is reversed.

(from Kaneko et al 1979)

sublamina a (Cajal's S1, 2 and 3), and sublamina b (Cajal's S4 and 5) similar to the subdivision of the cat's IPL. The terminals of OFF-bipolar cells were found in sublamina a for both mixed and cone bipolars; ON-bipolar cells of both types sent dendrites only to sublamina b. Famiglietti et al (1977) also found that OFF-(sustained) amacrine cells extended their dendrites into sublamina a, while dendrites of ON-(sustained) amacrine cells were confined to sublamina b. Most ON-OFF(transient) amacrine cells sent their dendrites to both sublaminae a and b in a stratified or diffuse branching pattern. Thus the identification of sustained amacrines as Cajal's (1893) monostratified amacrines, and of transient amacrines as Cajal's bistratified amacrines (Murakami & Shimoda, 1977) is seen to have a functional significance. Similar results were obtained for ganglion cells. It was found that the dendrites of OFF-centre cells terminated in sublamina a, while those of ON-centre cells extended to sublamina b. The dendrites of ON-OFF cells were found crossing the border between the two sublaminae.

Thus it appears that the vertebrate retina has separate pathways to convey ON and OFF signals to ganglion cells. The signals are first separated at the receptor-bipolar cell synapse and from there on the sign of the signal is preserved. Famiglietti et al (1977) and Naka (1977) suggested that ON bipolar cells connect only with ON-centre ganglion cells, OFF bipolars only with OFF-centre ganglions, and that this synapse must be excitatory to preserve response polarity. Miller & Dacheux 1976b, found that "inhibitory" responses from mudpuppy ganglion cells are, in fact, disfacilitation, further supporting the idea that bipolar-ganglion cell transmission is excitatory irrespective of the response polarity. This model of separate ON and OFF pathways is shown schematically in fig. 25 (from Kaneko et al, 1979 who, being the authors of Famiglietti et al, 1977, summarise their earlier work).

Amacrine cells - synaptic interactions and membrane properties

The results of Werblin and Dowling (1969) suggest that the synapse between bipolar and amacrine cells may all be excitatory as this type of connection makes the simplest circuit between the two kinds of neurone, with ON-bipolars connecting to ON-amacrines and OFF-bipolars to OFF-amacrines. ON-OFF amacrine cells are able to receive input from both ON- and OFF-bipolar cells. Toyoda et al, (1973) found that in sustained amacrine cells with antagonistic centre-surround organisation, the hyperpolarising response was accompanied by a resistance increase and the depolarisation by a resistance decrease. It was suggested that ON-centre amacrine cells received excitatory inputs from ON-centre bipolars at least in the receptive field centre, with a similar relationship between OFF-centre bipolar and amacrine cells. The ON-OFF amacrine cells were thought to receive balanced inputs (e.p.s.p.s) from both ON-centre and OFF-centre bipolar cells (fig. 26).

Werblin (1977) studied the membrane properties of the transient amacrine cell in the mudpuppy retina. He measured the voltage-current relationship and found it to be non-linear, with a region of "negative resistance" (fig. 27). He found that the response was caused by an inward (depolarising), monophasic synaptic current mediated by a conductance increase to ions with a reversal potential more positive than the dark (resting) level. This current generated a monophasic e.p.s.p. which could elicit an initial spike when it exceeded $\sim$4 mV. The spike rapidly boosted the membrane potential by about 30 mV or more. The generation of this spike as a "regenerative" ionic current in response to a certain threshold e.p.s.p. is consistent with the observed V-I relationship with its region of "negative resistance" (fig. 27). The monophasic form of the synaptic current is consistent with the finding that these amacrine cells receive only a depolarising input (Toyoda et al, 1973; Werblin & Copenhagen, 1974).

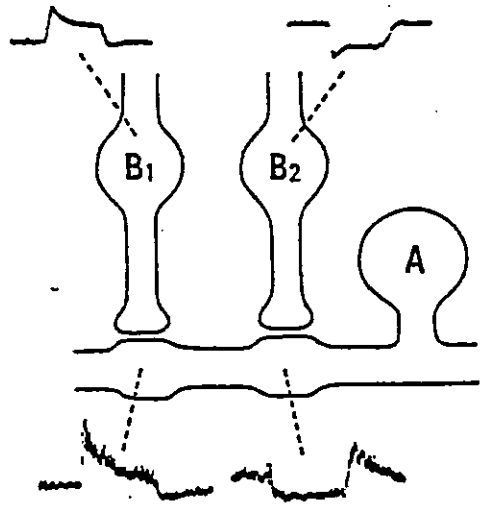

Fig. 26. A model proposed to explain the transient amacrine cell response. B_1, B_2, 'on' centre and 'off' centre bipolar cells respectively. A, transient ('on-off') type amacrine cell.

(from Toyoda et al 1973)

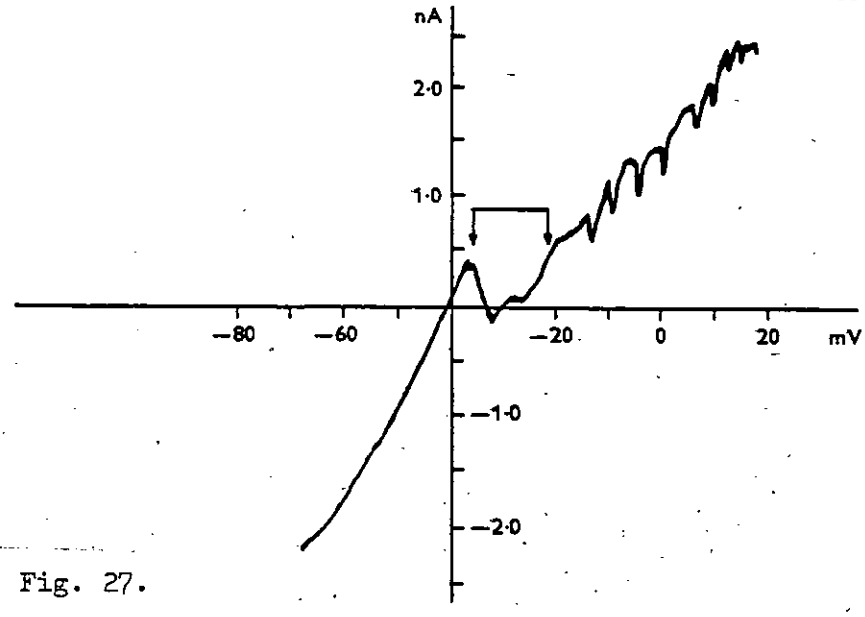

Fig. 27.

Current–voltage curve generated by 'sweeping' the potential from an initial hyperpolarization of −80 to +20 mV at 10 mV/sec under voltage clamp. A large negative resistance region spanning about 15 mV and 0·5 nA appeared at a depolarization of 4 mV above the dark level. A series of repetitive spikes was generated from −10 to +20 mV requiring an incremental clamping current of about 0·2 nA to maintain the potential ramp. The dark level is at the origin.

(from Werblin 1977)

Kaneko (1973) suggested that transient amacrine cells received input from bipolar cells with no colour coding, while the colour-coded, sustained amacrine cells were driven mainly by opponent-colour bipolar cells, with spatial information discarded in both cases. Since the giant ('rod') bipolar cells receive both rod and cone input it is likely that some amacrine cells have rod-driven responses under scotopic conditions. Dowling & Ripps (1977) recorded such a response in the all-rod skate retina consisting of a transient ON-depolarisation.

The spatial summation in amacrine cell receptive fields (Kaneko, 1973) has been attributed to lateral coupling between amacrine cells which is independent of the coupling of horizontal cells. Djamgoz & Ruddock (1978) found that in the roach retina, lateral transmission in amacrine cells (but not in horizontal cells) was blocked by local perfusion of Co^{++}. They concluded that amacrine cells are coupled to each other largely by means of chemical synapses. Naka & Christensen (1981) has also shown electrical coupling in amacrine cells of the catfish.

Synaptic input to ganglion cells

In the carp retina, Witkovsky & Dowling (1969) found that ganglion cells receive equal inputs from bipolar and amacrine cells. Comparing the sizes and spectral characteristics of receptive fields of bipolar, amacrine and ganglion cells of the goldfish retina, Kaneko (1973) found that the size of a ganglion cell centre was comparable to the size of the total receptive field of a bipolar cell. Bipolar and ganglion cells stimulated only in the field centres behaved similarly in a number of ways: there were opponent inputs from red and green cones, the red-sensitive area was smaller than the green-sensitive area, and the red responses had shorter latency than the green responses. Thus Kaneko (1973) suggested that information concerning the field centre was directly transmitted from bipolar to

ganglion cells. On similar grounds, sustained amacrine cells were thought to supply the surround information to ganglion cells.

Although it has been shown that amacrine and ganglion cells of the same response polarity (ON or OFF) extend their dendrites to the same sublamina of the IPL (Famiglietti et al, 1977) it is unlikely that the synaptic connections here are all excitatory. Miller (1979) has, in fact, suggested that amacrine-ganglion cell transmission is mostly inhibitory. Amacrine cells are thought to use various inhibitory transmitters including GABA and glycine. Further, putative neuroactive peptide transmitters have also been localised to specific amacrine cells (Stell et al, 1980). Thus it seems very likely that different kinds of amacrine cell play separate functional roles in influencing bipolar-ganglion cell transmission.

I.5 Ionic Bases of Electrical Activity in Retinal Neurones

I.5.i Introduction

The formulation of the ionic basis of electrical activity in the nervous system was initiated by Bernstein (1902) who used, for the first time, the electrochemical theories of Nernst. Work by Hodgkin, Huxley and Katz (Hodgkin & Katz, 1949; Hodgkin, 1951; Hodgkin & Huxley, 1952) revealed the ionic mechanisms responsible for electrical signalling in nerve axons. Hodgkin and Huxley formulated the equations which constitute a classic theory of the ionic basis of membrane potential and action potential generation in nerve axons and muscle. Subsequent work provided support for this theory and further information about the ionic basis of electrical activity (e.g. Hodgkin & Keynes, 1955a,b; Adrian, 1956; 1958; Hodgkin & Horowicz, 1957; 1959a,b; Fatt & Ginsbourg, 1958; Baker et al, 1962a,b; 1963). It is now generally accepted that the signalling ability of excitable cells depends on two factors:

i) the physiologically important inorganic ions (Na^+, K^+, Cl^-, Ca^{++}) are distributed in unequal concentrations on the two sides of the cell membrane, with each ion having its characteristic equilibrium potential as expressed by the Nernst equation:

$$E_x = \frac{RT}{Z_x F} \cdot \ln \left(\frac{a_x^{\,o}}{a_x^{\,i}} \right) \qquad (4)$$

where E_x is the equilibrium potential for the ion x; R is the universal gas constant; T is absolute temperature; F is the Faraday constant; $a_x^{\,o}$, $a_x^{\,i}$ are the activities* of the ion X on the outside and inside of the membrane respectively; Z_x is the valency of ion X.

ii) The cell membrane may become selectively permeable to different ions depending on its functional state. The prevailing transmembrane potential is determined by the relevant equilibrium potential (s) and the partial permeabilities of the membrane to those ions. Thus, a physiological effect resulting in an increase in permeability (conductance, g) of the membrane to an ion x (Δg_x +ve) will cause the membrane potential, E_m, to move towards the equilibrium potential of that ion, E_x. A decrease in permeability to ion x (Δg_x -ve) will cause the membrane potential to move away from E_x.

The mechanism described provides the basis for all electrical signalling in excitable cells and demonstrates the importance of ionic activities in cellular electrogenesis. It is the activities of various ions both in the extracellular environment and in the cytoplasm of a cell that define the functional character of that cell since they determine the potential levels between which the membrane potential can

*The activity of an ion, a_x, is related to its concentration, C_x, by the relation $a_x = \gamma_x C_x$, where γ_x is known as the activity coefficient.

move to give rise to the electrical response. These activity values can be measured directly with ion-sensitive microelectrodes.

I.5.ii Photoreceptors

Measurements of membrane resistance with a bridge circuit in gecko, mudpuppy and turtle retinae have shown that the response is associated with a resistance increase of the cell membrane. It has also been demonstrated that the resistance increase causes the hyperpolarisation and not vice-versa (Toyoda et al, 1969; Baylor & Fuortes, 1970). Werblin (1975b), using the voltage-clamp technique showed that the outer segment and the cell body of the mudpuppy rod photoreceptor possessed different electrical properties: a light-elicited resistance increase at the outer segment caused a potential-dependent transient resistance decrease at the inner segment.

In the dark the extracellular space around the tips of the photoreceptors is negative with respect to the basal ends of the receptors by about 5 mV, and this potential is reduced by a light stimulus. Penn & Hagins (1969) and Hagins et al (1970) attributed the voltage gradient across the rods of the rat retina to a 'dark current' of 71 pA per rod. Upon illumination this dark current was reduced. Sillman et al (1969a,b) investigated the extracellular mass receptor response in the frog retina. By ionic substitution, it was found that the amplitude of the photoreceptor response varied in direct linear proportion to the log. of the external sodium concentration; the relationship was simply inverted for the extracellular potassium. It was proposed that the dark current was due to Na^+ and that light caused a selective decrease in Na^+ permeability, but did not change the permeability to other ions. Hagins (1972) found that photoresponses of a variety of vertebrate rods and cones were abolished in the presence of ouabain in normal Na^+ concentrations and concluded that

sodium ions are pumped out of the inner segment by means of a metabolic mechanism. These results, together with the observation that the membrane resistance of the receptor outer segment increased during the light response, suggested that in the dark the outer segment membrane is permeable to Na^+ ions, keeping the cell depolarised. Light closes the Na^+ channels giving rise to a hyperpolarisation (fig. 28).

The internal transmitter of photoreceptors

The photopigment which effects the first stage in the transduction of light energy into the electrical activity of the photoreceptors is found in saccules which are separate from the cell membrane in rods. Thus it is necessary to propose a mechanism to effect the transition between the absorption of light and the closing of the Na^+ channels, i.e. an 'internal transmitter' which is involved in the transduction process. An internal action by Ca^{++} has been postulated since: i) increasing the extracellular Ca^{++} concentration was found to mimic the effect of light by reducing the dark current; ii) decreasing extracellular Ca^{++} severely reduced the light sensitivity of the dark current (Yoshikami & Hagins, 1973). It was proposed that the discs in the outer segments of rods are stores which accumulate Ca^{++} in the dark; light causes partial release of Ca^{++} ions which diffuse through the extrasaccular space to the outer membrane, when they bind to the Na^+ channels and close them (fig. 29). In cones, the blockage of ionic channels is supposed to occur following entry of external Ca^{++} brought about by an increased permeability of the outer segment membrane. Kaneko & Shimazaki (1975b) found that cones in the carp retina gave a prominent 'OFF' rebound in Ca^{++}-free medium. This enhancement of the 'OFF' response was not the result of interaction with other cells since it persisted after blockage of chemical transmission. It appeared to be

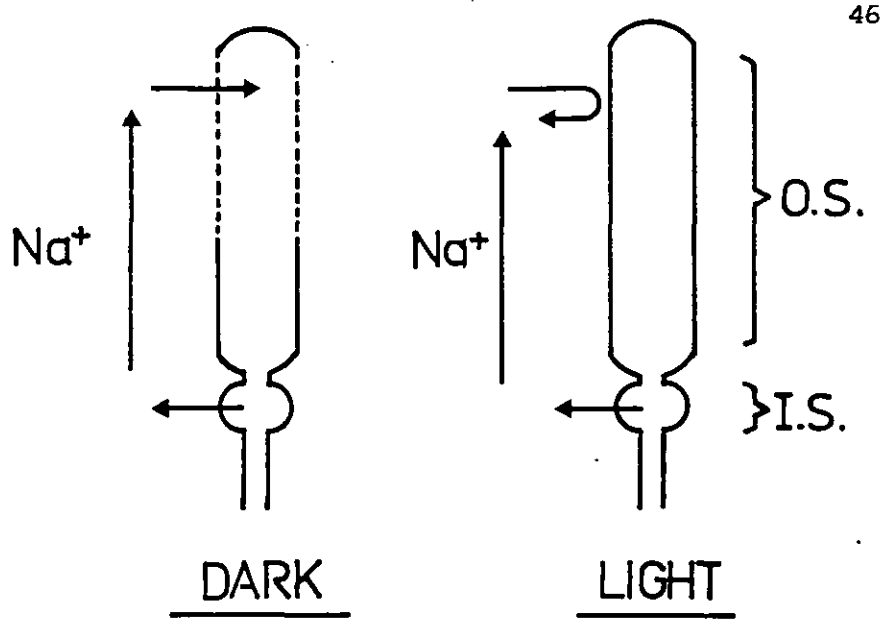

Fig. 28.

Na+ currents associated with rod photoreceptors. In darkness Na+ flows into the outer segment through the open Na+ channels and is extruded from the inner segment by a metabolic pump, causing an extracellular voltage gradient and Na+ current. In light the Na+ channels in the outer segment close, blocking the influx of Na+. However, Na+ continues to be pumped out of the inner segment thus giving rise to a hyperpolarisation of the receptor and a reduction in the extracellular potential gradient and current flow. O.S., Outer segment; I.S., Inner segment.

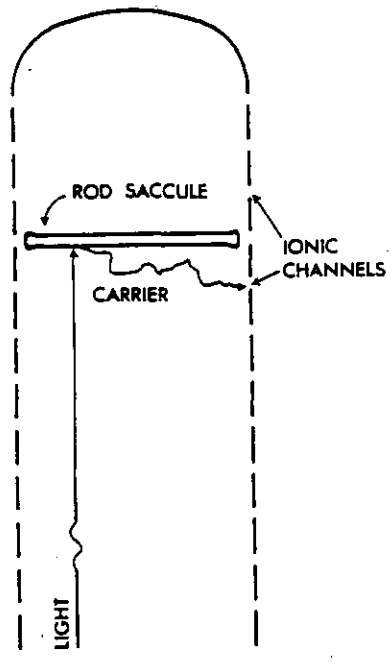

Fig. 29.

Schematic diagram showing the probable sequence of events whereby a photon absorbed by a rod saccule leads to a change in membrane conductivity.

(from Rodieck 1973)

produced by a change in the cone membrane properties by the removal of Ca^{++} suggesting enhanced Na^{+} permeability of the outer segment membrane in accord with the "Ca hypothesis". The physiological implications of the "Ca hypothesis" have been investigated and several other workers have also found evidence to support it e.g. Fatt and Falk (1977); Pinto et al, (1977); Hagins & Yoshikami (1977).

However, evidence casting doubt on the "Ca hypothesis" has also been found. Before the hypothesis was formulated, Arden & Ernst (1970) had shown that responses could be obtained from cones bathed in a Ca^{++}-free solution with a Ca^{++} chelating agent added to it such that the intracellular Ca^{++} would be reduced to a negligible level. Other workers (Bertrand et al, 1978; Arden & Low, 1978; Bastian & Fain (1979) have also questioned the validity of the Ca hypothesis. Doubt about Ca^{++} as the internal transmitter led to a search for other candidates. Bitensky et al, (1973) suggested that cyclic nucleotides might be involved in transduction. A light-activated phosphodiesterase(PDE) was discovered in rod outer segments (Bitensky et al, 1975) which catalyses the hydrolysis of cyclic guanosine monophosphate (cGMP). In neurones and other tissues the cyclic nucleotides are co-factors for a kinase which catalyses the phosphorylation of a membrane protein and this protein is believed to control the membrane permeability to ions. The finding by Woodruff et al, (1977) that there is a correlation between the permeability of the rod outer segment membrane and the level of cGMP suggests a model of transduction on the scheme shown in fig. 30.

The hydrolysis of cGMP leads to the production of H^{+} ions; this can be followed by the use of pH-sensitive electrodes or dyes in rod outer segment preparations. Thus, the velocity of hydrolysis has been measured by Liebman & Pugh (1979) who suggest a mechanism to explain the high gain of the process. Guanosine triphosphate (GTP)

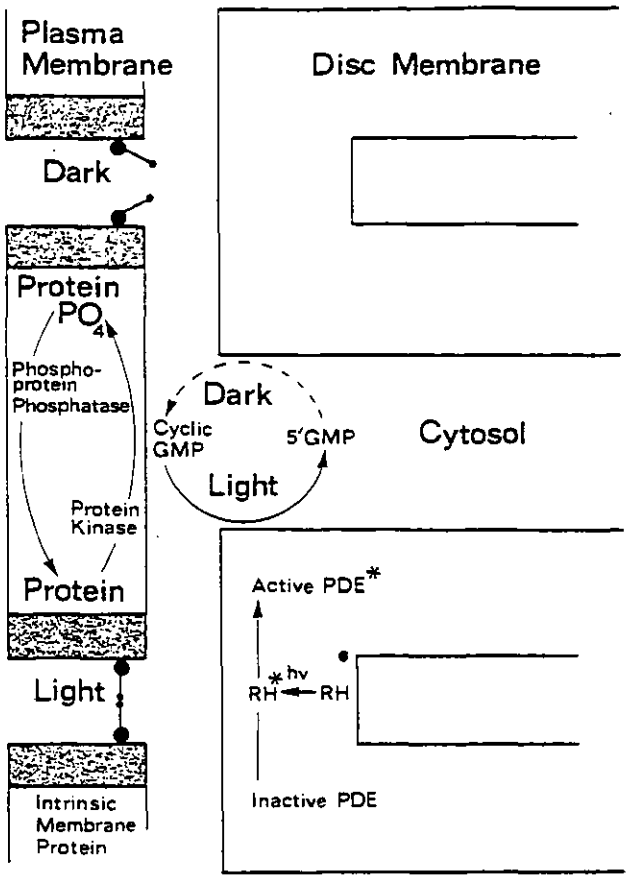

Fig. 30.

Mechanism proposed for cyclic nucleotide as internal transmitter in photoreceptors (from Ernst 1979)

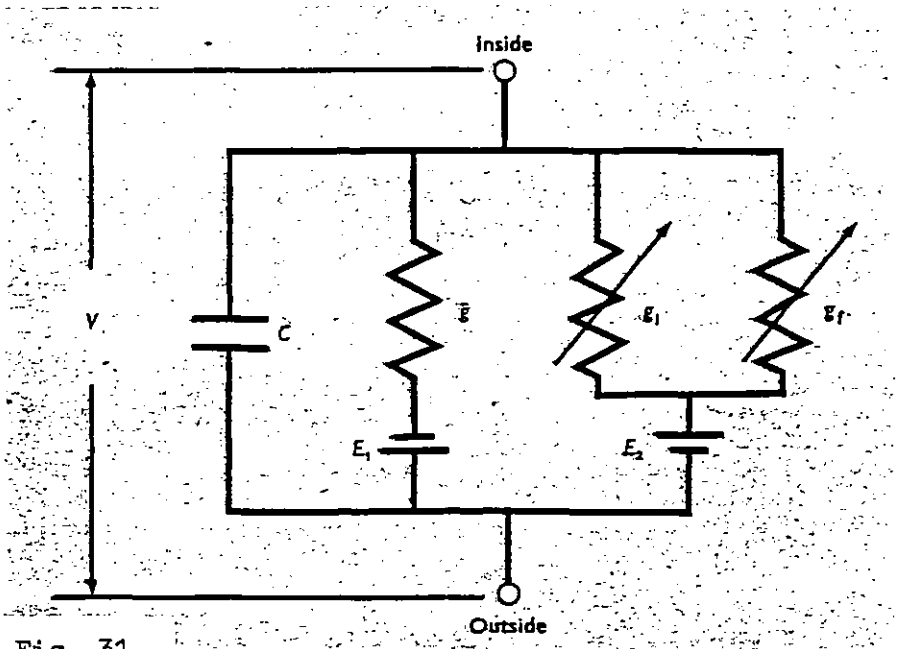

Fig. 31.

Equivalent circuit of the membrane of rod outer segment. C is the membrane capacity, $\bar{g}$ is a fixed conductance in series with the battery E_1 which limits the maximal amplitude of the light response. The two conductances g_l and g_t, are in series with the battery E_2. g_l is the light sensitive conductance and g_t is a voltage and time dependent conductance.

(from Cervetto et al 1977)

is required for the hydrolysis and adenosine triphosphate (ATP) is involved in the deactivation of PDE. The results show that light-activated cyclic nucleotide hydrolysis is fast enough to be involved in transduction and the process has enough gain.

At present, results are not conclusive enough to state that either the Ca hypothesis or the cyclic nucleotide hypothesis fully satisfy all the criteria for an internal transmitter in photoreceptors. Yoshikami et al, (1980) described light induced Ca^{++} effluxes from photoreceptors which were fast enough, large enough and of the spatial distribution to be expected from the Ca hypothesis. They claim that it only remains to link the Ca^{++} fluxes with enzymatic events in the disc membranes such as the hydrolysis of GTP and of cGMP and the binding of guanosine diphosphate (GDP).

The Ionic Bases of the Photoreceptor Current

Cervetto (1973) investigated the effects of changing external concentrations of Na^{+} and K^{+} on light-evoked responses of turtle photoreceptors. He found that the membrane potential of cones was controlled predominantly (but not solely) by Na^{+} in darkness and by K^{+} at the peak of the response. The ratio of K^{+} to Na^{+} permeability was not negligible in darkness, however, and it was proposed that the inner segments are constantly permeable to K^{+}, and that there is a light-dependent Na^{+} permeability in the outer segments. The results are consistant with a light-induced decrease in Na^{+} permeability in the outer segment membrane giving rise to the hyperpolarising response during which the membrane potential approaches the K^{+} equilibrium potential.

Results of Baylor et al,(1979a,b) suggest that the complexity of the voltage responses to bright illumination reflects an additional voltage-dependent conductance change (Fain et al, 1978). The nature

of this conductance was examined by Capovilla et al, (1980) by studying the influence of external K^+ and Cl^- on the membrane potential and responses of toad rods. The shape of rod responses to both bright and dim flashes was strongly dependent on membrane potential when modified by high external K^+, low external Cl^- or extrinsic current. The results suggested the existence of a voltage- and time-dependent conductance significantly active near the dark level of membrane potential. This can be represented by the electrical equivalent circuit of fig. 31 (Cervetto et al, 1977).

Vertebrate photoreceptors can be shown to have a variety of other voltage-sensitive conductances. For example, the current-voltage curve of rods shows a prominent outward rectification, like that observed in many nerve and muscle preparations (Jack, Noble & Tsien, 1975), which can be suppressed by TEA (tetraethylammonium chloride; Fain et al, 1977). TEA has been shown to block voltage-dependent K^+-channels in a variety of nerve and muscle cells (e.g. Armstrong, 1975). This suggests that rods have a voltage-dependent potassium conductance, perhaps similar to the delayed rectifier of axons (Hodgkin & Huxley, 1952). After treatment with 6-12 mM TEA, this K^+ conductance is suppressed and rods are capable of producing action potentials. These spikes have a time course similar to Ca^{++}-dependent action potentials in other systems and are much slower in rise time and longer in duration than Na^+-dependent action potentials of nerve and muscle (Fain et al, 1977). Under normal circumstances the inward Ca^{++} current does not become regenerative because it is matched by outward current through the voltage-sensitive K^+ conductance. Blocking the K^+ conductance with TEA destroys the balance between these two currents, and the Ca^{++} conductance becomes able to produce action potentials. The Ca^{++} conductance of rods probably serves to regulate the release of transmitter at the receptor synapse, and the K^+ conductance

serves as a kind of negative feedback to keep the rod membrane potential stable.

In addition to the potassium and calcium conductances, the rod membrane contains a third voltage-sensitve conductance which is at least partially permeable to sodium ions. This conductance is activated when the rod hyperpolarises and is responsible for the fast decay or 'initial transient' of the response to bright illumination. Preventing the activation of this conductance by perfusing the retina with 2 mM CsCl eliminates the fast decay and changes the waveform of the receptor response (Fain et al, 1978).

Miller & Dacheux (1976a) investigated the effects of a chloride-free (c-f) perfusate on the intracellular responses of photoreceptors in the mudpuppy retina. They found that the removal of external Cl^- did not result in a change of membrane potential but a slight decrease (10%) in response amplitude was observed, together with a small depolarising 'off' response. No change in input resistance of the cell was seen on exposure to c-f medium. These findings suggest that Cl^- is not a critical ion for receptor electrogenesis. Cl^- may, however, play some role in receptor function. O'Bryan (1973) has shown that at least one component of the feedback from horizontal cells onto cones is accompanied by an increase in conductance. Lasansky (1981) investigated this mechanism by recording responses of salamander cones to light on their surrounding area, using electrodes filled with different electrolytes, and current injection. He concluded that the depolarising response of cones to annular illumination (mediated by feedback from horizontal cells) was due to an increase in the Cl^- conductance of the cone membrane. Piccolino et al, (1980) found in the turtle retina, however, that this feedback pathway was mediated by a Ca^{++} conductance mechanism.

Oakley & Green (1976) and Oakley (1977) have shown that the light response of photoreceptors is associated with a decrease in extracellular K^+ concentration, C_K^o. In rod dominated retinae, the light-evoked decrease in C_K^o seems to be generated solely by the rods (Oakley & Green, 1976). A mechanism for the relationship between the receptor response and the decrease in C_K^o was suggested by Matsuura et al, (1978). In the dark the passive efflux of K^+ from the rod is balanced by an equal influx from the Na^+/K^+ pump. The light-evoked rod hyperpolarisation reduces the passive efflux with little effect on the pump, thus causing C_K^o to decrease. In order to test this hypothesis, Oakley et al (1979) measured light evoked changes in rod membrane potential and C_K^o under a variety of stimulus conditions. The C_K^o measurements were made with ion-sensitive microelectrodes. The results supported the hypothesis of Matsuura et al, (1978). Thus the light-evoked decrease in C_K^o seems to be a consequence of the rod membrane response to light.

I.5.iii Horizontal Cells

Kaneko & Shimazaki (1975b) investigated the effects of changing external ionic composition on synaptic transmission from receptors to horizontal cells in the carp retina. They found that when synaptic transmission was blocked the membrane potential of horizontal cells was highly dependent on external C_K, and that it corresponded with the expected level of the K^+ equilibrium potential, E_K. Under the same conditions, changes in external C_{Na} or C_{Cl} produced little change in the membrane potential. Thus Kaneko & Shimazaki (1975b) concluded that, free from the influence of transmitter substance, the membrane potential of horizontal cells is determined by E_K and that the hyperpolarising responses of the cells under normal conditions are

produced by E_m approaching E_K. It should be noted that the value of E_K used was strictly only an assumed value as it was not based on a quantitative determination of K^+ activity inside and around horizontal cells.

Kaneko & Shimazaki (1975b) also showed that in Na^+-free Ringers the membrane potential of the horizontal cells hyperpolarised and their light-evoked responses diminished (fig. 32). Because the membrane potential of cones is also highly dependent on external (C_{Na}) (fig. 33) in accord with Cervetto (1973), the observed effects on horizontal cells could not give rise to conclusive results. However, it was suggested that the results indicated indirectly a high Na^+ permeability of the horizontal cell membrane in the dark under the influence of the endogenous transmitter. The mechanism for the generation of S-potentials suggested by these results is summarised in fig. 34. The horizontal cell is maintained in depolarisation in the dark by a high conductance (closed switch) in series with E_D, the dark membrane potential to which Na^+ is contributing significantly. On illumination, R_D increases (open switch) and then the membrane potential is determined by the K^+ distribution across the membrane. This gives rise to the hyperpolarising response.

Waloga (1975) and Waloga & Pak (1976, 1978) showed in the axolotl retina that the membrane potentials and light-evoked responses of both receptors and horizontal cells were dependent on extracellular (C_{Na}) (fig. 35) but that these parameters were more Na^+-dependent for the horizontal cells than for the receptors (fig. 36). Replacement of extracellular Na^+ caused an increase in input resistance of the cell membrane, a hyperpolarisation of the membrane potential, and a diminution of the light-evoked response. The horizontal cell membrane potential was highly dependent on extracellular (C_{Na}). When extra-

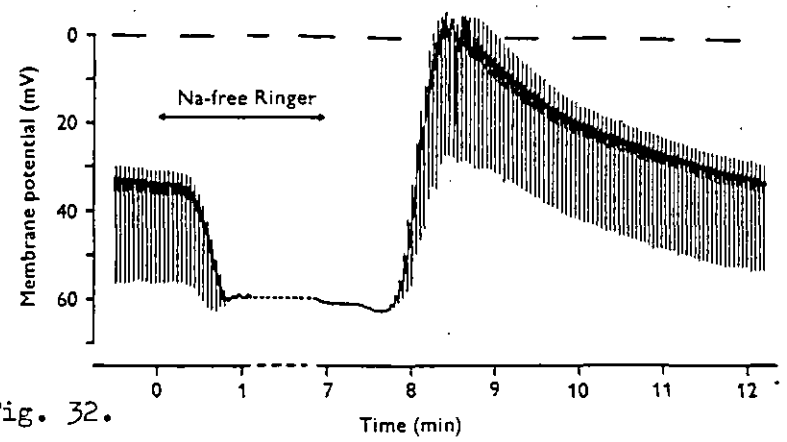

Fig. 32.

Intracellular recording from an L-type horizontal cell. In this experiment, only 620 nm flashes were used. At 0 min normal Ringer was switched to Na-free Ringer. At 7 min normal Ringer was reapplied to the retina. Since no membrane potential changes were seen between 1–7 min of perfusion with Na-free medium, this part of the record was cut out and shown with a dashed line. (from Kaneko & Shimazaki 1975b)

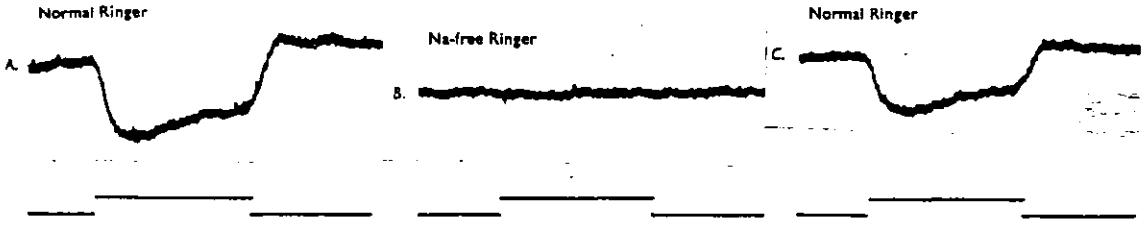

Fig. 33. Responses of a red-sensitive cone to diffuse 620 nm flashes (the same cell as in Fig. 2). *A*, in normal Ringer. *B*, 1 min after switching the perfusate to Na-free choline Ringer. *C*, 1 min after reapplying normal Ringer. (from Kaneko & Shimazaki 1975b)

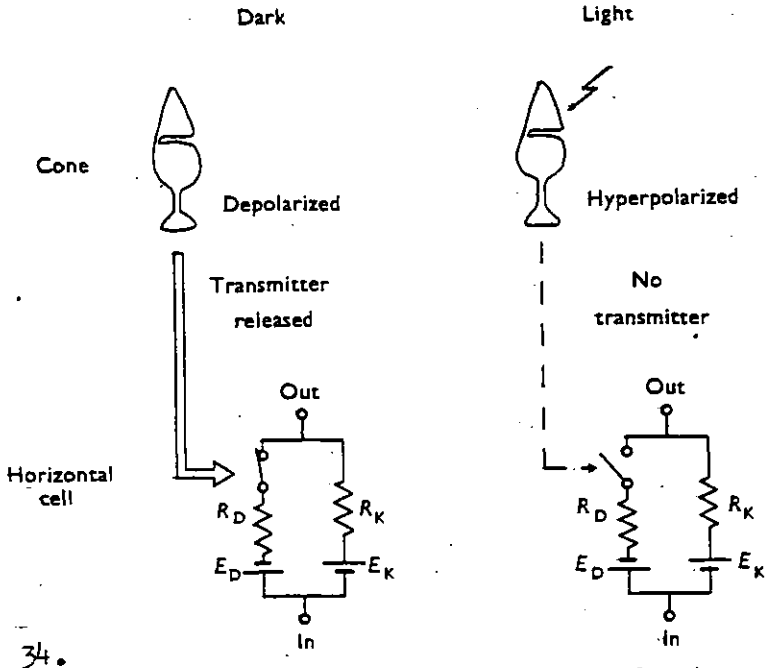

Fig. 34. Schematic diagram showing a model proposed to interpret the relationship between the light responses of cones and the transmitter release and the effects of transmitter substance on the horizontal cell membrane. The lower circuit diagram represents equivalent circuit of horizontal cell membrane. Changes in R_D should be gradual, but for simplicity, it is shown by opening (R_D increase) and closing (R_D decrease) the switch. E_D, equilibrium potential of the dark membrane potential; E_K, K equilibrium potential. (from Kaneko & Shimazaki 1975b)

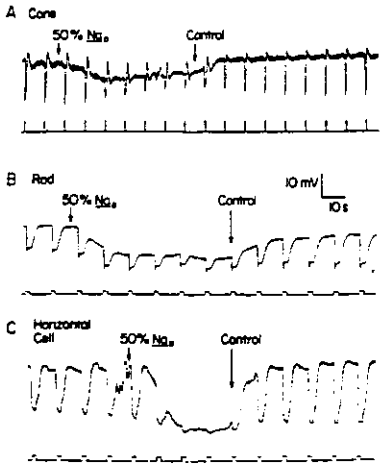

Fig. 35.

The effect of 50% Na_o solution upon receptor and horizontal cell potentials. The 50% Na_o solution hyperpolarizes the membranes and decreases the receptor potentials in both (A) cones and (B) rods. (C) 50% Na_o solution hyperpolarizes the membrane of the horizontal cell much more than the receptor membranes, and almost eliminates the light responses.

(from Waloga & Pak 1978)

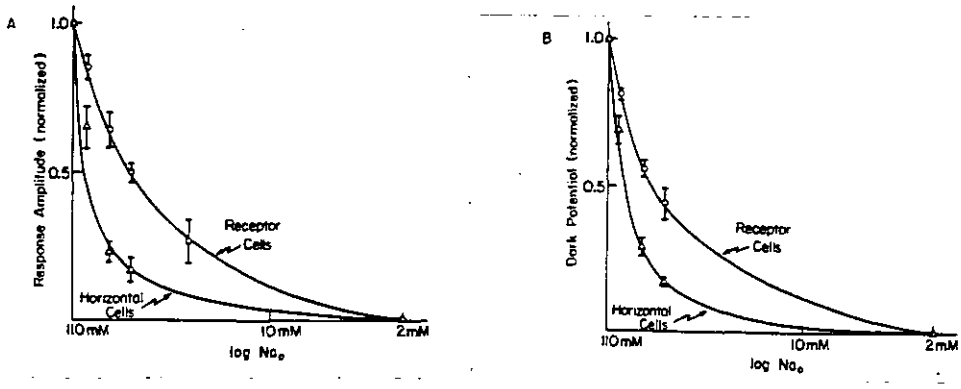

Fig. 36.

(A) The effect of decreasing Na_o on the light responses of receptors and horizontal cells. The horizontal cell responses display much stronger dependence on Na_o than the receptor potentials. Data are from cells which recovered completely upon return to the control solution after being bathed in several different Na_o solutions. All points, except the 26% Na_o (29 mM Na_o) were based on data obtained from either 14 rods and 3 cones, or 13 horizontal cells. The 26% Na_o points were obtained with either two rods and one cone, or two horizontal cells. For each cell, the amplitudes of the light responses were normalized with respect to the response amplitude for the same cell in the control bathing solution. (B) Effect of decreasing Na_o on the dark membrane potentials of receptors and horizontal cells. The membrane potential of the horizontal cell displays much stronger dependence on Na_o than the membrane potential of the receptor cell. For each cell, the dark membrane potentials at various Na_os were measured with respect to that obtained in 1% Na_o—taken to be very close to the maximum hyperpolarization obtainable in that cell. The "amplitude" of the membrane potential so obtained at each Na_o (the membrane potential at Na_o minus that at 1% Na_o) was then normalized with respect to the "amplitude" in control bathing solution for the same cell. All points were based on data obtained from either 14 rods and 3 cones, or 13 horizontal cells which recovered completely upon return to the control solution after being bathed in several different Na_o solutions.

(from Waloga & Pak 1978)

cellular (C_K) or (C_{Cl}) was varied the resultant change in membrane potential was predicted by the Nernst equation only if the variation was such that $C_K.C_{Cl}$ = constant. The results were consistant with the suggestion that the dark-released transmitter increased primarily the Na^+ conductance of the horizontal cell subsynaptic membrane. However, Waloga & Pak (1976) also found that the putative transmitter, aspartate (3 mM), could depolarise horizontal cells almost to the dark potential level in low external (C_{Na}) solution suggesting that the transmitter increased membrane conductance to ions other than Na^+ which could be involved in the dark depolarisation of horizontal cells.

Miller & Dacheux (1973) found that intracellularly recorded S-potentials in the rabbit retina were abolished by perfusion with a chloride-free (c-f) medium and that this effect was reversible. Cl^- was replaced by a large anion, usually SO_4^{2-}. In the mudpuppy retina, Miller & Dacheux (1976a) reported that in a c-f medium photoreceptor electrical activity was not affected (fig. 37) whilst the horizontal cells suffered firstly an early depolarisation accompanied by an enhancement of their light evoked responses, followed by a slow hyperpolarisation and consequent loss of response (fig. 38). The normal dark membrane potential of these horizontal cells was generally about -30 mV, whilst in the c-f medium, it reached about -60 mV (fig. 38). Most cells showed a progressive increase in input resistance as the cell hyperpolarised during the c-f effect. Miller & Dacheux (1976a) proposed a mechanism for the dark-depolarisation of horizontal cells in which the depolarisation is mediated by an increased Cl^- permeability. Thus, horizontal cells maintained internal (C_{Cl}) at a higher level than that for a passive Cl^- distribution so that the Cl^- equilibrium potential, E_{Cl}, was more positive than the membrane potential. The hyperpolarising responses arose from a light-mediated decrease in Cl^- permeability which caused the membrane potential to

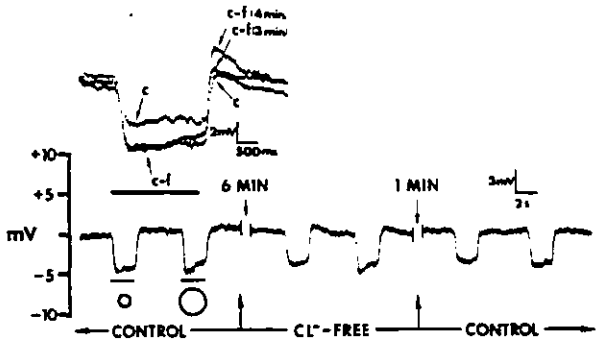

Fig. 37. C-f effects on intracellularly recorded receptors in perfused mudpuppy eyecup preparation. Responses on left were elicited by small spot and diffuse light stimulation in control Ringer. Middle section recorded 6 min after initiating c-f medium. Responses were slightly smaller and small off depolarization was seen. Responses on right were recorded 1 min after returning to normal Ringer showing slight reduction in response amplitude. Insert shows c-f effects on another receptor. Superimposed traces were elicited in control Ringer *(c)*, 3 and 4 min after initiating a c-f Ringer; all responses elicited by diffuse light stimulation. Note slight depolarization of recording observed in c-f responses. C-f medium resulted in increase in response amplitude (25%) and appearance of depolarizing off response. Irradiance: small spot 4.6×10^{-7} W/cm^2; diffuse 3.7×10^{-7} W/cm^2.

(from Miller & Dacheux 1976a)

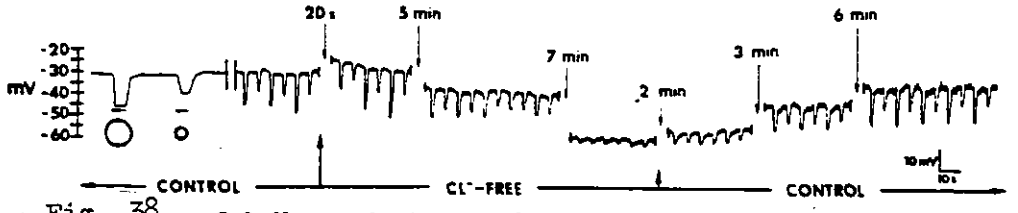

Fig. 38. C-f effects on horizontal cell activity. Left-hand section shows different amplitude responses to small spot and diffuse light stimulation. Remaining responses recorded at reduced speed, alternating small spot and diffuse light stimulation. C-f perfusate resulted in an early depolarization and increased response amplitude, followed by slow hyperpolarization of cell. After 5-min 20-s responses to diffuse and small spot stimulation were nearly equal in amplitude. After 12 min 20 s no slow hyperpolarization was evident and responses were small and irregular; cell had become hyperpolarized to about −60 mV. Returning to control Ringer did not elicit early transient changes in potential, but slow depolarization was accompanied by gradual recovery of light-evoked responses. Irradiance: small spot 4.6×10^{-7} W/cm^2; diffuse light 3.7×10^{-7} W/cm^2.

(from Miller & Dacheux 1976 a)

approach the K^+ equilibrium potential. This hypothesis would predict that the initial removal of Cl^- would shift E_{Cl} to a more positive value, causing a depolarisation as Cl^- moved out of the cell. This depolarisation would occur primarily at the subsynaptic membrane and during this period the response amplitude should increase. Then as Cl^- diffused out of the cell and was reduced in concentration, the membrane potential would hyperpolarise to approach the K^+ equilibrium potential as observed (fig. 38). The observed increase in input resistance is consistent with a steady loss of internal Cl^- and a reduction in the available anion to move through the synaptically opened channels. Thus this hypothesis explains the observed effects of the c-f medium on the electrical activity of horizontal cells.

Nelson (1973) studied horizontal cells in the mudpuppy retina using intracellular ion injection. With NaCl-filled microelectrodes the injection of Na^+ ions resulted in an increase in response amplitude in most cases. He argued that this result was not consistent with the idea that Na^+ was an important ion for maintaining the dark membrane potential of the horizontal cell since an increase in intracellular Na^+ would then result in a decrease in response amplitude. However, positive current injection could also lead to an increase in intracellular Cl^-, particularly in those regions of the cell where a high Cl^- permeability existed (Coombs et al, 1955). This would depolarise the cell and increase the response amplitude according to the hypothesis whereby the dark depolarisation is mediated by Cl^-, (the 'Cl^- hypothesis') rather than by Na^+ (the 'Na^+ hypothesis').

For the Cl^- hypothesis to be feasible a Cl^- distribution is required such that the transmembrane Cl^- equilibrium potential, E_{Cl}, is more positive than, or at least equal to, the dark membrane potential, E_m. In neurones, E_{Cl} is usually fairly close to E_m whereas E_{Na} is

much more positive (Ginsbourg, 1967). Thus the Na^+ hypothesis is accepted as being feasible in so far as $E_{Na} > E_m$ whereas to show that $E_{Cl} \geq E_m$ would require the measurement of E_{Cl} in single neurones by intracellular ion sensitive microelectrodes.

Miller (1978) also found that low extracellular Na^+ medium results in an uncoupling of low resistance junctions between horizontal cells in mudpuppy retina. It was shown that the increase in input resistance seen in low Na^+ medium was not due to a reduction in available Na^+ to move through synaptically opened channels, nor a decrease in synaptic input from the Na^+-sensitive receptors, since in normal Ringer a complete block of these channels with Co^{2+} caused no detectable change in input resistance. After blocking synaptic transmission, introducing low Na^+ again increased input resistance, showing that low (C^o_{Na}) effects do not depend upon the action of transmitter. It was also shown that the altered Na^+ environment did not change the resistance by modifying the extracellular resistive pathway. The conclusion that a low (C_{Na}) extracellular medium uncouples horizontal cells does not eliminate the possibility that Na^+ is involved in horizontal cell electrogenesis. It does suggest, however, that the uncoupling of the electroto ic junctions may lead to changes in response properties of horizontal cells which should be taken into account when performing low C_{Na} experiments and that perhaps the interpretation of these experiments which led to the Na^+ hypothesis (Kaneko & Shimazaki, 1975a,b) should be reconsidered.

Waloga (1975) investigated the effects of Cl^--free medium on horizontal cells of the axolotl retina. She found that responses were abolished but did not see the early depolarisation and enhancement phase shown by Miller & Dacheux (1976a) to be associated with the c-f effect in the mudpuppy retina. Waloga & Pak (1978) concluded that results obtained from the axolotl retina were inconsistent with the

Cl^- hypothesis.

Trifonov et al, (1974) suggest that the decrease in resistance of the non-synaptic membrane on hyperpolarisation could be due to the selective increase of permeability to K^+ or Cl^- or both. Byzov & Trifonov (1981) found that the non-synaptic membrane of horizontal cells in the goldfish retina was sensitive to extracellular (C_K) as expected. Decreasing extracellular C_K evoked hyperpolarisation and decreased membrane conductance for hyperpolarising current; increasing C_K caused the opposite effect. Ba^{2+} increased the slope of the hyperpolarising portion of the voltage-current curve without affecting the depolarising portion. Na^+ and Cl^- conductances were relatively small in the non-synaptic membrane. Increasing Ca^{2+} increased the slope of the depolarising portion of the voltage-current curve, but inhibitors of Ca^{2+} channels had no effect. It was concluded that the non-linearity of the horizontal cell non-synaptic membrane is explained by voltage-dependent K^+ channels activated by hyperpolarisation and, to some extent, by Ca^{2+} channels activated by depolarisation.

Johnson & Lam (1981) investigated the active and passive properties of the horizontal cell membrane. They used horizontal cells that had been dissociated from the catfish retina and electrically uncoupled. These isolated horizontal cells showed regenerative voltage responses which were blocked completely by application of the divalent cations Co^{2+}, Mn^{2+} or Ni^{2+}. These cations have all been reported to block inward Ca^{2+} currents in various systems. The addition of tetrodotoxin (TTX) to the bathing solution had apparently no effect on the regenerative responses. Thus the horizontal cell membrane seems to lack the TTX-sensitive Na^+ conductance mechanism found in nerve axons. It was concluded that the regenerative voltage responses recorded in isolated horizontal cells are TTX-insensitive (i.e. not Na^+ spikes) and are probably Ca^{2+}-dependent.

I.5.iv Bipolar Cells

ON-Centre Bipolar Cells

The light-evoked depolarisation of this cell is associated with a resistance decrease of the cell membrane (Toyoda, 1973; Nelson, 1973). Miller & Dacheux (1976a) recorded intracellularly from ON-centre bipolar cells in the mudpuppy retina. These cells were found to be sensitive to the removal of extracellular Cl^-: the loss of light response was accompanied by a slow small hyperpolarisation after an initial transient depolarisation. The response to an annulus was abolished before the response to a small spot of light. In the c-f medium at the time of response loss, light stimuli did not produce a conductance change. Recovery of the response in normal medium was accompanied by a return of the light-mediated conductance change. Effects of blocking synaptic transmission to ON-centre bipolars suggested that the dark-released transmitter has a hyperpolarising effect on these cells (Dacheux & Miller, 1976; Kaneko & Shimazaki, 1975a). One explanation is that the transmitter decreases the conductance to Cl^- and that internal (C_{Cl}) is higher than that for a passive distribution (Miller & Dacheux 1976a). This hypothesis would be consistent with the observed effects of the c-f medium and provide an ionic mechanism for the depolarising response to light. It was possible however that the action of the c-f medium was principally at the horizontal cell level and that a special interaction existed between the horizontal cell and the ON-centre bipolar cell.

Kaneko & Shimazaki (1975a) found that in the carp retina low external Na^+ abolished light responses and hyperpolarised the cell to a level close to maximal hyperpolarisation produced by surround illumination. Since cones are hyperpolarised by Na^+-free medium, probably no transmitter was released. Thus it was proposed

that the ON-centre bipolar cell membrane has a high Na^+ permeability when the transmitter is absent, and thus the removal of Na^+ would cause a hyperpolarisation. The effect of light would be to increase Na^+ permeability of the membrane causing depolarisation. This hypothesis is consistent with the observation that the input resistance is greater in the dark (Toyoda, 1973) as is the Cl^- hypothesis above.

Rod and Cone inputs

Saito et al,(1978) investigated the ionic mechanisms of rod and cone signals in the ON-centre bipolar cell of the carp retina. The results suggested that these cells receive depolarising inputs from both rods and cones but the two inputs are different in their ionic mechanisms. The information from rods is mediated by subsynaptic Na^+ channels and that from cones by K^+ and/or Cl^- channels. The two ionic components underlying the response must also be different in their time course to give the complex response pattern observed. The same relation of the rod and cone inputs to ON-centre bipolar cells has been suggested in the mudpuppy retina (Fain, 1975). Saito et al, (1978) found that the depolarising response of the ON-centre bipolar cell in scotopic conditions appears to be due to an increased conductance to ions having an equilibrium potential at about 20 mV. Because of the results of Kaneko & Shimazaki (1975a), Saito et al, concluded that information from rods was mediated by subsynaptic Na^+ channels. The depolarising component in the photopic retina appeared to be due to a decreased conductance to ions having an equilibrium potential at about -75 mV so it was proposed that information from cones was mediated by a permeability change of the subsynaptic membrane to either K^+ or to both K^+ and Cl^-.

OFF-Centre Bipolar Cells

The hyperpolarising response to light of these cells is associated with an increase in membrane resistance (Toyoda, 1973; Nelson, 1973). Miller & Dacheux (1976a) found that OFF-centre bipolar cells were relatively insensitive to removal of Cl^- but their antagonistic surround response was inverted to a hyperpolarising response (with the spot stimulus on continuously). Toyoda (1973) had suggested that the OFF-centre bipolar responses are generated in a similar way to L-type horizontal cell responses. This could be true as far as transmitter action and membrane resistance are concerned although different ionic mechanisms could be involved. The results of Miller & Dacheux (1976a) suggest that removal of external Cl^- differentiates between horizontal and OFF-centre bipolar cells in that although Cl^- may be proposed as the key ion in horizontal cell electrogenesis, it plays an insignificant role in generation of the responses of the bipolar cell. The loss of the antagonistic surround response in c-f. medium could be explained by the loss of the horizontal cell response, since these cells have been proposed to mediate the antagonistic surround (Werblin & Dowling, 1969). It is possible that Cl^- conductance changes in the bipolar cell were also involved in the loss of the surround response.

Since the OFF-centre bipolar cell central response does not seem to be Cl^--sensitive, Miller & Dacheux (1976a) suggest that this cell may depend on a high Na^+ conductance in the dark, and like the horizontal cell the non-synaptic region could be a K^+-dependent membrane. Kaneko & Shimazaki (1975a) did not record from enough OFF-centre bipolar cells to observe the effects of an altered Na^+ environment. However these authors do suggest that the ionic mechanism determining the membrane potential (non-synaptic membrane) of the OFF-centre bipolar cell is not completely the same as that for the

horizontal cell, since the response amplitude of the OFF-centre bipolar cell is not as large and the cell is hyperpolarised only to -40 mV by blocking the synapse.

I.5.v Amacrine Cells

These cells are quite difficult to penetrate and hold long enough to investigate ionic mechanisms by changing the external ionic environment. Miller & Dacheux (1976a) found that exposure to c-f perfusate abolished the ON-depolarisation of the ON-OFF amacrine cell but the OFF response remained at the same amplitude as in the control response. The ON depolarisation recovered on returning to normal Ringer solution, though the responses were smaller than they were initially. There were two possible explanations: (i) depolarisation is abolished because of a loss of input from the ON-centre bipolar; (ii) the loss of depolarisation could be due to the loss of a Cl^--dependent mechanism at the amacrine cell level, the depolarisation being due to an increased Cl^- permeability. Persistence of the OFF depolarisation in c-f medium would suggest that this response component is dependent on a different ionic mechanism such as increased Na^+ conductance. The transient effects of c-f media argue against (ii) since an expected initial exaggeration of the ON-response in comparison with the OFF response was not seen. Thus it seemed that Cl^- was not critical for amacrine cell depolarisation. An extension of this view would suggest that the light-evoked depolarisation of amacrine cells is probably dependent on Na^+.

Werblin (1977) found that the response of transient amacrine cells in the mudpuppy retina was caused by an inward monophasic current mediated by a conductance increase to ions with a reversal potential more positive than the dark level. Since the results of Miller and Dacheux (1976a) suggest that the conductance increase is not to Cl^-,

it is probable that the ion involved is Na^+.

I.5.vi Ganglion Cells

Since ganglion cells receive input which has been encoded by the rest of the retinal network of neurones, the effects of ion-substitution experiments on ganglion cell responses can not be expected to determine the ionic mechanisms involved. There are too many possible explanations for a given effect produced by ionic replacement at this level. The most that can be expected from this type of experiment is information about the interneuronal synaptic connections.

Miller & Dacheux recorded from ganglion cells in the retina of the rabbit (1973; 1975) and the mudpuppy (1976b) while subjecting the retina to perfusion with c-f medium. In the rabbit and mudpuppy, ON-centre cells showed a loss of both centre and surround responses in c-f medium and OFF-centre cells showed a loss of the surround mechanism. In the rabbit there was an enhancement of the OFF-centre response and in the mudpuppy the ON-component of ON-OFF cells was abolished in c-f medium. These results were explained by the loss of the ON-centre bipolar cell response that elicits the response of the ON-centre ganglion cell, and of the horizontal cell response which mediates the surround mechanism in OFF-centre ganglion cells. Thus the changes in ganglion cell responses in c-f medium could be explained in terms of the effects of the c-f environment on the neurones presynaptic to ganglion cells. However, Cl^--dependent inhibitory postsynaptic potentials (IPSPs) were observed in ON-OFF ganglion cells (Miller & Dacheux, 1976b). These IPSPs were preceeded by EPSPs and were apparently mediated by amacrine cells. The light-activated hyperpolarisation of OFF-centre cells was not the result of a Cl^--dependent IPSP but probably resulted from disfacilitation.

I.5.vii Methods for Determining Ionic Mechanisms

What is known about the ionic basis of the responses of retinal neurones has been mainly inferred from the results of experiments which involve the substitution of one particular ion in the extracellular perfusing medium. This type of experiment does not provide sufficient evidence whereby to determine the ionic bases of the electrical activity of a retinal neurone. One reason for this is that the interdependence of retinal neurones increases as one moves from photoreceptors to ganglion cells so that one has to consider the effects of ionic substitution on all cells presynaptic to the neurone in question as well as the possible effects on the latter itself. This introduces too many possible variables for a definite conclusion to be reached. Thus, although it has been generally accepted that the ionic substitution experiments of Hagins (1972) have shown that the photoreceptor response is based on a Na^+-dependent mechanism, even this is questionable as the reduction in external (C_{Na}) could cause an influx of Ca^{2+} due to a Na^+-Ca^{2+} exchange mechanism (Reeves & Sutko, 1980). The influx of Ca^{2+} could then be responsible for the loss of response by a blockage of ionic channels. This example shows how careful one needs to be in interpreting results of ionic substitution experiments as changing the concentration of one ion could give rise to effects due to a second ion because of an interdependent exchange mechanism between the two ions. At the level of horizontal cells, immediately postsynaptic to photoreceptors, there is doubt as to the interpretation of the results of ion-substitution experiments and for the other post-receporal neurones the uncertainty is even greater. The ionic substitution technique is not therefore an adequate method with which to investigate the ionic bases of neuronal electrical activity in a complex network such as the vertebrate retina. The method is not adequate because

it is not sufficiently direct and consequently it can not yield any definite conclusions. Further, lack of information on intracellular ionic activities of the common physiologically important inorganic ions (K^+, Cl^-, Na^+, Ca^{2+}) in retinal neurones has severely limited the understanding of the ionic bases of neuronal electrical activity. Only a direct quantitative determination of intracellular and extracellular ionic activities can serve to define the relevant ionic equilibrium potentials and thus provide a firm basis for the postulation of possible ionic mechanisms. Measurements of this kind can be performed with double-barrelled ion-sensitive microelectrodes. In the present study, ion-senstive microelectrodes have been used to measure the intracellular and extracellular potassium and chloride activites of horizontal cells in the roach retina.

PART B: ION-SENSITIVE MICROELECTRODES

I.6 Types of Ion Senstive Microelectrode (ISM)

Electrodes which gave a potentiometric response to the activity of one particular ionic species were developed by chemists for many different ions after the discovery of the pH electrode (Cremer, 1906). Such ion-sensitive electrodes were minaturised in a number of different ways for the determination of intracellular ionic activities (fig. 39a-e).

The first intracellular ISM was the pH-sensitive microelectrode developed by Caldwell (1954), who used essentially the same configuration as that of the laboratory pH-sensitive glass electrode (fig. 39a) which was miniaturised considerably and insulated with shellac rather than glass. Hinke (1959) made intracellular Na^+ and K^+ measurements in the squid axon with glass-insulated electrodes which used Na^+- and K^+-sensitive glass developed by Eisenman et al, (1957) (fig. 39b). Caldwell's and Hinke's electrodes both suffered from a major drawback in that their exposed ion-sensitive tips were at least 100 μm long. This meant that they could only be used in 'giant-size' cells, since in order to measure intracellular ionic activity correctly it is necessary to contain the ion-sensitive part of the electrode entirely inside the cell whilst keeping the rest of the electrode insulated.

The first reasonably "micro" ion-senstive electrodes were probably those made by Lev and Buzhinsky (1961) based on the design of Hinke's (1959) K^+-sensitive electrode but with the protruding tips being only a few μm long (fig. 39c). Even these electrodes, however, could only be used in large cells such as frog skeletal muscle fibres, due to the necessity for all of the protruding ion-sensitive glass to be inside the cell. Further, the ion-sensitive glass used had rather

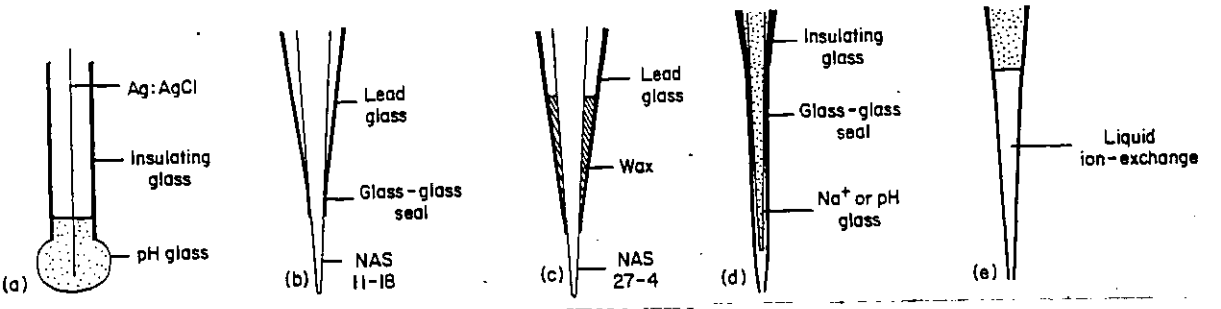

Fig. 39. Tip configurations of five different ion-sensitive electrodes. (a) Standard laboratory pH electrode, (b) Hinke design of Na^+-sensitive microelectrode, (c) Lev and Buzhinsky design of K^+-sensitive microelectrode, (d) recessed-tip Na^+-sensitive microelectrode (Thomas, 1970) and (e) liquid ion-exchanger microelectrode (Walker, 1971). (from Thomas 1978a)

Table 1. A classification of intracellular ion-sensitive microelectrod

Type of ISM Sensor	Primary Ion Sensed
Liquid state:	
Liquid ion exchanger	K^+, Cl^-, Na^+, Ca^{2+}
Neutral ion carrier	K^+, Ca^{2+}, Na^+
Solid-state:	
Glass membrane	Na^+, H^+, K^+
Metal	Cl^-, H^+

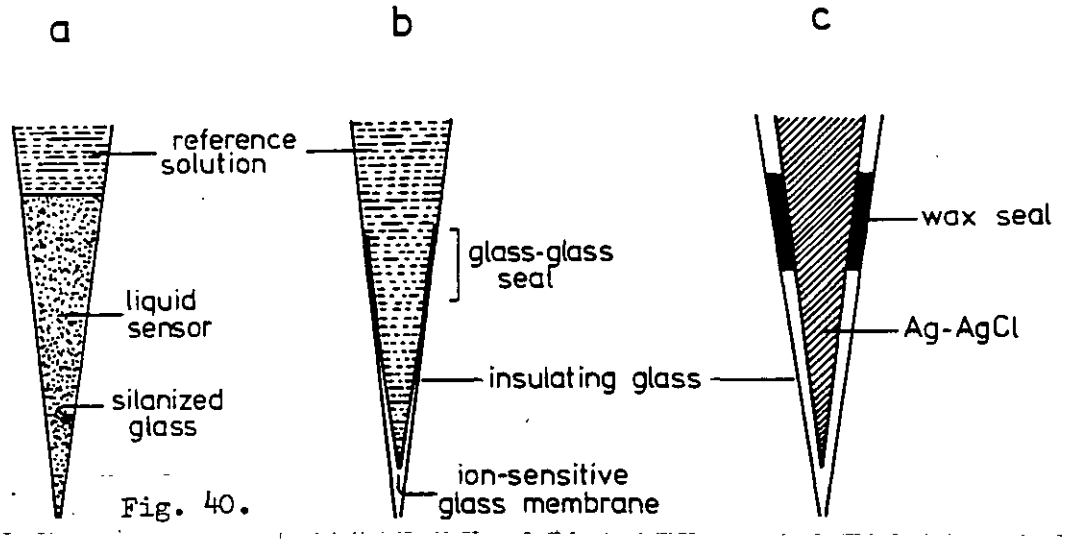

Fig. 40. The tip assembly of three different types of ISM (not drawn to scale). (a) Liquid-membrane ISM. The length of the liquid sensor column can be 200µm to several millimetres; the inside wall of the micropipette must be silanized. (b) glass membrane, recessed-tip type ISM; the recess volume is critical and determines the response time of the electrode. (c) Solid-state, metallic surface type ISM. (from Djamgoz and Laming 1981)

poor specificities. The problem of the protruding tip was solved by two new designs: the recessed tip configuration (fig. 39d) (Thomas, 1970; 1974, 1976) and the liquid ion-exchanger (LIX) microelectrode (fig. 40e) (Walker, 1971). With the recessed tip and LIX type of ISM only the extreme tip crosses the cell membrane, and remains within the cell. Since their tips can be made quite small ($\lesssim$0.5 μm in diameter), these are the only two types of ISM suitable for intracellular measurement of ionic activities in moderate-size cells. Intracellular ISMs have been classified according to the nature of the ion sensitive element as shown in table 1 (Djamgoz & Laming, 1981).

The liquid membrane ISMs use a LIX or neutral ion-carrier in the tip of a silanised glass microelectrode (fig. 40a); the solid state ISMs have ion-sensitive glass or a metal wire as the ion-sensitive element in a recessed tip configuration (fig. 40b,c). It should be noted that although glass is strictly not a solid the ion sensitive glass acts as a solid membrane with fixed interaction sites for ions so this classification is appropriate and practical.

I.7 Theory of the ISM Potential

An ISM is essentially an ordinary glass microelectrode fitted at its tip with an ion-sensitive component (membrane) which makes contact with the intracellular medium on the outside, and an appropriate back-filling solution on the inside. The electrical potential generated across the ion-sensitive membrane at the tip of an ISM, V_{ISM}, comprises the sum of two parts:

$$V_{ISM} = V_{ION} + V_{LOC} \qquad (5)$$

where V_{ION}: a potential that is dependent on the activity of the ion to which the ISM is sensitive, and V_{LOC}: a local potential that would be recorded by any ordinary microelectrode. To obtain V_{ION} alone, a second,

ion-insensitive, reference microelectrode is used, and its potential (V_{LOC}) is subtracted from V_{ISM}, using a differential measuring device.

The theory of the ion-sensitive electrode (ISE), was first formulated by Nikolsky (1937) and Eisenman et al, (1966). For the perfect ISE, the ion-sensitive membrane is absolutely selectively permeable, i.e. it is permeable to one ionic species, 'x', only. Ions 'x' can pass freely across the membrane meeting no resistance whatsoever whereas every other ion that may possibly be present in the sample solution meets an infinite resistance to attempted motion across the membrane which then constitutes an inpenetrable barrier. If there are two solutions, one on either side of the membrane, containing different concentrations of 'x', then an electric potential develops across the membrane, due to the diffusion of 'x' towards the side on which the concentration is less, until an equilibrium is established between the forces on 'x' due to the concentration gradient giving rise to the diffusion and the electric potential gradient which is a consequence of this diffusion.

The diffusive force on 'x' depends not exactly on the concentration of 'x' but on its activity. The activity is an "effective concentration" which gives the concentration of ions in the solution which are freely mobile (active) and so can contribute to the generation of an electrochemical potential. The mutual electrostatic attraction between anions and cations restricts their freedom to a certain extent so that a given fraction of the ions in a solution will be 'inactive' (not freely mobile). The more concentrated the solution the greater is the fraction of ions which are inactive. For the ion 'x', the activity, a_x, is related to the concentration, C_x, by the activity coefficient, γ_x as follows:

$$a_x = \gamma_x C_x \qquad (6)$$

where $\gamma \leq 1$ and depends on the concentration, or more precisely the ionic strength, of the solution. Strictly it is not possible to determine the activity coefficient of any one type of ion in solution in isolation from the others. Thus, in a solution of KCl it is not possible to measure the individual activity coefficients of K^+ and Cl^- but only a mean activity coefficient, $\overline{\gamma^2}_{KCl}$, defined by:

$$\overline{\gamma^2}_{KCl} = \gamma_K \gamma_{Cl} \tag{7}$$

The mean activity coefficient also depends on the ionic strength of the solution. Ionic strength, I, is defined by:

$$I = \tfrac{1}{2} \sum_{x=1}^{n} C_x Z_x^2 \tag{8}$$

when Z_x = charge on ion x, C_x is concentration of ion x, and there are n different ions in the solution (Walker, 1979; Bailey, 1980). If different solutions have the same ionic strength but different concentrations of a particular ion then the activity coefficient for that ion is the same in the different solutions.

An expression can be derived for the potential across a selectively permeable membrane (potential of a perfect ISE) based on electrochemical and thermodynamic principles (Cammann, 1979; Vesely et al, 1978; Koryta, 1975). The potential that is developed across the selectively permeable membrane, i.e. the equilibrium potential for ion 'x', is given by the Nernst equation and is related to the activities of ion 'x' on either side of the membrane as follows:

$$E_m = \text{Const.} + \frac{RT}{z_x F} \ln \frac{a_x(1)}{a_x(2)} \tag{9}$$

where E_m is the transmembrane potential; $a_x(1)$, $a_x(2)$ are activites of ion x on opposite sides 1, 2 of the membrane respectively; Z_x is the charge on ion x; R is the universal gas constant, T the absolute temperature and F the Faraday constant. For an ISE, one side of the

membrane, (2), will be the internal filling solution of the electrode and will thus be of constant composition, $a_x(2)$ = constant. Putting this into equation (9) gives the potential across the membrane, i.e. the electrode potential, as a function of $a_x(1)$:

$$E_m = E_o + \frac{RT}{Z_x F} \ln a_x(1) \qquad (10)$$

where E_o is a constant known as the standard electrode potential. This equation can be written in a more useful form, giving the electrode potential, E, as follows:

$$E = E_o + \frac{2.303RT}{Z_x F} \log_{10} a_x(1) \qquad (11)$$

Now it can be clearly seen that if the activity of an ion is increased by a factor of 10 then the potential of the electrode changes by $\Delta E \simeq 2.303RT/Z_x F$. For example at a temperature of 20°C for Na^+ or K^+, $\Delta E \simeq 58$ mV, so that a tenfold (decade) increase in a_{Na} will cause a potential rise of 58 mV in a Na^+ ISE. It can also be seen that for an anion, an increase in activity will cause a fall in potential.

I.8 Liquid Membrane ISMs

The most fundamental difference between the liquid membranes and the glass membranes arises from the greater mobility of the ionic species and the larger quantity of active material present in liquid membranes. This has some advantages, e.g. that the action of the membrane is faster than that of a glass membrane with fixed ion-exchange sites, but one disadvantage is that interfering ions also tend to get carried right into the sensor and take a long time to diffuse out while with glass membranes, interferents tend to stay near the surface and are easily washed away. This explains why glass electrodes can be used for a much longer time before their response starts to deteriorate, as the membrane is destroyed more slowly be interferents.

The properties and theory of both LIX and neutral ion-carrier membranes are discussed in detail by Koryta (1975). For liquid membranes selectivity is obtained when (a) one ionic species is much better than any of its rivals at entering the membrane; (b) no net steady state current is allowed to flow (Tsien, 1980). Condition (b) is imposed by connecting the ISM only to an electrometer of extremely high input impedance and low bias current. Thus at equilibrium the ions entering the sensor tip must be balanced by ions of the same sign leaving the sensor. The electrode potential is the agent which negotiates this balance and thus registers any change in the activity of the selected ion in the external solution.

I.8.i Neutral ion-carriers

Neutral ion-carrier membranes contain ionophores (macrocylic substances) dissolved in a suitable inert organic solvent. The structure of the ionophore forms a polar cavity in which one specific ion can be enclosed because of ion-dipole interactions. Thus one particular species of ion is enveloped in a hydrophobic shell and this obviously promotes the entry of this ion into the organic membrane phase. Morf et al, (1979) state that preference for divalent ions over monovalent ions can be enhanced by ligands which form thin rather than thick shells around the ion, by solvents of high dielectric constant and by an abundance of counterions (organic ions of opposite charge to that of the determinand) in the sensor.

The theory of these membrane potentials is given by Eisenman (1969), based on the concept of a very thin membrane. The resulting equation for the membrane potential is as follows, for one interfering ion y:

$$E_m = \frac{RT}{Z_x F} \ln \left\{ \frac{a_x(1) + k_{xy} a_y(1)^{Z_x/Z_y}}{a_x(2) + k_{xy} a_y(2)^{Z_x/Z_y}} \right\} \qquad (12)$$

where the terms are as before, with x being the primary ion, and y the interfering ion, and 1 and 2 refer to opposite sides of the membrane. The k_{xy} is defined as the selectivity coefficient of the 'membrane' for the ion 'x' over the interfering ion 'y'. If the solution on side (2) of the membrane is of constant ionic composition, equation (12) simplifies to:

$$E_m = E_o + \frac{RT}{Z_x F} \ln (a_x + k_{xy} \cdot a_y^{Z_x/Z_y}) \qquad (13)$$

This is known as the Nikolsky equation, which describes the potential of an ion-sensitive electrode.

Although ion carrier membranes are strictly electroneutral, with ion selectivity being due to complexation of the determinand ion with a macrocyclic compound in the sensor, such membranes used in ISMs would give rise to extremely high resistances and very slow response times. The resistivity of such membranes can be reduced by adding organic salts to raise the dielectric constant of the medium (Oehme & Simon, 1976; Steiner et al, 1979; Coles & Tsacopoulos, 1979). The organic salt added is often one of the ion exchanger substances which also enhance entry of the primary ion into the organic membrane phase by their own mechanism. Thus neutral ion-carrier membranes as used in ISMs may not act strictly as "pure" neutral ion carrier membranes, but the ionophores in the membrane do give by far the greater contribution to the ISM selectivity. Steiner et al, (1979) described a Na^+ ISM based on a neutral ion-carrier. Neutral ion-carriers have also been used in ISMs for K^+ (valinomycin), and Ca^{2+} as well as for Na^+ (Oehme & Simon, 1976; Coles & Tsacopoulos, 1979; Tsien, 1980; Rink & Tsien, 1980).

I.8.ii Liquid ion-exchangers

The term "ion-exchange electrode" is taken to mean an electrode

having as active material a charged ion-exchanger consisting of large organic molecules. The term is not used to denote any electrode for which ion-exchange at the membrane-solution interface contributes to the electrode potential as it would then include the glass electrodes. The liquid ion-exchanger electrodes consist of an inert organic solvent containing a dissolved ion-exchanger which selectively associates with certain ions present in solutions separated by the membrane. The ion-exchanger is insoluble in both of these solutions so the main difference from membranes with fixed sites (e.g. glass) is the free mobility of the ion-exchange sites within the membrane.

Organic solvents which have lone pair electrons on oxygen atoms but no exchangeable protons are well known to solvate cations much better than anions. Thus all the solvents commonly used for cation LIXs are such aprotic donor solvents. Anions are better solvated by solvents with hydrogen-bonded protons such as decanol (Tsien, 1980). The ion exchanger itself is basically a salt which influences the preference of the liquid membrane for one particular ion. Firstly there is a pronounced preference for either anions or cations depending on the nature of the salt. If the salt consists of a very hydrophobic (organic) cation and a rather hydrophilic anion, then anions will tend to leave the sensor and this, together with the condition of no net current encourages anions and not cations to enter the sensor in exchange. A salt of a hydrophilic cation (e.g. alkali metal ion) with a hydrophobic anion analogously favours cation selectivity. Secondly, the selectivity for one particular anion or cation occurs because of the order of hydrophobicity of the ions. The membrane will naturally be most selective for the most hydrophobic ion in significant concentration in the aqueous solution. This is the principle behind the Corning K^+ and Cl^- LIXs. For example, the K^+ LIX has a solvent of the aprotic donor type, and a salt with a very large and hydrophobic anion and a smaller and more hydrophilic

cation. The cation used is K^+ so that this ion both leaves and enters the sensor causing no long term changes in sensor composition. The sensor then responds to cations in order of their hydrophobicity so that it discriminates for K^+ against Na^+ by about 60:1 but K^+ is superseded by Cs^{++} and quaternary ammonium ions. These ions which supersede K^+ are normally assumed not to be present inside cells at sufficient concentration to cause problems. The Cl^- LIX behaves analagously to the K^+ LIX but favours anions according to their hydrophobicity. If any large monovalent anions are present they can cause significant interference.

A LIX was developed for Na^+ by Kraig & Nicholson (1976) and this was modified by O'Doherty et al (1979) who produced intracellular Na^+-sensitive LIX microelectrodes based on the antibiotic monensin. Electrodes produced with the former LIX showed a poor selectivity for Na^+ over K^+ (about 3:1), so O'Doherty et al (1979) proceeded to make another Na^+-sensitive microelectrode with a liquid membrane, based on a neutral ionophore, which was essentially free from K^+ interference and much faster in response than ISMs based on Na^+-sensitive glass. Kotera et al, (1979) reported an intracellular, double-barrelled Na^+ ISM based on HCl-treated monensin as LIX.

I.9 ISM's: Practical Considerations

The following is an account of the various properties of ISM's that have to be taken into consideration during practical applications.

I.9.i The double-barrelled ISM

As already noted (equation 5) the electrical potential developed by an ISM, V_{ISM}, with respect to the ground comprises the sum of two potentials:

$$V_{ISM} = V_{ION} + V_{LOC} \qquad (5)$$

V_{ION} is determined mainly by the activity of the ion to which the ISM is sensitive primarily; V_{LOC} is the local electrical potential (e.g. transmembrane resting potential, field potential) which would be recorded by any conducting element including an ISM. Thus, to obtain V_{ION} alone, it is necessary to measure V_{LOC} using an ion-insensitive (reference) electrode, and subtract the latter electronically from V_{ISM}. For intracellular measurements in large cells, two separate microelectrodes have been used; for intracellular measurements of ionic activity in medium/small-sized cells, however, it is necessary to bring the tips of the two microelectrodes to the same point in the form of a double-barrelled ISM. The double-barrelled ISM was first developed by Khuri (1971), and its tip assembly is illustrated in figure 41. So far, double-barrelled ISMs have been made using mostly a liquid membrane in the active barrel. Since liquid ion exchangers/neutral ion carriers exist already for K^+, Na^+, Ca^{2+} and Cl^-, and one for H^+(pH) has been reported recently (Ammann et al, 1981), double-barrelled ISMs can be made to record intracellularly the activities of the most important inorganic ions in cells.

I.9.ii Tip Size - Cell Membrane Damage

Double barrelled ISMs have larger tips than ordinary microelectrodes. How small the tip can be made is limited by several factors. The smaller the tip, the more difficult it is to get the liquid membrane column to the tip, and when filled, ISMs with extremely small tips will have intolerably high resistances. Furthermore, the silanisation of the active barrel means that the inside of the tip is coated with a layer of silicone. If the reaction between the silane and the hydrated glass surface goes to completion the silicone film tends to be 0.2 μm thick (Norton, 1944). Thus, if extreme precautions are not

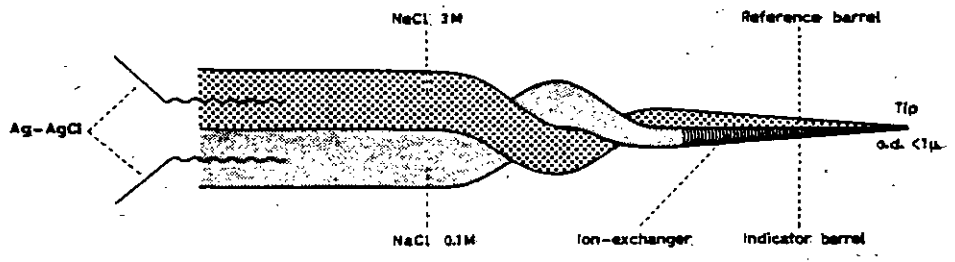

Double-barrelled, ion-selective liquid ion-exchange microelectrode.

Fig. 41. (from Khuri 1976)

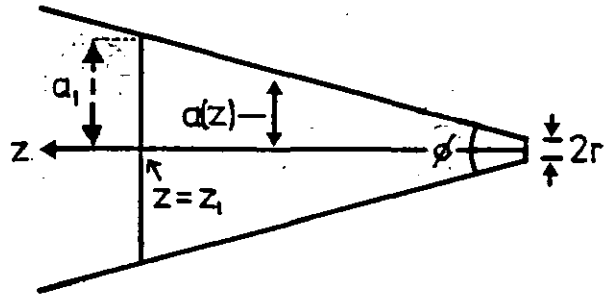

Fig. 42.

Schematic diagram of liquid membrane in tip of ISM. r is the radius of the tip, ø is the angle of taper of the shank which is assumed to be uniformly conical, z is an axial coordinate, a(z) is the radius of the liquid membrane column at distance z from the tip, and a is the radius at the meniscus of the liquid membrane ($a_1 = a(z_1)$)

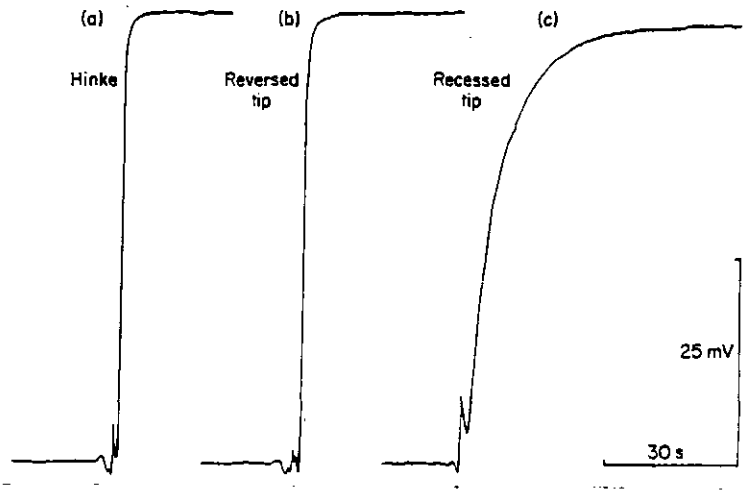

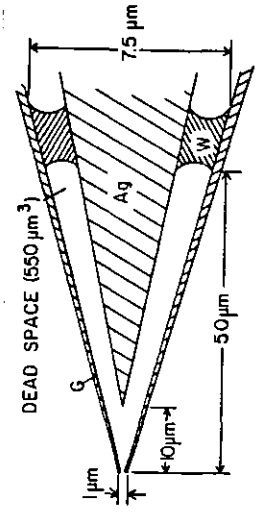

Fig. 43.

(a-c). Responses of three different Na+-sensitive microelectrodes to a rapid tenfold increase in external Na. (a) Protruding-tip (Hinke style) microelectrode, (b) reversed-tip, tip diameter 8 um and (c) recessed-tip, tip diameter 1 um. (from Thomas 1978 a) (d) Details of the tip of an Ag/AgCl - based Cl ISM. Dimensions given are averages for a nimber of electrodes. G, glass pipette, Ag, chlorided silver wire, W, wax seal (from Saunders & Brown 1977)

taken to silanise in a completely dry atmosphere (e.g. Coles & Tsacopoulos, 1977), then for properly silanised ISMs the internal tip diameter of the active barrel cannot be made much less than 0.5 μm without causing blockage of the tip. The tip size of a double-barrelled ISM is the combined external tip diameter of both active and reference barrels and so this can not be much less than 1 μm in practice. However, by using methods such as that of Coles & Tsacopoulos, (1977) for silanisation to carefully control the reaction between the silane and the glass surface it seems to be possible to produce thinner layers of silicone (polymerised silane) and thus make finer-tipped double-barrelled ISMs. For example, Dufau et al, (1980) claim to have produced working double-barrelled ISMs with mean tip diameters of 0.1 μm.

The limit on smallness of tip size of double-barrelled ISMs obviously puts a lower limit on the size of cell which can be penetrated without possible significant cell damage and consequent artefacts in measurements. However the size of cell that can be safely penetrated with a double-barrelled ISM knowing that both electrodes are in the same cell is still much smaller than that which can be penetrated simultaneously by a single ISM and its corresponding separate reference electrode. The effects of possible cell damage by the ISM and an artificial influx or efflux of ions via an imperfect glass to cell membrane seal or via the filling solution in the electrode are discussed by Zeuthen (1981).

I.9.iii Tip Resistances of ISMs

ISMs have a much higher electrical resistance than ordinary microelectrodes of comparable tip diameters because of the high impedance of the ion-sensitive element at the tip. This means that the response times are longer than those of ordinary microelectrodes so

there is a limit to the speed of electrical events that can be analysed in terms of ionic activities by ISMs. The high resistance of ISMs (10^9 - 10^{12} Ω) also causes problems with electrical noise and interference picked up from sources like static electricity on clothing and from a.c. mains leads. It is necessary to shield the preparation with a Faraday cage to reduce this interference. If only the preparation itself is shielded then access to it by the experimenter can be greatly restricted. If a Faraday cage large enough for the experimenter to work inside is used, the experimenter has to be careful to prevent introduction of static electricity into the cage and to restrict his movements while recording thus minimising static field instabilities.

The resistance of the liquid membrane in the tip of an ISM can be considered theoretically by making some simple assumptions. With reference to figure 42, if the resistivity of the liquid membrane is ρ and we neglect any conductivity through the glass wall then the total resistance of the liquid membrane column will be:

$$R = \frac{1}{\pi} \int_0^{z_1} \frac{\rho}{a^2(z)}\, dz = \frac{1}{\pi} \int_r^{a_1} \frac{\rho}{a^2}\, da \cot\frac{\phi}{2}$$

$$= \frac{\rho}{\pi} \cot\frac{\phi}{2} \left[-\frac{1}{a_1} + \frac{1}{r} \right]$$

For small tip diameters, $r \ll a$, this reduces to

$$R = \frac{\rho\cot(\phi/2)}{\pi r} = \frac{2\rho}{\pi r \tan\phi} \quad \text{(for small } \phi/2)$$

$$\therefore R = \frac{2\rho}{\pi r \phi} \qquad (14)$$

Thus for very small tip diameters, the resistance of an ISM is mainly dependent on the tip diameter and is independent of the length of the LIX column.

I.9.iv Response Times

The smaller the tip of an ISM, the higher is its electrical resistance, and the longer its response time. This means that the advantage of the recessed-tip type ISM over the Hinke type in terms of the smaller tip size is somewhat offset by the corresponding disadvantages of higher resistance and longer response time. The longer response time means that fast responses cannot be analysed. The responses of three kinds of glass ISM to an increase in C_{Na} are shown in fig. 43a-c. The 'reversed tip' electrode is another configuration of glass ISM made by Thomas (1969) about which he stated that the only advantage seemed to be that the response time was much faster than that of a recessed-tip ISM (Thomas 1978a). The tip size is certainly too large (5-10 μm) for intracellular use except in giant-size cells. The recessed tip ISM is the only one whose response is illustrated which is suitable for intracellular recording. Thus, it is seen from fig. 43 that the recessed-tip type ISM, designed for intracellular use, has a much longer response time than those of other designs with larger tips and that for a recessed-tip glass ISM this response time can be tens of seconds. In general, the metal ISMs tend to be as slow as the glass ISMs.

The liquid membrane ISM compares favourably with the recessed-tip type solid state ISM. The response times of LIX ISMs are in general of the order of the time constant (about 175 msec) of the input circuit of the amplifier (Coles & Tsacopoulos, 1979). This is much shorter than those of the corresponding solid state ISMs (Thomas, 1978a).

Neutral ion-carriers tend to have higher resistances than LIX solutions so that ISMs based on neutral carriers generally have longer response times than LIX ISMs. However response times of neutral carrier ISMs reported are still faster than those of corresponding

glass ISMs (Oehme & Simon, 1976; Steiner et al, 1979). Thus from the consideration of response times, the liquid membrane electrodes are better than the glass or metal recessed-tip ISMs. This is due to a large extent to the "dead-space" in the recess near the tip of the latter type of ISM, in which equilibration with the test solution has to take place. This is shown for a metal recessed-tip ISM in fig. 43d. In liquid membrane ISMs there is no dead-space as the ion-sensor is present at the very tip of the electrode and makes immediate direct contact with the test solution.

I.9.v Interference and Selectivity

Until recently, LIX ISMs were the only alternative to the solid state variety, and with the exception of the K^+ LIX (Corning, 477317), the former suffered from being rather poorly selective, compared to the glass type. With the introduction of highly selective neutral ion-carriers, the liquid membrane electrode began to look much more like the 'ideal' intracellular ISM. Because the K^+ LIX ISM was selective enough for intracellular use (given physiological ionic concentrations) it quickly superseded the glass K^+ ISM as it was easier to construct and had a much faster response time. The simpler design and better performance of the K^+ LIX ISM made it much more popular.

The neutral ion-carrier for K^+, valinomycin, however, has intrinsically a very high resistance as do other neutral ion carriers which is a serious problem for making ISMs. Usable intracellular ISMs are made by adding an organic salt to the ion-carrier to reduce the resistance. This reduces the selectivity to some extent but since the neutral ligands have excellent selectivities, the resulting ISMs still perform well (Oehme & Simon, 1976; Steiner et al, 1979; Coles & Tsacopoulos, 1979). The Na^+ LIX ISM at present has a poor selectivity compared with Na^+ glass ISMs (O'Doherty et al, 1979;

Kotera et al, 1979) although the latter group report intracellular Na^+ measurements with such a LIX electrode. Neutral carrier Na^+ ISMs have a better selectivity and good response times (Steiner et al, 1979). The only problem with this electrode seems to be that the Na^+: Ca^{2+} selectivity is not very good (Tsien, 1980) so that the glass Na^+ ISM is still the better electrode if Ca^{2+} interference is an important factor.

For Cl^- there is as yet no neutral carrier, and the Cl^- LIX (Corning 477315) is poorly selective as it responds to most similar anions e.g. HCO_3^-. The alternative metal ISM is more selective but is still liable to interference from several ions (Saunders & Brown, 1977). Ag-AgCl itself behaves like a "perfect" Cl^- electrode in response to pure Cl^- solutions but the metal ISM is used with caution as some work ers have found it to give erroneously high values for intracellular Cl^-, while others have not (Neild & Thomas, 1974 and cf. Armstrong et al, 1977 with Bolton & Vaughan-Jones, 1977). Some workers have used both LIX and metal ISMs to make intracellular a_{Cl} measurements (Saunders & Brown, 1977).

For Ca^{2+} there is no glass ISM and the LIX available is both poorly selective and highly resistive such that it is very problematic to measure intracellular Ca^{2+} (Brown & Owen, 1979; Tsien, 1980). A neutral carrier Ca^{2+} ISM has been developed in which the liquid sensor is gelled in the tip with PVC. This electrode has adequate selectivity and sharpness to measure Ca^{2+} inside cells which are only 12-15 μm across (Marban et al, 1980; Rink & Tsien, 1980). For H^+ the glass ISM seems to be more reliable than the antimony, and the former kind shows excellent selectivity (Green & Giebisch, 1974; Brown & Owen, 1979).

Since the ion-sensitive membrane of an ISE is not in practice absolutely selectively permeable to the primary ion, other ions interfere

by contributing to the ISE potential. Interfering ions contribute to the ISE potential to an extent described by a selectivity coefficient; the degree of selectivity of the electrode for the primary ion, x, with respect to an interfering ion, y, is expressed by the selectivity coefficient k_{xy} This may be defined by the following general equation for the electrode potential which is an extension of eqn. (11) taking account of interference:

$$E = E_o + \frac{2.303nRT}{Z_x F} \log_{10} (a_x + \sum_y k_{xy} a_y^{Z_x/Z_y}) \qquad (15)$$

where E_o, R, T, F, Z_x, a_x are as in eqn (11), Z_y is the charge on ion Y, k_{xy} is the selectivity coefficient of the ISE for ion 'x' against a particular ion 'y', and y represents all the different interfering ions; 'n' is an empirical constant (=1 if ISE gives Nernstian response to primary ion). This equation is applicable to nearly all ISEs (Bailey, 1980). In practice it is often sufficient to consider only one interfering ion, so that for principal ion 'x' and main interfering ion 'y', eqn. (15) becomes:

$$E = E_o + \frac{2.303nRT}{Z_x F} \log_{10} (a_x + k_{xy} a_y^{Z_x/Z_y}) \qquad (16)$$

The equation in this form is often referred to as the Nikolsky equation (Nikolsky, 1937) (cf eqn. 13). When an ISE is very selective for 'x' in comparison with 'y', then k_{xy} will be much less than unity. Conversely, if, as occasionally happens, the ISE responds preferentially to 'y' rather than 'x', k_{xy} will be greater than unity. For example, the selectivity coefficient of the Orion Ca^{++} ISE against barium ions, k_{CaBa} is 0.01 (Bailey, 1980); thus the electrode is 100 times more responsive to Ca^{2+} than to Ba^{2+}. However for the Cl^- ISE, k_{ClBr} = 300, i.e. there is a much greater response to Br^- than to Cl^- so this electrode can only be used to measure a_{Cl} in situations where interference by Br^- does not occur.

The value of k_{xy} is never constant for all activities of 'x' and 'y', although it is sometimes constant for a given ratio of the activity of 'x' to 'y' (Buck, 1974). ISEs based on liquid ion exchangers show large ranges in k_{xy} for a given 'x' and 'y'. The variations in k_{xy} are associated with the mechanism of the electrode response and with the changing environment of the ions in solution (Bailey, 1980). These factors also cause k_{xy} to depend upon the method used to determine it. Hence it is essential to know the details of the method of determining any quoted values fo k_{xy}.

Calibration of ISMs and Determination of k_{xy}

From equation (16) it follows that the selectivity coefficient of an ISE for the primary ion against the main interfering ion can be determined from potential measurements in solutions containing both the principal and the interfering ion or in separate solutions of the principal and interfering ions where the activities of these ions are known. Thus the methods for determining the selectivity coefficients can be classified into two groups: (1) those involving measurements of response in separate solutions of primary and interferent ions; (2) those measuring the response in solution containing a mixture of principal and interfering ions.

An ISE can be calibrated by measuring its potential response to a series of solutions containing different known activities or concentrations of the primary ion. The range of these activities in the calibrating solutions should be greater than the expected range in the preparation from which measurements are made. A calibration graph can then be drawn of ISE response, E, against log a_x which is used to convert measurements with the ISE in terms of potential into ionic activity values. For a perfect ISE it would be sufficient to calibrate in a series of solutions in which the primary ion is varied. However,

for real ISEs, interference from other ions must be accounted for. This may be achieved by recording the ISE response in solutions containing known activities or concentrations of the main interfering ion after calibrating in solutions containing the primary ion. This method will enable k_{xy} to be determined and so a correction can be made when comparing the calibration curve to the measurements to account for interference. Alternatively, the electrode may be calibrated in a series of solutions containing a mixture of both primary and interfering ions. This again enables k_{xy} to be determined but if these solutions are made up to resemble the expected situation in the preparation then interference is already accounted for in calibration; the calibration curve needs no correction and may be referred directly to the ISE measurements. Separate solution methods have been criticised (Thomas, 1978a) because they do not correspond to the real situation in analysis. Vesely et al, (1978) and Bailey (1980) described several methods for the experimental determination of k_{xy}. In the present study, the following methods were used for the initial characterisation of the liquid ion-exchanger, after which method 4 was used in the routine experimental procedure.

Method 1 If the ISE potentials are measured in separate solutions with the same activities of the primary (x) and interfering ion (y) with the same charge, Z, then the selectivity coefficient can be calculaated from the potential difference. From eqn. (16) if the ISE potential in the primary ion solution is denoted by E_x and that in the interfering ion solution by E_y, these are given by:

$$E_x = E_o + \frac{2.303nRT}{ZF} \log_{10} a_x = E_o + \frac{nRT}{ZF} \ln a_x$$

$$E_y = E_o + \frac{2.303nRT}{ZF} \log_{10} k_{xy} a_y = E_o + \frac{nRT}{ZF} \ln k_{xy} a_x \quad (\text{since } a_y = a_x)$$

$$\therefore E_y - E_x = \frac{nRT}{ZF} \ln k_{xy}$$

$$\therefore k_{xy} = e^{(ZF/nRT)(E_y - E_x)} \qquad (17)$$

Method 2 If a series of measurements is taken in separate solutions of x and y of various known activities (i.e. the ISE is calibrated firstly in solutions of x and then again in solutions of y) and the activities for $E_x = E_y$ are found (from the calibration graphs) then, from the equations above:

$$E_o + \frac{2.303nRT}{ZF} \log_{10} a_x = E_o + \frac{2.303nRT}{ZF} \log_{10} k_{xy} a_y$$

$$\therefore k_{xy} = \frac{a_x}{a_y} \qquad (18)$$

In addition to the criticism mentioned above, it has been pointed out (Pungor & Toth, 1969; 1970) that, during measurement of potential in solutions of ion y, an undefined concentration of ion x is formed at the tip of the ISE because of an ion-exchange reaction between x and y on the electrode membrane surface, thus introducing an error into the determination of k_{xy}. The values of k_{xy} obtained by separate solution methods often differ substantially from those obtained by mixed solution methods.

Method 3 In the first mixed solution method (Pungor & Toth, 1969; 1970), the electrode potential is measured in a series of solutions in which the activity of the principal ion, x, is varied and that of the interfering ion, y, is maintained constant. In this way the ISE is calibrated against a constant background of interfering ion. This method involves finding graphically the point at which the ISE is responding equally to both ions, i.e. from equation (16) the contribution of both ions x and y to the potential is equal when:

$$a_x = k_{xy} a_y^{Z_x/Z_y} \qquad (19)$$

For the usual case of $Z_x = Z_y$ and denoting the constant activity of interferent y by a'_y and the critical value of a_x for which ions x and y both contribute equally to the ISE potential by a'_x the value of k_{xy} is given by:

$$k_{xy} = \frac{a_x'}{a_y'} \qquad (20)$$

The value of a_y' is known and the value of a_x' is obtained graphically (fig. 44).

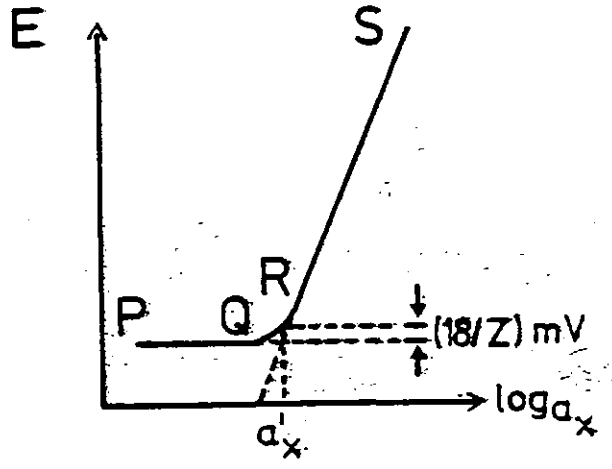

Fig. 44 Determination of k_{xy} in mixed solutions with constant activity of interfering ion (see text).

In the region RS in fig. 44 the ISE is showing a Nernstian response to ion x but as a_x decreases, the ISE is affected by the ion Y and in the region QR it is responding to both x and y; as a_x is decreased further, ion y has an increasingly dominant effect until in the region PQ the ISE is responding effectively only to the constant activity a_y' while the contribution from a_x is too negligible to be detected. The point at which the electrode is responding equally to x and y is the point of intersection of the linear extrapolations of PQ and SR (from equation (16)). The value of a_x at this point will be a_x' so having determined this value graphically, k_{xy} may be calculated from the formula of equation (20). This method is only suitable if PQ and RS are straight lines. In practice RS is usually a straight line but in the region PQ the ISE potential is subject to irreproducibility and drift. Thus it is better to determine the a_x' value by finding

graphically the point at which the difference between the experimental curve and the extrapolated Nernstian dependence (RS) equals $18n/Z_x$ mV. This follows simply from eqn. (16):

$$\therefore E = E_o + \frac{2.303nRT}{Z_x F} \log_{10} (a_x + k_{xy} a_y^{Z_x/Z_y})$$

Both ions are contributing equally to the potential when $a_x = k_{xy} a_y^{Z_x/Z_y} = a_x'$

$$\therefore E = E_o + \frac{2.303nRT}{Z_x F} \log_{10} (2a_x')$$

The response of the ISE in the absence of y is given by the extrapolation of SR as far as the limit of the Nernstian response. The difference in ISE potential in solutions of x with activity a_x' with and without y at activity a_y' is thus:

$$\Delta E = \frac{2.303nRT}{Z_x F} \left[\log_{10}(2a_x') - \log_{10} a_x' \right]$$

$$= \frac{2.303nRT}{Z_x F} \log_{10} 2$$

$$\therefore \Delta E = \frac{18n}{Z_x} \text{ mV (at } 25^{o}\text{C)} \qquad (21)$$

Thus by finding on the graph the activity of x at which the experimental line QR differs from the extrapolation of SR by $18n/Z_x$ mV the activity a_x' is determined. k_{xy} is then calculated by substitution into equation (20):

$$k_{xy} = \frac{a_x'}{a_y'}$$

Method 4 Another mixed solution method is to measure the response of the ISE in solutions of varying activity of the primary ion x, but of constant total ionic strength (see eqn (8)) such that as the activity of the primary ion increases, that of the interfering ion decreases correspondingly. This method was used by Thomas (1972) who calibrated a Na^+-sensitive microelectrode in solutions containing Na^+ and K^+ of constant total ionic strength. He assumed that since the

C_K in the calibrating solution was of the correct order, the ISM response was automatically corrected for interference by intracellular K^+. Thus since the calibrating solutions resembled the sample solutions in ionic strength and in concentrations of principal and interfering ions, the potential measurements could be converted to ionic activities using the calibration curve without the necessity to calculate selectivity coefficients. Similar methods for K^+ ISMs were used by Neher & Lux (1973) and by Coles & Tsacopoulos (1979) using Ringer solution in which NaCl is replaced by KCl to maintain constant total ionic strength.

The presence of the interfering ion in the calibrating solutions corrects for interference during the calibration so no subsequent correction need be made by calculating k_{xy} by one of the above methods and then using it together with estimated values of a_y in the sample. A further advantage of this method is that since the total ionic strength is constant the activity coefficient of a given ion must remain constant in the different solutions (as it is dependent on the ionic strength). The activity coefficient of an ion in any mixed solution of a certain ionic strength will be the same as that of a pure salt solution of that ion of the same ionic strength. Thus there is greater certainty about the value of activity coefficients than in methods using solutions where the total ionic strength is not constant. Also there is a greater probability that the selectivity coefficient will remain constant, for it has been suggested that k_{xy} may be different at different ionic strengths and will partly depend on the method used to calculate it (Moody & Thomas, 1971; Saunders & Brown, 1977). Thus this method of calibration has the advantages that the solutions can be made to resemble the ionic composition of the preparation (physiological preparations usually have constant total ionic strength throughout); the constancy of the total ionic strength means that the

ISE is likely to be well behaved during calibration - reference barrels often give an undesirable ion-sensitive response in a set of calibrating solutions which are not of constant total ionic strength (this may be due to tip potential); there is only a single value of the activity coefficient for the primary ion in the solutions and so activities are easily converted to concentrations and vice-versa; the calibration curve may be used to directly convert the ISE potential measurements into ionic activities without the need to calculate k_{xy} to correct for interference. (In practice the k_{xy} would be determined by one of the above methods for the particular ion-sensor used, and when a value of k_{xy} was well established so that the degree of selectivity of the ISM with that sensor was known, that ISM could be used to measure ionic activity using this calibration method with no further need to re-calculate k_{xy}).

Effects of reference barrel filling solution on activity measurements

The problem of which solution to use to fill the reference barrel of a double-barrelled ISM is one of finding a solution which will reduce tip and junction potentials (section I.9.vi) to a minimum and also not interfere with the measurement of ionic activity by the active barrel. For example, filling the reference barrel of a K^+- or Cl^--sensitive ISM with 3M KCl could cause erroneous measurements due to leakage of K^+ or Cl^- from the reference barrel. Finding the best solution can be a matter of trial and error. Berridge & Schlue (1978) repeated measurements with a double-barrelled K^+ ISM using firstly 2M KCl in the reference barrel and then two other filling solutions, one of which produced a large junction potential. Coles & Tsacopoulos (1979) tried five different reference barrel filling solutions for a K^+ ISM and found that 3M KCl had a clear effect on measurement of a_K, and 0.3M lithium acetate had the smallest junction potentials and did not

affect a_K measurements. Oakley et al,(1979) used 5M LiCl in the reference barrel of a double-barrelled K^+ ISM.

I.9.vi Tip potentials

A problem common to ordinary microelectrodes and reference barrels of double-barrelled ISMs is that of tip potential. This is not so much a problem for the active barrel, probably due to the organic nature of the liquid sensor. When, for example, a K^+-sensitive ISM is placed in a solution of KCl of the same concentration as that used to back-fill the active barrel (usually 0.5M) and this solution is at ground potential, the potential seen by the ion-sensitive barrel should be zero. Usually this potential is very near zero and so this is not a problem (Vyskocil & Kriz, 1972). However, the potential seen by the reference barrel in a solution at zero potential should also be zero and this is often not so in practice. The tip potential may be defined as the difference in potential between that seen by an intact microelectrode and by the same microelectrode with the tip broken off or a very low resistance electrode filled with the same solution. Adrian (1956) performed a careful study of tip potentials and showed that they were sensitive to the ionic composition of the medium outside the microelectrode tip. The larger the tip potential, the more sensitive it was to the change from 100 mM KCl to 100 mM NaCl for example. Thus, microelectrodes with large tip potentials gave false values for the E_m of frog muscle fibres because tip potential changed on entering the cell. Adrian therefore only used microelectrodes with tip potentials less than 5 mV.

The origin of tip potentials is unclear. It has been suggested that they are due to fixed anionic groups and free hydrogen ions forming a "double layer" along the inner glass wall of the microelectrode (Lavallée & Szabo, 1969). These workers proposed the equivalent circuit

of fig. 45 to account for the resistance and tip potential of a microelectrode made from glass of high resistivity so that the resistance across the wall could be neglected. There is a resistance R_W along the surface of the glass in parallel with another resistance R_O, the resistance of the bulk solution. It was proposed that R_W acts as a membrane permeable to cations only as it is constituted by the diffuse region of the double layer. When the microelectrode is filled with a KCl solution and immersed in a KCl solution of a different concentration, a potential E_K will appear in series with R_W. Then the microelectrode amounts to a K^+-sensitive electrode of resistance R_W shunted by a parallel resistance R_O, the latter constituted by the filling solution that is not in contact with the glass wall. The tip potential results from this potential E_K in series with R_W and in parallel with R_O.

A second possibility is that tip potentials originate from one or more interfacial potentials between glass and electrolyte solutions and the reduction in resistance of the glass wall near the tip due to hydration, swelling and perhaps dissolution. The tip potential would then be related to a voltage divider network as shown in fig. 46 and the observed correlation of tip potential with electrode resistance (tip potential increases with resistance) would follow (Agin, 1969). A further hypothesis is that hydration and swelling of the glass wall near the tip completely close the lumen. The system would then be one of a complete glass membrane which would show cation-exchanger properties (Agin, 1969). Since tip potentials are very unstable and one does not know how much they change on entering a cell, only by selecting microelectrodes with small tip potentials is the error from this source reduced to a minimum.

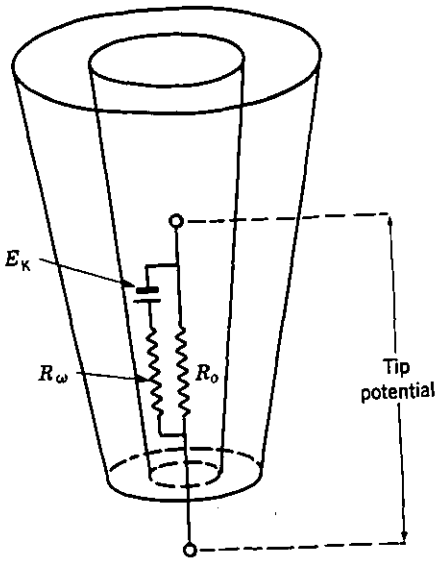

Fig. 45.

Fig. 6.5. Equivalent circuit of a high-resistivity glass micropipette electrode filled with KCl solution more concentrated than test solutions. (Symbols are defined in text.)

(from Lavallee & Szabo 1969)

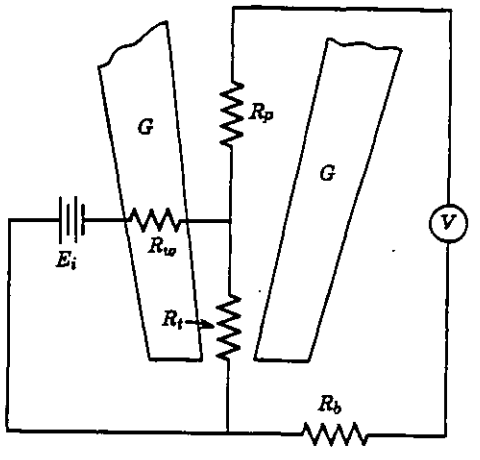

Fig. 46.

Equivalent circuit illustrating possible origin of tip potential. E_i is interfacial potential; G is glass wall of the microelectrode; R_p is resistance of bulk electrolyte in the pipette; R_t is resistance of the tip; R_w is resistance of the wall. R_b is resistance of the bath electrolyte; V is the voltage-measuring device.

(from Agin 1969)

Liquid Junction Potentials

A further potential generated at the tip which contributes to the microelectrode potential in addition to the tip potential is the liquid junction potential. This is a diffusion potential between the electrolytes of different composition in the electrode and the external solution. Nastuk & Hodgkin (1950) filled microelectrodes with 3M KCl to reduce the resistance and assumed provisionally that such electrodes had no junction potential error. This is because the junction potential depends on the profiles of the ions in the region where the two solutions mix. This potential is least dependent on the composition of the test solution when this boundary is sharp, the solution in the electrode has a higher concentration than the test solution, and the mobilities of the two ions being used in the filling solution are equal. The mobilities of K^+ and Cl^- are nearly equal and this is the reason for using KCl (Walker, 1979).

Adrian (1956) found that even electrodes filled with 3M KCl were not free from junction potentials, and that the potential was produced by a partial blocking of the tip which reduces mobility of Cl^- and exaggerates the difference in mobility of K^+ and Na^+. However it is generally accepted (Thomas, 1978a) that the error from liquid junction potentials is reduced to a minimum by using concentrated KCl as filling solution.

I.9.vii Potential Shunting, Capacitance and Inter-barrel Coupling

The very high resistance of some liquid membranes (e.g. that for Na^+) is comparable with the resistance of the glass wall of the electrode near the tip. This leads to the problem of shunting of the liquid membrane potential by capacitive and resistive leakage through the glass wall and this can lead to an overestimation of Na^+ activity (Lewis & Wills, 1980). Thus, attempts have been made to prevent any

leakage through the wall by shielding the electrode with a conductive layer on the outside of the electrode which is connected to an input-driven guard, and this is then insulated (Lewis & Wills, 1980; Wills & Lewis, 1980). Slightly different techniques of shielding the electrodes based on this concept are described by Suzuki et al, (1978) and Sachs & McGarrigle (1980). Shielding of the electrode in this way from the shaft down to very near the tip also solves another problem: the capacitance of the electrode to the tissue bath and surroundings causes interference, reduced fidelity and longer response time. These problems are mainly encountered in ISMs with very high impedance liquid membranes such as the neutral ion carrier for Na^+.

The effects of inter-barrel coupling constitute another problem in the use of double-barrelled ISMs. The first kind of effect is physical and is that of the liquid in the tip of one barrel crossing over to the other one. This problem should be solved by adequate silanisation (thus preventing entry of aqueous solutions into the active barrel) and ensuring that the reference barrel is not silanised at all (thus preventing entry of organic liquids into the reference barrel). Coles & Tsacopoulos (1979) bevelled the tips of double-barrelled ISMs to prevent LIX solution passing from the active to the reference barrel.

The second kind of coupling is electrical due to possible resistive and capacitive leakage through the glass separating the barrels very near the tip, and across the external solution at the tip due to the proximity of the two tips. The problem is worse if theta glass is used than if two separate capillaries are used for the two barrels as the former tends to have only a very thin glass partition between the barrels. The finer the tip of the ISM, the thinner is the partition between the barrels at the tip. The possibility of this coupling means that for double-barrelled ISMs to be used in experiments

it should be shown that it occurs only to a negligible extent. For example, Coles & Tsacopoulos (1979) showed that the reference barrel of a double-barrelled K^+ ISM recorded the same potential changes as an ordinary micro-electrode and then applied a voltage step change in the external solution. The reference barrel responded to the change as expected and only small electrical transient artefacts were seen in the K^+ signal after suitable adjustment of the positive capacitive feedback of the headstage amplifiers.

I.9.viii General Considerations

It has been argued in section I.5 (Ionic Bases of Electrical Activity) that ionic activities are of crucial importance in the functioning of an excitable cell as they determine both resting membrane potential and the ionic mechanisms underlying the electrical responses. Since ISMs are the most direct method of measuring intracellular ionic activities, they can be used in a wide range of both intracellular and extracellular applications. They have been used to make ionic activity measurements in skeletal muscle of various species e.g. frog (Lee & Armstrong, 1974) and rat (Kernan & MacDermott, 1976); in cardiac muscle of e.g. sheep (Ellis, 1977; Vaughan-Jones, 1977) and of guinea-pig and rabbit (Fry & Poole-Wilson, 1981); in the brain of e.g. cat (Lux, 1974; Heinemann & Lux, 1975; Somjen et al, 1976) and rat (Vyskocil et al, 1972; Gardner-Medwin, 1977); in photoreceptors of invertebrates (e.g. Brown & Ottoson, 1976; Saunders & Brown, 1977; Coles & Tsacopoulos, 1979), and extracellular space in the vertebrate retina (e.g. Oakley & Green, 1976; Oakley et al, 1979); in neurones of e.g. snail (Thomas, 1977; 1978b; Heyer & Lux, 1976) and Aplysia (Ascher et al, 1976; Russel, 1978); in mouse soleus muscle fibres (Aickin & Thomas, 1977); in absorptive cells lining the villi of Amphiuma small intestine (White, 1976); in epithelial cells of the rabbit urinary bladder (Lewis et al, 1978); in crayfish stretch receptor (Brown et al, 1978), and so on in many other

cells and extracellular environments. Thus the ISM has many biological and medical applications. A review of intracellular ionic activity measurements in nerve and muscle was produced by Walker & Brown (1977) and this was then updated (Brown & Owen, 1979).

There are several advantages of using ISMs apart from that of obtaining direct activity measurements (Thomas, 1978a). The response time of ISMs is reasonably fast, and if very fast responses are not being analysed, even the relatively 'slow' response time of the recessed-tip ISM is acceptable for making activity measurements. The information from ISMs is given in 'real time' without the need for time-consuming chemical procedures or long computations. In large cells it is even possible to record the activities of two or more ions simultaneously (Thomas, 1977; 1978b). The size of the ISM tip excludes the possibility of penetrating subcellular organelles so that activities are recorded only from the cytoplasm. Compared to that required for many techniques, the equipment required to make and use ISMs is fairly simple and inexpensive. Much of the equipment (e.g. oscilloscope and pen-recorder) would already be available in a physiology laboratory. Finally, since nothing is consumed by the ISM and only one cell is penetrated, it is possible to use ISMs in vivo on whole animal preparations.

Liquid membrane ISMs have better response times and are easier to make than solid state ISMs. In some cases, the recessed-tip electrodes still have a better selectivity than liquid membrane ISMs, but for most ions there is a liquid membrane available with adequate selectivity and the development of new LIXs and neutral carriers for ISMs is improving the selectivity of this type of electrode. One disadvantage of using a liquid membrane electrode is that it can only safely be used for at most a few days or a certain number of experiments, after which a new ISM must be made since the response starts to

deteriorate significantly after this time. The recessed tip ISM will last much longer and may even improve with use. This is not a very serious drawback though, since it is not too difficult to make a liquid membrane ISM before each day's experiments when a standard manufacturing technique has been developed. The liquid membrane ISM is probably the most versatile and simple of the various ISM designs since the shape of the shank near the tip and the size of the tip can be chosen to effectively penetrate and record from a given cell without constraints due to the shape of the tip of ion-sensitive glass or metal. It seems therefore that it is the liquid membrane ISM which holds the greatest potential for future development and for use as the 'ideal' intracellular ISM. The intracellular ion-sensitive microelectrode technique is being applied to neurones of the vertebrate (fish) retina for the first time in the present study.

The Aims and Scope of the Present Study

This thesis reports an experimental investigation of the ionic bases of the electrical properties of horizontal cells in a cyprinid fish, the roach (Rutilis rutilis) retina. The aim of this work has been to develop experimental methods in order to make direct quantitative measurements of extra- and intracellular ionic activities from these retinal neurones and to investigate any changes in ionic activity corresponding to the response to light. This is achieved in several stages:

1. The development of apparatus and techniques for the manufacture of double-barrelled ion-sensitive microelectrodes for K^+ and Cl^- which give an acceptable and reliable response to the activity of the relevant ion.

2. The construction of a system (including an optical stimulator) suitable for intracellular recording from single neurones in the isolated retina with double-barrelled ISMs. Refinement of the manufacturing technique for ISMs until they are capable of making reliable measurements of intracellular ionic activities in practice.

3. Measurement of the activities of K^+ and Cl^- in horizontal cells of the retina in the dark and during the response to light of various wavelengths. Investigation of the relationship between ionic equilibrium potentials, the saturation responses to light, and the level of membrane potential after spraying onto the retina the synaptic blocking agent, Co^{++} or the neurotransmitter dopamine.

CHAPTER II

APPARATUS, METHODS AND CALIBRATIONS

A walk-in Faraday cage was erected around a solid steel optical table to reduce to a minimum electrical noise and interference and mechanical instability during all experiments. Apparatus was constructed to provide the following functions:

1. Manufacture of double-barrelled ISMs with tip diameters ≤ 1 μm.
2. Calibration of ISMs for their response to ionic activity changes and evaluation of their performance.
3. Intracellular recording with ISMs and ordinary microelectrodes (OMs) from single neurones of the isolated fish retina.
4. Amplification, visual display, and recording on chart paper of the electrical signals produced by both ISMs and OMs.
5. Stimulation of the retina by light flashes of variable wavelength, intensity and duration.
6. Chemical perfusion of the retina by spraying.

II.1 Manufacture of Double-barrelled ISMs

The apparatus used in the manufacture of double-barrelled ISMs consisted of a number of different devices, each with a specific function. The apparatus will be described concurrently with the relevant methods.

II.1.i Preparatory work

Preliminary experiments were performed to determine the suitability of various kinds of glass capillary for the ion-sensitive (active) barrel of an ISM. It was found that capillaries containing a tubular filament, when made into microelectrodes (MEs) filled fairly easily with liquid ion-exchanger (LIX) and electrolyte, but this type of

ME did not constitute a suitable ISM active barrel as the LIX column tended to gradually reduce in length. This was presumably due to LIX proceeding up the filament, or the filament preventing adequate silanisation of the glass surface inside the tip of the ME. Capillaries of various diameters were also tested. Although there were difficulties involved in filling MEs made from unfilamented glass capillaries, the LIX column was stable in these MEs. The type of glass capillary chosen finally was an unfilamented, thin-walled capillary of 1.5 mm outer diameter (OD) and 1.05 mm inner diameter (ID).

Many trial-and-error experiments were performed to firstly produce suitably shaped single-barrel ISMs and to develop methods of silanising and filling with LIX and electrolyte, avoiding air bubbles. This involved using cat's whiskers (Thomas, 1978a), centrifugation (Plamondon et al, 1976) and local heating techniques (Zeuthen, 1971) to remove air bubbles and injection of electrolyte under pressure from a fine micropipette. Production of working single-barrel ISMs was followed by the development of a method for making double-barrelled ISMs. The technique used finally to manufacture double-barrelled ISMs is described below.

II.1.ii Method for production of double-barrelled glass micropipettes

Borosilicate glass capillary tubes of 1.50 mm OD and 1.05 mm ID (GC 150T-15 Clark Electromedical Instruments) were cut to produce lengths of 7.5 cm. Twenty of these lengths were placed vertically in a clean 250 ml beaker containing 8 ml of concentrated nitric acid in a fume cupboard. 2 ml of ethanol were added to the beaker. Within a minute or so the ethanol and acid began to react together violently, thus cleaning the glass. The reaction lasted about 5 minutes and then the beaker was taken out of the fume cupboard and the capillaries were washed 10 times in distilled water (a wash bottle was used to ensure

that the inside of the capillaries were rinsed as well as the outside). The capillaries were then placed in an oven at 100°C for 1 hour to dry. These capillaries that were to be used for the active barrels of ISMs were cleaned in this way to minimise problems in the subsequent construction of ISMs due to any extraneous substances contaminating the glass surfaces.

After drying in the oven the capillaries were paired with other capillaries which were used to make the reference barrels. These latter were borosilicate glass capillary tubes with an internal filament, an OD of 1.00 mm, and an ID of 0.58 mm (GC 100F-10, Clark Electromedical Instruments) which had been cut to produce lengths of 5 cm. A shorter filamented capillary was glued on to the middle of and parallel to a longer non-filamented capillary with four blobs of Araldite placed symmetrically near the ends of the shorter tube (fig. 47a). The capillaries were thus glued together in pairs and then placed horizontally in an oven at 100°C for 1 hour to polymerise the Araldite. After this, they were taken out of the oven and the longer member of each capillary pair in turn was clamped at both ends in the chuck jaws of a vertical electrode puller (Scientific Research Instruments; fig. 48a) such that the central part was positioned in the centre of a cylindrical heating coil with an ID of 4 mm made from 6 turns of resistance wire (fig. 47b). This electrode puller had been modified so that the upper chuck jaws could be rotated about a vertical axis with respect to the lower jaws. With the double capillary in this position (fig. 47b), a support of adjustable height was placed under the lower chuck so that the chuck was resting on it and the position of the upper chuck was fixed by means of a clamping screw on the puller. The controls on the puller were adjusted to give zero pulling force and maximum heating of the coil. After 10 seconds of heating, the glass softened and the upper chuck was unclamped.

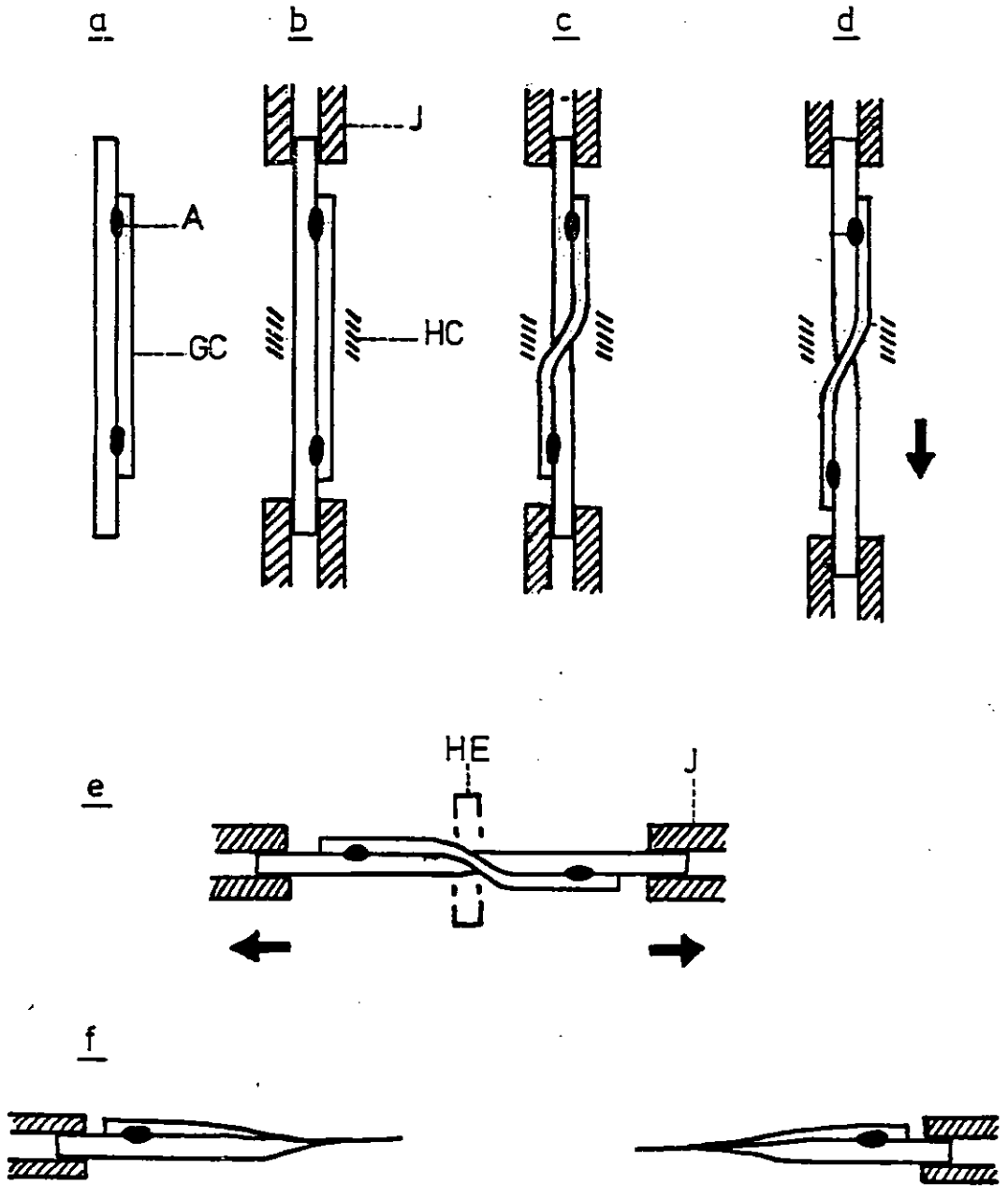

Fig. 47. a-f. Stages in the production of a double-barrelled micropipette from two separate glass capillary tubes. A - Araldite; GC - glass capillary; HC - heating coil; HE - heating element; J - chuck jaws of microelectrode puller.

a

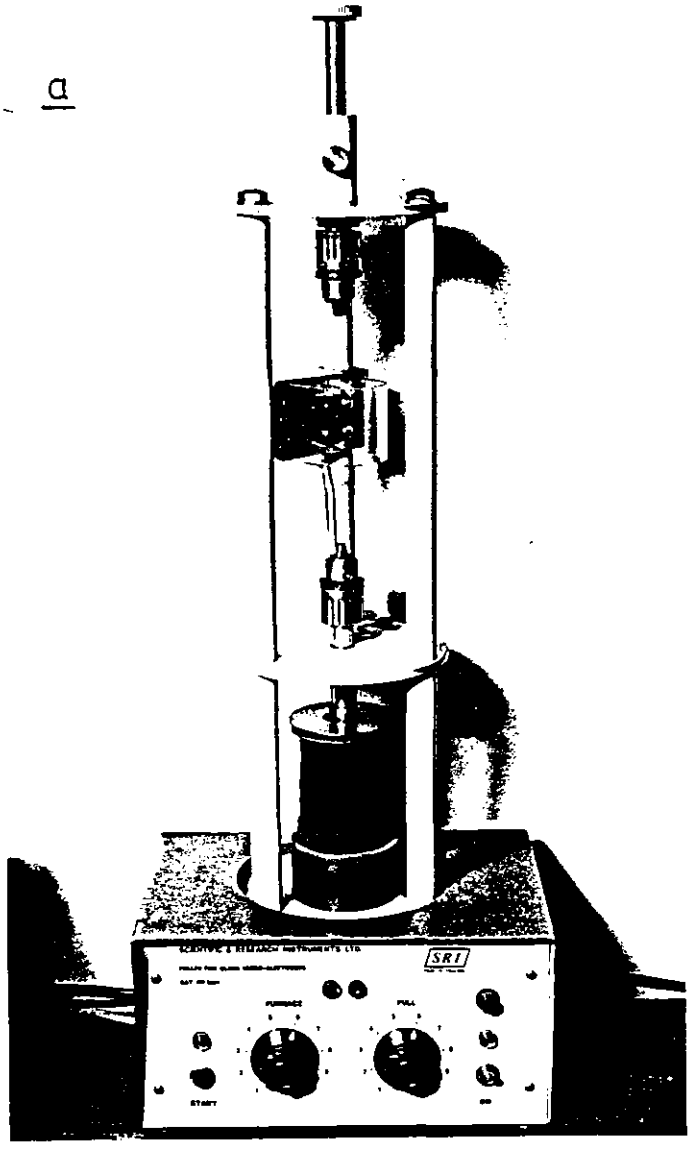

Fig. 48. Microelectrode pullers used in this study. a - SRI vertical puller; b - Clark horizontal puller.

b

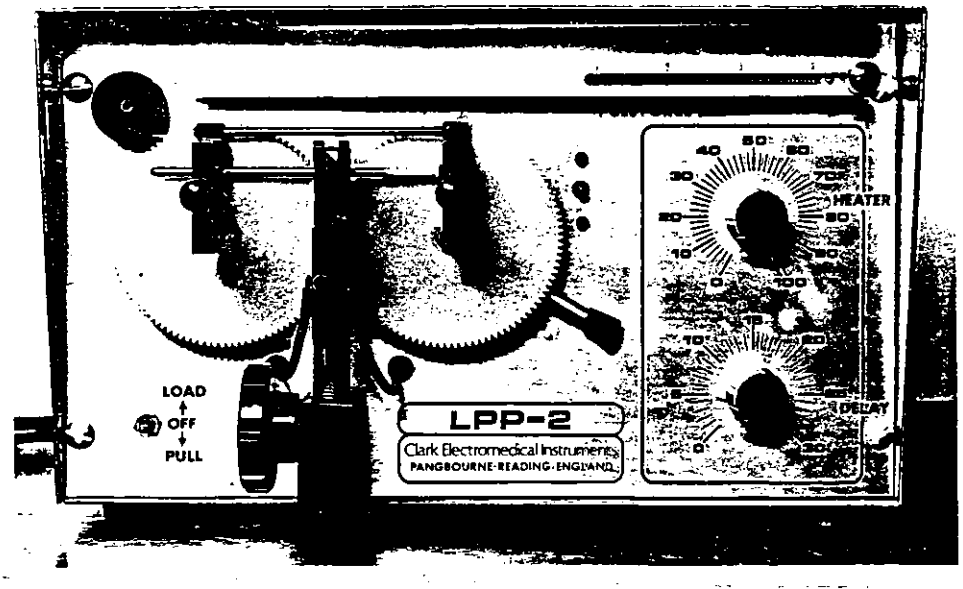

Being careful to maintain constant height, this chuck, holding the upper end of the double capillary was rotated through 180° and re-clamped. The heating was then terminated by switching off the puller. Thus, the two capillaries were twisted round each other by 180° (fig. 47c). This was to ensure that when the capillaries were pulled into micropipettes, each double-barrelled micropipette would have a single 'combined' tip consisting of the two adjacent tips of the two separate barrels. The next step was to stretch the twisted capillary pair slightly in order to optimise the shape of the shank of the micropipettes when they were pulled subsequently. This was achieved by lowering the height of the adjustable support under the lower chuck jaws by 2 mm, turning on the heating coil and allowing the capillaries to be stretched when the glass was softened as the lower chuck fell slowly under gravity until it rested on the support (fig. 47d). The heating was then turned off and the capillary pair was taken out of the jaws of the vertical puller.

The pulling of micropipettes from the capillary pair was performed by a Livingstone-type horizontal puller (Clark Electromedical Instruments, model LPP2, fig. 48b) which had controls for variable heating of an element formed from a U-shaped strip of platinum, variable pulling force and time of delay before 'pull' was effected (after heating had started). This puller was used because it was found that the vertical puller could not produce double-barrelled micropipettes with sub-micron tips. To pull a pair of micropipettes from a twisted and stretched capillary pair, the latter was clamped at both ends in the jaws of the horizontal puller, so that the central twisted part of the double capillary was positioned centrally inside the heating element (fig. 47e). It was important that the glass was heated, as nearly as possible, symmetrically about the axis of the length of the capillaries so that when micropipettes were pulled they would have

straight shanks terminating in fine tips (fig. 47f). Each micropipette was examined under a light microscope at x400 magnification to check that the shank was straight and of acceptable taper and that the tip was fine enough (≤1 μm in diameter). Acceptable double-barrelled microelectrodes were also examined in the scanning electron microscope to confirm their shapes, dimensions etc. An example is shown in fig. 49a,b. Microelectrodes with unacceptable features were discarded.

Microelectrodes were prepared in batches of 20 at a time. These were held vertically (tips up) in a specially-made metal holder and stored in a dessicator until the silanisation procedure.

II.1.iii Silanisation of the Active Barrel

The inside of the larger barrel of each micropipette needed to be silanised in order to make it hydrophobic/organophilic as this was to be used as the active barrel with the column of liquid ion-exhcanger in the tip. A small amount (2 ml) of silane (dimethyldichlorosilane, DDS; Sigma) was put into a small glass jar in a fume cupboard. This jar had a glass lid to fit it, in the centre of which was a hole of the correct size to accommodate the protruding back end of the active barrel of the double micropipette. Before each batch of micropipettes was silanised, two small pieces of filter paper and one of metal foil were placed over the hole in the lid and held down at the edges with masking tape. A hole was then made in the foil and paper, coincident with the hole in the lid, such that the protruding back end of a micropipette, when pushed through this hole would fit tightly (fig. 50). This arrangement was designed to ensure that when the lid was placed on the jar of silane and a micropipette was placed with its shaft end protruding through the hole as in fig. 50, the larger barrel would be silanised by DDS vapour while the smaller barrel remained unsilanised. This method was devised after some problems

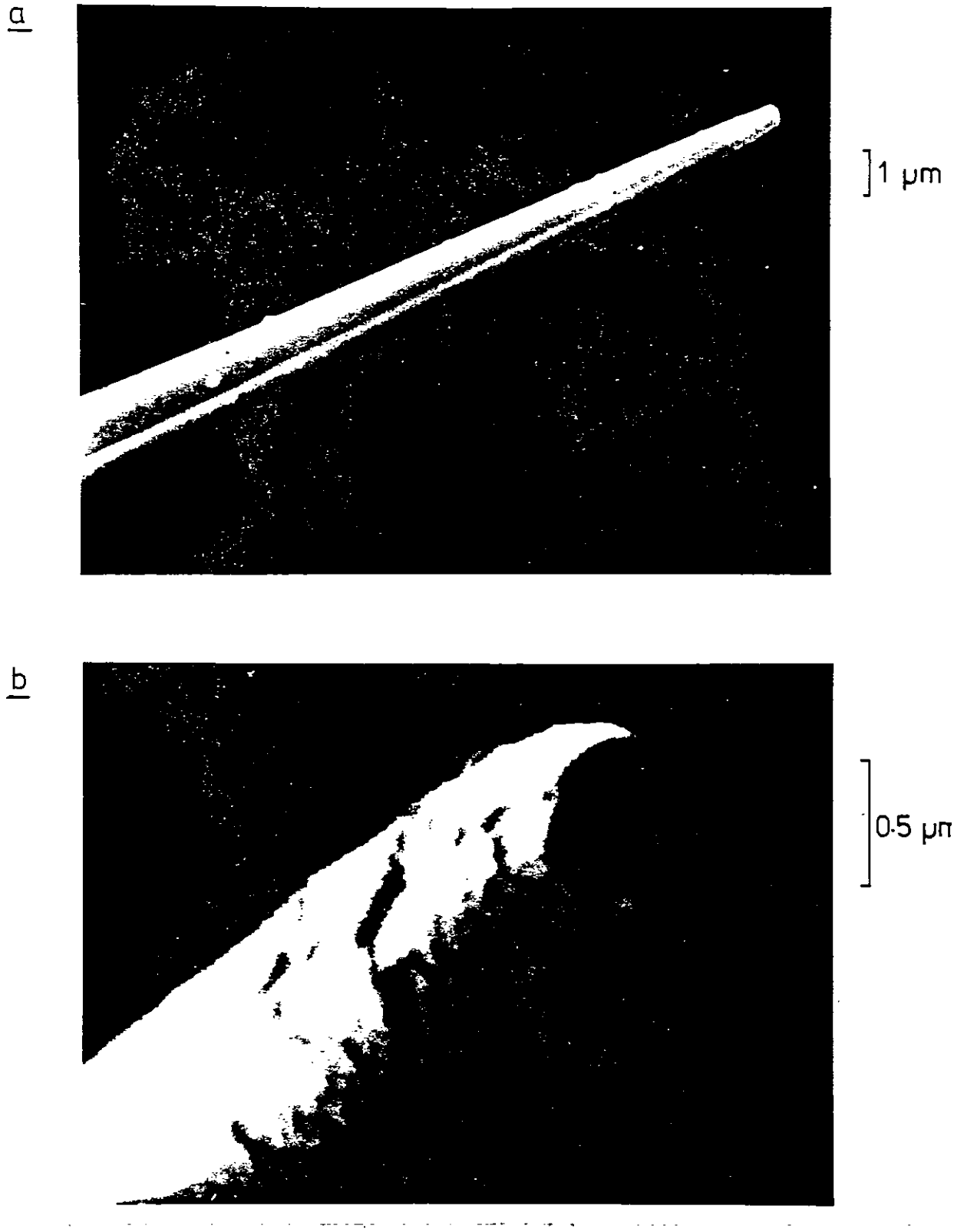

Fig. 49. a,b. Scanning electron micrographs of the tip of a double-barrelled ion-sensitive microelectrode. Calibration bars show the size of the tip (< 1 µm diameter) and part of the shank.

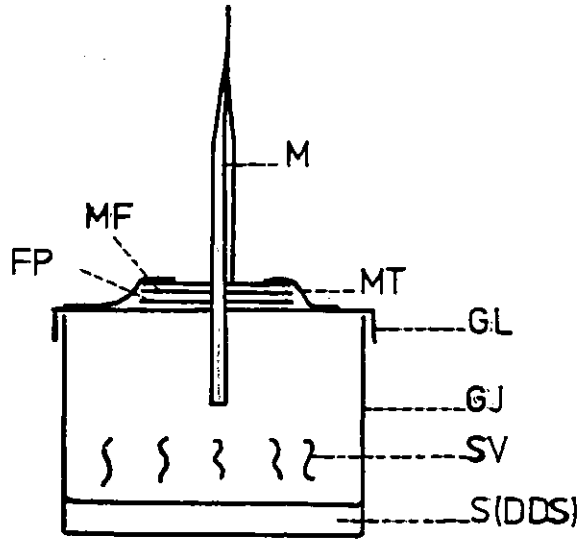

Fig. 50. Arrangement for the silanisation of the active barrel of a double-barrelled micropipette. M: micropipette; MF: metal foil; FP: filter paper; MT: masking tape; GL: glass lid; GJ: glass jar; SV: silane vapour; S(DDS): liquid silane (dimethyldichlorosilane).

Table 2. Effects of varying silanisation time

SILANISATION TIME (SECS.)	CONDUCTIVITY OF THE REFERENCE BARREL	CALIBRATION OF ISM
15	+ + + + + +	+ + − − − −
30	+ + + + + +	+ + + + − −
60	+ + − − − −	+ + − − − −
120	+ + − − − −	+ + − − − −

+ = conducting

− = non-conducting

+ = acceptable calibration

− = unacceptable calibration

connected with silanisation encountered in making ISMs. In general, if the active barrel was under-silanised, then the ion-sensitive electrode filling components were found to become unstable eventually. On the other hand, over-silanisation caused blockage in the tips of the active barrels, and 'spillage' of extra silane into the reference barrels prevented them from filling and conducting properly. A simple experiment was, therefore, carried out to establish the optimum silanisation conditions. The active barrels of 24 electrodes were silanised for 15, 30, 60 and 120 sec. (6 each), and then suitability of each to be turned into an ISM was tested, and assessed as shown in Table 2. In summary, microelectrodes silanised for 15 seconds were found not to calibrate well, whilst those silanised for 60 or 120 seconds suffered from blocked tips of reference barrels and hence also did not calibrate well. In conclusion, a duration of 45 seconds was chosen to be the optimum silanisation time.

When all the micropipettes in a batch had been silanised, they were placed (in their metal holder) in the oven at 100^{o}C for 1 hour. They were then taken out of the oven and stored in a desiccator.

II.1.iv Filling the Micropipettes

The smaller barrel was filled firstly with the appropriate salt solution to constitute the reference electrode (RB): 5M LiCl for K^+ ISMs; 85% 0.6M K_2SO_4 + 15% 1.5M KCl for Cl^- ISMs (Claire Aickin, personal communication). This barrel was filled before the active barrel because: (i) it avoided the situation of filling the active barrel (a more involved process) only to find that the reference barrel would not fill properly and conduct; (ii) the presence of electrolyte in the tip prevented liquid ion-exchanger from the active barrel tip crossing over to the empty RB tip and making the RB ion-sensitive when filled.

The reference barrel was filled using a 30g syringe needle and a 1 ml syringe. The tubular fibre inside this barrel enabled it to fill with electrolyte up to the very tip so that it made a good conducting electrode. The double-barrelled micropipette (DBM) was clamped in a crocodile clip, the jaws of which had been shaped and filled with dental wax so as to optimally hold the DBM. This modified clip was in turn held on an arm on the right-hand side of a pair of Prior micromanipulators mounted on an optical bench (MM1, fig. 51a) such that the shank and tip of the DBM could be viewed by a horizontal binocular microscope (fig. 51a,b; fig. 52). The microscope was calibrated by means of a graticule placed in one of the eyepieces. The DBM tip was viewed using a x20 objective when its size was being checked immediately after the micropipette had been pulled. A x3, and sometimes a x10, objective was used to view the DBM shank when it was being filled.

The filling of the active barrel proceeded in a number of steps:

1. A 10 mm long, 0.8 mm OD micropipette with a broken tip was waxed onto a fine hypodermic needle, which was attached to the body of a 1 ml disposable syringe. This was in turn connected to a 50 ml syringe via a short length of plastic tubing. This whole assembly was held upright in one of the left-hand micromanipulators (MM2, fig. 51a) above the DBM held on the right hand side. The tip of this broken micropipette was dipped into the pool of LIX in a small vial held by MM3 (fig. 51a) and a small quantity was sucked in. The 'electrode' was then lowered as far down as possible into the active barrel of the DBM under visual control, and a small drop of LIX was injected out by pressurising the syringe (fig. 51b). The injection micropipette was then removed from the inside of the active barrel.

2. A tightly fitting plastic tubing was attached to the back-end of the active barrel, and pressure exerted from another 50 ml syringe to force the drop of LIX to the tip of the electrode. Usually, such

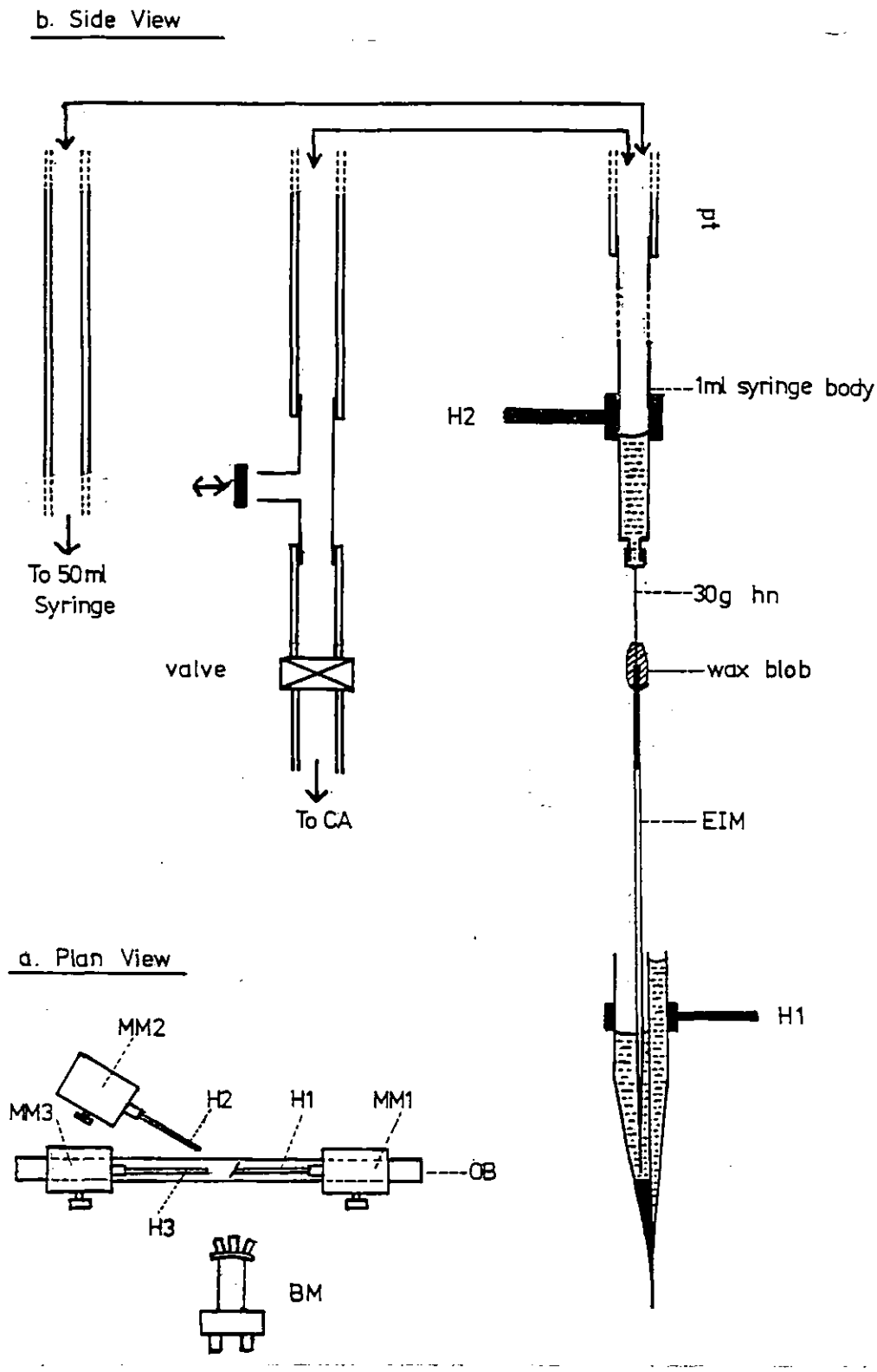

Fig. 51. a & b. Schematic diagram of apparatus for filling double-barrelled micropipettes. MM1, MM2, MM3: micromanipulators; OB: optical bench; H1: holder for double-barrelled micropipette; H2: holder for apparatus for injection of LIX and of electrolyte (b shows injection of electrolyte); H3: holder for vial of LIX; BM: binocular microscope; EIM: electrolyte injection micropipette; CA: compressed air source; hn: hypodermic needle; pt: plastic tubing.

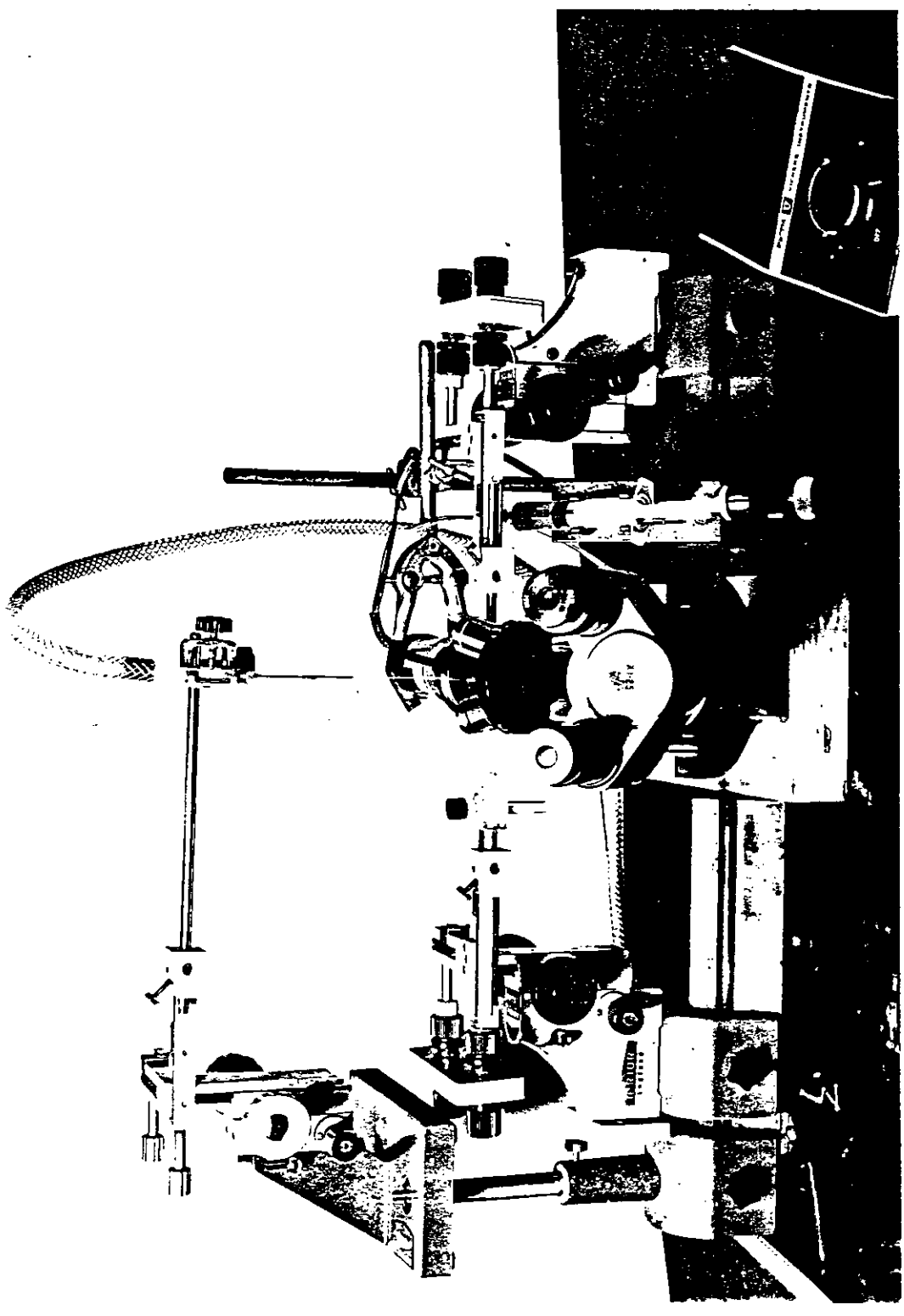

Fig. 52. Apparatus for filling double-barrelled micropipettes by injection of LIX and electrolyte. Compare with Fig. 51, a & b to discern the various parts of this apparatus.

pressure was sufficient to move the LIX a short distance, from where it 'took off' on its own by capillary action. By this means a few 100s μm - few mms of the tip of the active barrel was filled by a column of LIX.

3. Bevelling If the LIX did not move into the tip on its own or by pressure applied from the 50 ml syringe, the DBM was taken out of the apparatus and its tip bevelled slightly. For this a 'slurry beveller' of the type described by Lederer et al, (1979) was used. The bevelling medium consisted of about 10 ml of a mixture of (0.05 μm diameter) Al_2O_3 powder (20% by volume) in distilled water. This was kept in a plastic petri dish of 10 cm diameter placed on a 5 mm thick circular perspex plate that was attached to the shaft of a mains-driven clock-motor. The slurry medium was thereby rotated at 10 RPM, and the microelectrode, held in a clip and holder, was lowered by a Prior micromanipulator, under visual control, until its tip just touched the thick sediment (fig. 53a,b). The tip of the DBM was thus bevelled for a few seconds - 20 seconds, and then it was transferred to the microscope system to view its shank. Further application of back pressure usually moved the LIX to the tip; otherwise that DBM was discarded.

4. Back-filling the Active Barrel The active barrel was backfilled with electrolyte from the upper meniscus of the LIX to the top of the shaft using another broken glass micropipette connected to the body of a 1 ml disposable syringe, filled with the appropriate electrolyte and connected to a compressed air cylinder via a T-piece and valve (fig. 51b, fig. 52). The electrolytes used were: 500 mM KCl for K^+ ISMs and 500 mM NaCl for Cl^- ISMs. The electrolyte injection micropipette (EIM) was held in the appropriate micromanipulator (MM2, fig. 51a,b) and guided carefully into the active barrel. It was lowered until its tip could be seen inside the widest part of the shank under the microscope. Then, under microscopic observation the DBM was

a

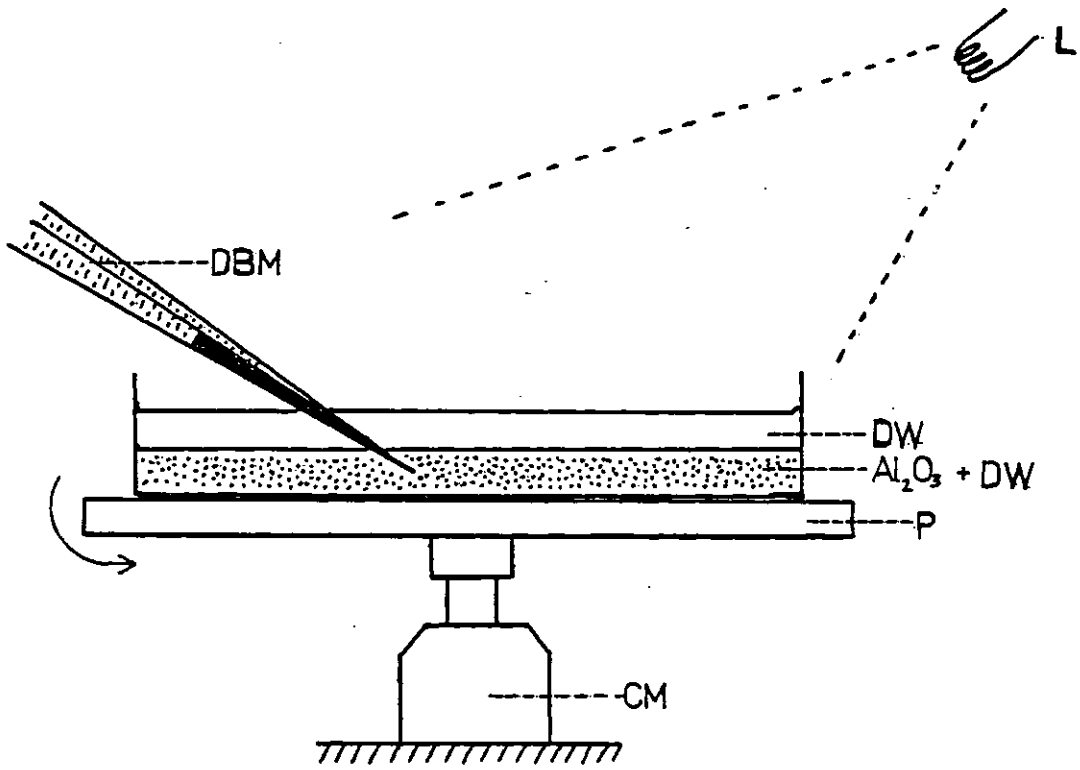

Fig. 53. a: diagram of; b: photograph of bevelling apparatus. DBM: double-barrelled micropipette; L: light; DW: distilled water; Al_2O_3: very fine particles of aluminium oxide; P: perspex plate; CM: clock motor.

b

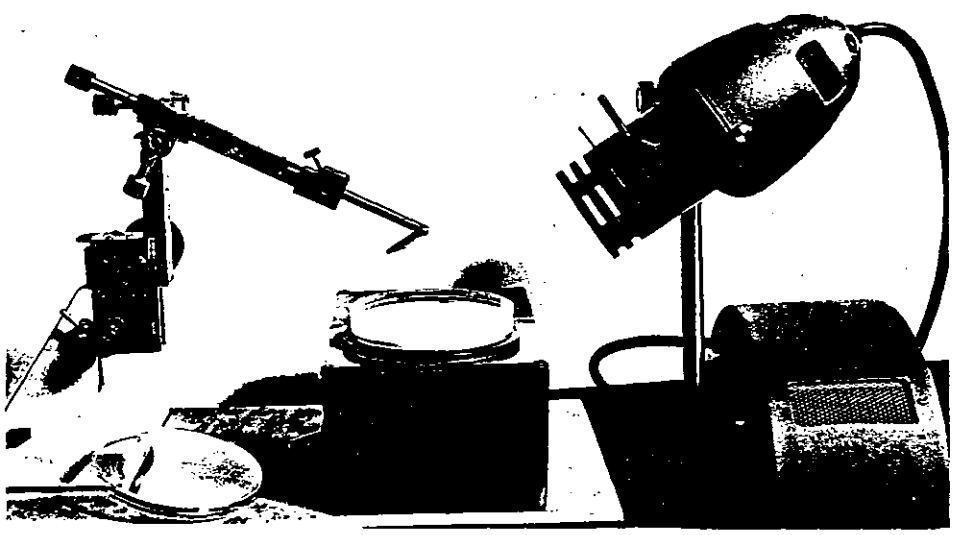

raised slowly until the EIM tip was positioned just above, but not quite touching, the upper meniscus of the LIX column (fig. 51b). The gas tap was then opened allowing air to escape through the outlet provided by the T-piece (fig. 51b). While viewing the tip of the EIM in the shank of the active barrel through the microscope, the outlet of the 3-way junction was blocked by the thumb, causing electrolyte to be injected into the shank, forming a junction with the LIX column. As the injected electrolyte started to fill the shank, the DBM was lowered so that the EIM tip always remained just below the upper meniscus of the electrolyte thereby avoiding the formation of air bubbles in the column of electrolyte already formed. Electrolyte was injected in this way until the upper meniscus had just passed the widest part of the shank. The thumb was then taken off the air outlet and the gas tap was closed. The EIM was taken out of the active barrel and the DBM was removed from the apparatus. The remaining part of the active barrel was filled with electrolyte by means of a 1 ml syringe and 30 g needle to produce a continuous column of electrolyte from the junction with LIX to the top of the shaft.

5. Provision for Electrical Connection In order to make electrical contact with the electrolyte solutions in the reference and active barrels of the DBM, chlorided silver wires were used. The reversible reaction between chloride ions in the electrolyte solution and in the solid AgCl coating on the Ag wire reduces the junction potential between the wire and the solution to a negligible minimum and produces a stable potential. 2 cm of each of a pair of 5 cm long silver wires were chlorided by electrolysis in a solution of 200 mM NaCl. The silver wires constituted the anode and a carbon rod acted as the cathode, whilst the DC current was supplied by a stimulator (model SD9, Grass Instruments) and measured by a DC multimeter (Levell Instruments). A current of 2 mA was passed for 2 minutes in order to

coat the ends of the wire with a uniform layer of AgCl. The wires were then placed, one in the active, and one in the reference barrel of the DBM with their 'chlorided' ends making contact with the electrolyte solutions in the barrels. The ends of the barrels were sealed off with sealing wax, and the free ends of the wires were soldered onto miniature metal pins (fig. 54).

II.2 Recording System

A Faraday cage was built from Dexion framework and a fine expanded copper mesh around a large solid steel optical table. The Faraday cage was large enough for the experimenter to work inside thus providing a shield against external sources of electrical interference (Figure 55a,b). The heavy steel optical table was found to provide an excellent mechanically stable working platform for testing ISMs and for electrophysiological intracellular recording experiments. A pair of precision micromanipulators (Zeiss) mounted on a large heavy base-plate were placed on the table (fig. 55a,b) and between them a recording platform was constructed on this base plate (fig. 56). This platform consisted of a square 0.5 inch-thick metal table with a circular hole in the centre for the light beam to enter. The platform was fitted with the XY-controls of a microscope stage so the recording chamber could be moved around relative to the light beam. Above the recording platform, a binocular zoom stereo-microscope (Zeiss) was situated for visual examination of the preparation during recording (fig. 56). The electronic equipment used was set in a recess inside a Faraday cage so that the cage interior was well shielded from all a.c. mains inputs (fig. 55a,b; fig. 57).

The electronic equipment consisted of:

1. A dual-differential electrometer (WPI Model F223) to the probes ('head-amplifiers') of which the ISM was connected via small metal

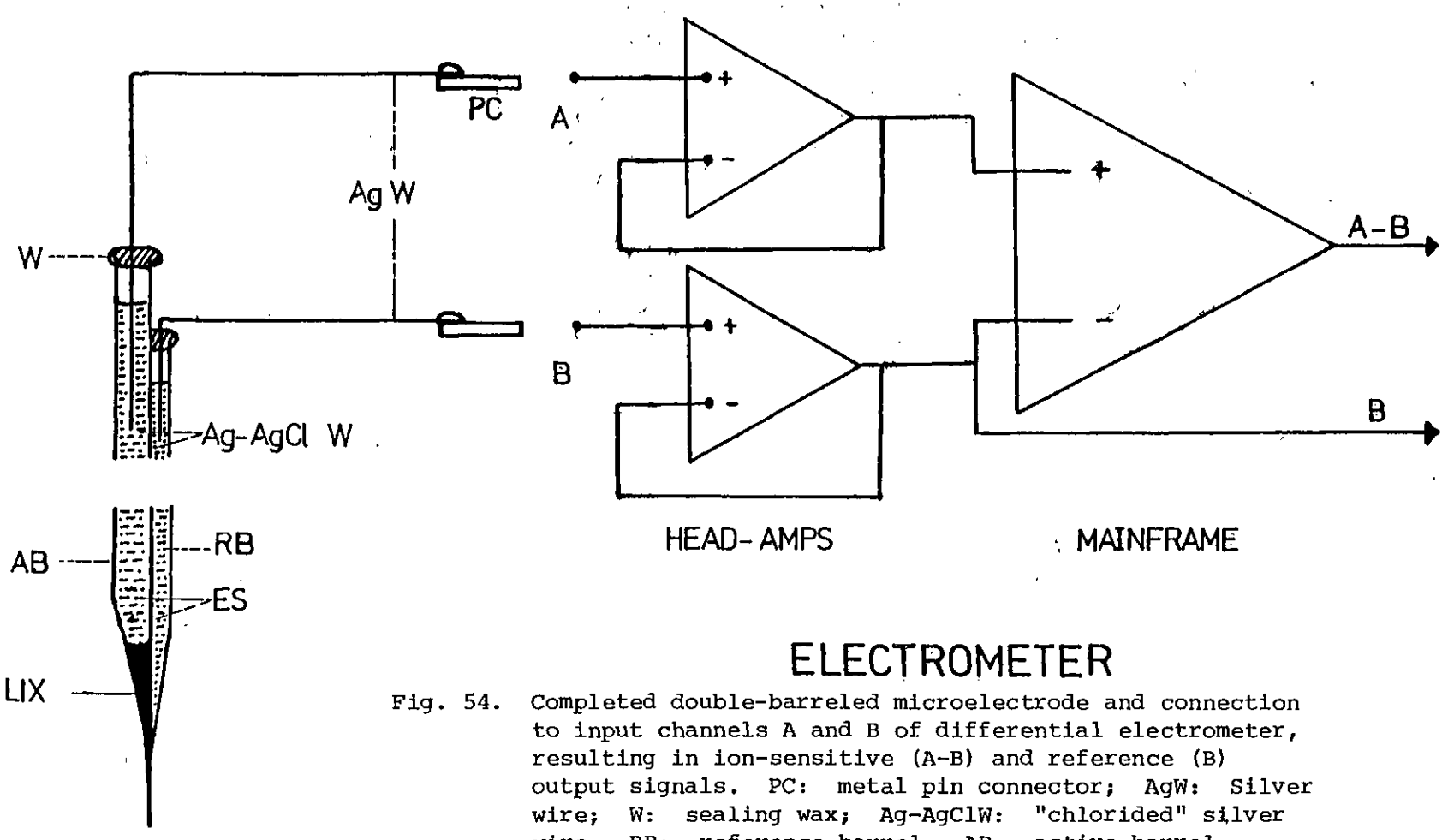

Fig. 54. Completed double-barreled microelectrode and connection to input channels A and B of differential electrometer, resulting in ion-sensitive (A-B) and reference (B) output signals. PC: metal pin connector; AgW: Silver wire; W: sealing wax; Ag-AgClW: "chlorided" silver wire; RB: reference barrel; AB: active barrel; ES: electrolyte solutions; LIX: liquid ion-exchanger.

a

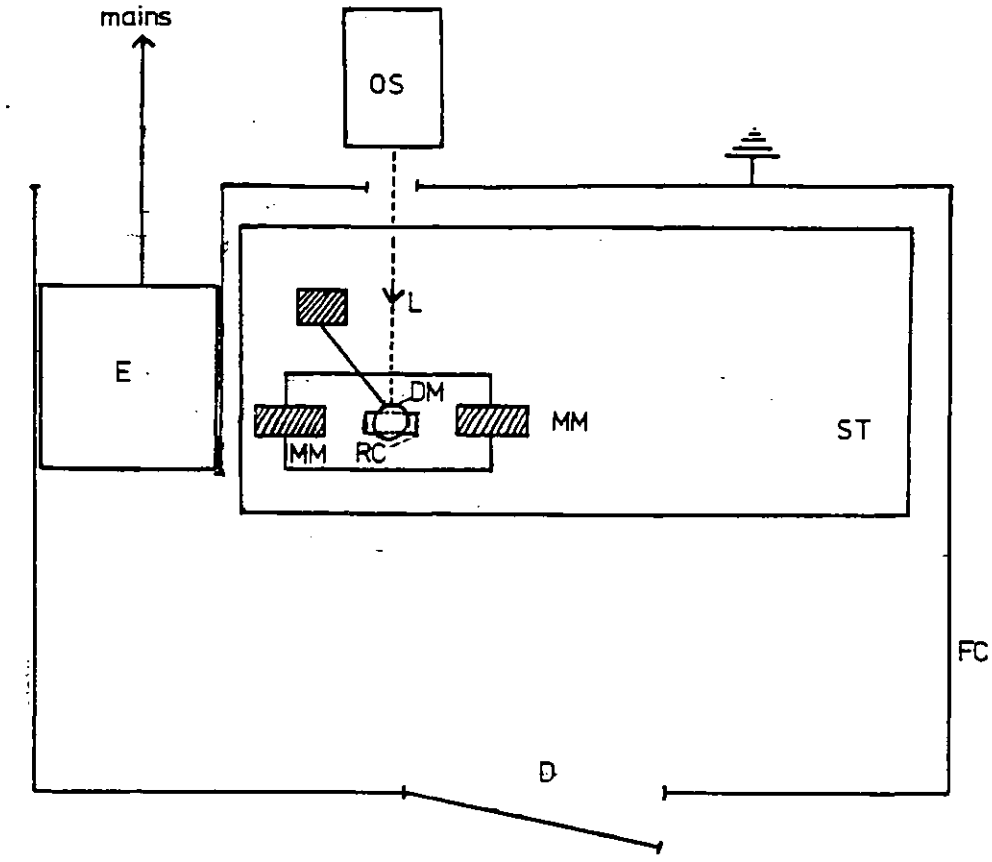

Fig. 55. a: Schematic diagram of Faraday cage and associated equipment from above. FC: Faraday cage; D: door; ST: steel table; MM: micromanipulators; DM: dissecting microscope; OS: optical system; L: light beam; RC: recording chamber; E: electronic equipment.
b: photograph of equipment inside Faraday cage.

b

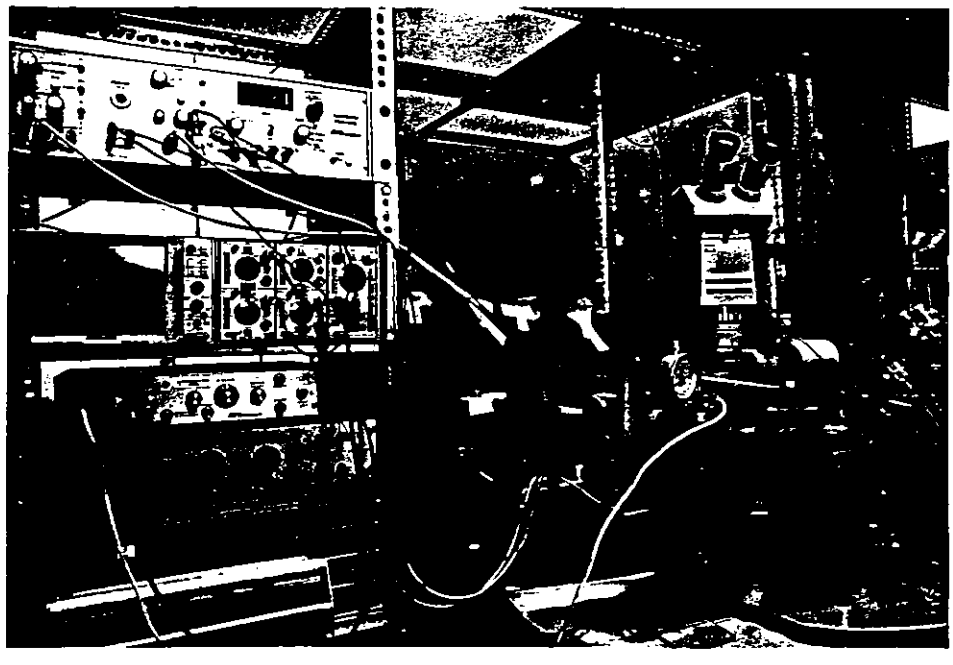

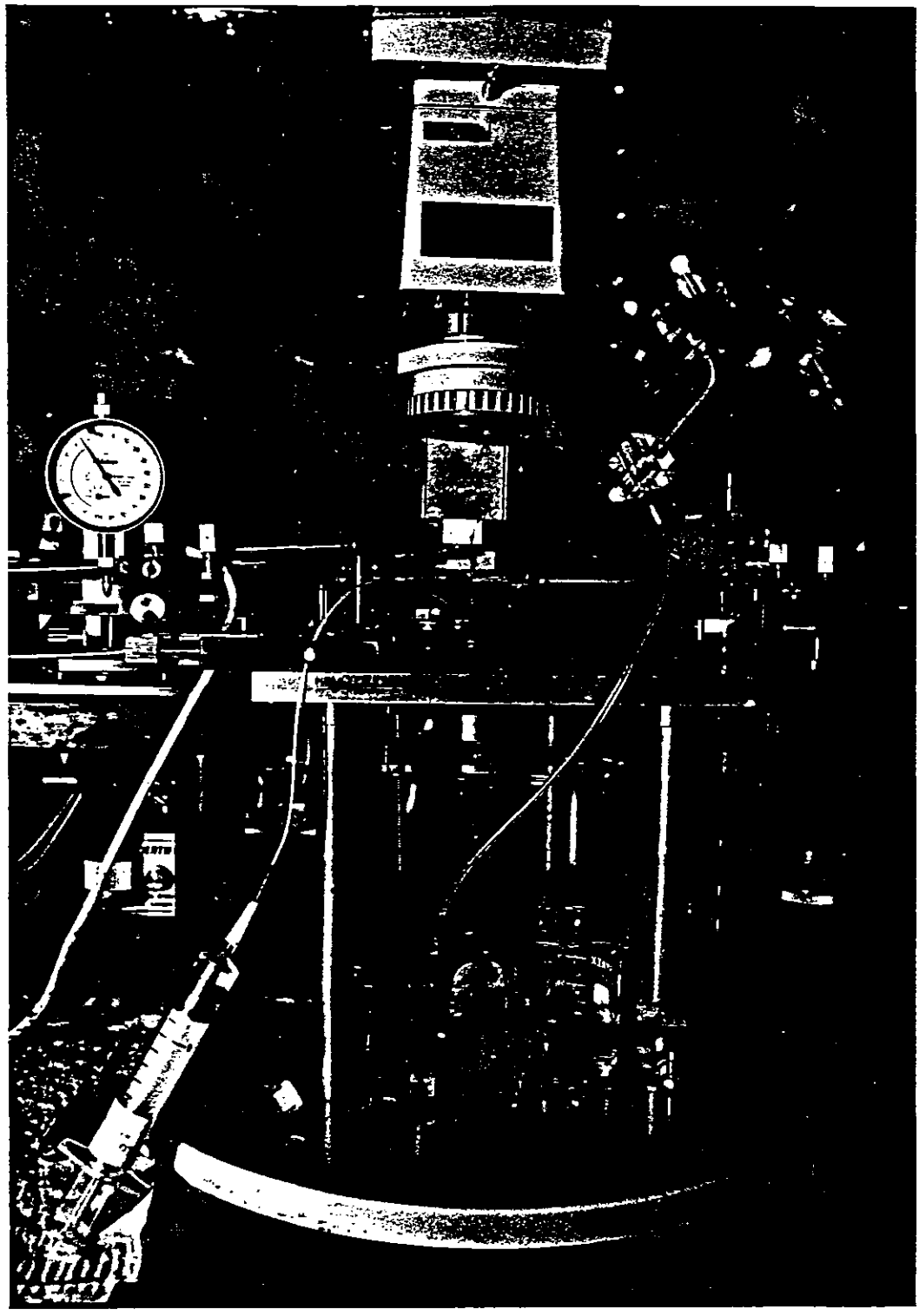

Fig. 56. Photograph of recording platform above which is seen a microelectrode held by a micromanipulator and the dissecting microscope.

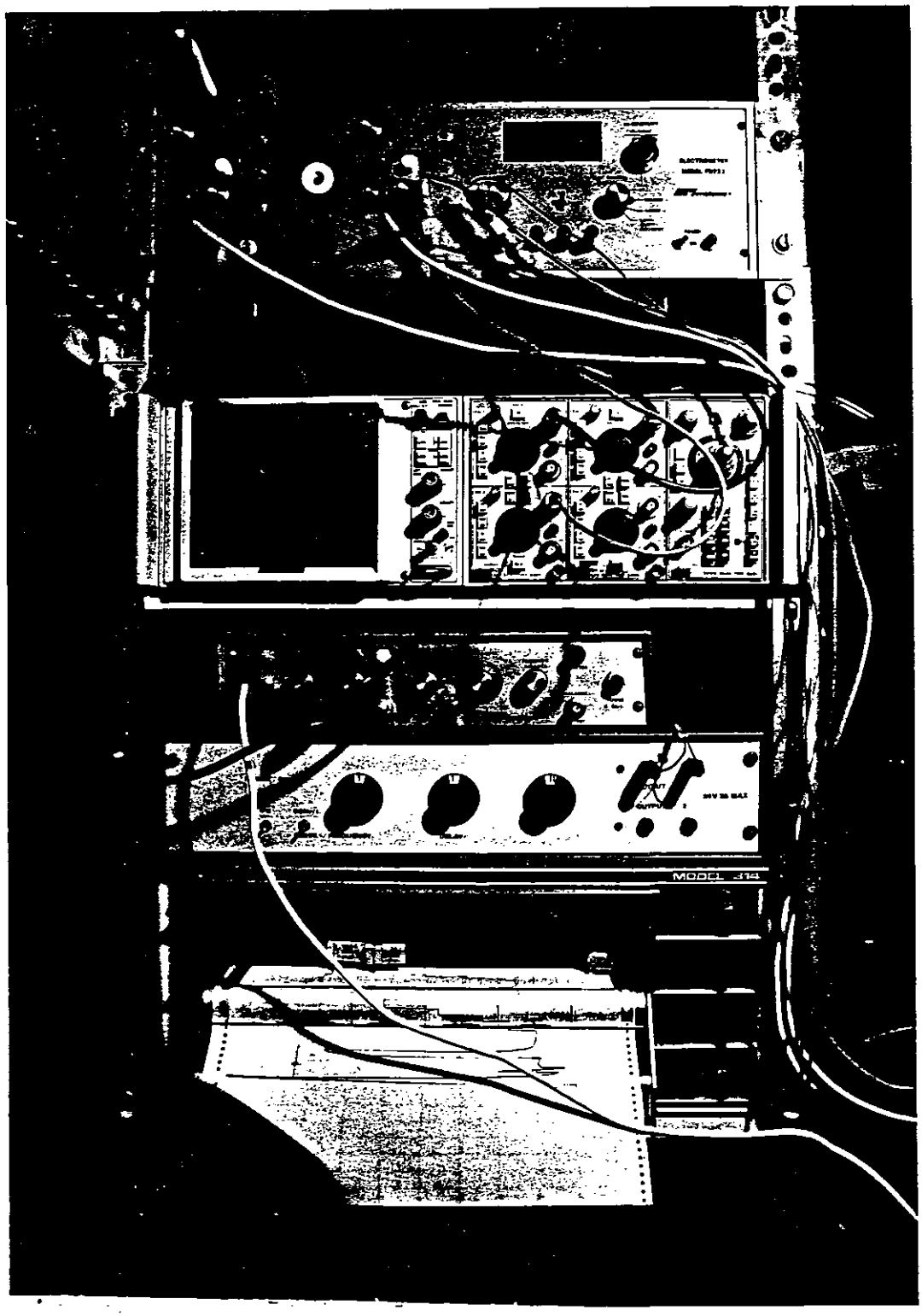

Fig. 57. Photograph of electronic equipment: electrometer, oscilloscope, amplifier, pulse generator and chart recorder (see text).

connectors (fig. 54). The active barrel was connected to channel A and the reference barrel to channel B, so that the output of the B channel monitored the membrane potential of cells whilst the differential output A-B represented the response of the ISM to ionic activity changes. The electrometer had the following manufacturers' specifications:

(i) Input impedance = $10^{15}\Omega$

(ii) Input capacitance = 1.0 pF

(iii) Input leakage current = 10^{-14}A maximum

(iv) Response time = 0.5 μsec 10-90%.

2. A 2-channel chart recorder (Bryans Model 300) for monitoring outputs (A-B) and (B) from the electrometer.

3. A 2 beam storage oscilloscope (Tektronix Model 5113), which was connected in parallel to the chart recorder.

4. A unity gain, high input impedance amplifier (WPI, model M701).

5. A delayed pulse generator (for operating a shutter in the light beam).

The 'earth' connection in the mains plug of each of these instruments was disconnected, and each device was earthed on its panel by connecting its chassis to an aluminium common earthing bar at the back of the Faraday cage. This 'bus' bar was in turn connected to the mains earth via a plug, thereby ensuring that no earth loops were created.

II.3 Calibration of ISMs

In order to calibrate the ISM a 'calibrating apparatus' was constructed from perspex to provide access for the ISM tip to a small chamber into which solutions of varying ionic composition could be passed and quickly changed (fig. 58). The outlet of this chamber was

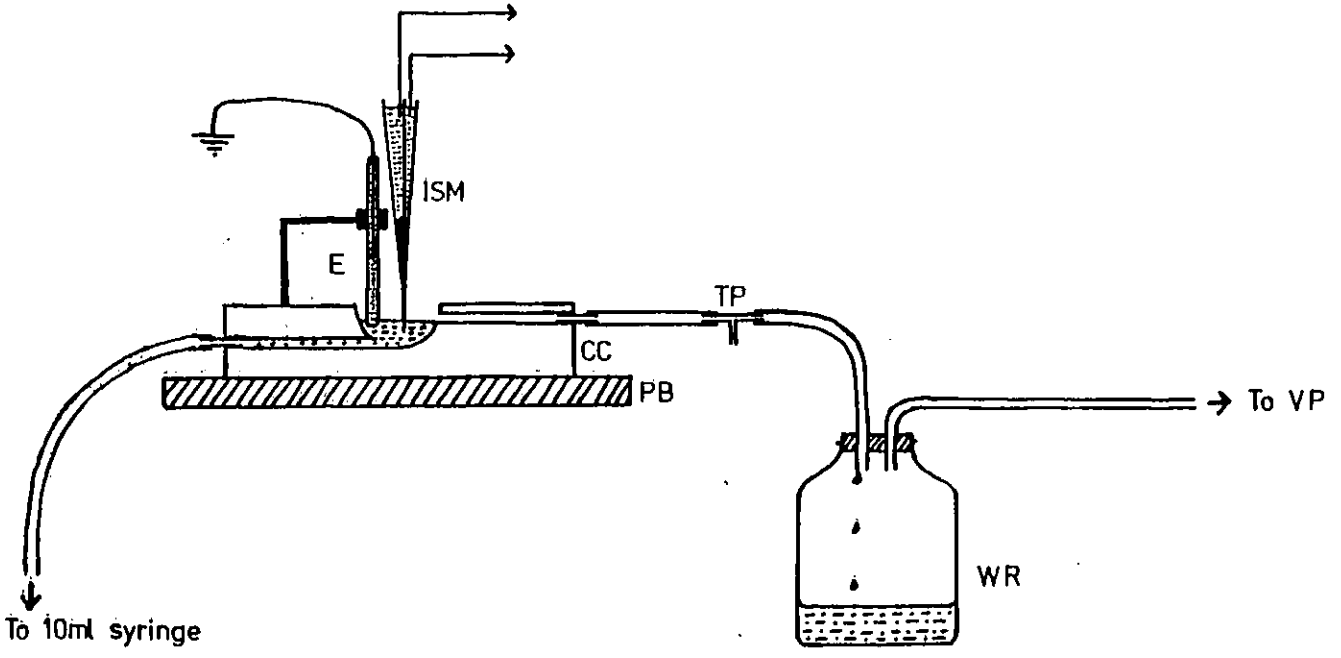

Fig. 58. Diagram of system for calibration of an ion sensitive microelectrode (ISM). E: earth electrode (Ag-AgCl/Agar-Ringer); CC: calibrating chamber; PB: perspex base-plate; TP: T-piece; VP: vacuum pump; WR: waste reservoir.

connected to a vacuum pump via a T-piece and 1ℓ glass bottle which acted as a vacuum chamber and collected the used solution. Solutions were passed into the chamber from a set of 10 ml syringes. The calibrating module was placed in the XY controls on the platform and the ISM was held tightly in a modified crocodile clip on the end of a brass rod clamped in the right-hand micromanipulator. Probes from the electrometer were mounted on the back of the platform. In order to firstly test the resistance of both barrels of the ISM the connections to the electrometer probes were made as described earlier (fig. 54). The solution of highest concentration from the series of calibrating solutions appropriate for the ISM being tested (see below) was then injected into the calibrating chamber from a 10 ml syringe. This solution in the chamber was 'earthed' by a glass capillary containing agar-Ringer (Appendix 1) and a Ag-AgCl contact connected to the chassis-earth of the electrometer (fig. 58). (This 'floating earth' system was devised so that the same 'earth' could be used both for calibrating ISMs and for the retina in experiments and thus potential readings from an ISM during an experiment could be reliably referred to the ISM calibration recorded on the chart paper.) The tip of the capillary was dipped into the solution and the resistances of the two barrels were measured using the constant current supply ('Electrode Test') switches on the electrometer. Deflection of either of the two switches passed a small current (1 pA) across the corresponding electrode thereby causing a voltage shift at the output of 1 mV per 1000 MΩ.

If the resistance measurements showed that the ISM conducted well in both barrels with stable potential readings and the resistances were within the normally expected range of values (see Results chapters), then the ISM was calibrated. A series of calibrating solutions was prepared for each kind of ISM (K^+ and Cl^-) and stored in 500 ml bottles

and 10 ml syringes in a refrigerator. Each series of solutions was of constant total ionic strength. The series of calibrating solutions for the different ISMs were prepared from 'Analytical Reagent' grade chemicals according to the formulae given in Appendix 2. To calibrate the ISM, solutions were passed through the calibrating chamber starting with the solution in which the primary ion for the ISM was most concentrated. 5ml of each solution was passed through the chamber by injection from a 10 ml syringe whilst the excess solution was removed in a controlled manner using the vacuum system (fig. 58). The last $\sim$1 ml of each solution was left in the chamber and the ISM's response to that solution was recorded on the chart paper. The responses of both barrels (channels A-B and B) were recorded simultaneously (fig. 54). After the experiment the ISM was re-calibrated to check that there had been no significant change in calibration during the course of the experiment (see Criteria for Selection of Results section II.7). Before the analysis of the experimental data, the calibration trace on the chart recording was converted to a calibration curve on a log-linear graph so that ionic activity measurements could be made from the experimental traces using this graph. Activities were derived from concentrations of the primary ion in the solutions by means of standard activity coefficients. (Because the solution in a given calibrating series were of constant total ionic strength the activity coefficient for the relevant ion was the same for all solutions of that series). For the calibration curve the potential seen by the ISM in the solution containing the highest concentration of primary ion was defined as zero potential. Examples of the calibrations of ISMs showing the raw data from the chart recorder and the corresponding calibration curves are given in fig. 59a,b for a K^+ ISM and fig. 60a,b for a Cl^- ISM.

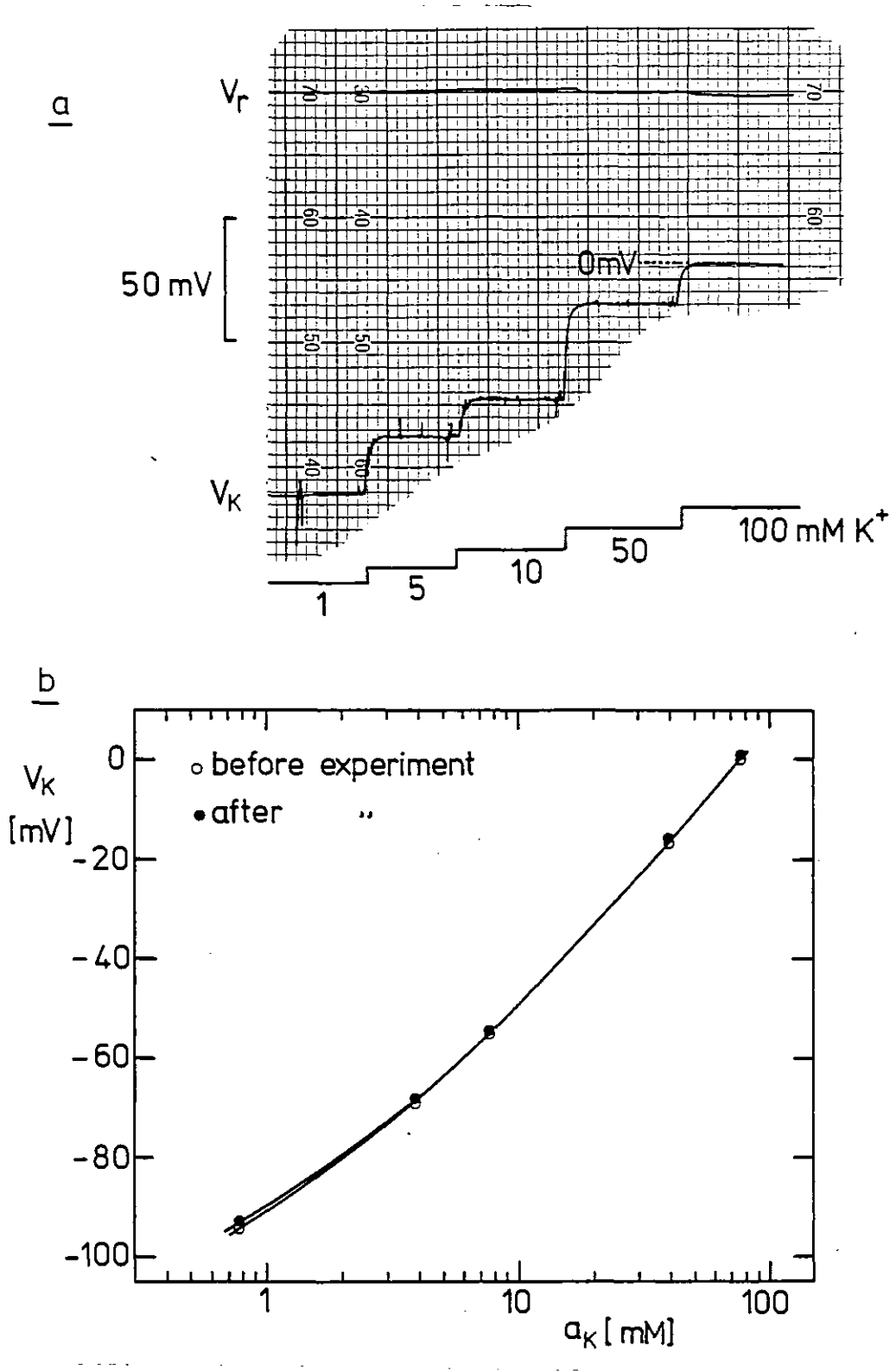

Fig. 59. a: calibration of a K^+ ISM and b: the resulting calibration curve. V_r is the potential seen by the reference barrel and V_K is the differential potential signal which is dependent on a_K.

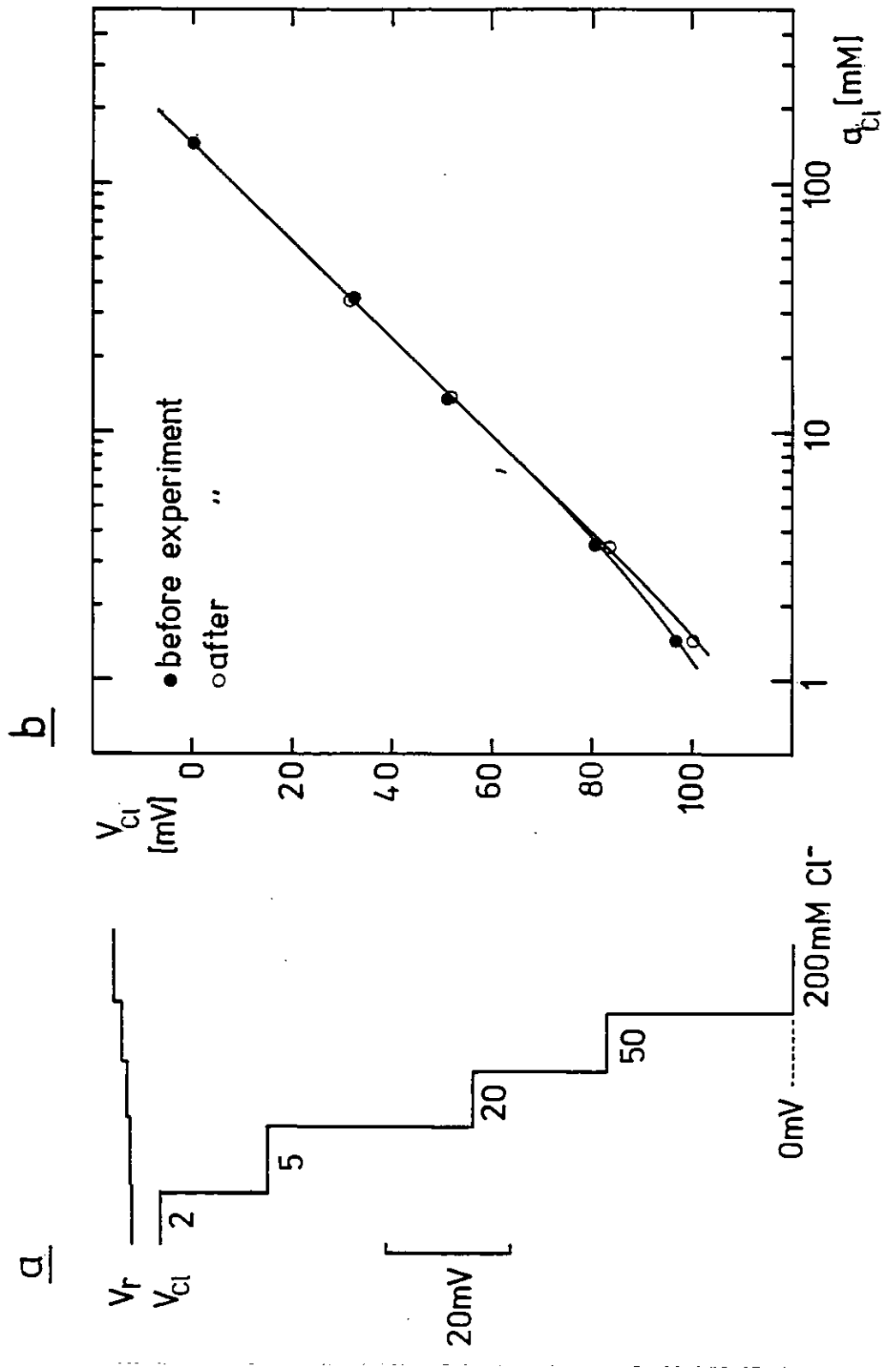

Fig. 60. a: Calibration of a Cl^- ISM and b: the resulting calibration curve. V_r is the reference barrel potential and V_{Cl} is the a_{Cl}-dependent potential.

Stability and test for possible light sensitivity of Ag-AgCl reference electrodes

A simple experiment was devised to test the stability of an electrolyte-filled glass reference microelectrode in which contact with the electrolyte was made via an Ag-AgCl wire. The experiment was also designed to test for any sensitivity to light of the potential seen by the Ag-AgCl wire. The reference electrode tip was placed in a bath of 100 mM KCl which was earthed and the potential seen by the electrode was recorded by taking readings from the electrometer at 1 minute intervals for a period of 53 minutes. During this period the light-stimulus was turned on and off several times. The results of this experiment are shown in fig. 61. It is seen that after the electrode has reached a steady state potential reading (8 minutes) it remains very stable (to within 0.5 mV in 45 minutes) and there is no variation of potential corresponding with the onset and offset of light.

II.3.i Interference and Selectivity - Characterisation of Orion and Corning LIX's for K^+

The degree of interference to the response of an ISM to its primary ion 'x' by an interfering ion 'y' is expressed by the selectivity coefficient k_{xy} in the Nikolsky equation (see Introduction Section I.8.i). The Nikolsky equation can be fitted to the calibration curve of an ISM by taking k_{xy} as a variable parameter to be empirically determined. A numerical method for doing this is given in the example of Appendix 3. The selectivity of an ISM for its primary ion against the main interferent is a characteristic of the liquid ion-exchanger. Before using a LIX ISM to determine the activity of the primary ion in an experimental situation, an ascertainment of the selectivity of the LIX against the main interfering ion to be encountered in the

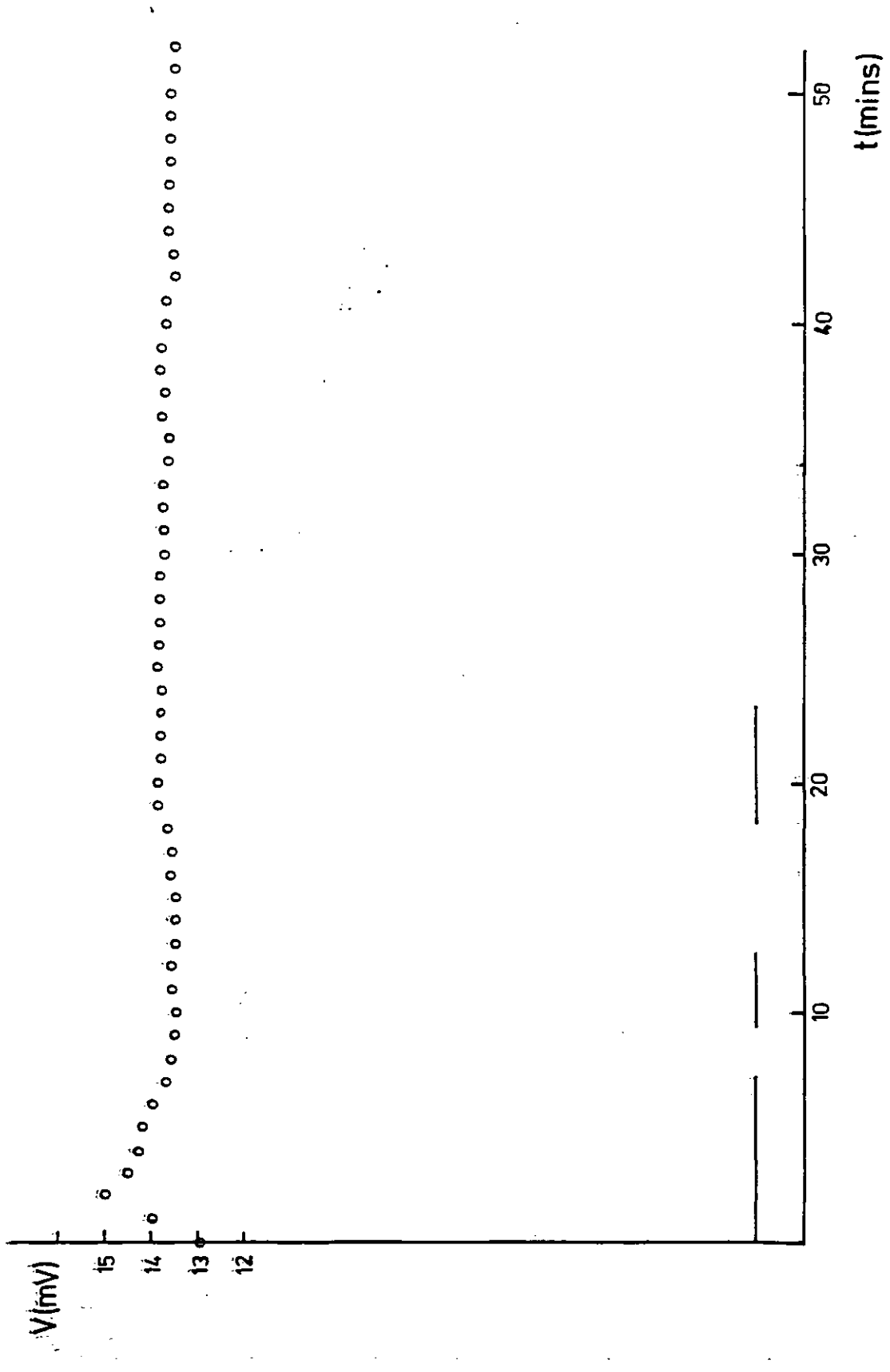

Fig. 61. Offset potential with respect to earth seen by a fine (high resistance) reference electrode, V, plotted against time, t. The bars above the abscissa represent the onset of light.

experimental situation would show whether the LIX was satisfactory for that purpose. The only LIX available when the technique for making conducting ISMs had been developed was that made by Orion for K^+ and Cl^-. Since this LIX had not been used widely, the selectivity had not been well established in any reports. Thus, the selectivity of the Orion K^+ LIX was determined against Na^+ as interferent by calibrating the ISM in four different series of solutions of various ionic compositions. The formulae for these calibrating solutions are given in Appendix 2. The value of k_{KNa} was calculated from the calibration curves in three different ways. The method used to determine k_{KNa} from the calibration curves is described in section I.9.v. The procedure for calibration of a K^+ ISM in the four series of solutions and making three determinations of k_{KNa} was repeated for twelve different ISMs. The information from the twelve graphs of calibration curves was compiled into a single graph of four calibration curves by calculating the mean and standard error values for all the corresponding points on the graphs. The resulting graph is shown in Appendix 2. The mean and standard error values for the three different determinations of k_{KNa} were also calculated and are as follows:

Method 1. KCl + 10 mM NaCl solutions:

$k_{KNa} = 0.40 \pm 0.06$

Method 2. KCl + 50 mM Na Cl solutions:

$k_{KNa} = 0.16 \pm 0.03$

Method 3. KCl + NaCl

Separate Solutions:

$k_{KNa} = 0.41 \pm 0.10$

Thus after the systematic determination of k_{KNa} for the Orion K^+ LIX, it was concluded that this LIX was not selective enough for K^+ over Na^+ to provide the basis for an ISM to measure a_K in retinal neurones. Even the most favourable estimate for k_{KNa} (= 0.16 ± 0.03) means that the ISM

would only be selective for K^+ against Na^+ by about 6:1 and in the extracellular environment of the neurones it might be expected that the ratio $(C_{Na}):(C_K)$ could be 10:1.

K^+ ISMs were finally made using the Corning LIX (Code 477317; kindly made available by H.M. Brown). Although the use of Corning liquid ion-exchangers for K^+ and Cl^- and their selectivities had been reported (e.g. Walker, 1971; Brown, 1976), the selectivity of the Corning K^+ LIX was determined in a similar way to that of the Orion LIX for comparison. k_{KNa} was calculated from the calibration curves in three separate ways for eight different ISMs (App. 2). The results in terms of mean and standard error values for k_{KNa} were as follows:

Method 1. KCl + 10 mM NaCl Solutions:

$k_{KNa} = 0.06 \pm 0.01$

Method 2. KCl + 50 mM NaCl solutions:

$k_{KNa} = 0.026 \pm 0.005$

Method 3. KCl + NaCl Seperate Solutions:

$k_{KNa} = 0.0088 \pm 0.0001$

These values compare very well with the value of 0.02 reported by Brown (1976). Thus, as shown previously by others, ISMs using Corning K^+ LIX are adequately selective for K^+ over Na^+ for intracellular measurements of K^+ activities. Following this characterization procedure, K^+ ISMs were routinely calibrated in mixed solutions of constant total ionic strength with K^+ being replaced by Na^+. This ensured that the effect of interference by Na^+ was already compensated for during the calibration and the experimental traces could then be referred to the calibration traces to determine ionic activity values.

II.4 The Optical Stimulator

A single beam optical system was constructed to provide light stimuli to the retina. The system consisted of a 150W tungsten-halogen

lamp LS, which was driven by a DC power supply (Gould, MG 24/8), and cooled by an electric fan. A pair of converging lenses L_1 and L_2 focussed the lamp filament onto a small hole at the centre of an iris diaphragm, ID (Fig. 62) An electromagnetic shutter S (Ledex) was positioned in front of the iris diaphragm and was driven by a delayed-pulse generator. Light from the hole in the iris diaphragm (regarded as a 'point source') was collimated into a parallel beam by an achromatic lens, L_3, and the beam directed into the Faraday cage. The spectral content and the illumination level of the beam were controlled by a linear interference filter (400-700 nm) and by a set of neutral density filters covering a 4 log unit range. A circular stop, O, placed before the filters acted as the object to be focussed on the retina. The beam was deflected upwards by a prism P (figs. 62, & 63) placed in a holder on the base of the micromanipulators, and a de-magnified image of O was formed on the surface of the retina by a low power (x3) microscope objective (figs. 62 & 63), which was held just underneath the hole in the centre of the platform by an objective holder (from an old microscope) so that its position could be adjusted. For routine stimulation of the retina, light flashes of about 620 nm wavelength were used. The illumination level of these flashes were 1 $\mu W/mm^2$, as measured by a digital radiometer (Macam Model PR 3010). The optical densities of the neutral density filters were also confirmed for white lights using this radiometer.

II.5 The Atomising System

In some experiments, it was necessary to apply a chemical to the retina. Since it was desired not to treat the retina with any artificial salines, this application was made by atomising the chemical onto the retina from a concentrated stock solution. The atomiser consisted of a broken micropipette held vertically in a clamp, with

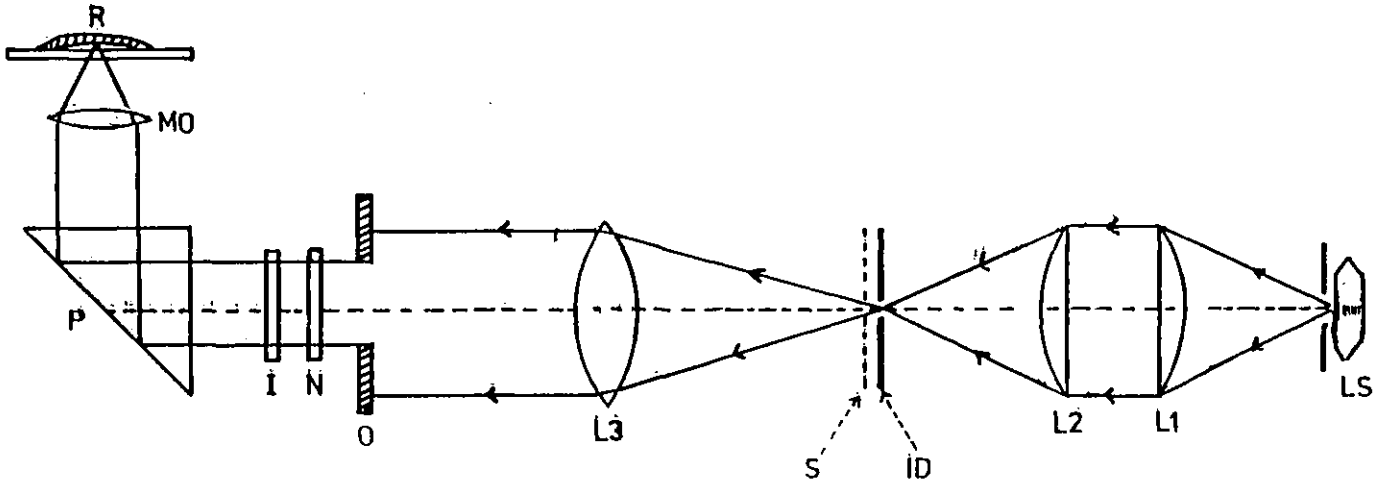

Fig. 62. The optical system. LS: light source; L1, L2: converging (focussing) lenses; ID: iris diaphragm; S: shutter; L3: collimating lens; O: circular stop; N: neutral density filter; I: linear interference filter; P: prism; MO: microscope objective; R: retina.

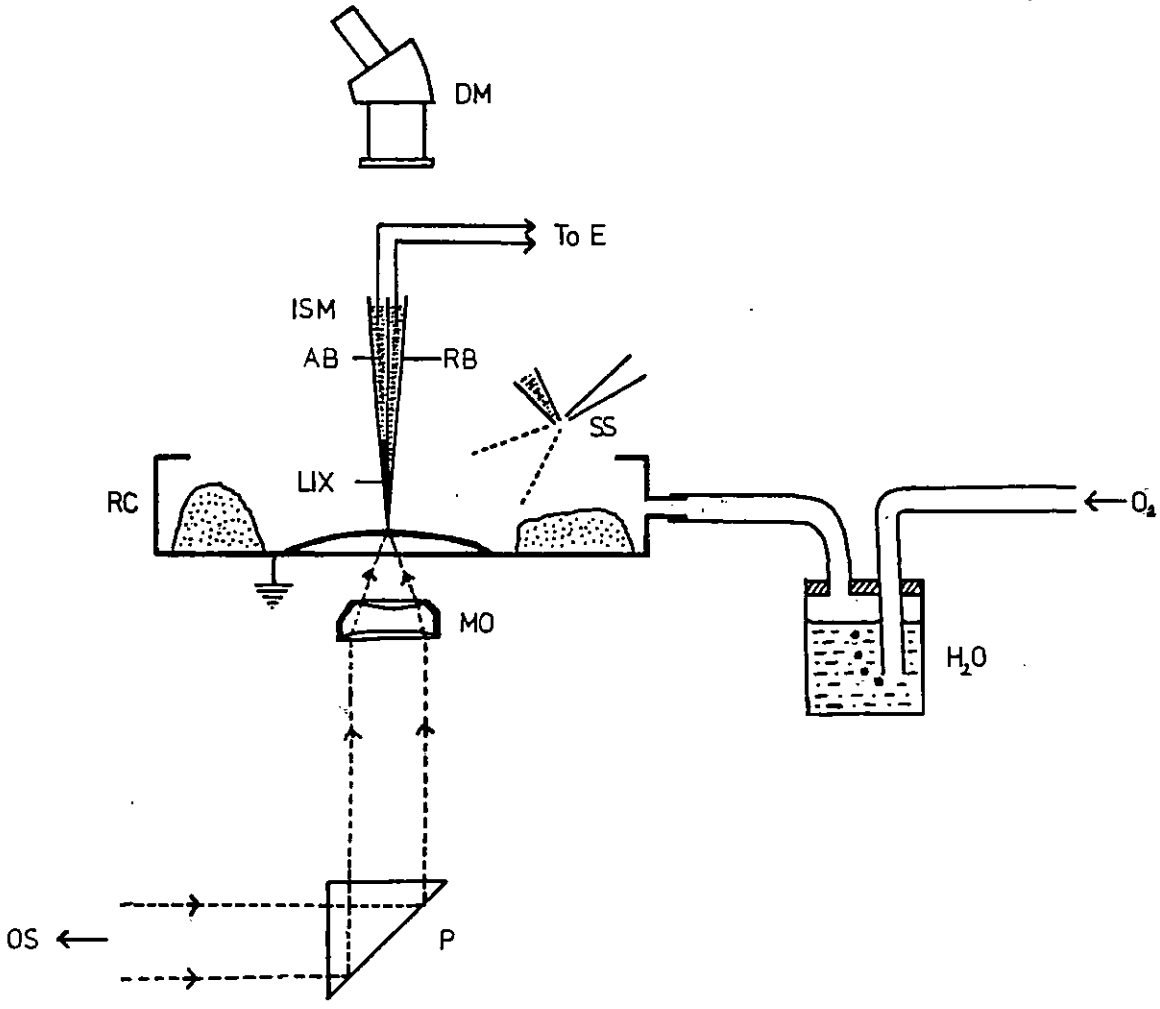

Fig. 63. Set-up for recording from retina with an ion-sensitive microelectrode (ISM); DM: dissecting microscope; E: electrometer; AB/RB: active/reference barrel; SS: spraying system; RC: recording chamber; LIX: liquid ion-exchanger; MO: microscope objetive; P: prism; OS: optical stimulator. Rate of O_2 supply was adjusted by a regulator.

its end connected via a plastic tube to a small amount of the stock solution (fig. 64a; fig. 56). The end of a pasteur pipette was drawn in a flame and the tip of this was held perpendicular to the broken micropipette in a right-angle clamp (fig. 64a). The large end of the pasteur pipette was connected to a cylinder of compressed air via a T-piece, valve and regulator, in that sequence. The assembly of 'glass' capillaries was held above the recording chamber (fig. 63; fig. 56). By applying an air jet at a pressure of about 5 lb/sq.in, a low pressure region was created at the tip of the vertical electrode which caused the solution to be sucked up and atomized onto the retina.

The atomising system was calibrated by spraying a solution of 2.5M KCl (normally used for filling ordinary microelectrodes) onto microscope slide cover slips for 1, 2 and 5 seconds at a time, and determining the weight of KCl salt drying on the cover slips. This was repeated 6 times, the results averaged and plotted as shown in figure 64b. The atomiser sprayed linearly for the first 2 seconds or so of the application of air pressure. Most sprays were in fact for 2 seconds or less. Assuming that the retina is a flat disc of 8 mm diameter and 0.4 mm in thickness, the calibration graph can be used to establish that the spraying of a 1M solution for 1 second results in an effective intra-retinal concentration of about 25 mM, assuming that the amount of solution sprayed spreads uniformly throughout the retina. In other words for a 1 second spray, the effective final intra-retinal concentration of a given chemical solution is 1/40 of the concentration of the stock solution.

II.6 Experimental Procedures

An ISM was manufactured, as described in section II.1, and calibrated a number of times until two subsequent calibrations, separated by some 20 minutes, were exactly the same; this was taken to be a sign

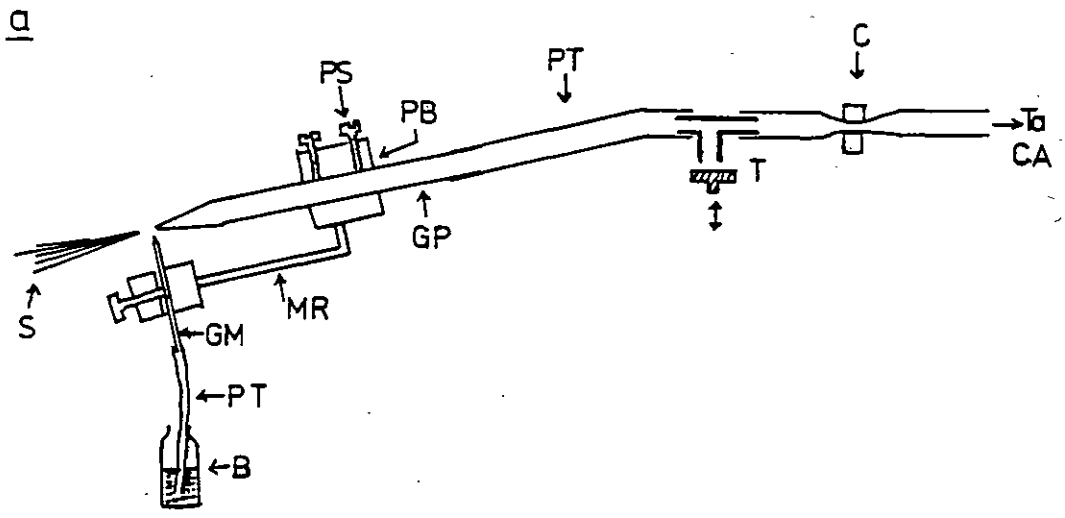

Fig. 64. a: spraying system for application of chemical solutions to the retina. CA: compressed air source:, C: clamp; T: tap to turn on spray; PT: plastic tubing; PB: perspex block; PS: plastic screws; GP: glass pipette; MR: metal rod; GM: glass micropipette; B: bottle containing solution to be sprayed; S: fine spray aimed at retina.
b: Results of calibration of spraying system. Graph shows mass, M, of KCl from solution sprayed against time, t, of spraying. Each point represents an average from 6 repeated trials.

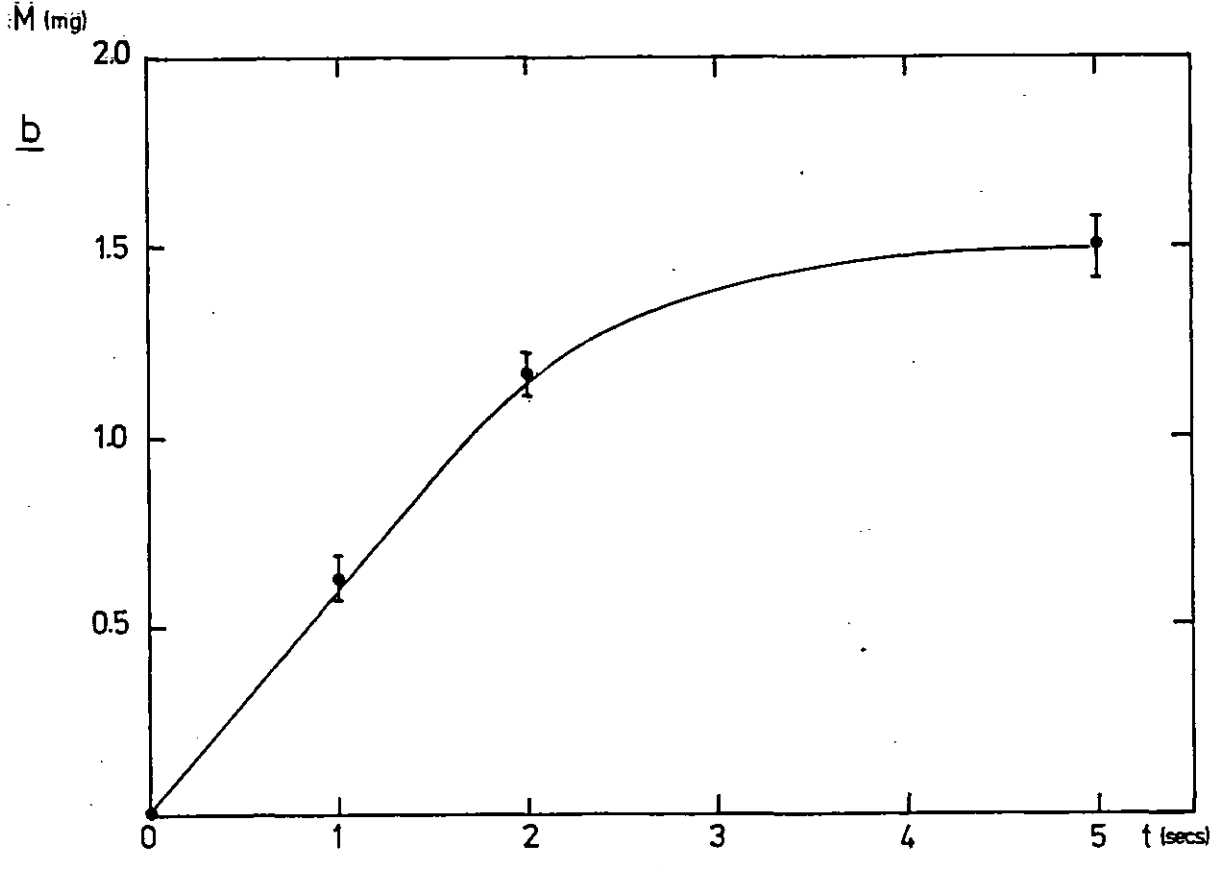

of a stable ISM. A fish was then put in to a large bin full of aerated, cold tap water and kept in the dark for 50-60 minutes. All experiments were carried out on the retina of the roach (Rutilus rutilus), which belongs to the family Cyprinidae, which also includes the goldfish, the carp, the tench, the rudd and the bream. At the end of the dark-adaptation period, the ISM was calibrated again to make sure that it still calibrated as previously, and if so, the fish was taken out of the dark, and killed under dim red light in the darkened recording room. One eye was then removed, cut around equatorially, and the top half consisting of the cornea and lens discarded. The retina was peeled off the inside of the eye-cup by cutting the optic nerve, and placed receptor-side upwards in the centre of a 10 cm square perspex recording chamber. The purpose of dark adaptation was to cause the pigment epithelium to withdraw from the neural retina, so the latter could be peeled off without damaging the photoreceptors. In the recording chamber, the isolated retina was surrounded by a crescent of Kleenex that had been saturated with distilled water. The retina was earthed on one side using the same Ag/AgCl-Agar earth electrode as that used for the calibration of the ISM. The chamber was gassed continuously with moist oxygen (fig. 63). These precautions ensured that the isolated retina remained in good functional order for at least one hour. The retina was stimulated with light flashes entering the recording chamber from underneath, so the direction of light entry into the retina was as in the normal eye. The electrode was then advanced onto the retinal surface under direct microscopical control, and recordings began.

II.7 Criteria for Acceptance of Results from Intracellular Recording Experiments

The ISM technique is susceptible to several possible sources of

error. Following each recording session, therefore, the results, recorded on chart paper, were analysed, and the following criteria were used to evaluate and select the results for final acceptance:

1. Calibration of ISM must correlate before and after experiment to within 5 mV at all points, to ensure that the calibration of the ISM did not change during the experiment;

2. Extracellular levels of potential (B) and ionic activity (A-B) must be steady to within 2 mV, to ensure that sudden and transient changes in ISM calibration did not occur due to tip blockage etc.;

3. Deflection of traces on penetration of cell should be sharp - a sign of a 'healthy' or undamaging electrode penetration;

4. Intracellular levels of potential and ionic activity must be clear and steady for at least 30 seconds; although cells that could be maintained for up to 20 minutes did not show significant changes from the initial readings;

5. Magnitude of normal membrane potential should not be less than 15 mV unless depolarising agents were used; this avoided counting cells that might have been damaged;

6. There should be a good correlation between membrane potentials measured by the ISM and those measured by an ordinary microelectrode in the same retina.

CHAPTER III

POTASSIUM ACTIVITY MEASUREMENTS

Measurements of intracellular K^+ activity, a_K^i, in horizontal cells of the roach retina and of extracellular K^+, a_K^o, around these cells were made using double barrelled K^+ ISMs. In this chapter the results obtained from these measurements are described.

III.1 Derivation of Results from the Recorded Traces

The chart recording from the beginning of an experiment shows the calibration of a K^+ ISM followed by traces produced when the ISM touches the surface of the retina and commences to record the extracellular K^+ activity, a_K^o, by means of the a_K-dependent voltage V_K (fig. 65a). In the presentation of the results of this study, the K^+-sensitive differential potential is denoted by V_K and the membrane potential (the electrical potential of the inside of the cell with respect to the outside) at any time is represented by V_m, whereas the notation E_m exclusively represents the resting membrane potential. Similarly for the Cl^- results, where the Cl^--sensitive potential is denoted by V_{Cl}. The V_K trace (representing a_K) quickly reaches a steady state value which is used to determine the value of a_K^o. The level of the V_K trace is referred to the calibration trace to obtain a voltage reading, V_K^o. This reading of V_K^o is then referred to the calibration curve of the ISM to determine the value of a_K corresponding to V_K^o, which is a_K^o. This procedure is shown schematically in fig. 65a,b. The chart recording of an ISM penetrating and remaining inside a horizontal cell for some time enables the intracellular K^+ activity, a_K^i, for that cell, to be determined in a manner similar to that for a_K^o. The potential difference between the levels of V_K inside and outside the cell, ΔV_K^i, is measured and the voltage $(V_K^o + \Delta V_K^i)$,

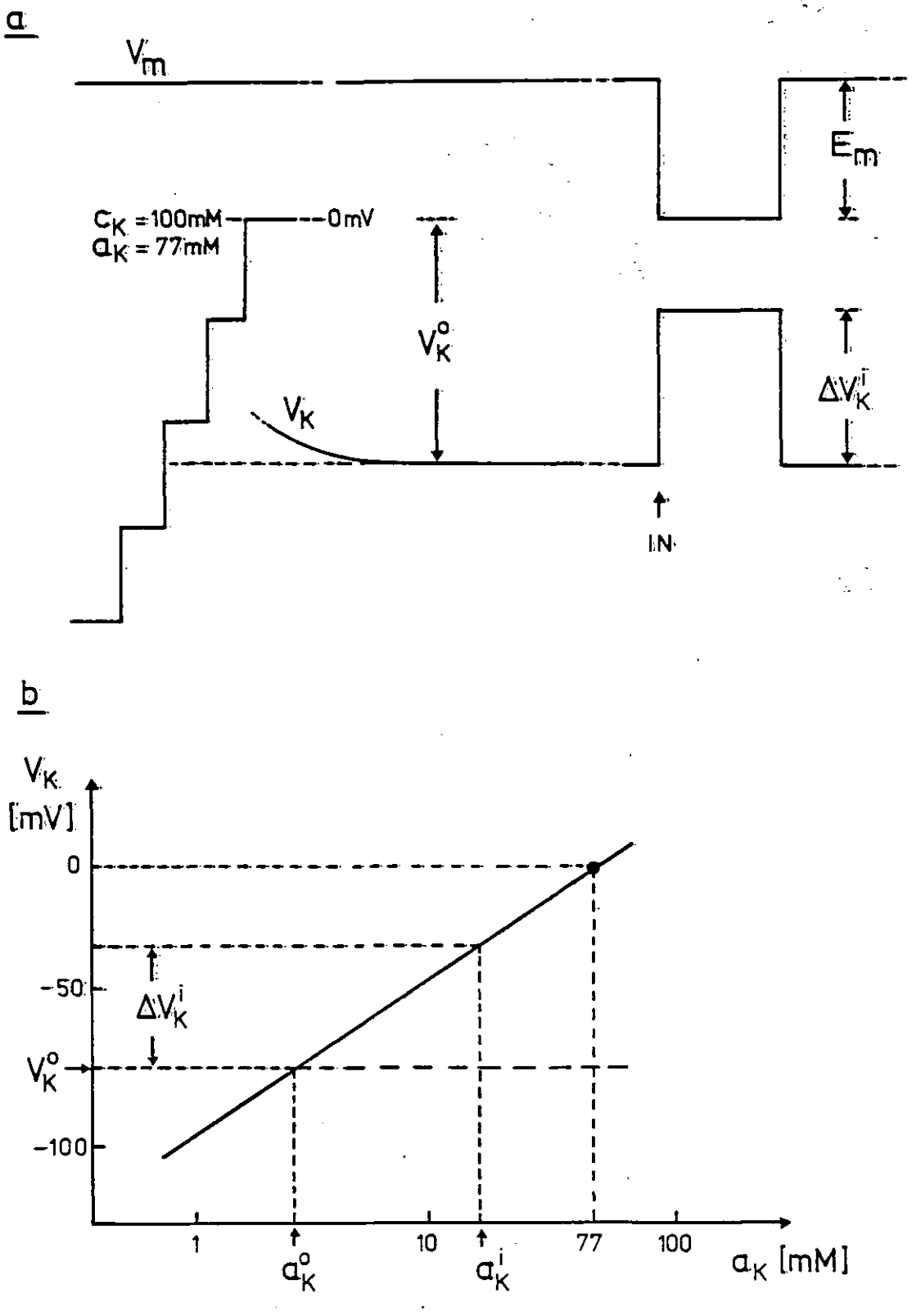

Fig. 65. a: Schematic diagram showing how V^o_K and V^i_K are determined from the ISM calibration trace and the recording of the extracellular potential and a cell penetration (starting at 'IN'). V_m is the reference potential and V_K is the K^+-sensitive potential.
b: Determination of the intracellular level of a_K by the calibration curve (see text).

when referred to the calibration curve yields the value of a_K corresponding to this voltage, viz a_K^i (fig. 65a,b).

The value of Em for the horizontal cell is read directly from the hyperpolarising deflection of the reference barrel, V_m, trace upon penetration of the cell (fig. 65a). Thus when a_K^i and E_m has been determined for a particular horizontal cell, it remains to calculate the value of the potassium equilibrium potential, E_K, for that cell. The value of E_K is computed from the corresponding values of a_K^o and a_K^i and the slope factor, 58 mV / tenfold change in a_K^i, derived from the Nernst equation (see equ. 11, p 73 et seq.), using the relation:

$$E_K = 58 \log_{10} \frac{a_K^o}{a_K^i} \quad (mV) \qquad (22)$$

When E_K has been determined the value of E_K is compared with that of E_m, so that the possible role of K^+ in the generation of the electrical responses of the horizontal cells can be evaluated.

Tables 3 and 4 show the results of a_K and E_m measurements on L_1- and C_b-type horizontal cells, respectively, which were selected according to the criteria described in chapter II, section 7. This means that the great majority of actual recordings of cell penetrations were rejected on these grounds in order to obtain a final list of results which were reliable. The results are presented in the format of a list composed of groups of cells which were well-penetrated and held for each ISM. The first column gives the number of the ISM with which the recordings were made. The second and third columns give the resistances of the reference barrel and ion-sensitive barrel respectively for that ISM. The fourth column gives the value of a_K^o which is pertinent to all the cells for a given retina which are numbered in the fifth column. The next two columns give the

values of resting membrane potential, E_m, and intracellular K^+ activity, a_K^i, measured by the ISM. The next column gives the values of K^+ equilibrium potential, E_K, for these cells, calculated as described above (eqn. 22). The last column shows the relation between E_K and E_m for each cell expressed as the difference value $E_K - E_m$. This value was found to be always negative so that for horizontal cells in the roach, E_K is always more negative than E_m. Table 3 comprises results from 102 L_1-type horizontal cells and Table 4 12 C_b-type cells. The results for the C_b-type cells came from the same retinae as those for the L_1-type cells but good penetrations of C_b-type cells were much more difficult to obtain.

III.2 Extracellular K^+ Activity Measurements

An actual recording from the beginning of an experiment showing the calibration of the ISM followed by the ISM touching the retina and recording the extracellular K^+ activity is shown in fig. 66. It can be seen that the a_K-sensitive V_K trace quickly reaches a steady state value and this is used to calculate a_K^o as described above (see fig. 65). It was found that a_K^o did not change significantly throughout the horizontal cell layer. Since on leaving a cell the V_K trace always returned to the same level as that before penetration a_K^o had the same value on both sides of and throughout the horizontal cell layer (fig. 67). Further it was found that a_K^o did not increase by more than 10% of its original value throughout the duration of an experiment (40-60 minutes) (fig. 68). In appendix 4, it has been shown that an increase of 10% in the extracellular activity of an ion 'x' will cause a change in the corresponding E_x of only 2.4 mV, for a given value of a_x^i. The value of a_K^o was monitored continuously during these measurements, and any slight changes in time were taken into account in calculating a_K^i and E_K (fig. 65a,b).

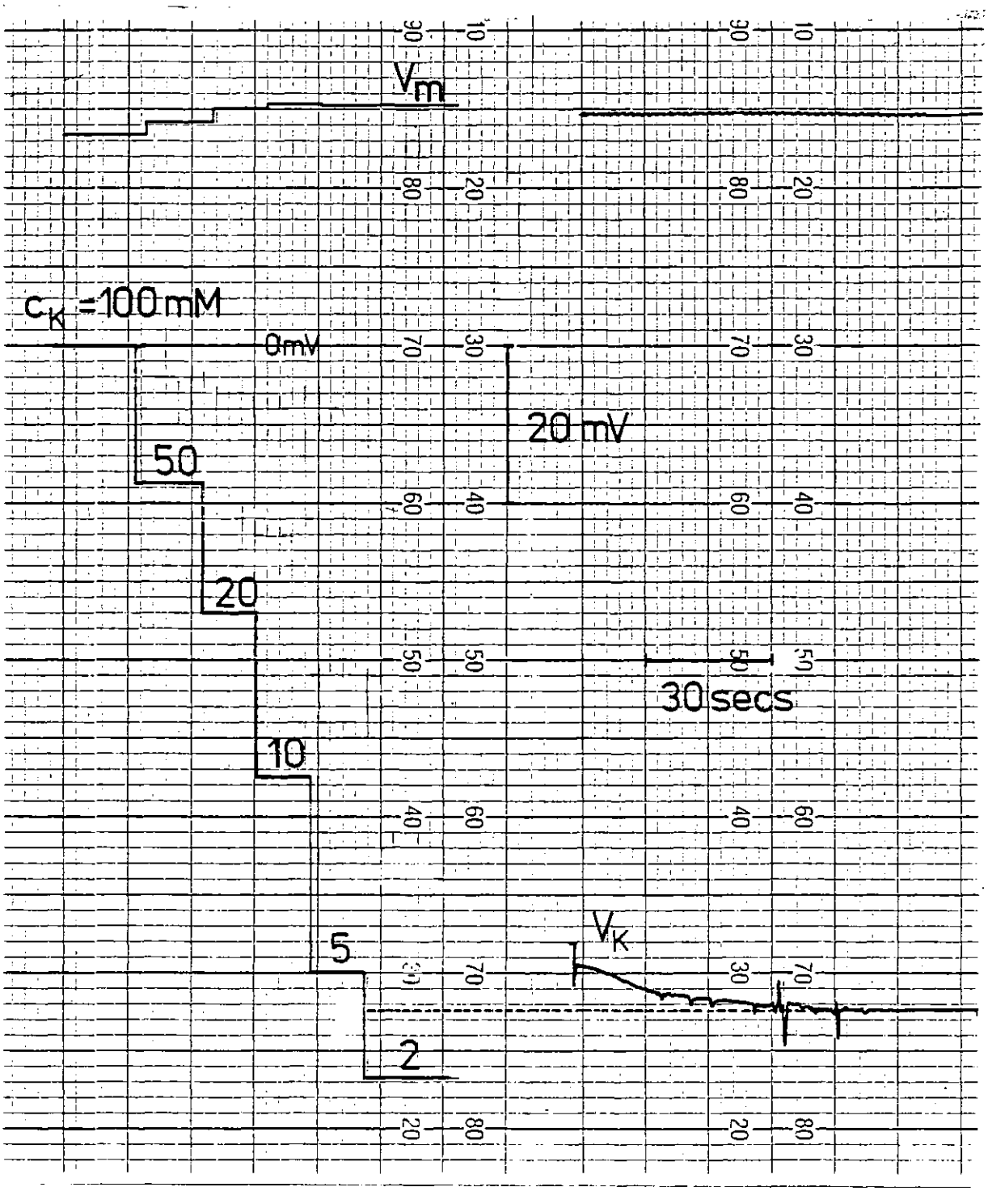

Fig. 66. Raw data from the chart recorder at the beginning of an experiment. The calibration of the ISM showing the concentrations of K^+ at each step is followed by the response of the ISM as it touches the retina.

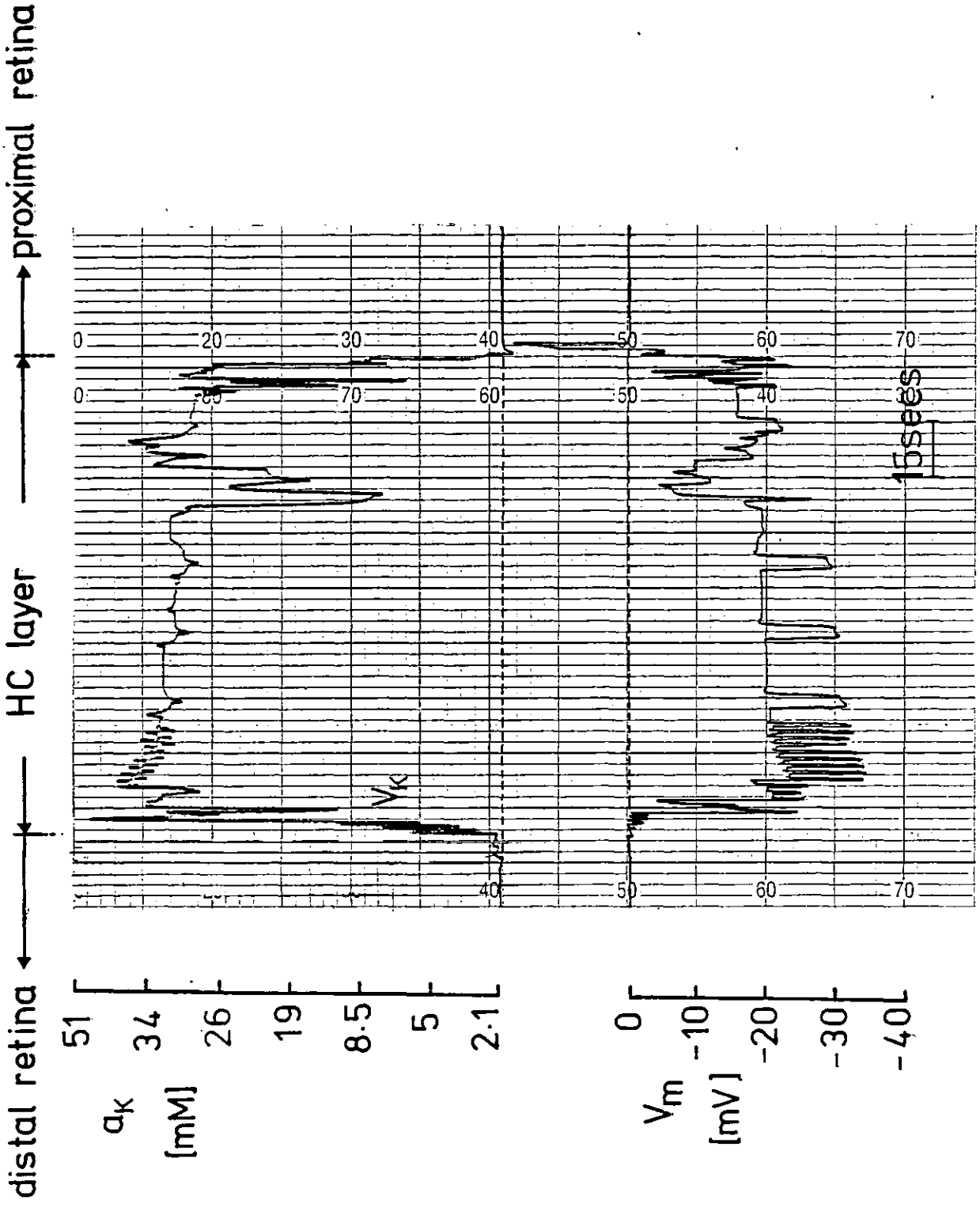

Fig. 67. Recording from the retina as the ISM is advanced through the horizontal cell (HC) layer showing that the extracellular levels of a_K and V_m are the same on both sides of this layer.

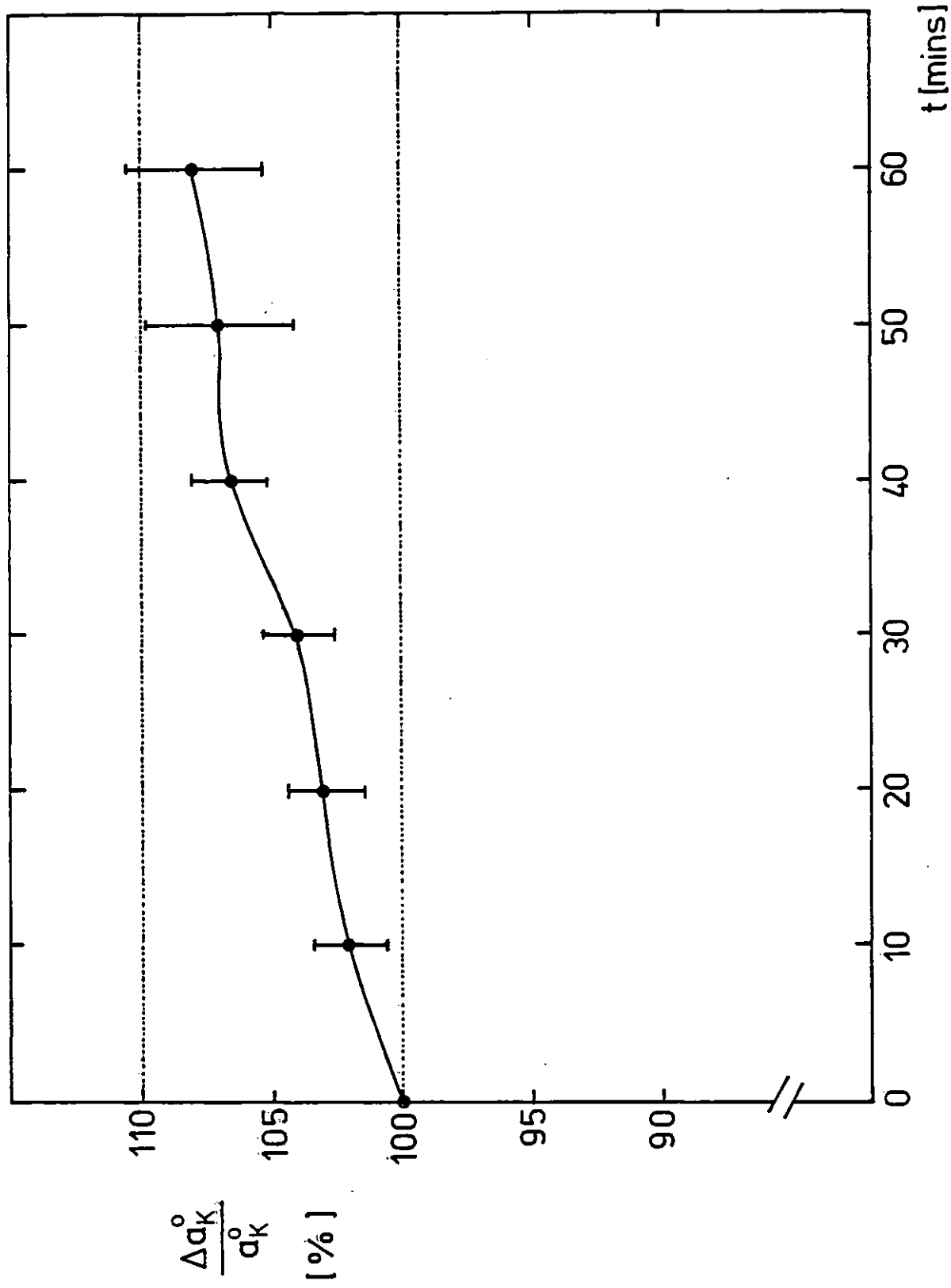

Fig. 68. Graph showing increase of a^o_K (as a % age of the original value) with time. Results are averaged from measurements of a^o_K during 10 experiments. Broken lines represent original a^o_K and 10% increase in a^o_K.

The frequency distribution of a_K^o obtained from 25 retinae is shown in fig. 69 by means of a histogram divided into intervals of 1 mM. This interval is appropriate because the a_K^o were estimated to one significant figure after the decimal point. The interval to the immediate right of an integer x contains results with values from x to x + 0.9. The mode of the a_K^o distribution occurs at the same interval as the mean value of 3.4 mM (Table 5, section III.9). The distribution is almost symmetrical with only a very slight tendency towards higher values than the mean showing that the median is also close to the mean and mode. Further the distribution is a fairly narrow one with most of the results quite close to the mean value.

III.3 Intracellular K^+ Activity Measurements

The penetration of an L_1-type horizontal cell with a K^+ ISM is shown in fig. 70. The upper trace shows K^+ activity which has been calculated from the V_K trace and ISM calibration. The lower trace shows the electrical potential measurement obtained from the reference barrel of the ISM, which was recorded simultaneously with the activity signal. Initially the K^+ ISM measures a_K^o (about 3 mM) and the external potential (0 mV) which was used as the reference level from which to measure E_m. The ISM then penetrated the horizontal cell (at the point marked 'IN') seen by the rapid deflections in both traces which quickly reached new levels, the E_m being about -35 mV and the intracellular a_K being about 90 mM. As soon as the ISM was in the cell, hyperpolarising responses to (red) light flashes were seen which were just over 10 mV in magnitude, and corresponding deflections were seen in the a_K trace. The transient deflections seen in the a_K trace at times corresponding to the onset and offset of light most probably arise as the result of the difference in time responses between the

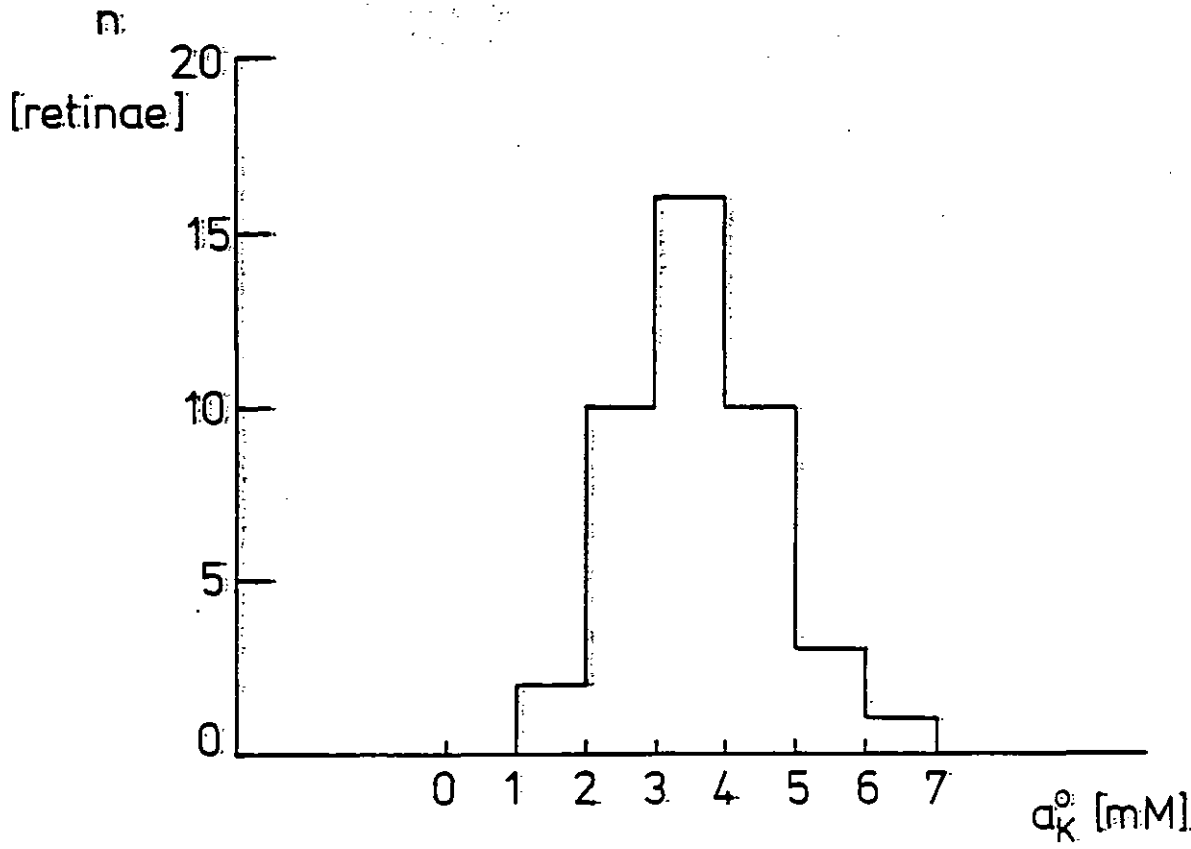

Fig. 69. Histogram of frequency distribution of a^o_K values obtained from 25 retinae.

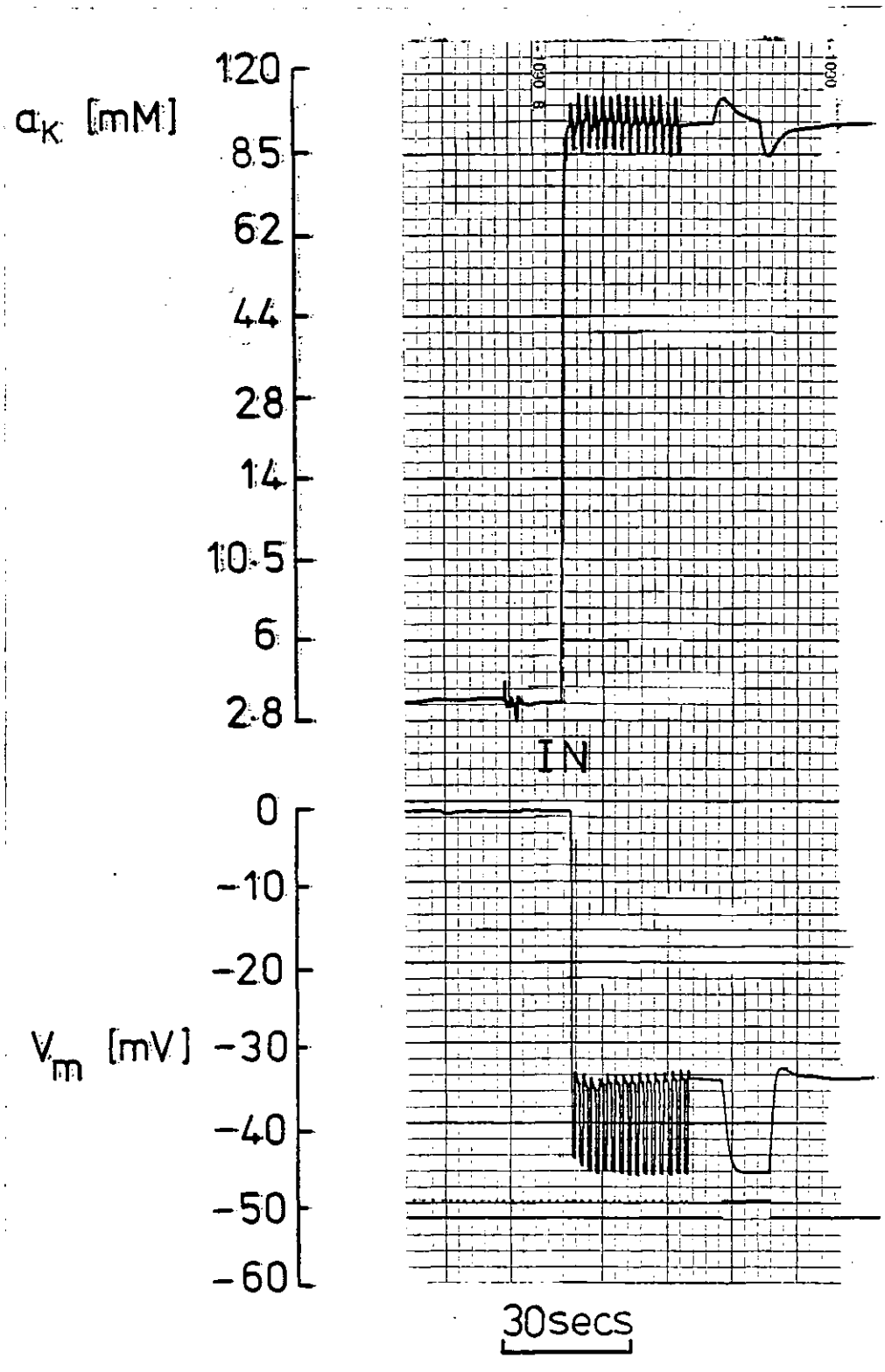

Fig. 70. Chart recording showing penetration of an L_1-type horizontal cell with a K^+ ISM. Upper trace is the K^+-sensitive potential and lower trace the reference (membrane) potential.

two barrels A and B of the ISM. This causes a transient artefact in the differential (A-B) response whenever there is a fast change in the channel B response. A mathematical analysis to describe the nature of this differential time response artefact is derived in Appendix 5.

In order to test that the electrometer was subtracting the channel B (reference barrel) signal from the channel A (active barrel) signal perfectly to produce the ionic activity-dependent signal 'A-B', a simple experiment was performed. A double-barrelled microelectrode was constructed using 1 mm diameter filamented glass capillary tubing for both barrels. Each barrel was then filled with 2.5 M KCl solution, connected to the electrometer as normal and used to record from several horizontal cells in a retina as in a normal experiment. It was found that when the electrode tip made a good penetration of a horizontal cell so that both barrels (channels A and B respectively) were recording the same electrical response, the output of the differential channel 'A-B' did not change by more than 0.5 mV. During the response of the cell to sustained light stimulation the differential reading remained constant (fig. 71). Thus, there were no discernable artefacts due to a possible imperfect subtraction of B from A, and the electrometer's electronic subtraction was reliable.

A histogram of the distribution of a_K^i values for L_1-type horizontal cells is shown in fig. 72, in which the abscissa is divided into intervals of 10 mM. The intervals are such that results having the value of the number to the immediate left of an interval are contained within that interval as is the case in all subsequent histograms. The mean value of a_K^i obtained from 102 cells is 57±2 mM. This distribution of a_K^i values is less regular than the a_K^o distribution, but it shows a distinct peak in the region of the mean. For C_b-type cells the mean value of a_K^i was 54±6 mM (Table 5).

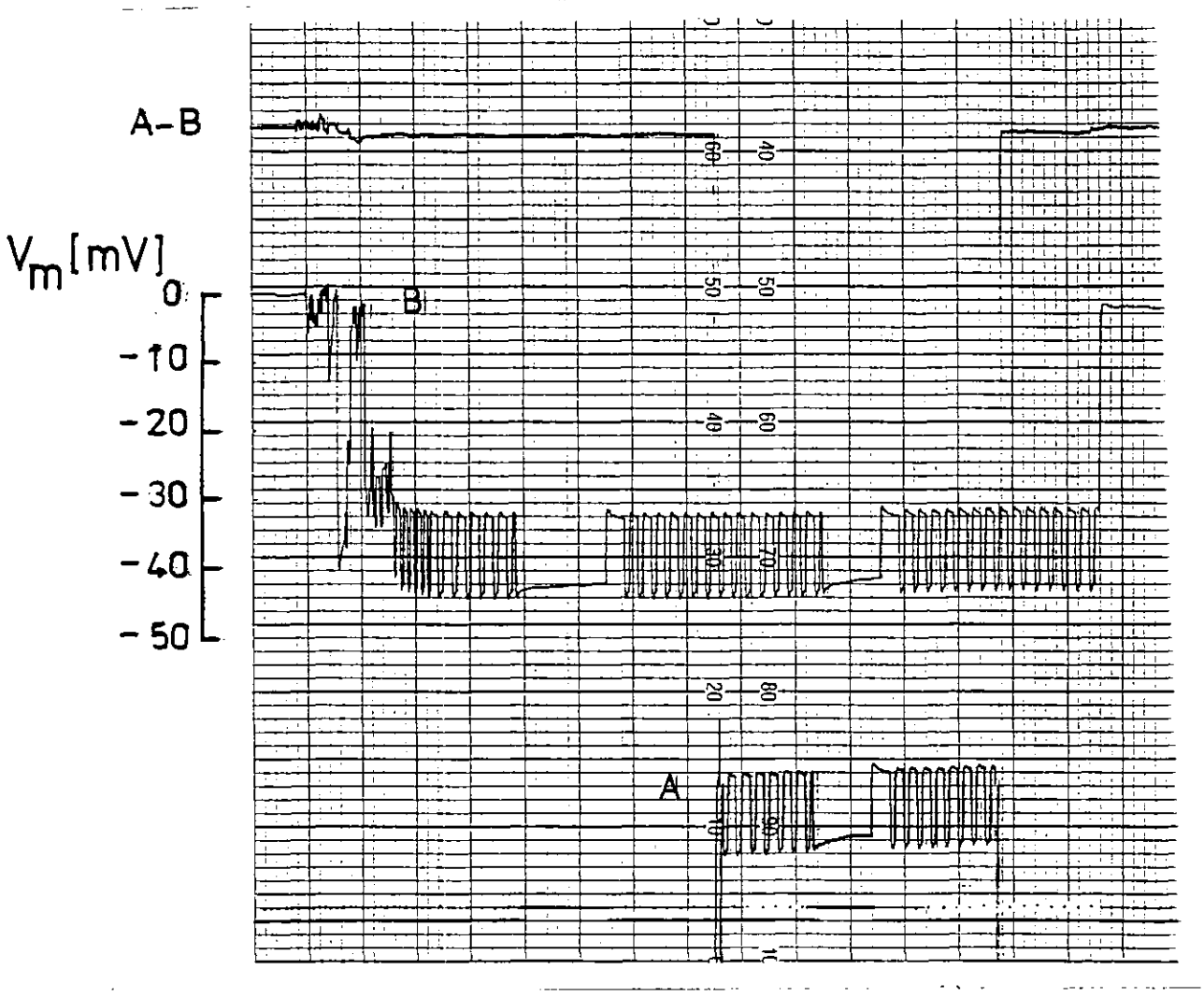

Fig. 71. Chart recording from experiment with "double reference-barrel" microelectrode to investigate the electrometer's subtraction of channel B from channel A. The penetration of an L_1-type horizontal cell is shown by the channel B (lower) trace and hyperpolarising responses to flashes to red light are seen whilst the differential output A-B is steady. Switching to channel A shows that both barrels of the electrode are recroding the same electrical potential changes. Switching back to the output A-B gives a steady response showing that there is no discernable error in the electrometer's subtraction of the response of channel B from that of channel A.

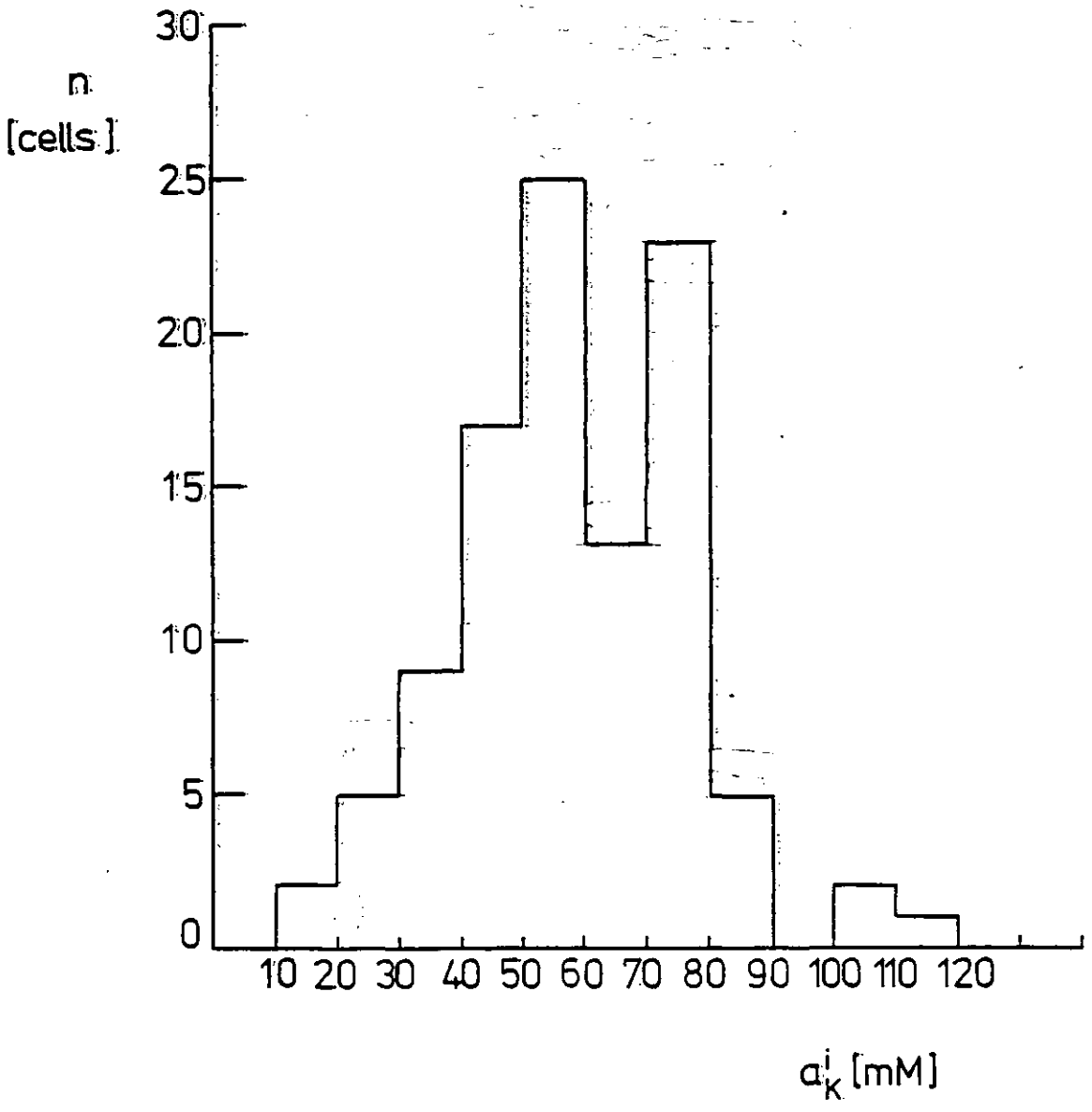

Fig. 72. Histogram of frequency distribution of a^i_K values obtained with K^+ ISMs from 102 L_1-type horizontal cells.

III.4 Distribution of E_K

For each horizontal cell from which a good recording was obtained, the value of E_K was calculated as described in section III.1. A histogram of the distribution of E_K values for 102 L_1-type cells obtained from ISM measurements is shown in fig. 73. The mode interval of the E_K distribution is very close to the mean value of -70±2 mV. In every L_1-type horizontal cell from which data was accepted, E_K was more negative than the corresponding E_m value. The average value for the difference E_K-E_m was -35±2 mV. The mean value of E_K for C_b-type cells was -65±4 mV, and that of the difference E_K-E_m was -33±5 mV.

III.5 Measurements of E_m with K^+ ISMs and Ordinary Microelectrodes

A histogram of the distribution of E_m values obtained from the same 102 L_1 cells with K^+ ISMs is shown in fig. 74. The histogram is divided into intervals of 5 mV. It shows a peak in the interval -30 to -35 mV which is very close to the mean value -35±1 mV (Table 5, section III.9). This is a fairly wide distribution (range from -15 to -74 mV with a significant number of results at all points within the range -20 to -49 mV). This histogram represents a distribution which seems to be neither symmetric nor regular but it should be compared to the histogram of the distribution of E_m for L_1 cells obtained with ordinary microelectrodes (OMs) comprising many more (411) results (fig. 75). This shows that, assuming E_m can be measured in horizontal cells reliably with OMs, the 'real' situation is quite a wide distribution of E_m values. This suggests that the width of the E_m distribution obtained with ISMs does not reflect merely an inaccuracy in the measurement technique. Furthermore the mode occurs at the same interval in both distributions, although the peak is not so distinctly defined in the OM E_m distribution. This distribution for E_m obtained

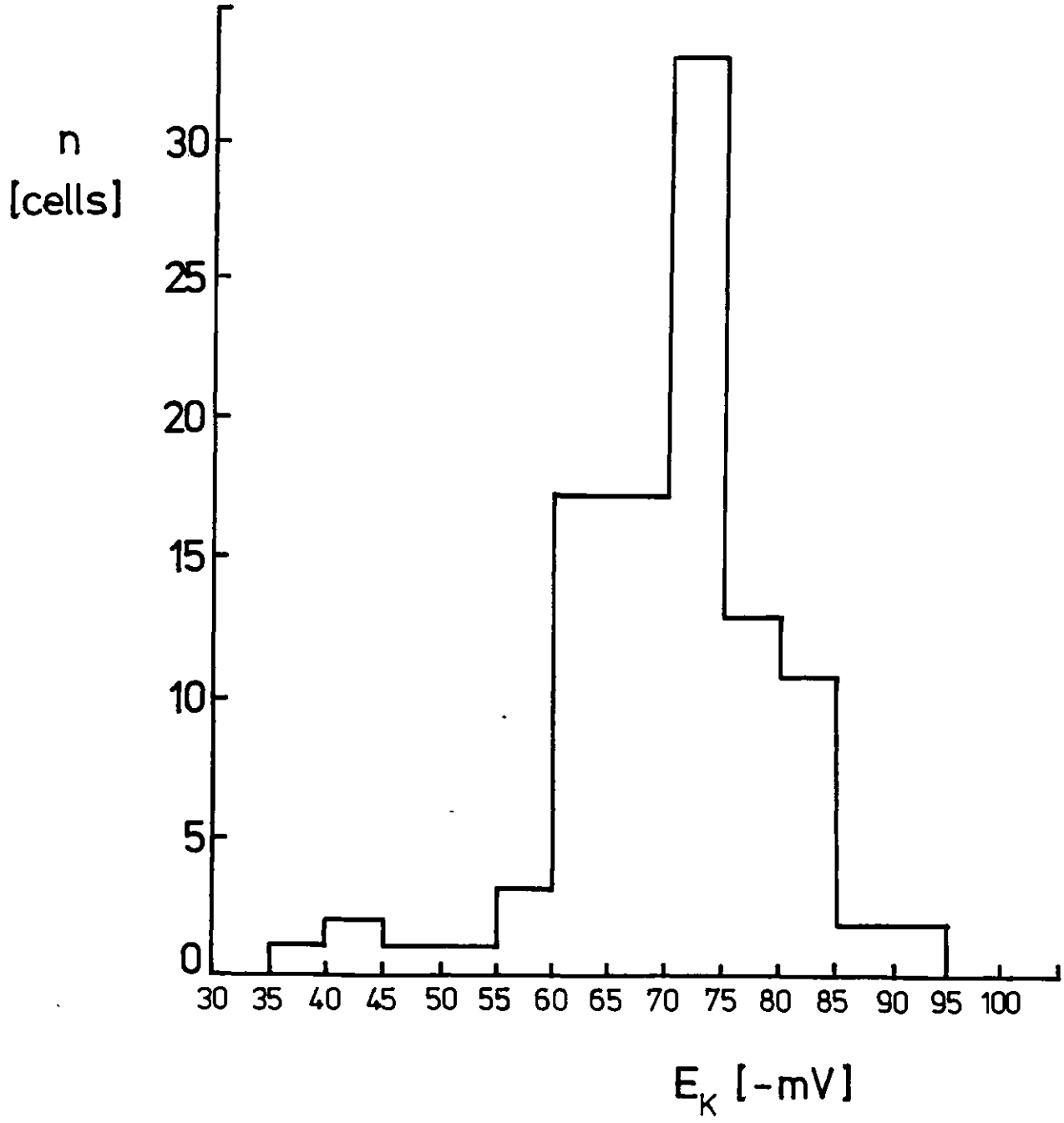

Fig. 73. Histogram of E_K values obtained with K^+ ISMs from 102 L_1-type horizontal cells.

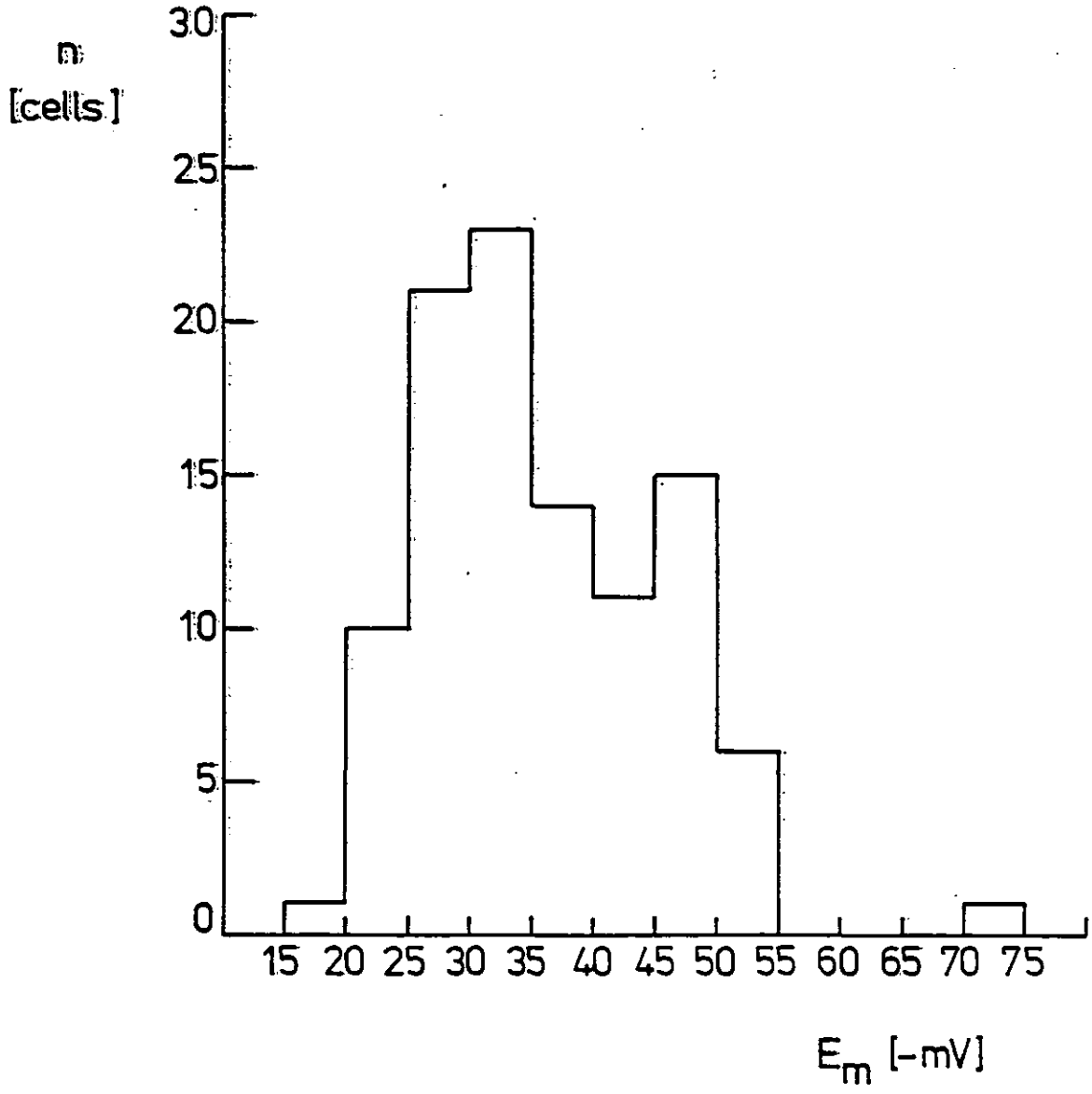

Fig. 74. Histogram of values of the resting membrane potential (E_m) obtained with K^+ ISMs from 102 L_1-type horizontal cells.

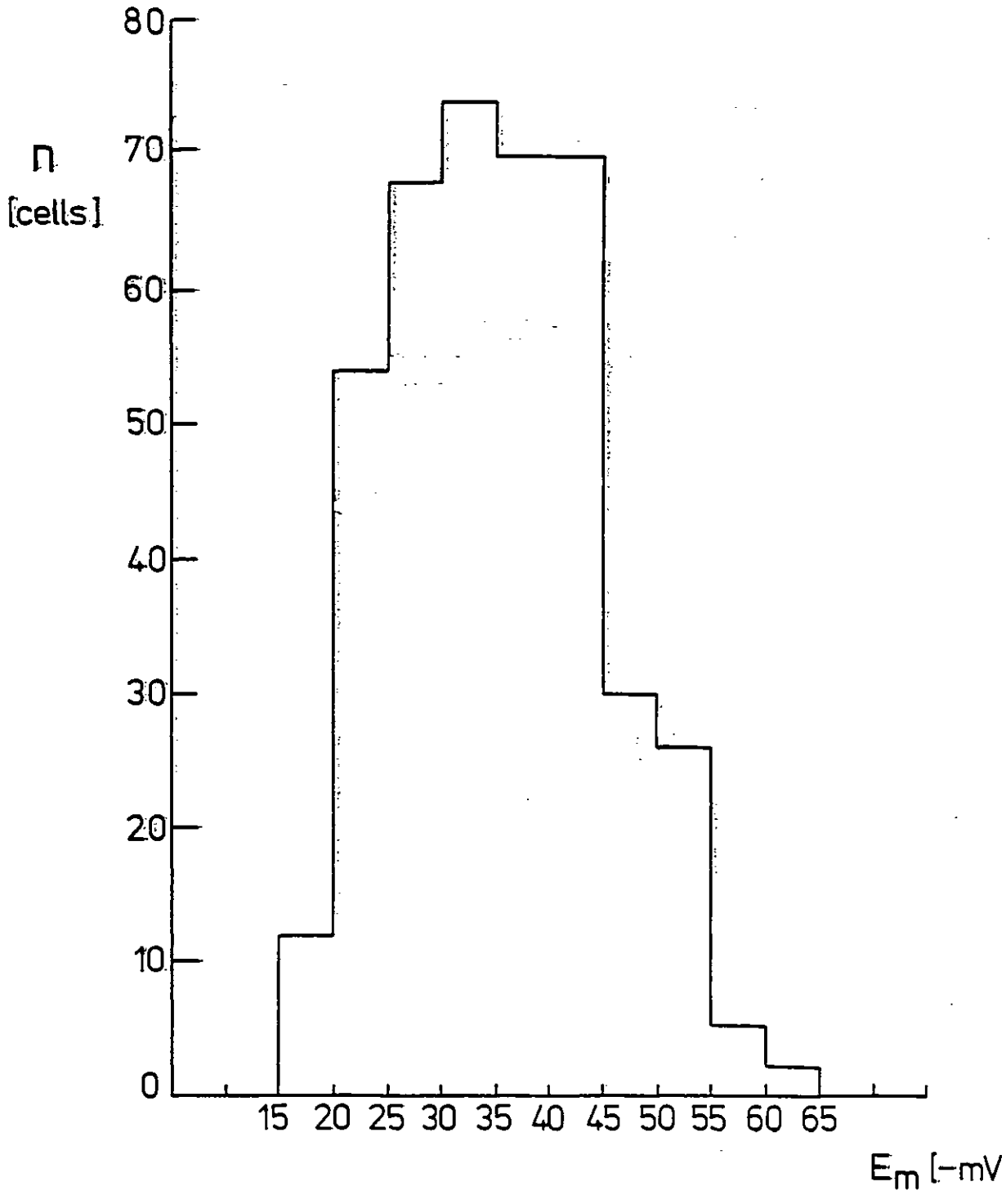

Fig. 75. Histogram of E_m values obtained with ordinary microelectrodes from 411 L_1-type horizontal cells.

with OMs suggests that all values between -20 and -49 mV are quite common. The ISM E_m distribution can thus be seen to represent a sample of the wider distribution from many more results obtained with OMs. The mean value of E_m obtained with K^+ ISMs for C_b cells was -30±3 mV (Table 5).

To make a more accurate comparison between the results for E_m obtained with ISMs and OMs, the measurements of E_m made with an ISM and an OM in the same retina are shown in a pair of histograms (fig. 76). The distribution of E_m from the ISM was obtained from 8 results and that from the ordinary microelectrode from 20 results. The histograms are very similar with a common mode, the same width and a similar distribution of results. This strongly supports the contention that measurements of E_m made with K^+ ISMs selected by the criteria described at the end of chapter II are as reliable as those made with OMs.

These histograms, which show the comparison between distributions of E_m measurements obtained with ISMs and OMs, also show that there is no artefactual error in the measurement of E_m by ISMs due to the use of 5 M LiCl as the reference-barrel filling solution. The OMs filled with 2.5 M KCl gave a very similar E_m distribution to the ISMs, the reference barrels of which were filled with 5 M LiCl. Although 5 M LiCl was an 'unusual' electrolyte for filling a microelectrode it proved to be most suitable as a K^+ ISM reference-barrel filling solution (see section V.2).

To further test the reliability of the measurement of E_m with ISMs the relationship between the measured E_m and the value of the reference-barrel resistance, R_r, was investigated. This is shown in fig. 77 in which are plotted the means and standard errors of the E_ms of groups of cells penetrated by ISMs with given values of R_r. This graph incorporates the 102 results and shows that there is no significant dependence of E_m on R_r, as the best straight line that could be drawn

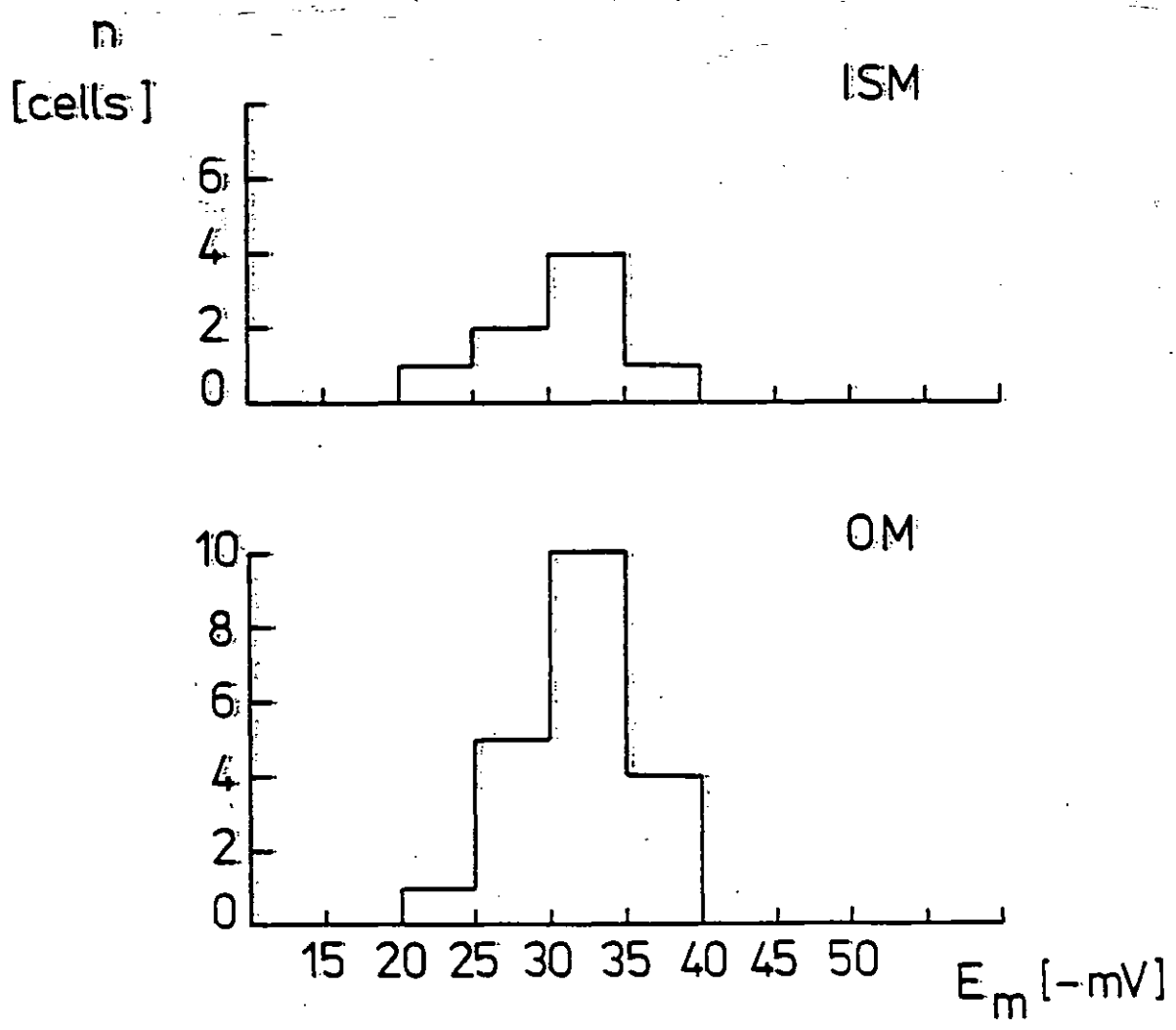

Fig. 76. Histogram of E_m values obtained from a single retina with ISMs (upper) and ordinary microelectrode (lower) for comparison.

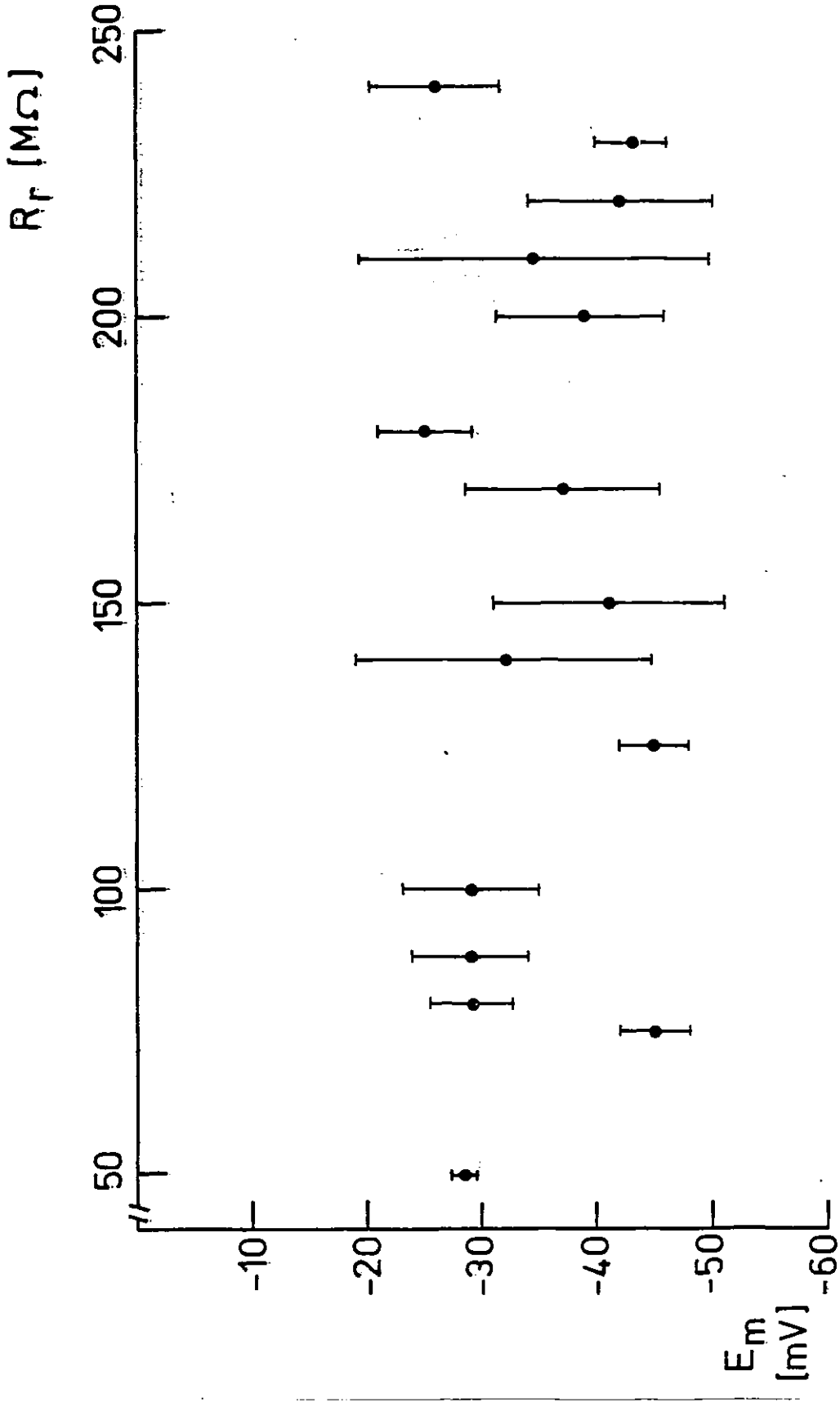

Fig. 77. Plot of mean and standard errors of E_m values recorded by ISMs with given values of reference barrel resistance, R_r. This shows that there is no significant dependence of E_m on the value of R_r.

through these points would have a correlation coefficient of only 0.1. Thus, there is very little error in estimation of E_m due to tip potentials in the reference barrels of ISMs, since tip potentials are related to the resistance R_r (section I.9.vi). If tip potentials in the ISMs were affecting the results by causing an error in the estimation of E_m, this would result in the observed value of E_m having a significant dependence on R_r. The relationship demonstrated in fig. 77 shows that this is not the case.

It is concluded that the dark resting potentials of the horizontal cells can be of any value in the range -20 to -50 mV. This wide range of values is probably due to (i) adaptational state of the retina; it was always observed that as the retina light-adapted during the course of an experiment, the resting potentials became more hyperpolarised, and (ii) the effect of isolation of the retina on the integrity of the photoreceptor input to the horizontal cells; some patches of the retinal surface could be seen under the dissecting microscope to be rather sparsely populated with photoreceptors, and in such retinal regions relatively more hyperpolarised resting potentials were obtained.

III.6 Comparison of E_K with E_m

The histogram of the distribution of E_K is shown together with the histogram of the E_m distribution obtained with ISM measurements in fig. 78. This pair of histograms superimposed shows the relationship between the frequency distributions of E_m and E_K which have both been described separately above. There is only a small amount of overlap between the distributions of E_m and E_K and this diagram shows clearly that E_K is significantly more negative than E_m for L_1-type horizontal cells by an amount of the order of E_m itself.

The difference between E_K and E_m is shown for both L_1-type

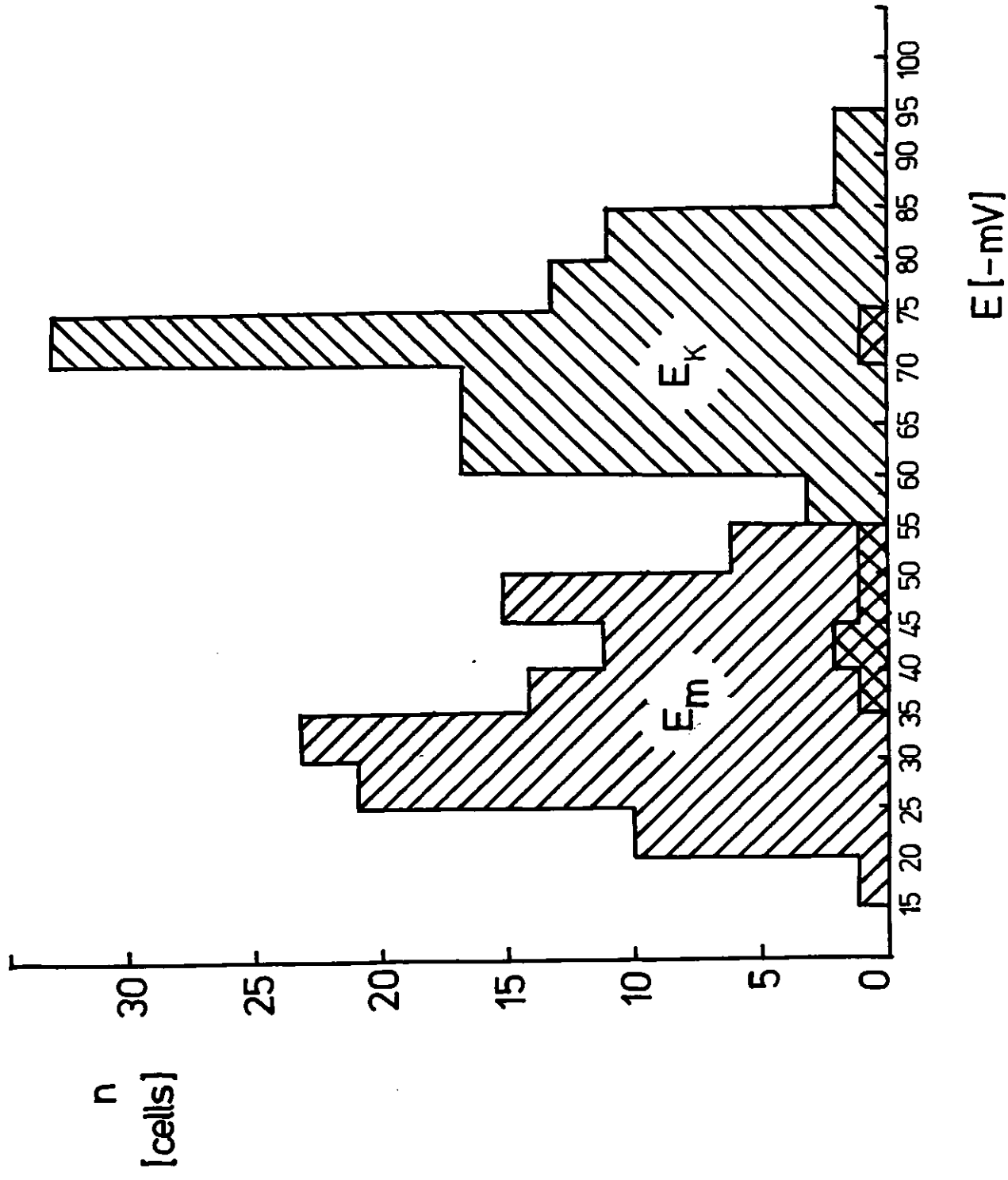

Fig. 78. Histograms of E_m and E_K distributions shown on the same abscissa for comparison.

and C_b-type horizontal cells in fig. 79. The unbroken lines represent the mean values of E_m and E_K for both L_1- and C_b-type cells and the broken lines represent the standard errors associated with these mean values.

A further aspect of the relationship between E_m and E_K is represented in fig. 80 where individual E_K values are plotted as points on a graph with E_m as abscissa (i.e. each point represents a single L_1-type horizontal cell). The broken line represents the equality: $E_m = E_K$, and all the points are above this line showing that E_K was always more negative than E_m for L_1-type horizontal cells.

Since it was well established that E_K was always significantly more negative than E_m, the relationship between E_K and E_m could be further investigated by ascertaining how the difference E_K-E_m varied with E_m. Figure 81 shows a plot of E_K-E_m against E_m for L_1-type horizontal cells. The points represent the 102 individual results. This distribution shows that the difference E_K-E_m decreases with increasing E_m, suggesting that the contribution to E_m from E_K, i.e. from K^+, is greater for cells with larger values of E_m than it is for those with smaller E_ms for L_1-type horizontal cells.

III.7 E_K and Hyperpolarisation of Horizontal Cells

To investigate the possibility that E_K defines the level of maximum hyperpolarisation of the membrane potential, V_m, experiments were performed using variable light intensity and application of the synaptic blocking agent, Co^{++}, onto the retina. Examples of the raw data obtained from such experiments are shown in the recordings of figs. 82 and 86. In fig. 82 the upper trace shows K^+ activity and the lower trace shows the membrane potential recording of the reference barrel, V_m. This recording shows the penetration of an L_1-type horizontal cell and responses elicited by red light flashes. After

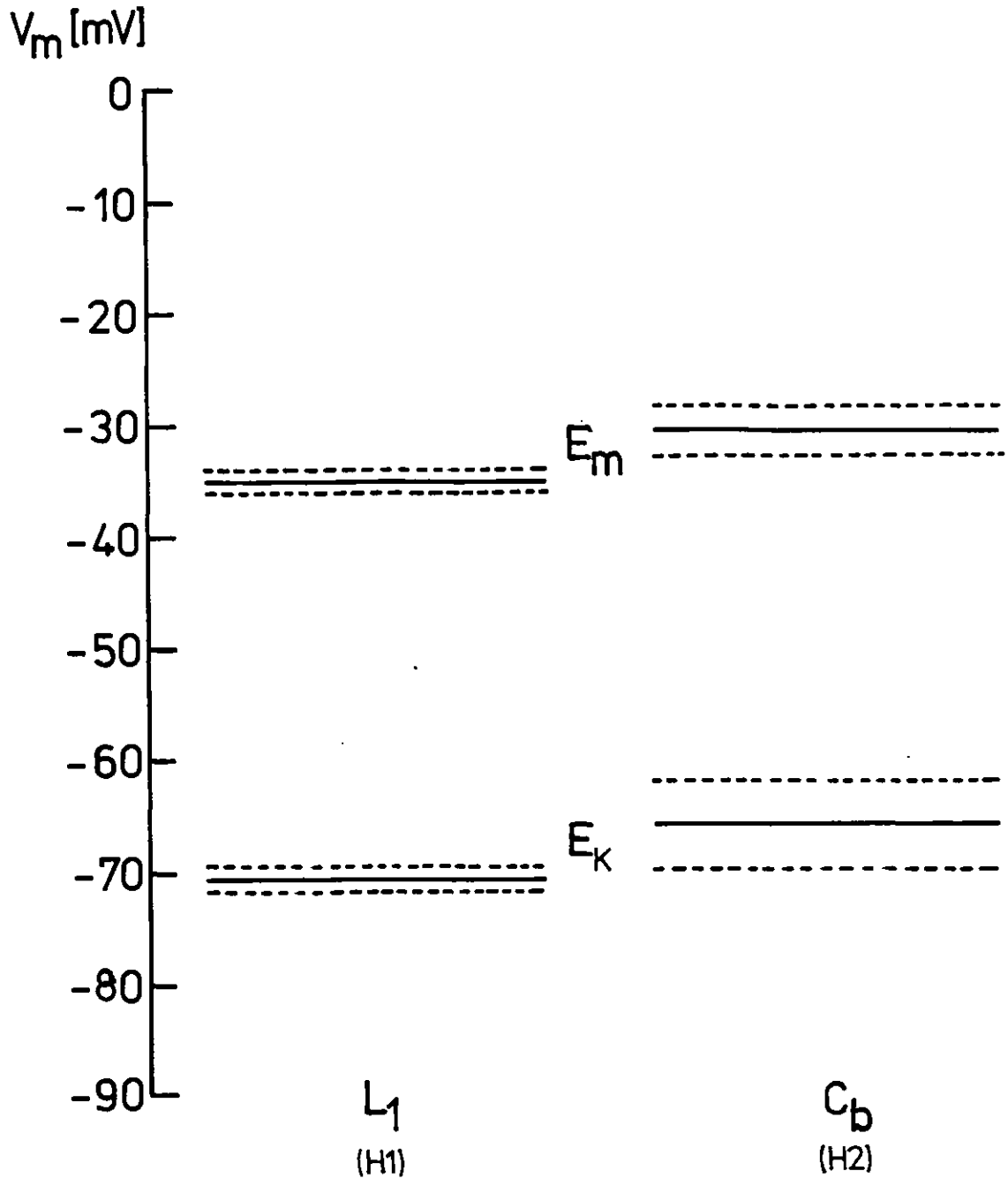

Fig. 79. Diagram showing the potential levels of E_K and E_m in both L_1 and C_b type horizontal cells. Heavy lines represent mean values and broken lines the corresponding standard errors.

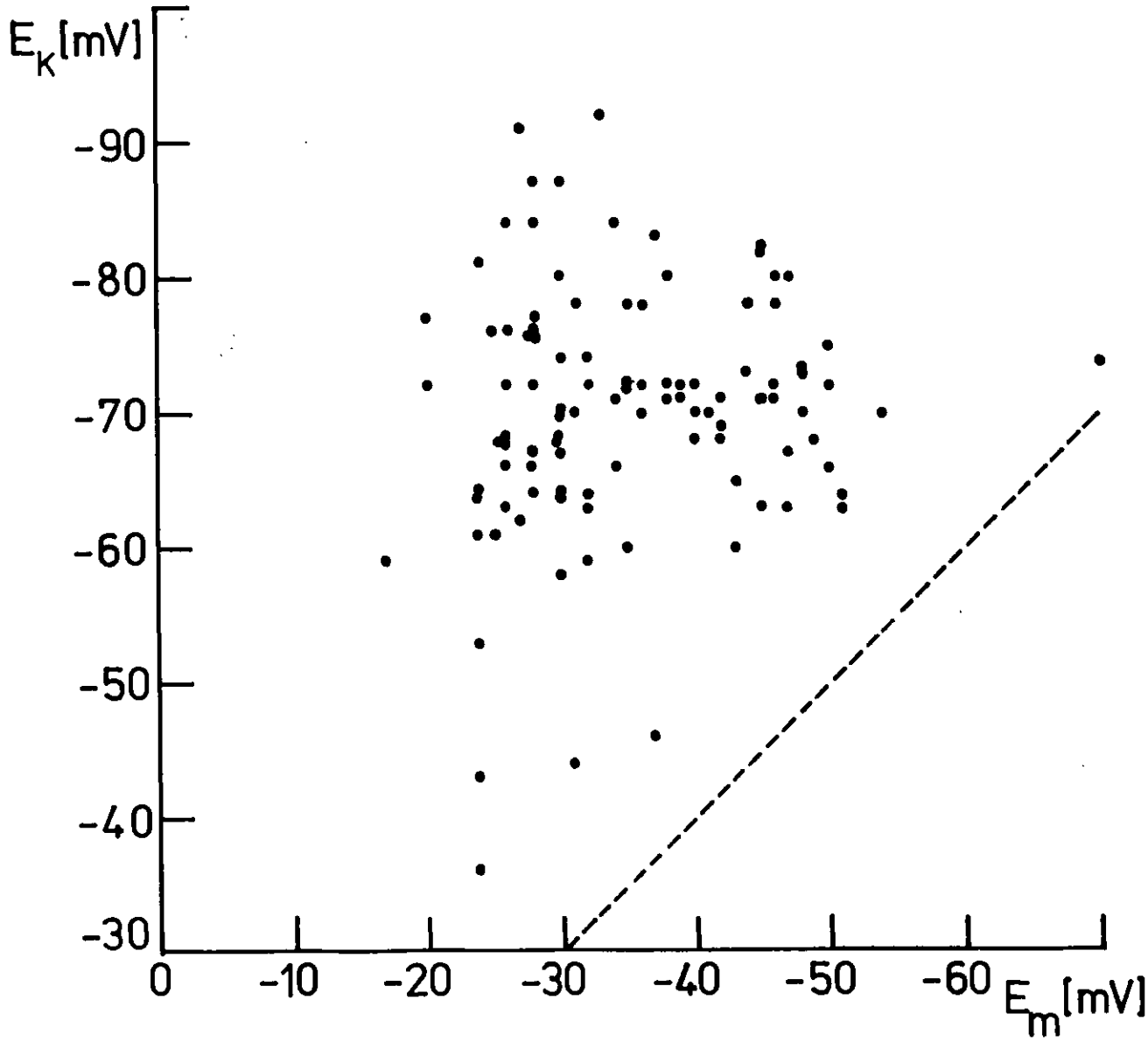

Fig. 80. E_K versus E_m as a distribution of points, each representing a single L_1-type horizontal cell. The broken line denotes the equality $E_K = E_m$ and shows that for all the cells $|E_K| > |E_m|$.

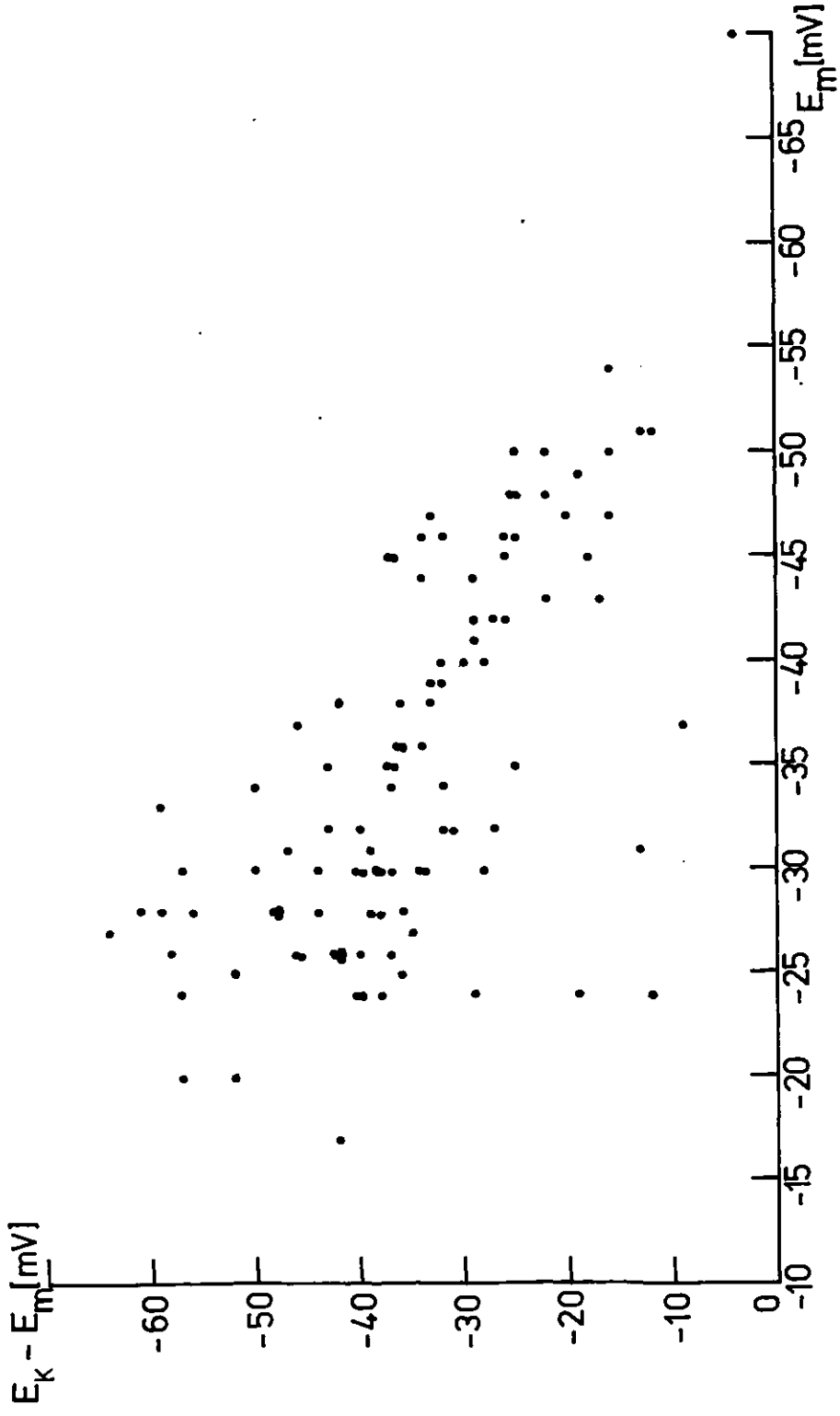

Fig. 81. Distribution of E_K-E_m versus E_m with points representing L_1-type horizontal cells. The difference, E_K-E_m, is greater for the smaller values of resting membrane potential, E_m.

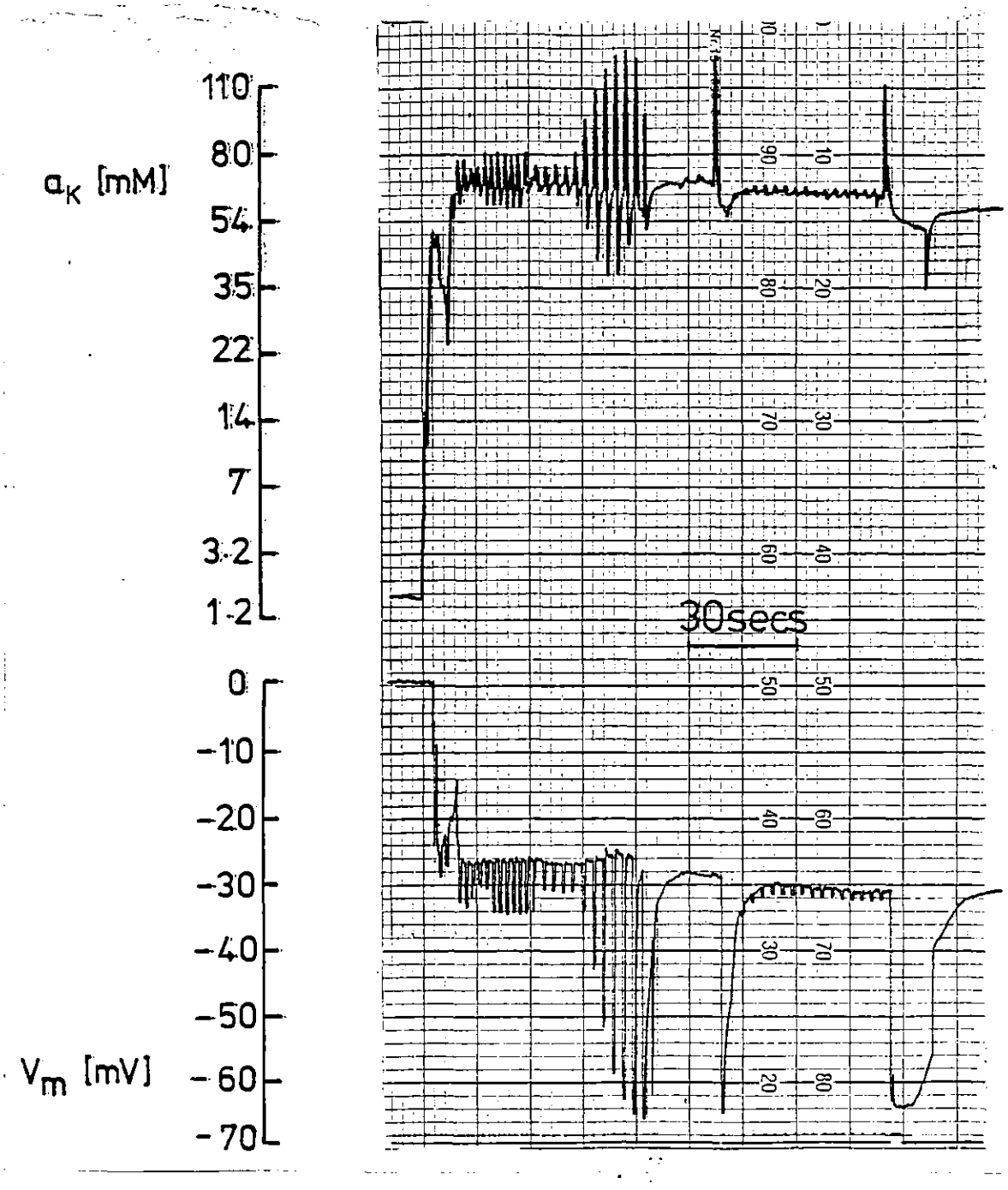

Fig. 82. Penetration of and intracellular recording from an L_1-type horizontal cell showing the responses to red light flashes of increasing intensity and to a short period of sustained illumination (see text).

a number of flashes, the light intensity was reduced and this is seen as four hyperpolarising responses of reduced amplitude. Then the light intensity was increased by one step (0.5 log units) for each flash by using a series of neutral density filters. This is shown by the hyperpolarising responses of increasing amplitude. There were eight different steps of increasing light intensity and the response increased with each step until at the penultimate step, the response was nearly saturated and so there was only a slight increase in the amplitude of the response between this and the last step. After a short rest period and another bright flash, the light intensity was returned to the normal level and it was seen that the responses were smaller due to light-adaptation of the photoreceptors. Finally a bright red light was held on for a short period and the response of the a_K trace showed a clear decrease in a_K^i during this maintained hyperpolarisation. (This phenomenon of change in a_K^i corresponding to the response of the cell to maintained illumination is discussed in section III.8). Thus the recording of fig. 82 shows that as the light intensity was increased a maximum amplitude of hyperpolarising response was defined.

The effect of spraying Co^{++} onto the retina while recording from an L_1-type horizontal cell is shown in the recording of fig. 83. This is a recording from an L_1-type horizontal cell with an ordinary microelectrode. It shows the hyperpolarising responses to increasing intensity of (red) light which reached a saturation level of maximum hyperpolarisation, followed by the response to the application of Co^{++}. The spraying of Co^{++} caused the cell to hyperpolarise rapidly from its resting membrane potential, E_m, to a level which corresponded to the maximum level of hyperpolarising response. (An example of the response to application of Co^{++} to the retina while recording from an L_1-type cell with a K^+ ISM is shown in fig. 86).

Fig. 83. Effect of spraying Co^{++} on the intracellular response and membrane potential (V_m) of an L_1-type horizontal cell. Recording was made with an ordinary microelectrode.

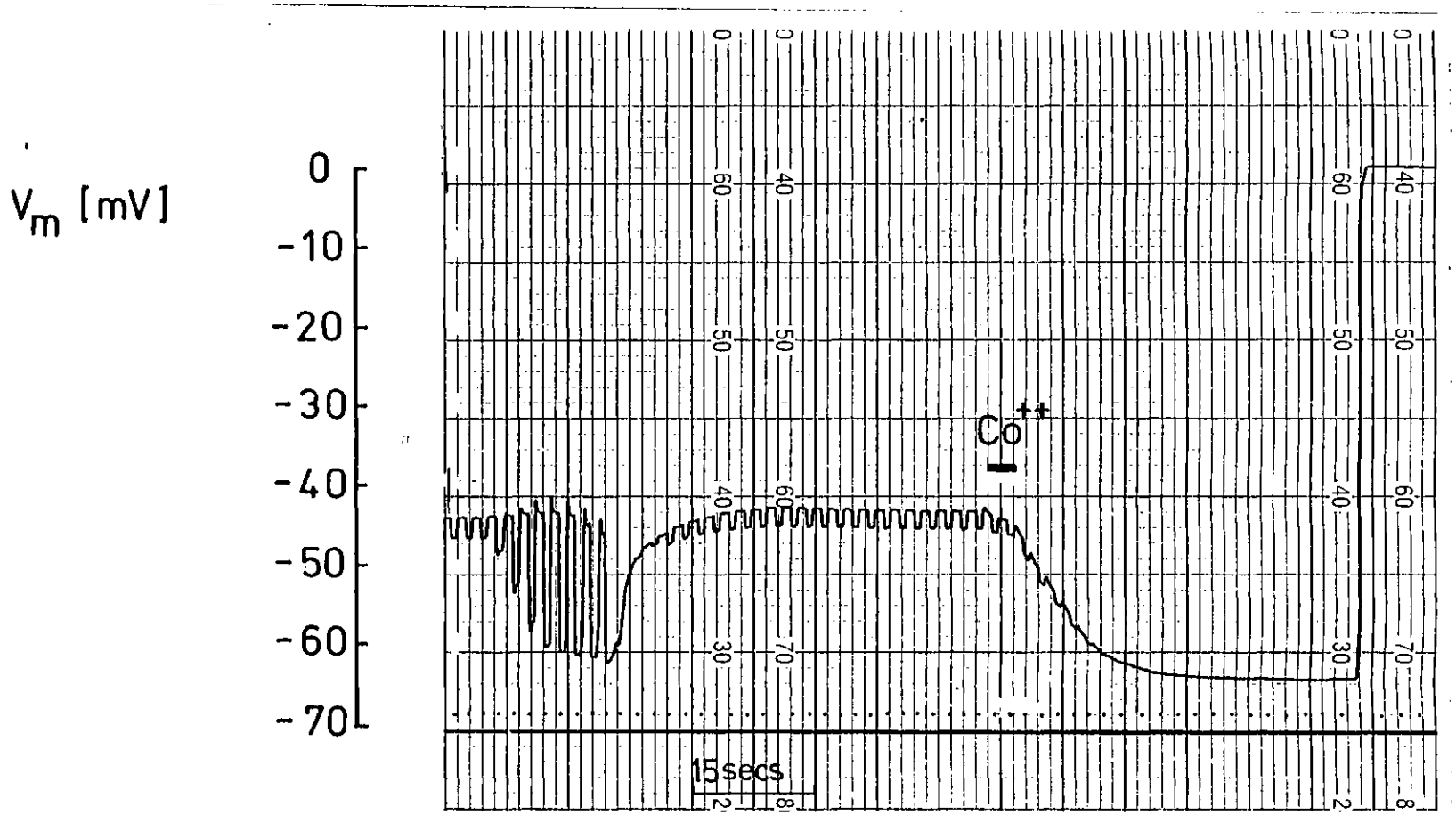

This type of experiment serves to show the analogy between decreasing the subsynaptic membrane conductance of horizontal cells by shutting off transmitter release from the photoreceptors using bright light (Trifonov, 1968) and by using a synaptic blocking agent (Co^{++}). The results from these experiments could be used to determine whether the maximum level of hyperpolarisation reached corresponded to the K^+ equilibrium potential, E_K, for a given cell. The results of experiments using increasing light intensity are shown in fig. 84. This shows the results from five different L_1-type cells on a graph with voltage as ordinate and log of intensity of light-stimulus as abscissa (V-log I plot). The resting membrane potentials, E_m, for the five different cells are shown by horizontal lines adjacent to the five corresponding symbols each of which represents a single cell. The results are plotted as points which represent the level of hyperpolarisation of the membrane potential, V_m, for each cell, in response to the stimulus light intensity which was increased in steps of 0.5 log units. There are nine different steps. The horizontal lines in the lower half of the diagram represent E_Ks for the different cells represented by their symbols. It is shown that for the cells represented by filled and open squares the response saturated at 3.0 log units above threshold and furthermore, for these two cells the level of hyperpolarisation of the saturating light response corresponded to only 1mV and 2mV below E_K for the 'closed' and 'open square' cells respectively. The 'closed triangle' cell response saturated at only 2 mV below E_K. The 'open circle' cell response saturated at 2.5 log units above threshold with a level of hyperpolarisation 4 mV below E_K. Finally the 'filled circle' cell response saturated at 3 log units above threshold at a level 2 mV above E_K. This shows that the maximum hyperpolarisation response to light intensity corresponds closely to E_K for each cell. The level of hyperpolarisation reached in response to Co^{++} application also corresponds

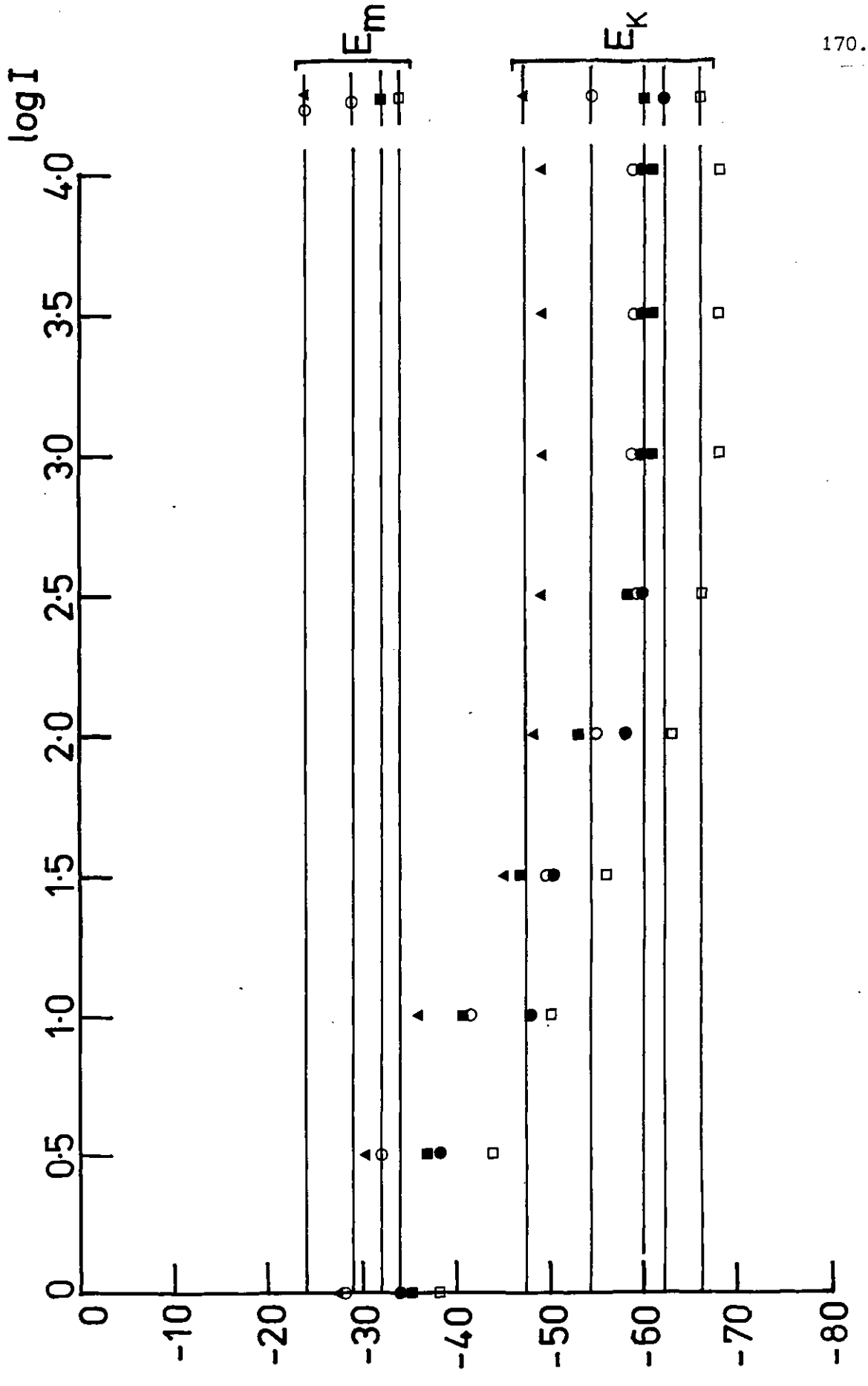

Fig. 84. Results of experiments on five L_1-type horizontal cells (represented by different symbols) in which (red) light intensity was increased until the response saturated. Membrane potential (V_m) is plotted against log. of intensity (I) of light stimulus. There is a close correspondence between the maximal hyperpolarisation level in response to light and the level of E_K for each cell. E_K was calculated from the value of a_K^1 for each cell during the response to saturating light.

to this level and hence to E_K (figs. 83, 86).

III.8 Changes in a_K^i during Light-Evoked Responses

It was noted that in fig. 82 there was a decrease in a_K^i during the maintained hyperpolarisation of V_m in response to saturating red light. Figure 85 shows another typical example of the decrease in a_K^i seen corresponding to a hyperpolarising response of V_m. In this case $\Delta a_K^i = -4$ mM while $\Delta V_m = -10$ mV. A decrease in a_K^i is also seen corresponding to a hyperpolarisation elicited by Co^{++} application. An example of this effect is shown in fig. 86 which is a recording with a K^+ ISM from an L_1-type cell. Firstly light of increasing intensity was flashed and then Co^{++} was sprayed onto the retina. The level of maximum hyperpolarisation to saturating light intensity corresponded to the level of hyperpolarisation elicited by Co^{++} application. Corresponding to the Co^{++}-induced hyperpolarisation of V_m, the level of a_K^i was seen to decrease by 5 mM.

Changes in a_K^i corresponding to maintained hyperpolarisation or depolarisation of V_m in a C_b-type horizontal cell are shown in the recording of fig. 87. The cell had a dark resting potential of -22 mV and a_K^i = 26 mM, and at first showed hyperpolarising responses of about 20 mV magnitude to 450 nm blue light flashes. During the sustained hyperpolarising response to maintained light stimulation, a_K^i decreased gradually by some 4 mM, as in the case of L_1-type units. On return to flashing stimuli, a_K^i gradually returned to its original value. At the point marked 'R', the light stimulus was changed to 620 nm red, in response to which the cell gave depolarising responses of about 5 mV magnitude, and at the point of stimulus change, showed a rapid increase in a_K^i to 28 mM (2mM above the original value). During continued flashing of the red light stimulus, the value of a_K^i settled back to its original value of 26 mM, whilst the membrane

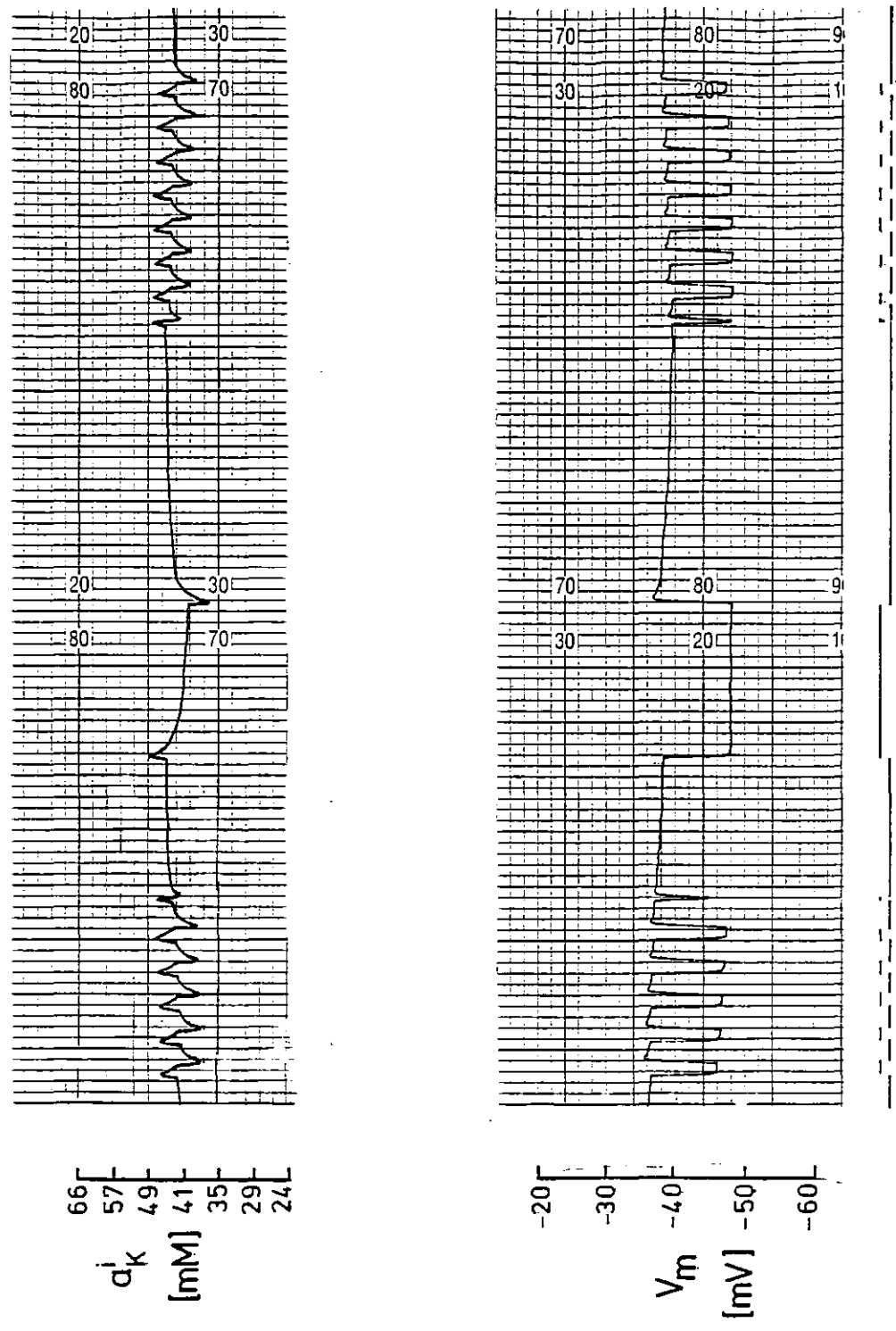

Fig. 85. Intracellular recording from an L_1-type horizontal cell with a K^+ ISM showing K^+ activity (a^i_k) and membrane potential (V_m) responses to flashes of red light and to a period of sustained illumination. Upward deflection in the stimulus monitor (lowermost) trace represent the onset of light.

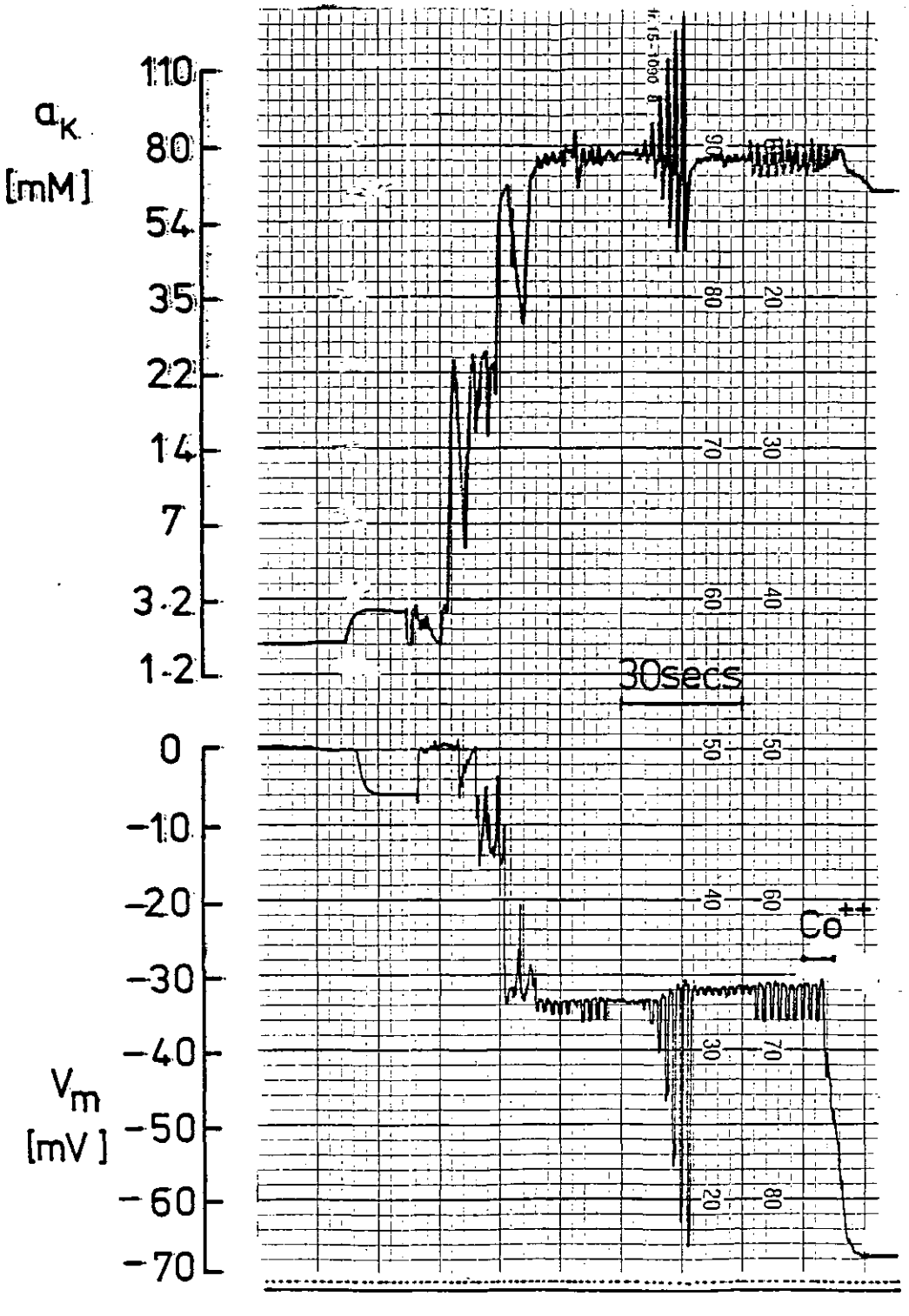

Fig. 86. Penetration of and intracellular recording from an L_1-type horizontal cell with a K^+ ISM showing responses to light of increasing intensity and the effect of application of Co^{++} to the retina. The hyperpolarised level of V_m brought about by Co^{++} is very close to the level of the hyperpolarising response to red light of saturating intensity.

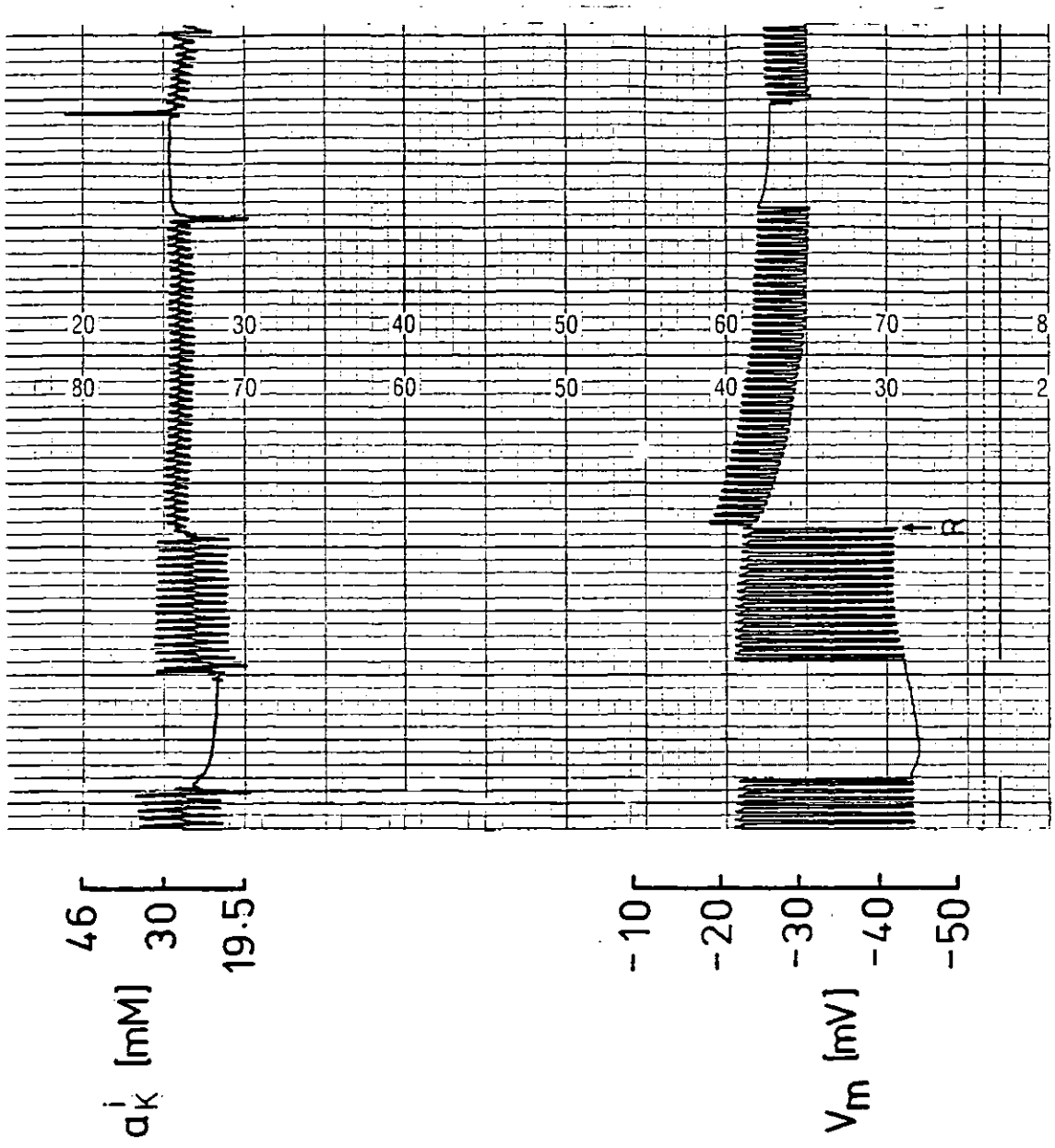

Fig. 87. Intracellular recording with a K^+ ISM from a C_b-type horizontal cell showing hyperpolarising responses in the V_m trace to blue light flashes and then depolarising responses to red light flashes (starting at 'R'). There are also short periods of sustained illumination with each of the two different stimulus wavelengths. Onset of light is denoted by upward deflection in the stimulus monitor (lowermost) trace.

potential relaxed to a more hyperpolarised level (E'_m = -31 mV). During sustained depolarising response to maintained red light stimulation, a^i_K increased again to 28 mM.

The decrease in a^i_K corresponding to the hyperpolarising response to the maintained blue light could be due to an increased K^+-permeability of the horizontal cell membrane while the increase in a^i_K corresponding to the depolarising response to the maintained red light could be due to a decrease in K^+-permeability of the cell membrane. These changes in a^i_K are discussed more fully in the Discussion chapter (section V.4).

III.9 Summary of Results

The results presented in this chapter are summarised in Table 5 which shows the quantities obtained by combining the results of Tables 3 and 4 to produce mean and standard error values for the parameters of interest. The mean, $\bar{x}$, and standard error, SE, were calculated by the usual formulae:

$$\bar{x} = \frac{1}{n} \sum_{i=1}^{n} x_i \qquad (23)$$

$$SE = \sqrt{\left[\frac{1}{n(n-1)} \sum_{i=1}^{n} (x_i - \bar{x})^2\right]} \qquad (24)$$

where x_i represents the ith value of the population of n values. The number of significant figures which could be meaningfully stated was objectively determined by the accuracy of the standard error according to the number of results (Barford, 1967). Thus the number of significant figures quoted is never greater than that determined by this criterion. The last significant figure of the standard error was adjusted accordingly (i.e. rounded up according to the 'error' in the standard error determined by the number of results) and then the standard error was rounded up again to the next integer value in all

cases except that of the a_K^o value for which the first decimal place was maintained as one of the two significant figures. Mean and standard error values are given for: resistance of the reference barrel of a K^+ ISM, R_r, from 25 values; resistance of the active barrel of a K^+ ISM, R_a, from 25 values; extracellular K^+ activity, a_K^o, and corresponding K^+ concentration value C_K^o from 25 values; resting membrane potential of an L_1-type horizontal cell, $E_m(L_1)$, from 102 values; resting membrane potential of a C_b-type horizontal cell, $E_m(C_b)$, from 12 values; intracellular K^+ activity in L_1-type cells, $a_K^i(L_1)$, and corresponding K^+ concentration value, $C_K^i(L_1)$, from 102 values; intracellular K^+ activity in C_b-type cells, $a_K^i(C_b)$, and corresponding K^+ concentration value, $C_K^i(C_b)$, from 12 values; K^+ equilibrium potential in L_1-type cells, $E_K(L_1)$, from 102 values, and in C_b-type cells, $E_K(C_b)$, from 12 values; difference of E_K and E_m in L_1-type cells, $(E_K-E_m)(L_1)$, from 102 values, and in C_b-type cells, $(E_K-E_m)(C_b)$, from 12 values.

The following observations of interest are prompted by these results: the mean concentration of extracellular K^+ (C_K^o = 4.6 mM) is higher than that normally used in Ringer solutions to perfuse the retina (2.5 - 3.6 mM; Appendix 7); intracellular K^+ activity is much higher than the extracellular K^+ activity for all horizontal cells, by a factor greater than 10; E_K is more negative than E_m by a significant amount such that $E_K - E_m$ is of the order of E_m itself; because E_K is more negative than E_m, there must be at least one other ionic mechanism involving an ion X such that $E_x > E_m$ in order to maintain the observed level of the resting (dark) membrane potential, E_m, in horizontal cells. Further discussion of these results will be found in chapter V.

Table 3. K^+ Activity Measurements on L_1(H1)-Type Horizontal Cells

ISM No.	R_r (MΩ)	R_a (MΩ)	a_K^o (mM)	Cell No.	Em (mV)	d_K^i (mM)	E_K (mV)	E_K-E_m (mV)
E180	150	12K	2.5	1	-46	60	-80	-34
				2	-45	65	-82	-37
E182	75	12K	4.0	3	-43	52	-65	-22
				4	-47	56	-67	-20
E186	80	10K	2.1	5	-35	48	-78	-43
E199	140	9K	6.2	6	-37	38	-46	- 9
				7	-70	115	-74	- 4
				8	-24	50	-53	-29
				9	-51	75	-63	-12
E193	150	12K	3.8	10	-51	50	-64	-13
				11	-47	48	-63	-16
				12	-50	55	-66	-16
E203	200	15K	4.6	13	-49	70	-68	-19
				14	-54	77	-70	-16
E204	200	10K	2.9	15	-37	80	-83	-46
				16	-36	46	-70	-36
				17	-40	44	-68	-28
				18	-45	74	-82	-37
				19	-47	67	-80	-33
				20	-38	47	-71	-33
E206	210	24K	3.5	21	-24	15	-36	-12
				22	-45	44	-63	-18
E209	220	16K	4.6	23	-35	77	-72	-37
				24	-44	102	-78	-34
				25	-46	100	-78	-32
				26	-48	82	-73	-25
				27	-50	87	-75	-25
				28	-50	77	-72	-22
				29	-39	77	-72	-33
				30	-42	67	-68	-26
				31	-42	70	-69	-27
				32	-24	24	-43	-19
EK38 S=60	140	30K	1.8	7	-26	50	-84	-58
				15	-31	40	-78	-47
				16	-27	67	-91	-64
				17	-33	70	-92	-59

Table 3. (Continued)

ISM No.	R_r (MΩ)	R_a (MΩ)	a_K^o (mM)	Cell No.	E_m (mV)	a_K^i (mM)	E_K (mV)	E_K-E_m (mV)
EK30	80	20K	3.8	3a	-26	65	-68	-42
				3b	-32	85	-74	-43
				4	-32	78	-72	-40
				5	-30	56	-64	-34
				6	-31	70	-70	-39
				7	-24	56	-64	-40
				9	-17	44	-59	-42
				10	-28	56	-64	-36
				14	-24	54	-64	-40
EK31	200	18K	5	2	-34	72	-66	-32
				6	-32	56	-59	-27
				9	-32	65	-64	-32
EK35	180	12K	3.8					
S=60				7	-30	70	-74	-44
				8	-28	75	-76	-48
				13				
				15	-25	75	-76	-52
EK36	150	15K	3.8	15	-24	44	-61	-38
S=65				25	-30	38	-58	-28
EK41	100	16K	2.7					
S=59								
				4	-30	65	-80	-50
				11	-26	75	-76	-46
EK42	50	4K	2.4	6	-28	50	-76	-48
S=64				12	-28	50	-76	-48
				22	-30	34	-67	-37
				23	-28	32	-66	-38
EK43	100	14K	2.6	1	-40	42	-70	-30
S=64				4	-30	38	-68	-38
				9	-26	38	-68	-42
				21	-26	36	-66	-40
				24	-28	44	-72	-44
				25	-30	42	-70	-40
				26	-30	42	-70	-40
				27	-26	38	-68	-42

Table 3. (Continued)

ISM No.	R_r (MΩ)	R_a (MΩ)	A_K^o (mM)	Cell No.	E_m (mV)	a_K^i (mM)	E_K (mV)	E_K-E_m (mV)
EK38 S=63	140	30K	2	4	-25	22	-61	-36
				16	-26	34	-72	-46
				19	-36	44	-78	-34
				21	-32	24	-63	-31
				24	-38	48	-80	-42
EK39 S=63	200	15K	4	2	-38	70	-72	-36
				3	-30	60	-68	-38
				9	-28	58	-67	-39
				10	-30	52	-64	-34
				14	-36	70	-72	-36
				19	-40	70	-72	-32
				23	-46	70	-72	-26
				26	-48	65	-70	-22
EK40 S=62	240	22K	2.4	2	-28	50	-77	-59
				3	-28	65	-84	-56
				5	-30	75	-87	-57
				9	-28	75	-87	-61
				10	-24	58	-81	-57
				12	-20	50	-77	-57
				14	-20	42	-72	-52
EK40 S=59	240	22K	3.8	13	-34	78	-84	-50
				20	-34	48	-71	-37
E215	230	24K	3.3	33	-48	62	-73	-25
				34	-46	57	-71	-25
				35	-41	54	-70	-29
				36	-44	62	-73	-29
				37	-45	57	-71	-26
				38	-42	57	-71	-29
				39	-39	57	-71	-32
E213	88	17K	4.9	40	-35	85	-72	-37
				41	-27	57	-62	-35
				42	-26	59	-63	-37
E212	170	14K	2.6	43	-43	28	-60	-17
				44	-31	14.5	-44	-13
E210	150	12K	2.6	45	-35	28	-60	-25

Table 4. K^+ Activity Measurements on C_b (H2) Type Horizontal Cells

ISM No.	R_r (MΩ)	R_a (MΩ)	a_K^o (mM)	Cell No.	E_m (mV)	a_K^i (mM)	E_K (mV)	E_K-E_m (mV)
EK30	80	20K	3.8	20	-22	40	-56	-34
EK31	200	18K	5	1	-22	56	-59	-37
				5	-28	46	-55	-27
EK38	140	30K	1.8	1	-32	48	-83	-51
				14	-31	50	-84	-53
EK39	200	15K	4	24	-42	48	-63	-31
EK40	240	22K	2.4	13	-30	50	-80	-50
"	"	"	3.8	6	-38	85	-78	-40
				9	-28	65	-71	-43
EK83	400	30K	7	1	-44	52	-50	- 9
				2	-42	57	-53	-11
				3	-40	52	-50	-10

Table 5. Summary of Results of Potassium Activity Measurements

a_K^o	=	3.4±0.1 mM	C_K^o	=	4.6±0.1 mM
$E_m(L_1)$	=	-35±1 mV			
$E_m(C_b)$	=	-30±3 mV			
$a_K^i(L_1)$	=	57±2 mM	$C_K^i(L_1)$	=	77±3 mM
$a_K^i(C_b)$	=	54±6 mM	$C_K^i(C_b)$	=	73±8 mM
$E_K(L_1)$	=	-70±2 mV			
$E_K(C_b)$	=	-65±4 mV			
$(E_K-E_m)(L_1)$	=	-35±2 mV			
$(E_K-E_m)(C_b)$	=	-33±5 mV			

All figures given are mean ± standard error

CHAPTER IV

CHLORIDE ACTIVITY MEASUREMENTS

The results from measurements of intracellular K^+ activity (Chapter III) show that the resting (dark) membrane potential, E_m, of both L_1- and C_b- type horizontal cells is significantly more positive than the K^+ equilibrium potential, E_K. This suggests that another ion with an equilibrium potential more positive than E_m contributes to the generation of the resting membrane potential. Thus measurements of intracellular Cl^- activity were made in the roach retina to determine E_{Cl} in horizontal cells and to investigate the possible role of Cl^- in cellular electrogenesis. These experiments were carried out using double-barrelled Cl^--sensitive microelectrodes based on the Corning exchanger 477315.

IV.1 Derivation of Results from the Recorded Traces

The traces on the chart recording from the beginning of each experiment showing the calibration of the Cl^- ISM and the response of the ISM as it touched the retina are used to determine a^o_{Cl} in a manner similar to that described for K^+ in section III.1. Zero potential is taken as the response shown by the V_{Cl} trace to the calibration solution with the highest activity of Cl^-, which is the most negative potential step of the calibration, thus all measured potentials have positive values. Values for E_m and a^i_{Cl} are obtained by noting the deflections of the V_m and V_{Cl} traces respectively upon penetration of a horizontal cell as described for K^+ in section III.1. For each horizontal cell the Cl^- equilibrium potential, E_{Cl}, is calculated from the values of a^o_{Cl}, a^i_{Cl} and the slope factor, 58mV , using the equation:

$$E_{Cl} = 58 \log_{10} \frac{a^o_{Cl}}{a^i_{Cl}} \quad (mV) \qquad (25)$$

The results of these measurements on L_1- and C_b-type horizontal cells are compiled in Tables 6 and 7 respectively. These results were selected according to the criteria described in section II.7 and consequently the great majority of recordings of cell penetrations were rejected in order to produce a reliable final list of results. The format of presentation of the results in Tables 6 and 7 is similar to that of Tables 3 and 4 (section III.1). Table 6 comprises results from 84 L_1-type horizontal cells and Table 7 14 C_b-type horizontal cells.

IV.2 Extracellular Cl^- Activity Measurements

A recording from the beginning of an experiment, showing the calibration of a Cl^- ISM followed by the response obtained as the ISM touches the retina is shown in fig. 88. This illustrates the determination of a^o_{Cl} by referring the steady-state level of V_{Cl} to the calibration trace. The V_{Cl} trace always returned to the same 'baseline' level on leaving a cell as that before penetration, and so a^o_{Cl} was found to have the same value throughout and on both sides of the horizontal cell layer (fig. 89). Furthermore, it was found that a^o_{Cl} increased only slightly ($\ll$10%) throughout the duration of an experiment (40-60 minutes) (fig. 90). It has been shown that a change in a^o_{Cl} of 10% would cause a change in E_{Cl} of only 2.4 mV, for a given value of a^i_{Cl} (Appendix 4). This value is, in fact, much less than the difference $(E_{Cl}-E_m)$ obtained consistently (section IV.5). The reading of a^o_{Cl} was monitored continuously during the experiments and any significant changes were taken into account when calculating a^i_{Cl} and E_{Cl}.

The frequency distribution of a^o_{Cl} values obtained from 25 retinae is presented as a histogram, in which the abscissa is divided into intervals of 10 mM (fig. 91). The mode of this distribution is the interval which contains the mean value. The mean value of a^o_{Cl} is 95±6 mM, which corresponds to a concentration of 128±8 mM, assuming that

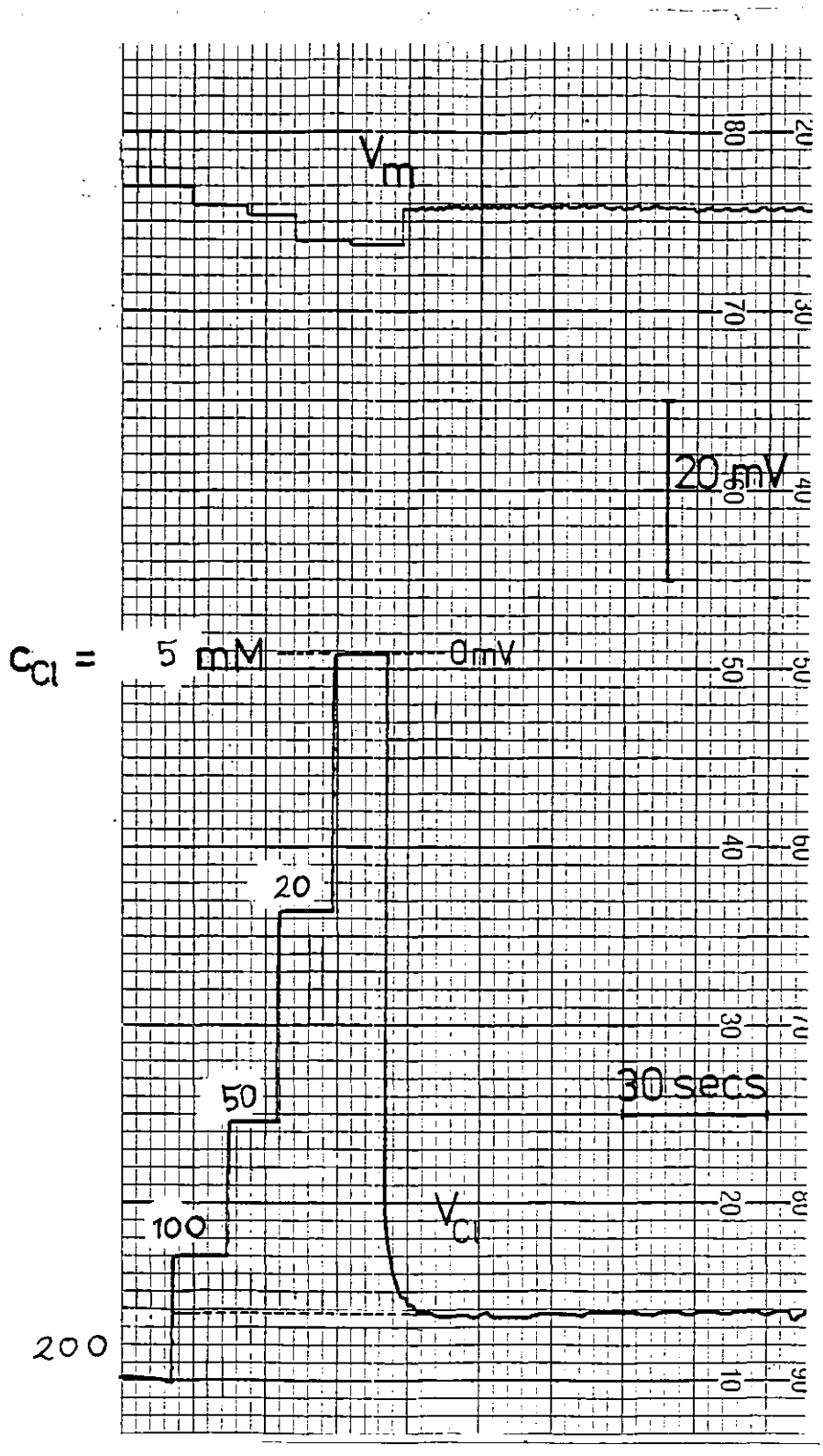

Fig. 88. Recording from the beginning of an experiment showing calibration of Cl^- ISM and values of Cl^- concentration (C_{Cl}) at each step, followed by response of ISM as it touches the retina. Upper trace shows membrane (reference barrel) potential, V_m, and lower trace shows Cl^- sensitive potential.

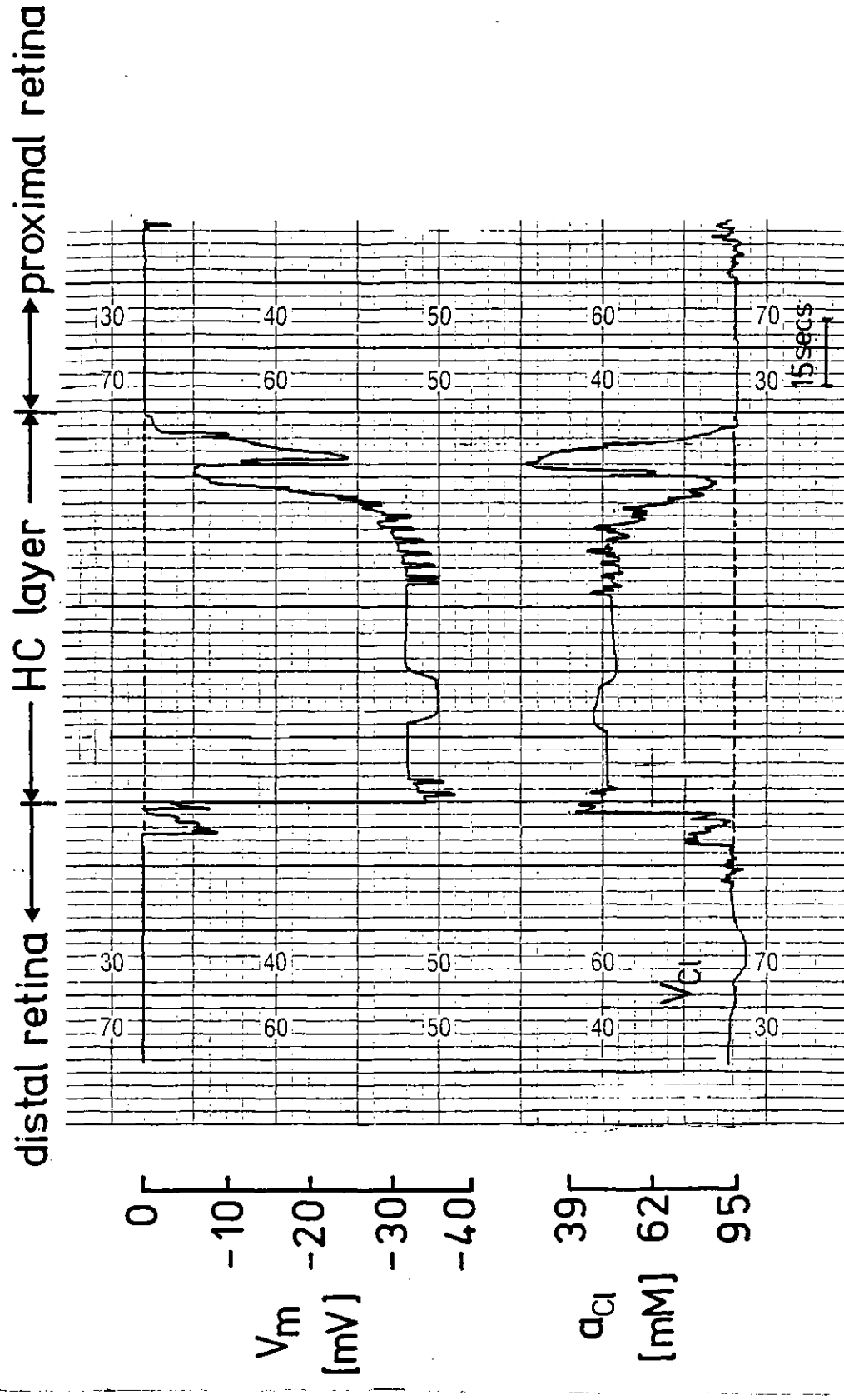

Fig. 89. Recording from the retina with a Cl^- ISM as it is advanced through the horizontal cell (HC) layer to the proximal retina. Upper trace shows membrane potential, V_m (reference barrel potential) and lower trace shows Cl^- activity (differential Cl^--sensitive potential). Extracellular levels of a_{Cl} and V_m are the same on both sides of this layer.

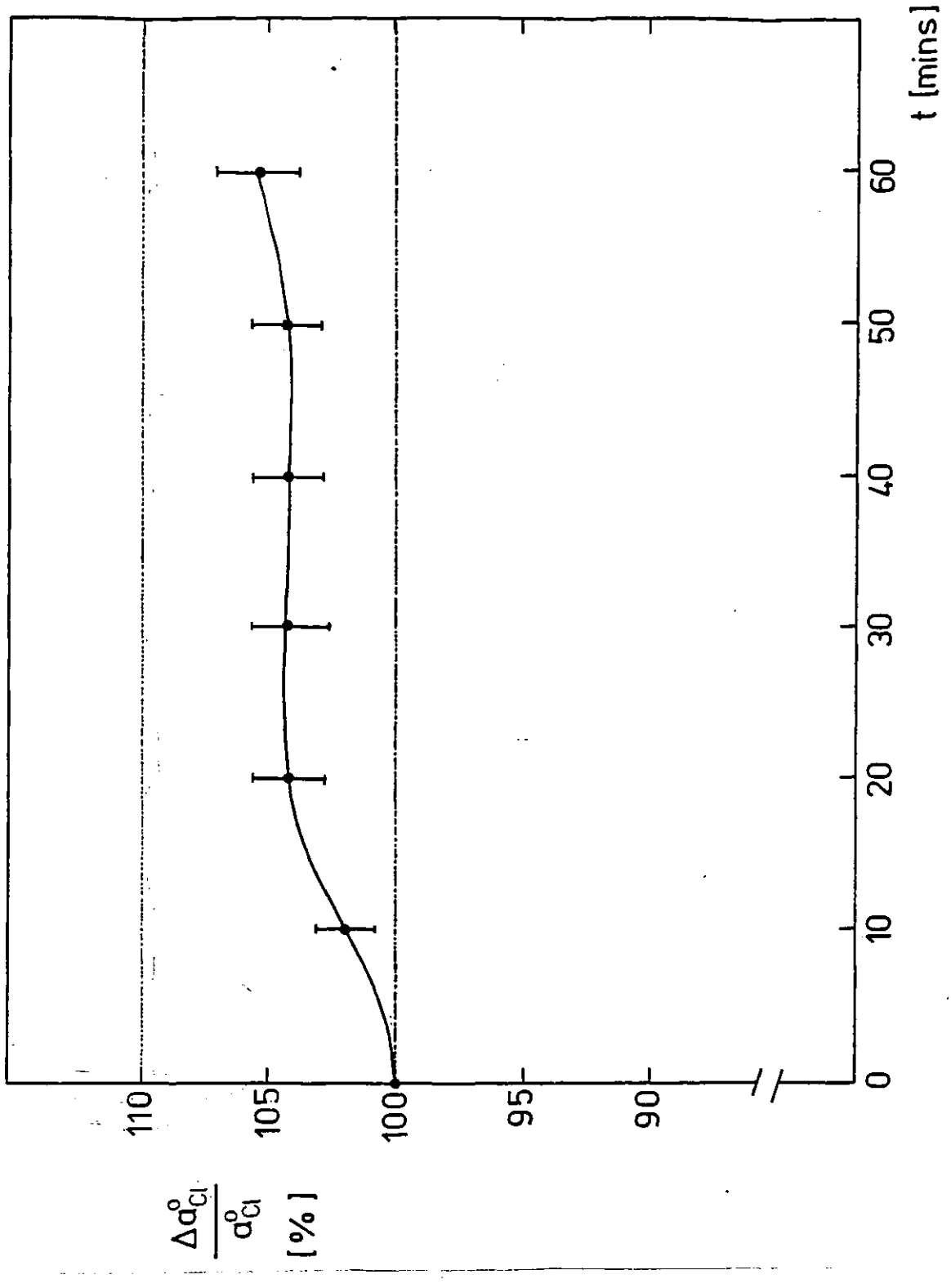

Fig. 90. Graph showing increase in extracellular Cl^- activity, Δa^{o}_{Cl}. Expressed as a percentage of the original value, a^{o}_{Cl}, with time. Means and standard errors are plotted which represent the results from 10 experiments. Broken lines deonte original level of a^{o}_{Cl} and 10% increase in a^{o}_{Cl}.

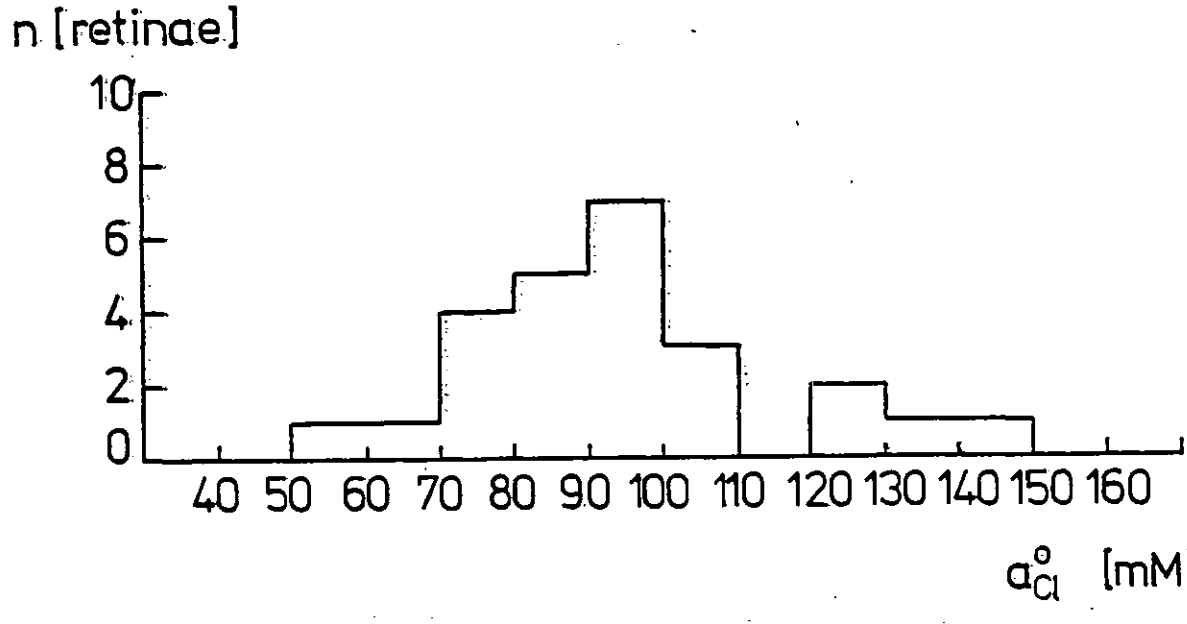

Fig. 91. Histogram of frequency distribution of a^{o}_{Cl} values obtained with Cl^{-} ISMs from 25 retinae.

γ_{Cl} = 0.74 (see discussion in sections V.4,5). A significant feature of this result is that a^{o}_{Cl} has a wide distribution (range 50-150 mM) i.e. a^{o}_{Cl} varies considerably from retina to retina, although for a given retina it has always been found that $a^{i}_{Cl} < a^{o}_{Cl}$ and $|E_{Cl}| < |E_{m}|$ (section IV.3 and IV.4). The physiological implications of these results and relationships are discussed in section V.5.

IV.3 Intracellular Cl^- Activity Measurements

The penetration of an L_1-type horizontal cell with a Cl^- ISM is shown in fig. 92. The upper (V_{Cl}) trace shows Cl^- activity while the lower (V_m) trace shows electrical potential measured by the reference barrel. Initially, the Cl^- ISM measures the a^{o}_{Cl} (89 mM) and the external potential (0 mV) which is used as the reference level from which to measure E_m. The ISM then penetrates the horizontal cell (at the point marked 'IN'), seen by the rapid deflection in both traces which quickly reach new levels, the E_m being about -35 mV and the a^{i}_{Cl} being around 40 mM. As soon as the ISM is in the cell, hyperpolarising responses to red light flashes are seen, which are just over 10 mV in magnitude, and corresponding artefactual deflections are seen in the V_{Cl} trace (section III.3 and Appendix 5). For every horizontal cell investigated a^{i}_{Cl} was less than the corresponding a^{o}_{Cl}. The mean value of a^{i}_{Cl} obtained from 84 L_1-type horizontal cells in accordance with the criteria outlined in section II.7, is 47±2 mM, which corresponds to a concentration of 64±3 mM. The histogram of the distribution of these a^{i}_{Cl} values is given in figure 93, which also shows that the interval at which the mode occurs also contains the mean.

As already noted in Chapter III, satisfactory measurements from C_b-type horizontal cells were more difficult to obtain. Fourteen cells were investigated successfully. The mean a^{i}_{Cl} value found (47±3 mM) is exactly the same as the value obtained for the L_1-type cells.

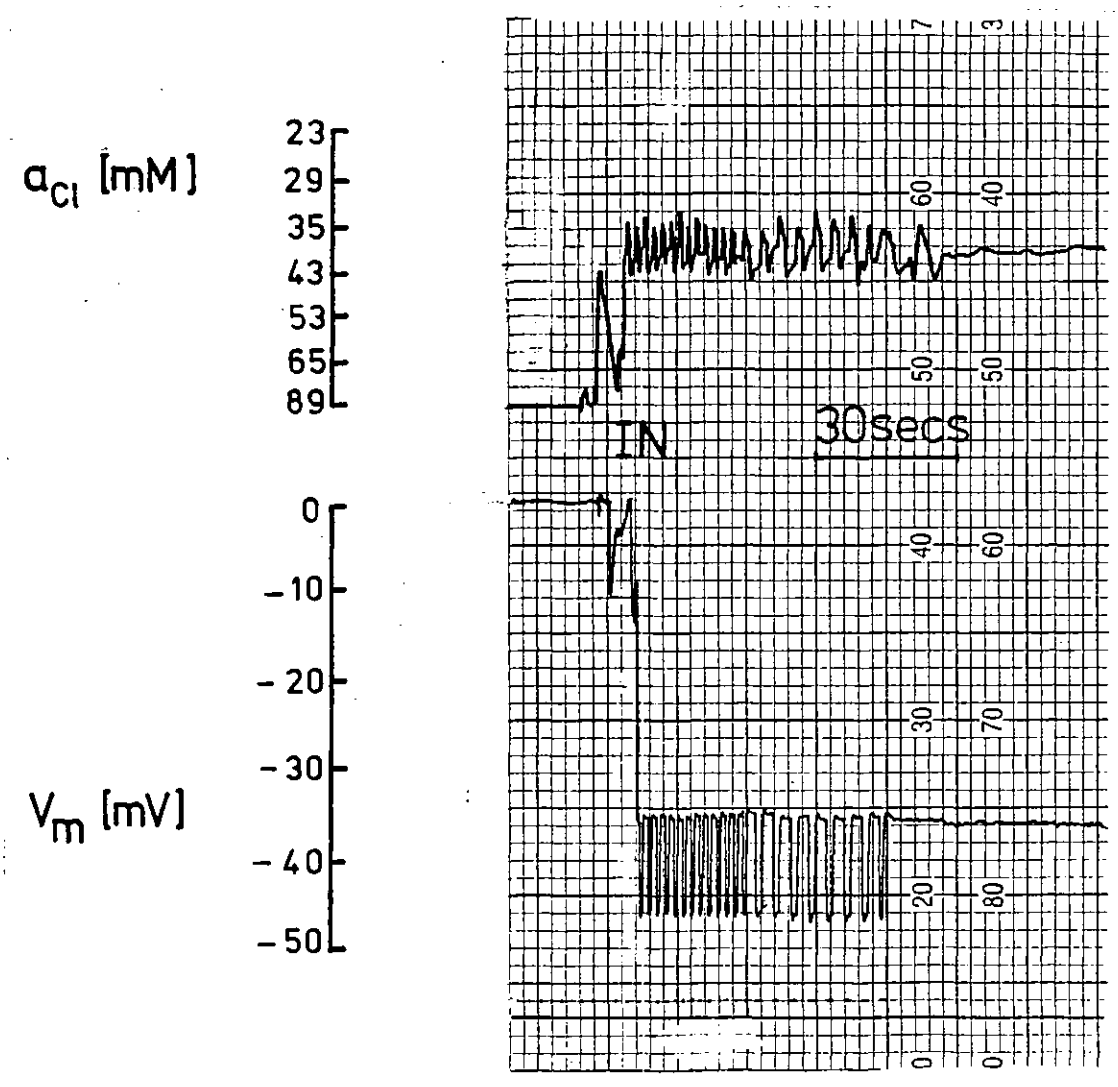

Fig. 92. Penetration of and intracellular recording with a Cl^- ISM from an L_1-type horizontal cell showing responses to red light flashes, denoted by upward deflection in the stimulus monitor (lowermost) trace.

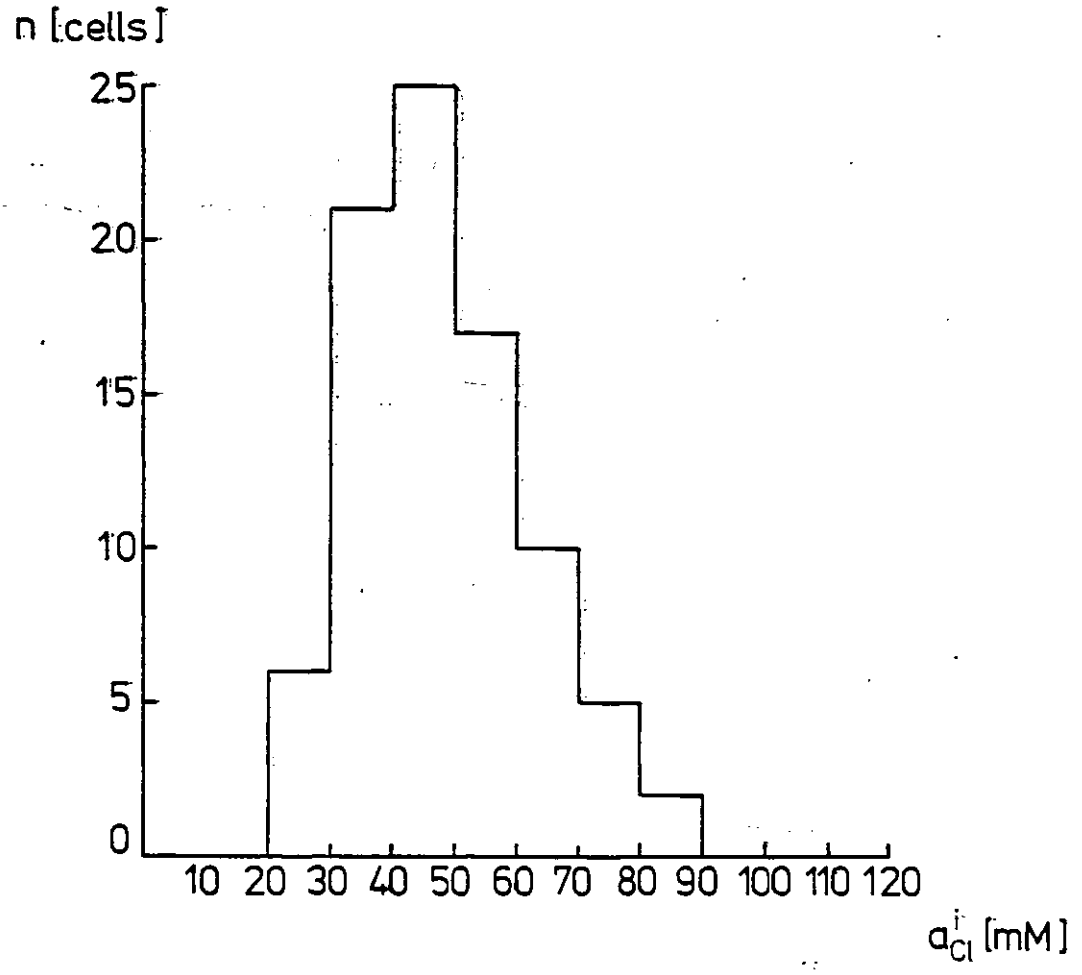

Fig. 93. Histogram of frequency distribution of a^i_{Cl} values obtained with a Cl^- ISMs from L_1-type horizontal cells.

IV.4 Distribution of E_{Cl}

E_{Cl} values for the horizontal cells were calculated using equation 25 (section IV.1). A histogram of the distribution of the E_{Cl} values obtained from the 84 L_1-type cells is shown in fig. 94. This distribution is quite narrow with a sharp peak for the mode, and this interval contains the mean value, -19 ± 2 mV. This narrow distribution of E_{Cl} values further supports the suggestion that the wide range of a^o_{Cl} values observed is not caused by experimental error since these a^o_{Cl} measurements are used to calculate E_{Cl} values, and they produce a very consistent E_{Cl} result.

Similarly, for the 14 C_b-type horizontal cells studied, the mean value of E_{Cl} found is -22 ± 2 mV.

IV.5 Comparison of E_{Cl} with E_m

The histograms of the distribution of E_{Cl} and E_m obtained with Cl^- ISMs for the same population of 84 L_1-type horizontal cells, are shown together on a common abscissa for comparison in fig. 95. There is a small amount of overlap between the distributions of E_{Cl} and E_m but it is clear that E_{Cl} is significantly more positive than E_m such that the magnitude of the difference between E_{Cl} and E_m is about the same as that of E_{Cl} itself. This is a significant finding since it shows that in L_1-type horizontal cells of the roach retina, Cl^- is not passively distributed across the cell membrane, but that it must be actively transported into the cell and could possibly contribute to an electrogenic mechanism in these cells. Further it shows that the level of E_{Cl} with respect to E_m is such that Cl^- could possibly be involved in maintaining the depolarised level of the dark resting membrane potential, E_m.

E_{Cl} is more positive than E_m by an average of 12 ± 2 mV for L_1-type horizontal cells, and 11 ± 2 mV for C_b-type cells.

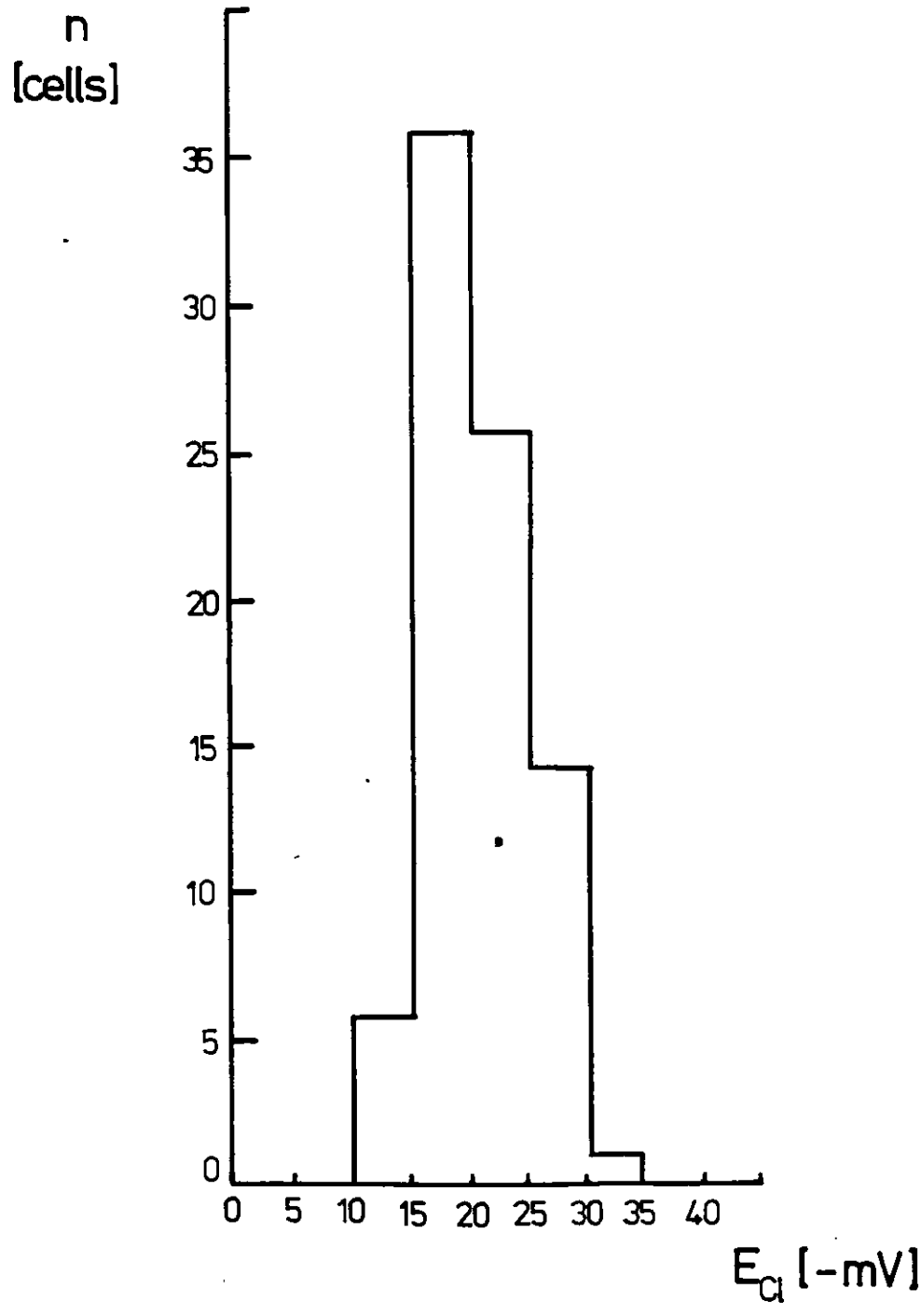

Fig. 94. Histogram showing distribution of E_{Cl} values for L_1-type horizontal cells obtained with Cl^- ISMs.

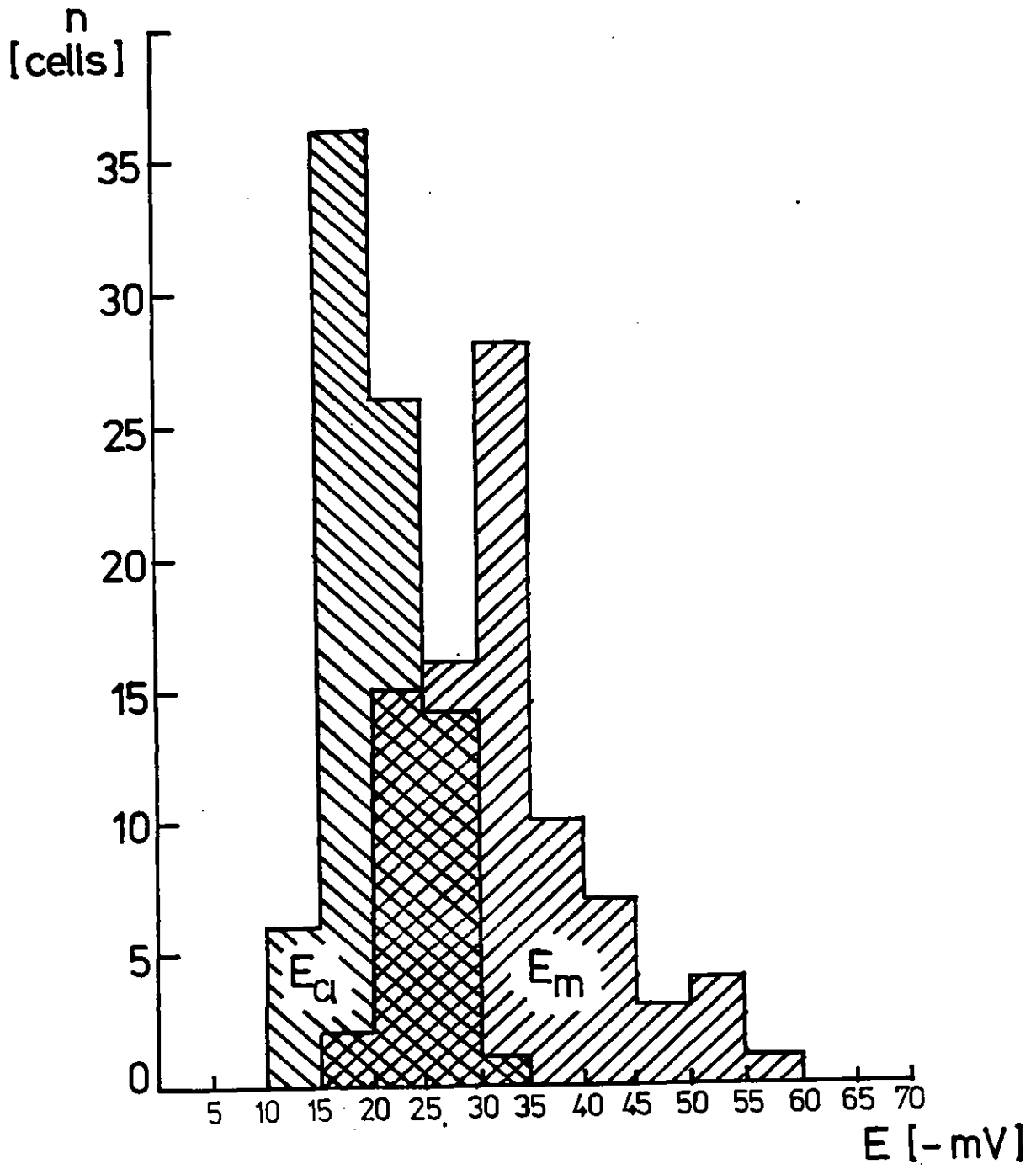

Fig. 95. Histogram of distribution for E_{Cl} and E_m in L_1-type horizontal cells shown on a common abcissa for comparison.

The difference between E_{Cl} and E_m is shown in fig. 96 for both L_1-type and C_b-type horizontal cells using an ordinate representing potential across the cell membrane, V_m. The unbroken lines represent the mean values of E_{Cl} and E_m for L_1-type cells on the left and C_b-type cells on the right, and the broken lines represent the corresponding standard errors. It is seen that E_{Cl} is significantly more positive than E_m for both types of cell.

The relationship between E_{Cl} and E_m is represented in fig. 97 as a distribution of points each representing a single L_1-type horizontal cell with its own values of E_{Cl} and E_m, plotted on a graph with E_{Cl} as ordinate and E_m as abscissa. The broken line represents the equality, $E_m = E_{Cl}$. The distribution of points with respect to this line shows that for all cells in which measurements were made and selected according to the criteria, E_m was more negative than E_{Cl}. The solid line is a linear regression of the points with a slope of 0.27 and a correlation coefficient of 0.53.

As the position of E_{Cl} with respect to E_m in L_1-type horizontal cells is now firmly established, the relationship between E_{Cl} and E_m can be further investigated by ascertaining how $E_{Cl}-E_m$ varies with E_m. This relationship is shown in fig. 98 with points representing single L_1-type horizontal cells on a graph with $E_{Cl}-E_m$ as ordinate and E_m as abscissa. The diagram shows clearly that the difference $E_{Cl}-E_m$ increases as E_m increases in magnitude and thus in the cells with the deeper resting membrane potentials, the E_{Cl} is more widely separated from E_m than it is in the cells with smaller E_ms. Thus, given that the dark resting membrane potential, E_m, is determined by two or more ionic mechanisms and that one of these may involve Cl^-, this relationship between $E_{Cl}-E_m$ and E_m suggests that the contribution of Cl^- to the generation of E_m is greater in those cells with smaller membrane potentials. It has already been shown that $(E_K - E_m)$ has the inverse relationship with E_m

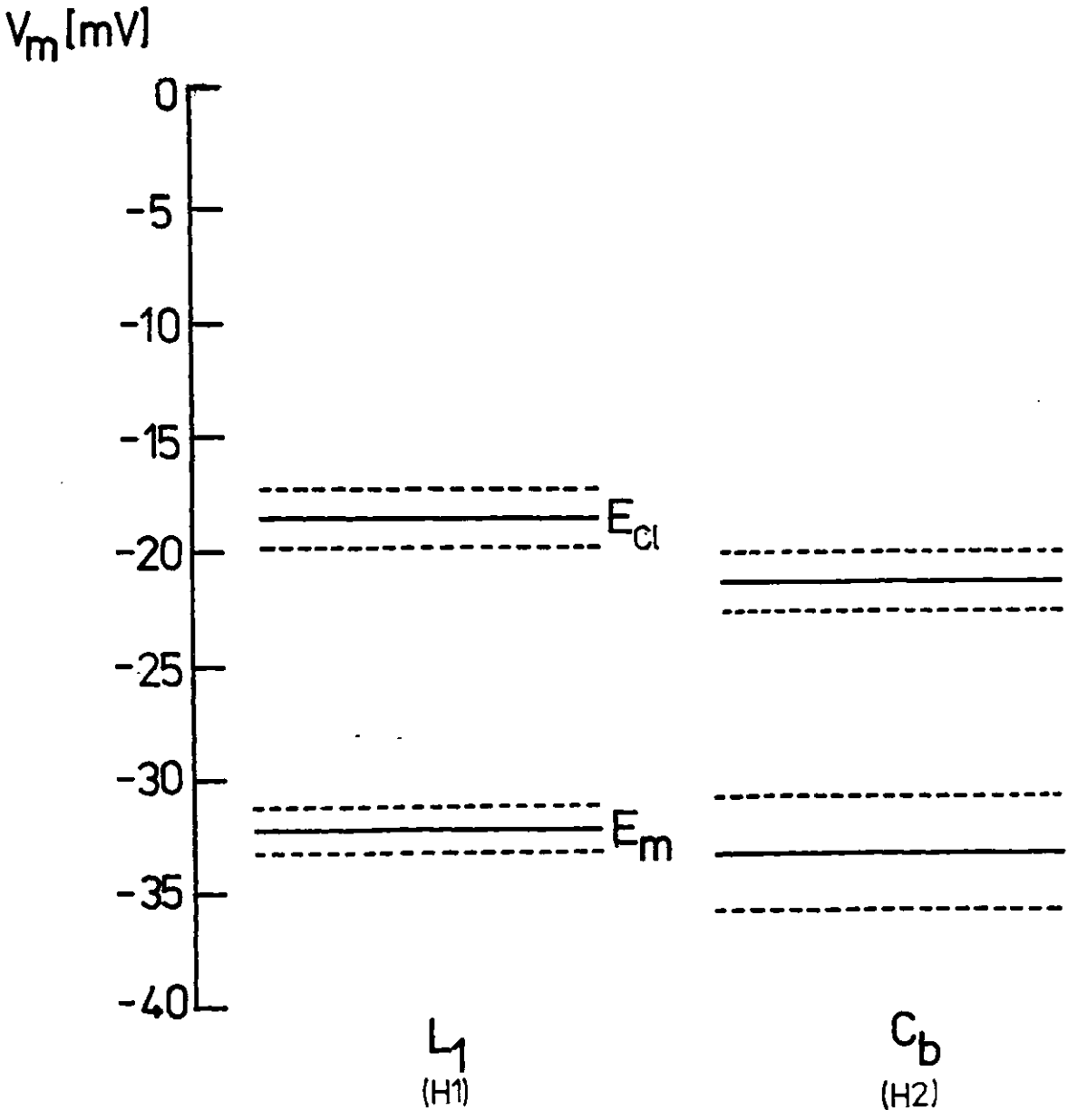

Fig. 96. Diagram showing potential levels of E_{Cl} and E_m for both L_1- and C_b-type horizontal cells. Heavy lines represent mean values and broken lines the corresponding standard errors.

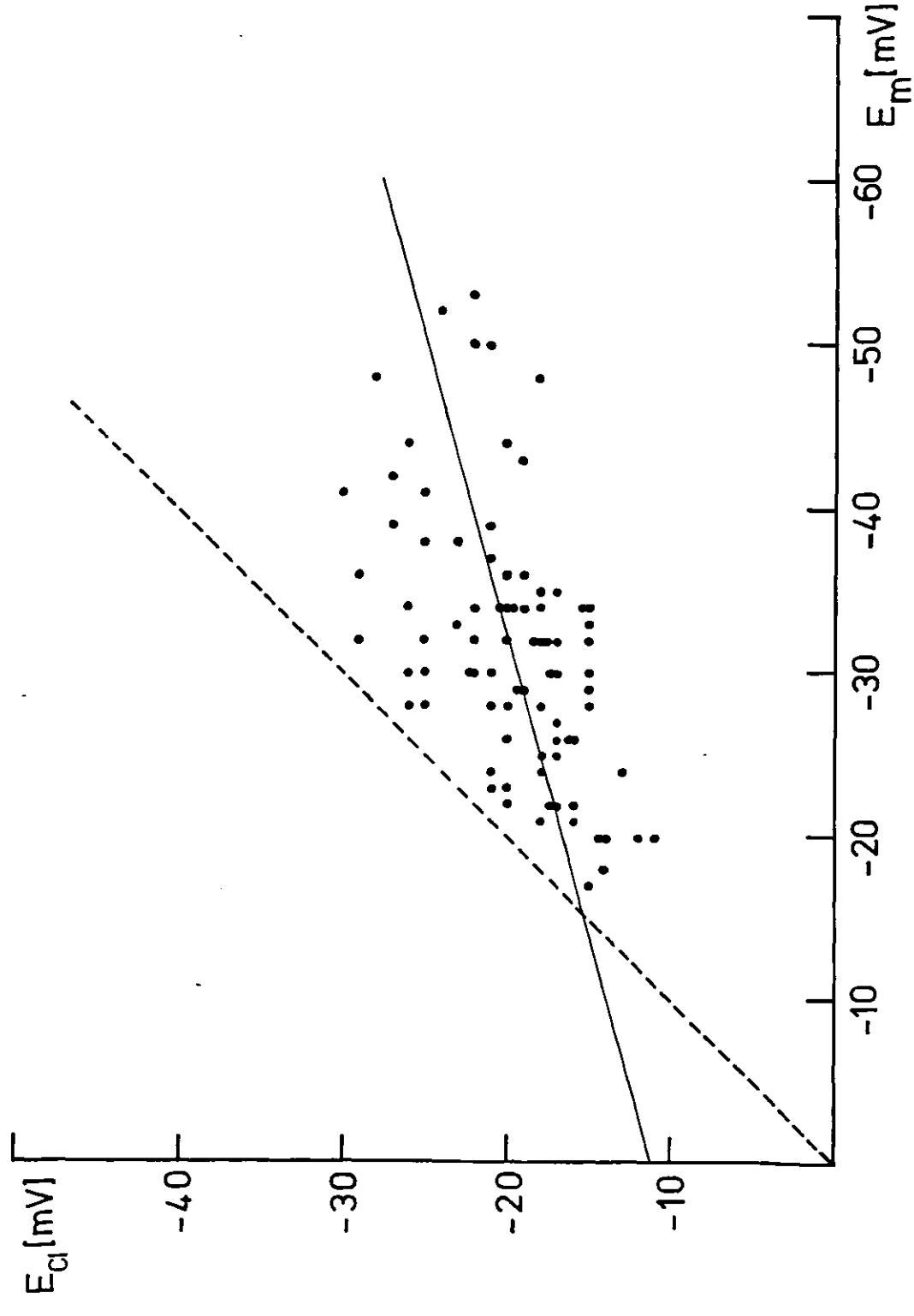

Fig. 97. Distribution of points representing L_1-type horizontal cells showing the relationship between E_{Cl} and E_m for these cells. The solid line is a linear regression of the points and the broken line denotes the equality, $E_m = E_{Cl}$ showing that for all the cells, $|E_{Cl}| < |E_m|$.

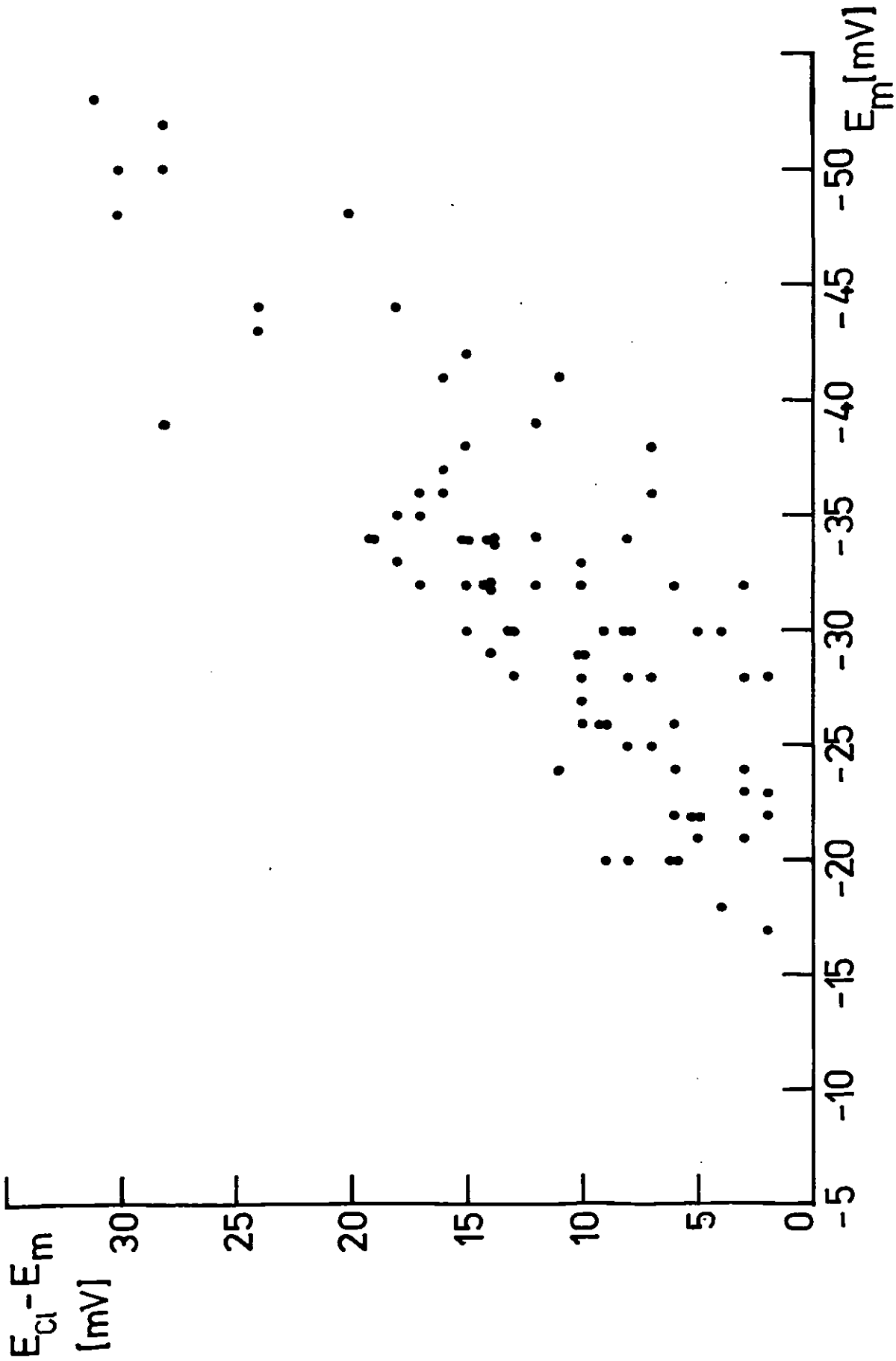

Fig. 98. Distribution of E_{Cl} - E_m versus E_m for L_1-type horizontal cells. The difference, $E_{Cl}-E_m$, is greater for the larger values of E_m.

(fig. 81, section III.6).

IV.6 Measurements of E_m with Cl^- ISMs and Ordinary Microelectrodes

As noted in section II.7, a major criterion that needs to be satisfied before any ISM data can be accepted, is that resting membrane potentials recorded by ISMs should be the same as those recorded by ordinary microelectrodes. In order to meet this criterion, the distributions of E_m for L_1-type horizontal cells obtained with ordinary microelectrodes (OMs) and Cl^- ISMs were recorded in the same retinae, and are compared in the histograms of fig. 99a and b, respectively. The shaded histograms represent E_m distributions obtained from a single retina with OMs from 13 cells (a) and with Cl^- ISMs from 7 cells (b). These histograms are similar with a common mode. The larger unshaded histograms represent distributions of E_m for L_1-type horizontal cells obtained from measurements with OMs (a) and Cl^- ISMs (b) in the same retinae. The OM histogram for E_m consists of 67 measurements and the ISM histogram for E_m contains 84 results. The two distributions have a common mode with the peak more emphasised in the ISM histogram; in this histogram the interval of the mode contains the mean value of -32±1 mV. The mean value of E_m obtained with ordinary microelectrodes is -36±1 mV. The modes of these two E_m histograms and the more comprehensive one shown in fig. 75 are identical, and the ISM histogram can be seen to represent a part of the larger distribution. Thus, the irregularities in the ISM histogram are probably due to the limited number of results arising from the strict selection criteria. Since the Cl^- ISM distribution for E_m is essentially similar to the OM distribution it is suggested that ISMs do not cause any significant cell damage and that tip potential effects are negligible.

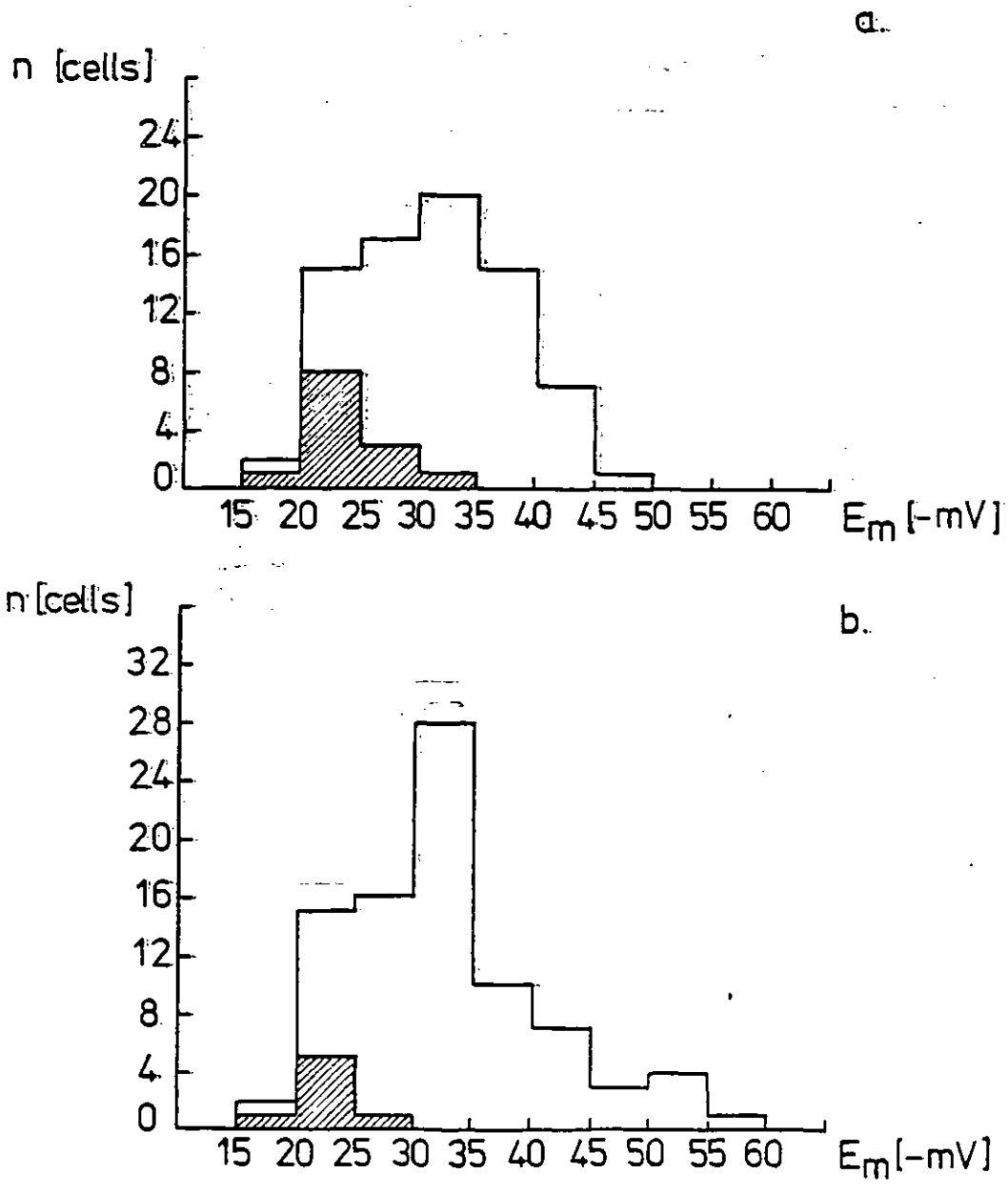

Fig. 99. Histograms showing comparison of E_m distribution obtained with Cl^- ISMs (a) and with ordinary microelectrode (b). The shaded histograms represent results from a single retina.

IV.7 Changes in a^i_{Cl} During Light-Evoked Responses of Horizontal Cells

An intracellular recording with a Cl^- ISM from an L_1-type horizontal cell is shown in fig. 100. The lower trace shows the membrane potential, V_m, and the upper trace the intracellular Cl^- activity, a^i_{Cl}. This L_1-type cell had an E_m of -23 mV and the V_m trace shows the hyperpolarising responses to saturating red light of nearly 30 mV amplitude which were obtained. The V_{Cl} trace shows that a^i_{Cl} in the dark was 75 mM. The transient responses in the V_{Cl} trace are most probably due to the differential time response artefact (Appendix 5). To investigate the change in a^i_{Cl} during the light-response, the light was held on for a short-time, shown by the upward deflection of the stimulus-monitor trace below the V_m trace. It is seen that the level of a^i_{Cl} decreased during the sustained light-stimulus by 20 mM.

This change in a^i_{Cl} which occurs during the response to light in L_1-type cells is such that Cl^- flows out of the horizontal cell during hyperpolarisation. This is inconsistent with the hypothesis that the light-evoked hyperpolarisation is due solely to a decrease in Cl^--permeability in the subsynaptic membrane of the horizontal cell corresponding to the reduction in transmitter from the photoreceptors during the light-stimulus. The observed changes in a^i_{Cl} are consistent, however, with a passive movement of Cl^- across the cell membrane in response to the shift in trans-membrane electrical potential, V_m. If there is a light-evoked, synaptically driven increase of a^i_{Cl}, it seems to be obscured by the larger effect of the membrane potential (electrical gradient) change. All of the L_1-type horizontal cells studied showed either a light-evoked decrease of a^i_{Cl} or no change. The hyperpolarisation response of C_b-type horizontal cells was also associated with a similar effect whilst depolarisation responses to red light stimuli were accompanied by an increase of a^i_{Cl}, again, as expected from the change of membrane potential. These results on changes in a^i_{Cl} during the light-

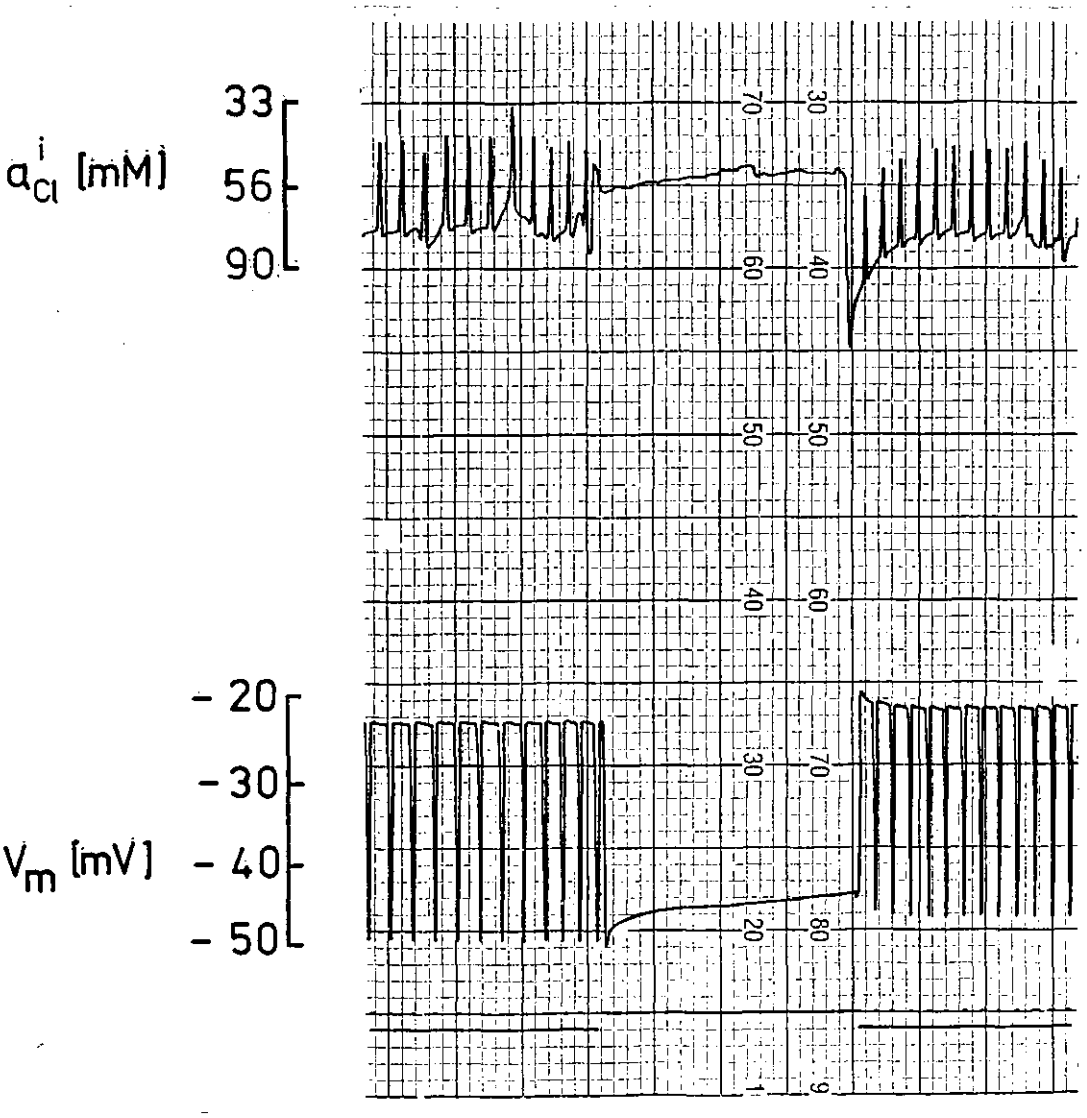

Fig. 100. Intracellular recording from an L_1-type horizontal cell with a Cl^- ISM showing responses to flashes of red light and to a period of sustained illumination. Onset of light is denoted by upward deflection in the stimulus monitor (lowest) trace.

evoked responses of the horizontal cells cannot be interpreted further without voltage-clamping their membranes. They are, however, discussed further in Chapter V.

IV.8 E_{Cl} and Depolarisation of C_b-Type Horizontal Cells

In the absence of voltage-clamping, results on changes in a^i_{Cl} during the light-evoked responses of the horizontal cells are inconclusive. Since E_{Cl} is always more positive than E_m in both L_1- and C_b-type units, Cl^- can only be involved in a depolarising response of these cells. Since C_b-type units depolarise in response to red light stimulation, experiments were undertaken to test whether the saturation level of these depolarisations coincided with the corresponding E_{Cl} levels. Thus, V-log I curves were obtained from 3 C_b-type units, and the results are summarised in fig. 101. This is a plot of membrane potential, V_m (ordinate) against log. of light intensity (abscissa). The points represent the depolarising responses to red light of the C_b-type horizontal cells, as the intensity is increased in steps of 0.5 log units, with a different symbol for each cell. With these depolarising responses, increasing light intensity causes the response to saturate at some point after which further increase of intensity would often bring about a decrease in response amplitude. The broken lines in the lower part of the figure represent E_ms of these cells depicted by their symbols and those in the upper part represent their respective E_{Cl}s. The 'triangle' cell response saturated at an illumination level 3.0 log units above threshold, at a level of depolarisation corresponding exactly with E_{Cl}, after which a decrease in response amplitude to supersaturation intensity is seen. This effect is also seen to a lesser extent in the responses of the cell represented by the 'square' symbol. These responses saturated at 3.0 log units above threshold at a level 1 mV below E_{Cl}.

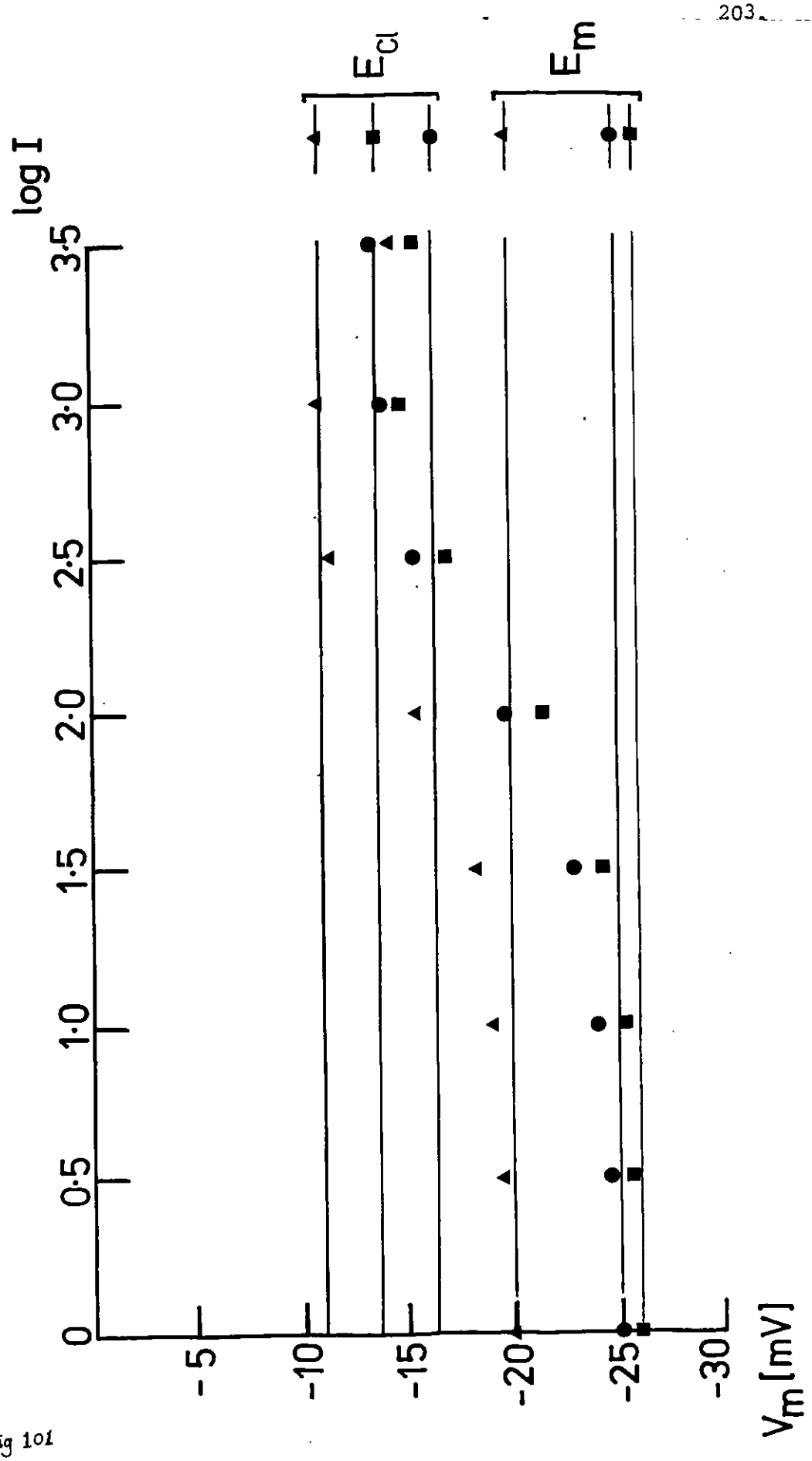

Fig 101

Results from experiments using flashes of red light of increasing intensity while recording from C_b-type horizontal cells with Cl^- ISMs. Results from three cells are shown. Membrane potential (V_m) is plotted against log of intensity (I) of light stimulus. E_{Cl} was calculated for each cell from the value of a^i_{Cl} during the response to saturating light.

The 'circle' cell reached near saturation at 3.5 log units above threshold at a depolarisation level 3.5 mV above E_{Cl}. Thus there seems to be a correspondence between the maximal depolarisation response of a C_b-type horizontal cell to red light of increasing intensity and the E_{Cl} of that cell. This suggests that the depolarisation response may be mediated by a light-elicited permeability increase to Cl^- in the sub-synaptic membrane of C_b-type horizontal cells.

IV.9 E_{Cl} and Depolarisation of L_1-Type Horizontal Cells: Effects of Dopamine.

As noted in the preceeding section, if chloride ions are involved in horizontal cell membrane electrogenesis, they can only contribute to depolarising, i.e. excitatory responses, assuming that the underlying synaptic mechanism is conventional whereby transmitter molecules open ionic channels. L_1-type horizontal cells are known to receive two sets of excitatory synaptic input, one from cone photoreceptor cells, the other from the interplexiform cells. The neurotransmitter operating at the former is not known, whilst there is reasonable evidence that the interplexiform cell of the cyprinid fish retina uses dopamine as its transmitter (Dowling & Ehinger, 1975). Thus, experiments were undertaken to explore the possibility that the excitatory, depolarising action of dopamine on L_1-type horizontal cells might involve Cl^-.

Stable measurements were obtained from 41 L_1-type horizontal cells in 8 retinae following application of dopamine (plus sodium ascorbate) to the retina. In each retina a small number of control impalements were made to establish that Cl^- readings were in accordance with measurements described earlier in the untreated state of the retina. Readings were taken following spraying of the retinae with 0.1 mM dopamine and 10 mM ascorbate, the latter being included to prevent enzymatic oxidation of the amine in the retina. Results are given in figures 102-106, and are

summarised in Table 8.

Following application of dopamine, L_1-type horizontal cells were found to have relatively depolarised resting potentials (E_m = -12±1 mV cf. - 32±1 mV control) (fig. 102, Table 8). The a^i_{Cl} of the cells showed a clear increase from a control value of 47±1 mM to 55±2 mM. Figure 103 shows a pair of histograms on a common abscissa, which compare the distributions of a^i_{Cl} before (fig. 93) and after dopamine application. This increase in a^i_{Cl} would be expected from the depolarisation of the membrane potential. The distribution of E_{Cl}s before and after dopamine application is given in fig. 104, which shows that dopamine causes a shift in E_{Cl} to smaller values. The mean (± S.E.) of the 'after' distribution is -13±2 mV compared to -19±2 mV for the 'before' distribution (Table 8). Figure 105 shows the comparison of distributions of E_m and E_{Cl} after dopamine application. These distributions display a very close correspondence. After dopamine application the mean (±S.E.) values for the distribution of E_m =-12±1 mV, and for E_{Cl} = -13±2 mV and for $E_{Cl}-E_m$ =-0.7±0.3 mV (Table 8). This data is also presented in graphical form in fig. 106 which shows the relationship between E_{Cl} and E_m for the population of cells studied both before and after dopamine application. The distribution of points denote the E_{Cl} vs E_m relationship for the 41 cells studied in dopamine-treated retinae. These points can be fitted with a straight line of slope 0.77 by linear regression, the correlation coefficient being 0.91. This is drawn as a solid straight line 'D', whilst the similar line obtained for the control data (fig. 97) is also included as the straight line 'C' for comparison. A straight line 'T' of slope 1 is shown as the theoretical line of equality of E_m and E_{Cl}. As seen in fig. 106, following application of dopamine to the retina, E_m's become very close in magnitude to the corresponding E_{Cl}'s: $E_{Cl}-E_m$ =-0.7±0.3 mV cf. 12±2 mV control (Table 8).

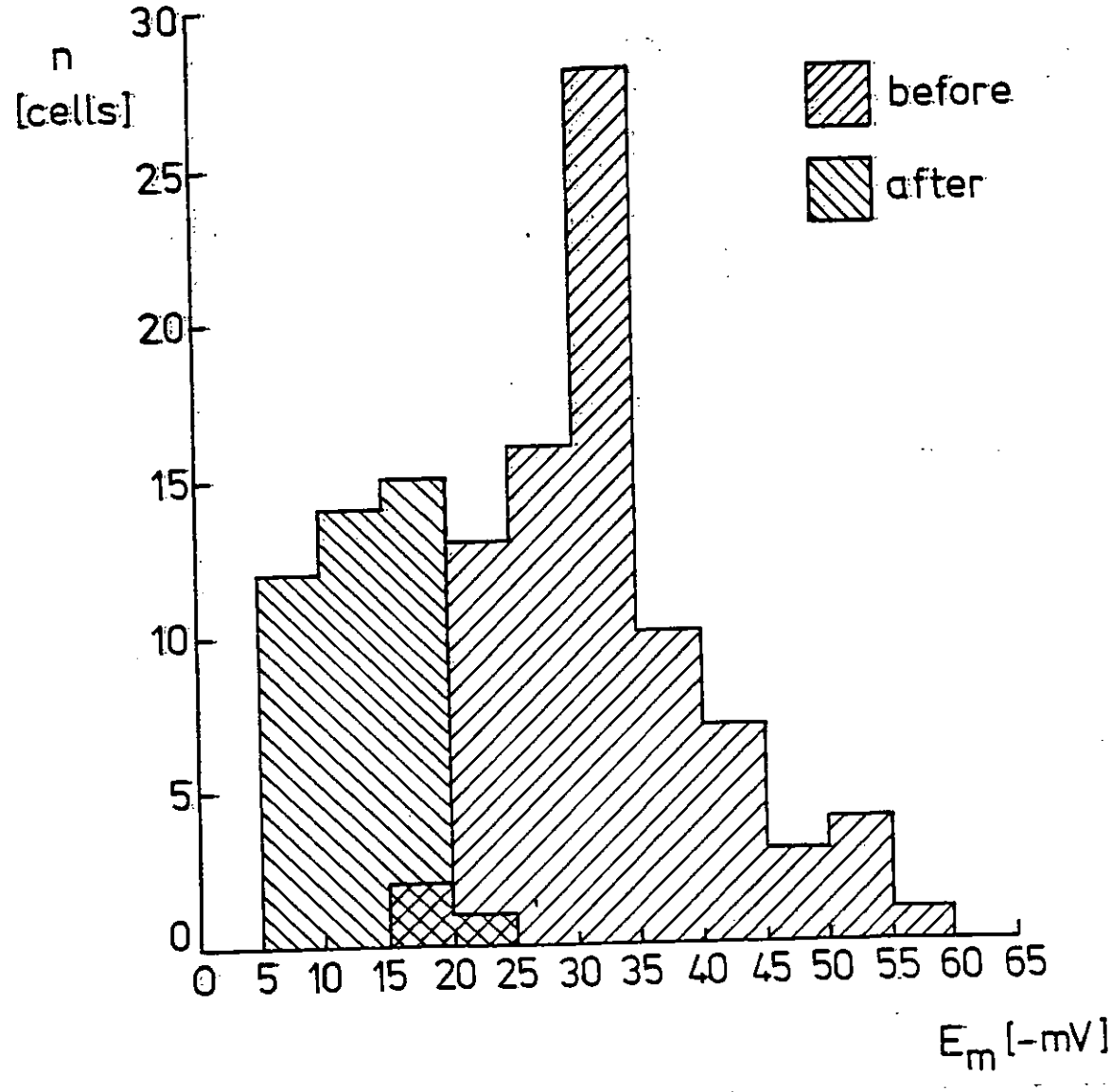

Fig. 102. Histograms of E_m distribution for L_1-type horizontal cells both before and after application of dopamine to the retina, shown on a common abscissa for comparison.

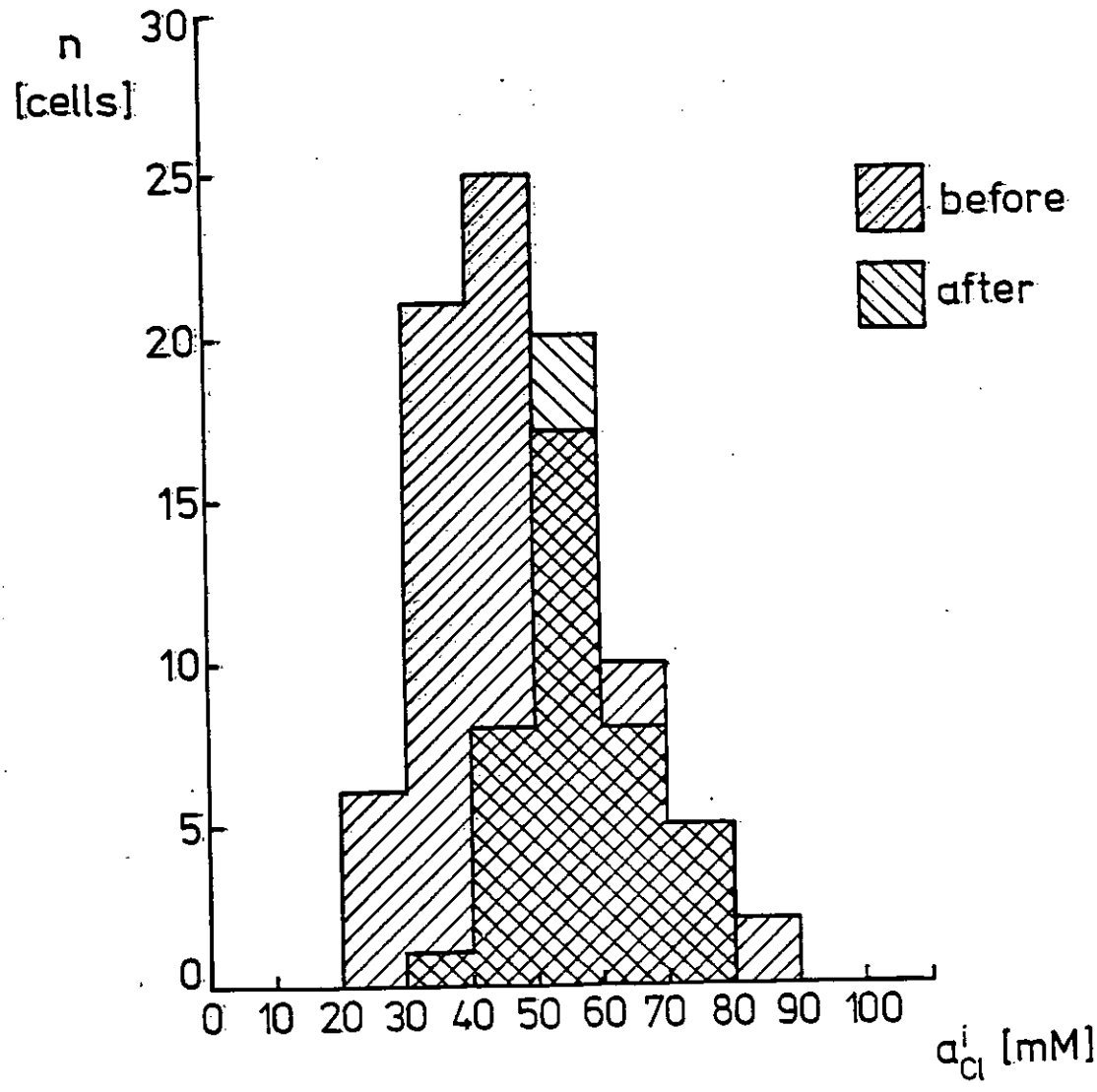

Fig. 103. Histogram of distribution of a^i_{Cl} for L_1-type horizontal cells both before and after application of dopamine to the retina.

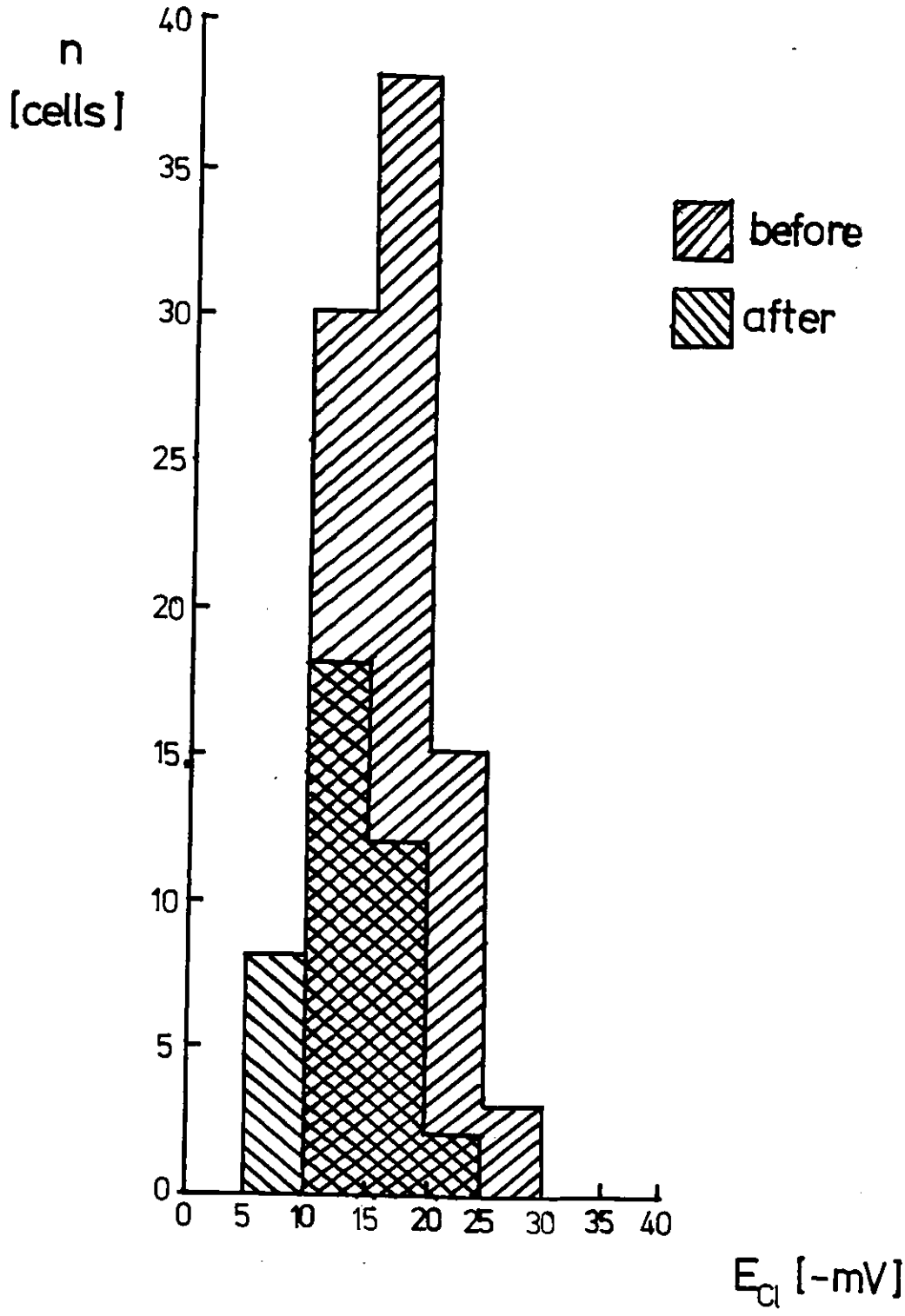

Fig. 104. Comparison of distributions of E_{Cl} for L_1-type horizontal cells before and after dopamine application to the retina

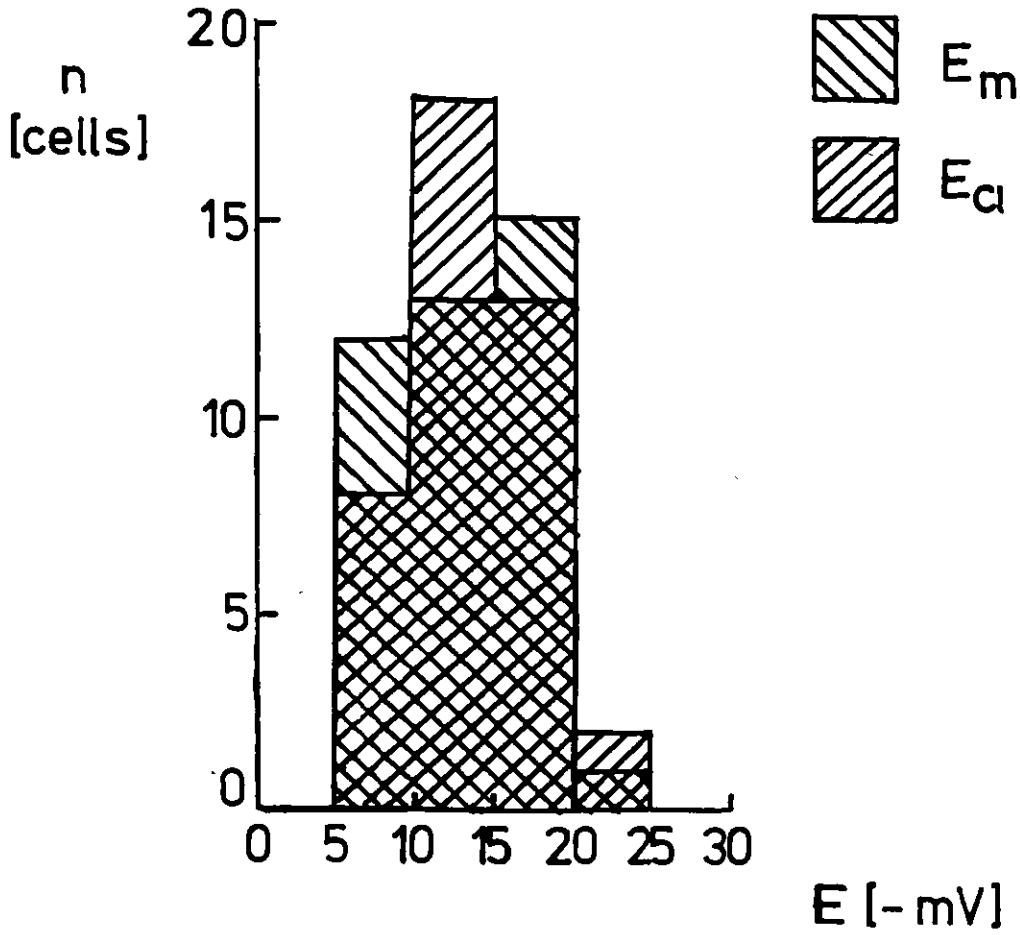

Fig. 105. Histograms showing comparison between distributions of E_m and E_{Cl} for L_1-type horizontal cells after application of dopamine to the retina.

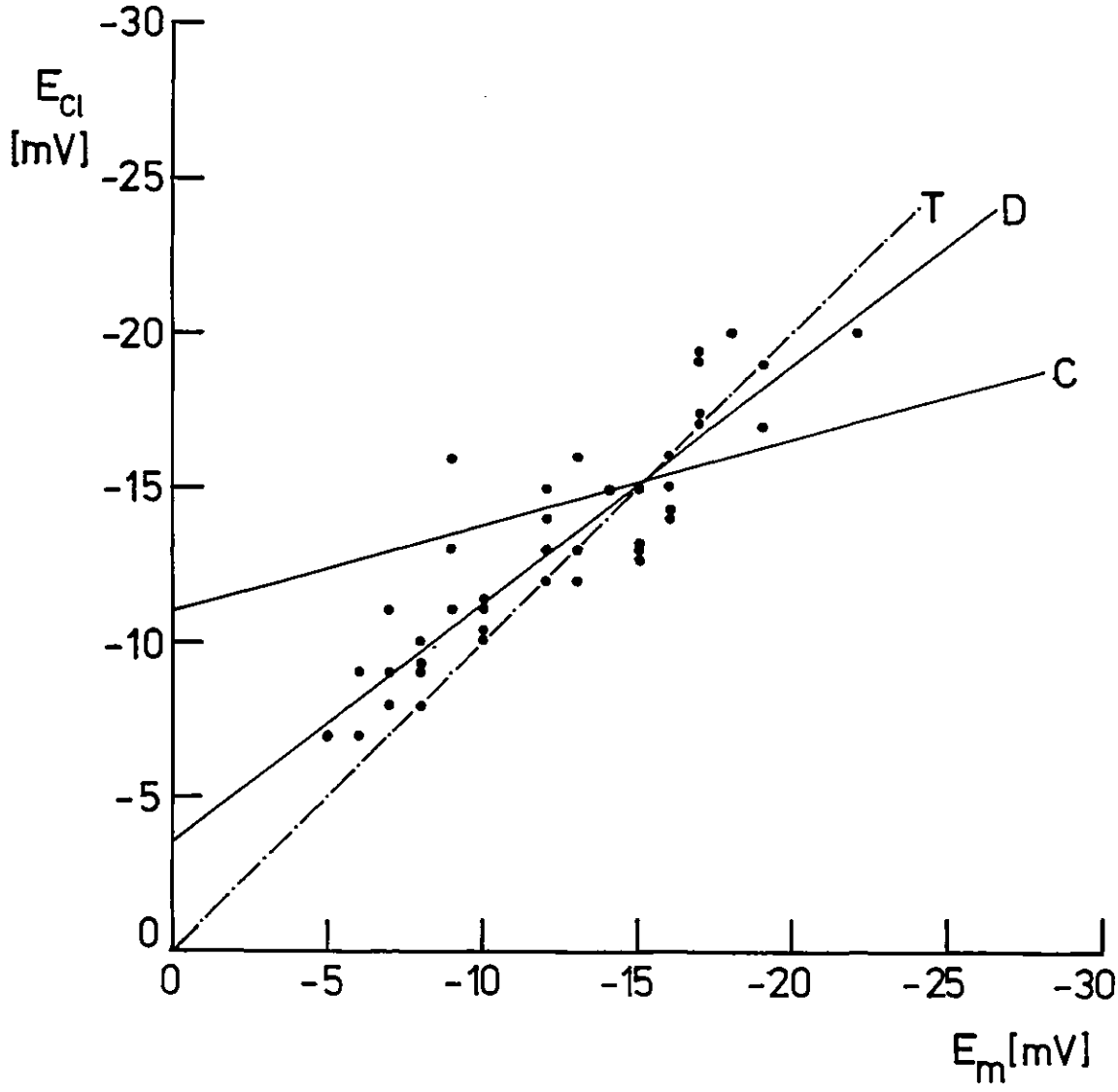

Fig. 106. Distribution of points representing L_1-type horizontal cells showing relation between E_{Cl} and E_m after dopamine application. D is a line of linear regression of these points; C is the line of linear regression for the points representing E_{Cl} versus E_m before dopamine application (Fig. 96) for comparison; T is a line representing the equality $E_m = E_{Cl}$.

Thus dopamine has the effect of abolishing the potential difference between E_m and E_{Cl} in L_1-type horizontal cells by depolarising E_m and also to a lesser extent E_{Cl}. These results are consistent with the hypothesis that dopamine acts by opening Cl^- channels in the horizontal cell membrane. Since the interplexiform cells use dopamine as a transmitter, it is possible that the feedback pathway from interplexiform cells to horizontal cells is used to control dopamine-sensitive Cl^- channels in the subsynaptic membrane of L_1-type horizontal cells.

IV.10 Summary of Results

The results on control Cl^- activity measurements presented in this chapter are summarised in Table 9 which shows the physiological parameters obtained from combining the results listed in Tables 6 and 7 to produce mean and standard error values. The number of significant figures quoted is never greater than that determined by an objective criterion (Barford, 1967) and values were rounded up to the next integer (see section III.9). Mean and standard error values are given for parameters corresponding to those for the K^+ results (section III.9).

These results suggest the following observations of interest: $\bar{a}^o_{Cl}$ is higher than $\bar{a}^i_{Cl}$ by about a factor of 2; the value of $\bar{c}^o_{Cl}$ (128±8 mM) is higher than that normally used by some workers to perfuse retinae in fish Ringer solutions (range 88.1 to 126.9 mM; Appendix 7); $\bar{E}_{Cl}$ is more positive than $\bar{E}_m$ and its magnitude is about half that of $\bar{E}_m$ so that the magnitude of $\overline{E_{Cl}-E_m}$ is similar to that of $\bar{E}_{Cl}$ itself. After application of dopamine to the retina, however, $\bar{E}_{Cl}$ is almost exactly the same as $\bar{E}_m$ (Table 8).

Table 6. Cl^- Activity Measurements on L_1(H1)-Type Horizontal Cells

ISM No.	R_r (MΩ)	R_a (MΩ)	a^o_{Cl} (mM)	Cell No.	E_m (mV)	a^i_{Cl} (mV)	E_{Cl} (mV)	$E_{Cl}-E_m$ (mV)
EC 11	300	120K	80	1	-48	32	-28	20
S=56				4	-41	36	-25	16
				5	-44	35	-26	18
				8	-50	41	-22	28
EC 17	400	250K	125	1	-33	75	-15	18
S=48				2	-50	60	-21	30
				6	-28	75	-15	13
				7	-24	65	-18	6
				12	-38	56	-23	15
				13	-28	50	-25	3
				14	-33	56	-23	10
EC 18	500	320K	54	4	-48	26	-18	30
S=48				6	-52	20	-24	28
EC 21	580	300K	130	1	-22	70	-17	5
S=47				3	-23	65	-20	3
				4	-22	66	-20	2
				12	-18	80	-14	4
				17	-26	66	-20	6
				18	-20	80	-14	6
EC 23	400	250K	95	1	-25	52	-17	8
S=49								
EC 27	350		90	1	-32	50	-15	17
S=48				10	-36	42	-19	17
EC 28	500	180K	95	7	-34	54	-15	19
S=52				8	-36	42	-20	16
				9	-34	42	-20	14
				13	-44	42	-20	24
				21	-25	46	-18	7
				22	-26	48	-17	9
				23	-22	50	-17	5
EC 31	500	200K	143	2	-35	70	-18	17
S=42				3	-43	65	-19	24
				4	-29	65	-19	10
				5	-21	70	-18	3
				6	-30	58	-22	8
				8	-28	52	-18	10
				12	-34	65	-19	15
				17	-29	65	-19	10
				24	-32	60	-22	10
				25	-30	58	-22	8
				30	-32	46	-29	3
				35	-30	52	-25	5

ISM No.	R_r (MΩ)	R_a (MΩ)	a^o_{Cl} (mM)	Cell No.	E_m (mV)	a^i_{Cl} (mV)	E_{Cl} (mV)	$E_{Cl}-E_m$ (mV)
EC 32	1000	200K	75	19	-34	25	-26	8
S=44				20	-24	32	-21	3
				21	-28	25	-26	2
				23	-23	32	-21	2
				25	-28	32	-21	7
				27	-36	23	-29	7
				28	-30	40	-15	15
				29	-30	32	-21	9
				30	-30	25	-26	4
EC 34	300	275K	90	1	-28	42	-20	8
S=47				2	-37	40	-21	16
				5	-38	34	-25	7
				6	-42	30	-27	15
				8	-39	30	-27	12
				9	-30	46	-17	13
EC 39	500	390K	80	4	-34	32	-22	12
S=44				5	-32	38	-18	14
				6	-34	36	-20	14
				7	-35	40	-17	18
				9	-32	40	-17	15
				10	-34	38	-18	15
				12	-32	30	-25	6
				14	-34	36	-20	14
EC 57	280	100K	74	18	-29	40	-15	14
S=53				21	-30	36	-17	13
				22	-27	36	-17	10
				24	-24	43	-13	11
EC 58	160	120K	74	27	-32	33	-20	12
S=52								
EC 59	110	94K	85	34	-32	42	-18	14
S=52				36	-32	42	-18	14
				38	-34	47	-15	19
EC 60		124K	100	45	-26	52	-16	9
S=51				46	-39	44	-21	28
				53	-53	42	-22	31
				57	-41	31	-30	11
EC 62	102	62K	89	58	-26	48	-16	10
				59	-22	48	-16	6
				61	-17	50	-15	2
				63	-20	57	-11	9
EC 63	95	73K	95	70	-21	50	-16	5
S=54								
EC46	115	50K	64	1	-20	40	-12	8
S=57				2	-20	37	-14	6

Table 7. Cl^- Activity Measurements on C_b(H2) Type Horizonal Cells

ISM No.	R_r (MΩ)	R_a (MΩ)	a^o_{Cl} (mM)	Cell No.	E_m (mV)	a^i_{Cl} (mM)	E_{Cl} (mV)	$E_{Cl}-E_m$ (mV)
EC 11(C) S=55	300	120K	80	3	-29	49	-17	12
EC 17(C) S=48	400	250K	80	8	-36	52	-25	11
EC 28C S=52	500	180K	95	12	-44	46	-18	16
				16	-35	46	-18	17
					-32	38	-24	8
EC 31C S=42	500	200K	143	8	-32	52	-25	7
				10	-25	58	-22	3
				15	-32	58	-22	10
				17	-26	58	-22	4
					-22	58	-22	0
EC 32C S=44	1000	200K	75	26	-44	19	-33	11
EC 59 S=52	110	94K	85	37	-25	45	-16	9
EC 60 S=51		124K	100	51	-56	33	-29	27
EC 62 S=52	102	62K	89	60	-31	44	-18	13

Table 8. Effects of Dopamine on L_1-type Horizontal Cells

	CONTROL	0.1 mM DOPAMINE
E_m (mV):	-32±1	-12±1
a^i_{Cl} (mM):	47±1	55±2
E_{Cl} (mV):	-19±2	-13±2
$E_{Cl}-E_m$ (mV):	12±2	− 0.7±0.3

All figures given are mean ± standard error

Table 9. Summary of Results of Chloride Activity Measurements

a^{o}_{Cl}	= 95±6 mM	C^{o}_{Cl}	= 128±8 mM
$E_m(L_1)$	= -32±1 mV		
$E_m(C_b)$	= -34±3 mV		
$a^{i}_{Cl}(L_1)$	= 47±2 mV	C^{i}_{Cl}	= 64±3 mM
$a^{i}_{Cl}(C_b)$	= 47±3 mV	$C^{i}_{Cl}(C_b)$	= 64±4 mM
$E_{Cl}(L_1)$	= -19±2 mV		
$E_{Cl}(C_b)$	= -22±2 mV		
$E_{Cl}-E_m(L_1)$	= 12±2 mV		
$E_{Cl}-E_m(C_b)$	= 11±2 mV		

All figures given are mean ± standard error

CHAPTER V

GENERAL DISCUSSION AND CONCLUSIONS

V.1 General Comments

The principal aims of the present study were threefold:

1. Design and construction of a system suitable for fabricating double-barrelled ion-sensitive microelectrodes (ISMs) based on liquid ion-exchangers. This system was based on that described by Thomas (1978a). ISMs were manufactured according to the method of Berridge and Schlue (1978), which was modified and improved as described in Chapter II.

2. Design and construction of an electrophysiological system suitable for intracellular recording from retinal neurones with ISMs, in the dark or during light stimulation. This system was based on Svaetichin's (1953) original design, and has been described in Chapter II.

3. To use these ISMs and the electrophysiological system to obtain intracellular recordings of ionic activity and membrane potential from luminosity (L_1) and chromaticity (C_b) type horizontal cells in the retina of a common cyprinid fish, the roach (Rutilus rutilus). Thus, intracellular potassium and chloride activities of these neurones have been measured for the first time. These results have been presented in chapters III and IV.

The principal objectives of the present study, therefore, have been largely achieved.

V.2 A General Discussion of the ISM Technique

As noted in equation 5.(I.7), an intracellular ISM measures the membrane potential as well as an activity-dependent potential. In order to evaluate the latter, it is necessary to subtract the membrane potential (recorded by an ordinary microelectrode) from the ISM

potential. In the case of large (e.g. snail) neurones that can also be visualised, this can be achieved by impaling a single cell with two separate microelectrodes under microscopic observation. In the present study, however, this procedure was not possible, so double-barrelled ISMs had to be developed. An initial step in the manufacture of an ISM based on a liquid ion-exchanger (LIX) is the silanisation of the active barrel. Silanisation is required in order to make the interior of the glass micropipette hydrophobic/organophilic. This, in turn, ensures that the column of LIX is held firmly at the tip of the microelectrode and that the back-filling solution does not creep to the tip thereby creating a low-resistance shunt. Silanisation also overcomes the tendency of untreated glass to behave to some extent like a cation-sensitive electrode (Walker, 1976). A variety of silanes and silanisation techniques have been used (e.g. Zeuthen et al, 1974; Oakley, 1977; Coles & Tsacopoulos, 1977). In the present study the method of Berridge and Schlue (1978) was used as it was simple and effective. This involved exposing the wide end of the active barrel to the vapour of dimethydichlorosilane (DDS) for 30 to 60 seconds, and then heating the micropipettes at 100^{o}C in an oven for one hour.

Following silanisation, a small quantity of LIX was injected by pressure into the shank of the active barrel from a smaller-diameter micropipette with a broken tip. Walker (1971) originally recommended the use of LIX columns some 200 μm in length. It is possible, however, to use longer columns (which would make the micro electrodes easier to manufacture) without adverse effects on the electrode resistance or response time, since it has been shown (Armstrong & Garcia-Diaz, 1980) that the resistance, R, of the LIX column in electrodes with very small tips can be approximated by the equation:

$$R = \frac{2\rho}{\pi r \phi} \qquad \text{(equation 14; section I.9.iii)}$$

where ρ = resistivity of the LIX; r = radius of tip; ϕ = angle of taper of shank. Thus, the dependence of the ISM resistance on the length of the LIX column is negligible compared with its dependence on the tip size if small.. In the present study, LIX columns of up to 5 mm were used as reported for ISMs made by Zenthen et al, (1974) and Coles and Tsacopoulos (1979).

The ISMs used in the present study had tip diameters in the range 0.5 to 1 μm (fig. 49a,b). Coles and Tsacopoulos (1979) suggested that the reaction of the silane with the hydrated glass surface on the inside of the micropipette produces a silicone layer of about 0.2 μm thickness. This would imply that the tip diameters of the ISMs produced in this way would have a lower limit of about 0.4 μm. This appeared to be true for the ISMs fabricated during the course of the present study. These ISMs, however, were found to cause no significant damage to the membranes of the horizontal cells, which in the fish retina, are several tens of microns in diameter (Stell, 1972).

Tip potentials constitute an inescapable problem with microelectrode recordings. Tip potentials seem to arise from the presence of an aqueous salt solution inside the tip of a glass microelectrode (section I.9.vi), and therefore, create a problem mainly for ordinary microelectrodes and for the reference barrels of double-barrelled ISMs. For the ISMs used in the present study, the potential recorded by the ion-sensitive barrel when the tip was immersed in an earthed solution of composition identical to that of the backfilling solution, was never more than 2 mV different from the theoretically predicted 0 mV reading. The same has been observed by Vyskocil and Kriz (1972). The tip potentials associated with the reference barrels of the ISMs could only have been eliminated by increasing the tip sizes of the ISMs. This was undesirable, however, since it would lead to damage of the cell membranes, and leakage of the solutions from the electrodes.

The standard method of breaking the tips of electrodes to measure tip potentials was not performed in the present study since it was found that the performance of an ISM often improved on the following day, so ISMs were kept for as long as possible without their tips being broken. Instead, the effect of the ISM tip potentials on the membrane potential (E_m) measurements was investigated by measuring E_m's in a given preparation independently using ordinary microelectrodes of 60-80 MΩ resistances, filled with 2.5 M KCl. Results were accepted only if the two sets of measured E_m values had the same mean, and had similar distributions. Good agreement was usually found between these two sets of values (e.g. figs. 76, 99), thereby suggesting that the tip potentials had been minimised sufficiently so as not to affect adversely the E_m measurements.

Further, investigations performed on the relation between E_m's measured by ISMs and the corresponding values of the reference barrel resistances showed no significant correlation between these two parameters (fig. 77). This evidence provides further support for the claim that tip potentials in these ISMs have been sufficiently minimised, since tip potentials large enough to cause significant artefacts in the measurement of potential would give rise to a dependence of E_m on the reference barrel resistance, R_r.

Another technical consideration concerns the possible dependence of the ISM response upon the value of the total ionic strength of the calibrating solutions. In this study the K^+ ISMs were calibrated in solutions of total ionic strength = 100 mM, while the Cl^- ISMs were calibrated in solutions of total ionic strength = 200 mM. It is obviously necessary that the calibrating solutions define a range of ionic activities which covers the range of activities for that ion measured in the experimental situation. It was found that a range of 0-100 mM concentration was sufficient for the K^+ measurements, while the

measurement of a_{Cl} required a greater range and so 0-200 mM (concentration) was chosen as this was adequate and convenient. The total ionic strength in the retina itself was estimated to lie somewhere between 100 and 200 mM (an exact estimate can not be made without knowledge of the activities of all the physiologically important ions in the retina). Thus the calibrating solutions approximated the environment of the retina in ionic strength, but the question remained as to how closely the calibrating solutions should resemble the retina in order to produce reliable measurements; also was it justifiable to use 100 mM total ionic strength solutions to calibrate K^+ ISMs and 200 mM total ionic strength calibrating solutions for Cl^- ISMs? The effect of doubling the total ionic strength of the calibrating solutions (from 100 to 200 mM) on the response of the ISM was calculated (Appendix 6). It was shown that the maximum change in the ISM potential caused by this difference in total ionic strengths corresponds to a change in ionic activity of less than 1 mM. This change is greater than that due to the difference in total ionic strength between the calibrating solution and the retina since this has an intermediate value between 100 and 200 mM. Thus any error arising from choosing the total ionic strength as described was shown to be negligible. Finally, Thomas (1978a) has suggested that the best filling solution for an ordinary microelectrode would be a non-aqueous liquid ion-exchanger equally sensitive to K^+ and Na^+ but insensitive to divalent cations. Subsequently, Thomas and Cohen (1981) reported such a solution. An attempt was made during this study to obtain a sample volume of this solution, but it was not successful!

V.3 A General Discussion of the Experimental Procedures

The functioning of neurones involves trans-membrane flow of ions, the latter being controlled by specific ionic and electrical gradients

which may exist across the membrane. In the long term, the trans-membrane ionic gradients are maintained by metabolic pumping mechanisms.

The current, I_x, generated by the trans-membrane flow of ions of species 'x' is given by

$$I_x = g_x (E_m - E_x)$$

where g_x = conductance of the membrane to the ion 'x'

E_m = resting membrane potential

E_x = equilibrium potential of the ions 'x'.

As noted in equation 4,

$$E_x = \frac{RT}{FZ_x} \ln \frac{a_x^o}{a_x^i}$$

where R = the universal gas constant,

T = the absolute temperature

F = the 'Faraday' constant

Z_x = valency of the ion 'x'

a_x^o = extracellular activity of the ion 'x'

a_x^i = intracellular activity of the ion 'x'

The present study was based on measurements of the intracellular and extracellular potassium and chloride ion activities of the horizontal cells, the calculations of the individual equilibrium potentials, and their comparison with the corresponding membrane potentials. Since, in this study, it was intended to measure the 'natural' values of these ionic activities, the isolated retina was not superfused with any 'artificial' salines. Instead the isolated retina was kept in a moist oxygenated atmosphere which enabled it to continue its function in a normal manner, as judged from the nature of the electrical responses elicited from neurones, for up to two hours. In order to ensure that the retina did not suffer from dehydration to the extent that artefactual errors were introduced into the measurements of ionic activity, the value of the extracellular activity was constantly monitored during the

course of each experiment. This activity value remained constant for 40 to 60 minutes, after which it began to rise slowly presumably due to dehydration of the retina beginning to take effect. If the rise in the extracellular ionic activity was estimated during the experiment to be approaching 10% of the original value, the experiment was terminated, and the ISM re-calibrated. In appendix 4, it has been estimated that if, during an experiment, the extracellular activity of an ion 'x' increased by 10% (say, due to dehydration), the effect upon the calculated equilibrium potential, E_x, would cause merely a difference of less than 2.4 mV. Since a difference between the membrane potential E_m and E_x of less than 2.4 mV would not be significant the criterion of not allowing Δa_x^o to increase beyond 10% was sufficient. In this study the following values were obtained.

$E_K - E_m$ = −35±2 mV (L_1 units); −33±5 mV (C_b units)

$E_{Cl} - E_m$ = +12±2 mV (L_1 units); +11±2 mV (C_b units)

The fact that the isolated retina was not superfused in this study could not, therefore, have introduced significant errors into the ionic activity measurements.

Admittedly, the superfusion technique can be very advantageous especially in pharmacological studies in which the reversibility of the action of a chemical would normally be required to be tested. When investigating the ionic bases of membrane potentials, however, ionic substitutions in the superfusate have to be controlled very carefully. Firstly, when testing the contribution of an ion 'x' to a membrane potential E_m, the 'classical' procedure has been to replace 'x' with another 'y' that may also be contained in the superfusate (e.g. K^+ replaced by Na^+). This is not ideal procedure if both 'x' and 'y' are simultaneously making contributions to E_m. Secondly, the trans-membrane flow of ions may be coupled such that an alteration in the extracellular activity of the ion 'x' might affect the permeability of

the membrane to another ion 'z', such that the secondary effect would give rise to a membrane current I_z. For example, many excitable cells contain a Ca^{2+}-activated K^+ conductance mechanism (Meech, 1978); also, replacement of extracellular Na^+ may cause an increase in intracellular Ca^{2+} (Baker & Singh, 1981), which could lead to further membrane potential changes.

In conclusion, use of the non-superfused isolated retinal preparation eliminated these problems, and allowed the natural values of the ionic activities to be determined within the rigid set of criteria used.

V.4 Potassium Activity Measurements

The results of extracellular potassium activity measurements (a_K^o) in the roach retina, and intracellular potassium activity measurements (a_K^i) in L_1- and C_b-type horizontal cells have been presented in Chapter III. The mean value of a_K^o obtained from this study, 3.4±0.1 mM, corresponds to a concentration, C_K^o, of 4.6 mM based on an estimated activity coefficient γ_K of 0.74 for the retina (for 100 mM total ionic strength, γ_K = 0.77, and for 200 mM total ionic strength, γ_K = 0.717, Weast, 1971). This value of C_K^o is slightly higher than that used by most other workers in Ringer solutions to superfuse the cyprinid fish retina; extracellular potassium concentrations used were in the range 2.5 to 3.6 mM (Appendix 7). Thus, the first quantitative determination of a_K^o in the cyprinid fish retina with ISMs, reported in this thesis, has shown that the amount of K^+ in the extracellular environment has been underestimated. An underestimation of C_K^o in a Ringer solution which was used to superfuse the retina would tend to produce larger than 'normal' membrane potentials (and perhaps make the results look slightly better than they would with the real C_K^o).*

The mean value of a_K^i in L_1-type horizontal cells obtained,

* see facing page (223a)

57±2 mM, corresponds to an intracellular K^+ concentration, C_K^i of 78 mM, using $\gamma_K = 0.74$. This is considerably different to the indirectly estimated values of C_K^i of 125 mM and 118 mM obtained for the horizontal cells of the carp retina (Kaneko & Shimazaki, 1975a; Tachibana, 1981). Although some values of C_K^i greater than 100 mM were obtained in this study, it can be concluded that the value of C_K^i or a_K^i obtained indirectly from ionic substitution experiments can be vastly over-estimated. The value of E_K in horizontal cells, obtained from a_K^i, was shown to be the baseline for the saturation hyperpolarising responses of these cells. This was as expected from the K^+ distribution in neurones and the predicted position of E_K (e.g. Kaneko & Shimazaki, 1975b) but it was demonstrated for the first time in this study that there is an exact quantitative equivalence between the value of E_K and the maximal hyperpolarisation level reached by the cell following blockage of photoreceptor input to the cells by light stimulation or Co^{2+} application.

The change of a_K^i seen coincidentally with light stimulation was observed only in about 50% of the horizontal cells tested. However, in those L_1 type cells that did show this effect, the intracellular potassium activity always <u>decreased</u> during sustained light-evoked hyperpolarisation. The maximum value of a_K^i decrease seen was 12 mM. C_b type horizontal cells also showed this effect. One would expect that a_K^i would change as a result of the hyperpolarisation of the membrane potential, but in this case, the expected change would be an <u>increase</u> in a_K^i assuming constant membrane permeability to K^+. Such a change was never observed during light-evoked hyperpolarisation of the horizontal cells. This effect can, however, be explained by postulating a voltage-dependent K^+-permeability of the horizontal cell non-synaptic membrane such that hyperpolarisation causes an increase in permeability and depolarisation causes a decrease. Such a voltage-

dependent conductance mechanism has already been proposed in the horizontal cells of fish and amphibian retinae (Trifonov et al, 1974; Byzov & Trifonov, 1981; Werblin, 1975a). Werblin (1975a) has specifically suggested that the light-evoked hyperpolarization of horizontal cells in the mudpuppy retina is accompanied by a potential-dependent increase in permeability of the non-synaptic membrane. This property of the non-synaptic membrane appears to be common to both L_1 and C_b type horizontal cells (fig. 21). (See 'Further Discussion', pp. 237a,b).

V.5 Chloride Activity Measurements

The results of extracellular chloride activity (a^o_{Cl}) measurements in the roach retina, and intracellular chloride activity (a^i_{Cl}) measurements in L_1- and C_b-type horizontal cells have been presented in Chapter IV. a^o_{Cl} had an average value of 95±6 mM, which corresponds to a concentration of 128±8 mM, assuming $\gamma_{Cl} \simeq \gamma_K = 0.74$ as in section V.4. This value is fairly close to the concentrations of Cl^- included in physiological salines by several workers (Appendix 7). However, ISM measurements have shown clearly that the a^o_{Cl} values have a wide range (50-150 mM) i.e. the value of a^o_{Cl} can vary significantly from retina to retina. For the horizontal cells of a given retina, however, a^i_{Cl} values were consistently lower than the value of a^o_{Cl}, and E_{Cl} values were consistently more positive than the corresponding E_m values.

Since the distribution of Cl^- across the horizontal cell membrane is not passive ($E_{Cl} \neq E_m$) and a^i_{Cl} is greater than that for a passive distribution, it is postulated that Cl^- is actively 'pumped' into the horizontal cells by a mechanism which may obtain energy from the metabolic ATP cycle. An inwardly directed Cl^- pump has been established in the squid axon, in which a^i_{Cl} was over twice that for a

passive distribution, and this was not due to any substantial binding of intracellular Cl^- (Keynes, 1963). Also, the influx of Cl^- was not linked to the transport of the cations by the Na^+-K^+ pump. Other neurones, however, (e.g. snail neurones) are known to have a Cl^-/HCO_3^- exchange mechanism which is involved in regulating the intracellular pH (Russell, 1980).

The 'chloride' ion-exchanger, Corning 477315, used in the present study is, in fact, an anionic exchanger. The other main anion in the retina from which some interference in ISM measurements might be expected is bicarbonate. It has been shown that chloride ISMs based on Corning 477315 have a selective ratio over HCO_3^- of 20:1 (Walker, 1971). At present, it is not certain what role, if any, HCO_3^- might have in retinal function, but since some workers have left out HCO_3^- completely from their Ringer's solution (Appendix 7), and still had 'normally' functioning retinae, it would appear that HCO_3^- is not crucial to the electrophysiological functioning of the fish retina. One possible method of eliminating HCO_3^- interference might be to use Ag-AgCl type chloride ISMs. In one study, Owen et al, (1975) measured a^i_{Cl} in a giant cell of Aplysia with both Cl^-LIX and Ag-AgCl type ISMs. Average values of a^i_{Cl} were 38 mM and 152 mM for Cl^- LIX and Ag-AgCl ISMs, respectively. It was concluded that the apparently high value of a^i_{Cl} measured with Ag-AgCl electrodes was due to interference from Br^-, which exists at a concentration of 1 mM inside these cells. Thus, although the contribution of HCO_3^- to Cl^- measurements can be determined in principle by using Ag-AgCl ISMs, this type of ISM is more difficult to fabricate, and also suffers from interference problems to such an extent that it can be very unreliable (Thomas, 1978a).

Potassium activity measurements in the roach retina showed that $E_K < E_m$ by some 35 mV in L_1-type horizontal cells. It followed

from this that the horizontal cell membrane in the dark had also to be permeable to another ionic species 'x' with $E_x > E_m$. The chloride activity measurements were carried out to test whether the distribution of Cl^- across the horizontal cell membrane was consistent with the above requirement. It was indeed found that E_{Cl} is more positive than E_m, for every L_1-type horizontal cell investigated, by an average of 16 mV. This raises the possibility that Cl^- is the ion involved at the red-sensitive cone L_1-type horizontal cell synapse, which is known to be excitatory and active in the dark (Trifonov, 1968). The distribution of Cl^- is such as to depolarise the membrane from its resting potential when Cl^- permeability is increased since Cl^- would actually tend to leave the cell interior under the resultant force due to both its electrochemical gradient and the membrane potential. If Cl^- was indeed involved at this synapse, then blockage of synaptic transmission by saturating light stimulation should lead to an increase in a^i_{Cl}. In fact, in horizontal cells that did demonstrate a light-evoked change of a^i_{Cl}, the opposite was observed i.e. a^i_{Cl} decreased during light stimulation. This is, however, to be expected from the influence of enhanced membrane hyperpolarisation during the light-evoked response. The ideal way to investigate light-evoked changes in a^i_{Cl} would be to voltage-clamp the horizontal cell membrane during light stimulation, so the effect of membrane potential hyperpolarisation could be eliminated. Horizontal cells are electrically coupled, however, and in the fish retina, it has been demonstrated that this coupling spreads over most of the retina (Norton et al, 1968). As a result the space constant of the horizontal cell layer is too large for the cells to be voltage-clamped effectively by current-injection from a point source (Lamb, 1976). Instead, a chemical manipulation of the system was tried. It is known that external (H1 type) horizontal cells, which

generate L_1-type responses receive synaptic input also from inter-plexiform cells (Dowling & Ehinger, 1975). The interplexiform cell - horizontal cell synapse is excitatory and dopamine is its transmitter in the cyprinid fish retina. Thus one possibility is that Cl^- ions are involved at this synapse, rather than at the photoreceptor input synapse. This possibility was tested by recording from L_1-type horizontal cells in the roach retina, following application of about 0.1 mM dopamine. In agreement with the above suggestion dopamine application caused a decrease in a^i_{Cl}, presumably as the result of an increase in g_{Cl} of the horizontal cell membrane, and the membrane potential of the cells was depolarised such that $E_m \simeq E_{Cl}$ (section IV.9). Although the dopamine experiments do not prove that Cl^- is involved at the interplexiform cell synapse on to horizontal cells, the results of the experiments are consistent with this idea. Two other pieces of evidence have been obtained, which indirectly support this hypothesis:

(i) J.I. Toyoda (personal communication) has made preliminary measurements of a^i_{Cl} with ISMs in horizontal cells of the carp retina superfused with a physiological saline. No consistent relationship between E_{Cl} and E_m could be found, although normal S-potentials could be generated with $E_{Cl} < E_m$. Taken together, these observations suggest that (a) Cl^- is not crucial to the generation of S-potentials since E_{Cl} could be more negative than E_m, but light-evoked responses can still be generated i.e. Cl^- are not related to the photoreceptor synaptic input. It has been shown that in the absence of the interplexiform cell input, horizontal cells can still respond to light although their adaptational properties change (Djamgoz et al, 1981). (b) As shown in this study, a^o_{Cl} has a wide range of values (fig. 91). An artificial physiological saline with an 'abnormal' Cl^- concentration used to bathe

the retina may have an adverse effect on the E_{Cl} vs. E_m relationship. To stress again, 100% of the horizontal cells investigated in this study had $E_{Cl} < E_m$.

(ii) J.S. Rowe and K.H. Ruddock (personal communication) have tested the action of dopamine on the horizontal cell membrane potential in the roach retina. It was found that dopamine depolarised some cells and hyperpolarised others. This observation can be interpreted by assuming that following treatment of the retina with the artificial physiological saline, E_{Cl} vs. E_m relationships for the horizontal cells were altered, so that for some cells E_{Cl} became more negative than E_m, and these cells were hyperpolarised by dopamine, which, according to the hypothesis presented in this study, opens chloride channels and thereby causes E_m to move towards E_{Cl}.

A different interpretation can be suggested for the involvement of Cl^- in C_b-type horizontal cells. The red-sensitive depolarisation of C_b-units is due to an inhibitory GABAergic input from L_1-type cells (Stell et al, 1977; Fourtes & Simon, 1974; Djamgoz & Ruddock, 1979). Red light stimulation hyperpolarizes L_1-units, reduces the amount of GABA released by the latter onto green-cone terminals, and as a result of this dis-inhibition, green-cones depolarise, and they, in turn, depolarise C_b-units, i.e. depolarisation of C_b-units is associated with an increase in synaptic membrane conductance. If Cl^- is involved at this synapse, then during light stimulation a^i_{Cl} should decrease, but the opposite was observed. This effect is what is expected however from the depolarisation of the membrane potential, and any truely light-evoked change in a^i_{Cl} could only be investigated under voltage-clamp conditions. Whilst this discrepancy cannot be resolved without voltage-clamping the C_b-type horizontal cell membrane, V-log I curves obtained for the depolarising component of C_b responses show that

the maximum depolarisation level reached by a C_b unit in response to red light stimulation is close to the level of E_{Cl} for that unit. Some C_b units reach this level at moderate levels of light intensity, and a further increase in intensity, leads to a smaller response amplitude (fig.101). It has been suggested that C_b units in the goldfish retina also receive synaptic input from another type of interplexiform cell which uses glycine as its transmitter (Marc, 1980). Another consideration in parallel with the suggestion for the L_1-units, is that Cl^- is involved at this synaptic input. Glycine, however, hyperpolarises C_b units, and if this effect is indeed mediated directly by the glycinergic interplexiform cell, it implies that this synaptic input is inhibitory, in which case Cl^- could not be involved since $|E_{Cl}|<|E_m|$. The possibility that glycine might cause hyperpolarisation by decreasing g_{Cl}, however, cannot be excluded although this would be an unconventional mode of action for a synaptic transmitter.

There is also substantial evidence for the involvement of Na^+ in horizontal cell membrane electrogenesis (Kaneko & Shimazaki, 1975a,b). The interpretation of these low Na^+/ionic substitution experiments was questioned by Nelson (1973) and Miller (1978). The decoupling effect of low Na^+ observed by Miller (1978) could occur since reduction of external Na^+ may lead to an increase in Ca^{2+} influx (Baker et al, 1969). Loewenstein (1975) has shown that an increase in intracellular Ca^{2+} activity can uncouple low resistance junctions in epithelial cells and Miller (1978) suggested that in low Na^+ horizontal cells would also uncouple and as a result amplitudes of their light-evoked responses decrease. Preliminary experiments carried out towards the end of the studies reported here, showed that Na^+ is distributed in such a way that E_{Na} is more positive than OmV and hence more positive than the membrane potential. One possibility is that Na^+ is the ion involved at the cone-horizontal cell excitatory

synaptic input, in accordance with the suggestion of Kaneko & Shimiazaki (1975a,b). Horizontal cells have also been shown to produce Ca^{2+}-dependent regenerative responses to membrane depolarisation (Johnston & Lam, 1981). The physiological role of these Ca^{2+}-mediated events in horizontal cell function is still to be investigated.

V.6 An Electrophysiological Model of the Horizontal Cell Membrane

Horizontal cells function as interneurones integrating information concerning spatial distribution of light intensity in the retina and accordingly controlling photoreceptor-bipolar cell transmission in the outer plexiform layer. They also encode information concerning the chromatic content of the visual stimulus. The synaptic organisation of L_1(H1) type horizontal cells (excluding connections with bipolar cells) is illustrated in figure 107. L_1-type horizontal cells receive synaptic input from red-sensitive cones (transmitter unidentified) and synapse back onto the same cones via inhibitory GABAergic synapses. Horizontal cells of a given functional type are coupled laterally through electrical junctions. They also receive excitatory synaptic input from the dopaminergic interplexiform cells, which are themselves driven by bipolar and amacrine cells in the inner plexiform layer.

The measurements of extracellular potassium and chloride activities in the roach retina and values of a^i_K and a^i_{Cl} in L_1-and C_b-type horizontal cells obtained for the first time using intracellular ISMs, have led to the quantitative determination of the potential levels of E_K and E_{Cl} (with respect to E_m) in both these types of unit. These results are summarised in fig. 108.

Previously published data and information obtained during the present study can be combined to make up an electrophysiological model of the L_1(H1) horizontal cell membrane, as shown in fig. 109. At the first stage, the membrane mechanism of electrogenesis is

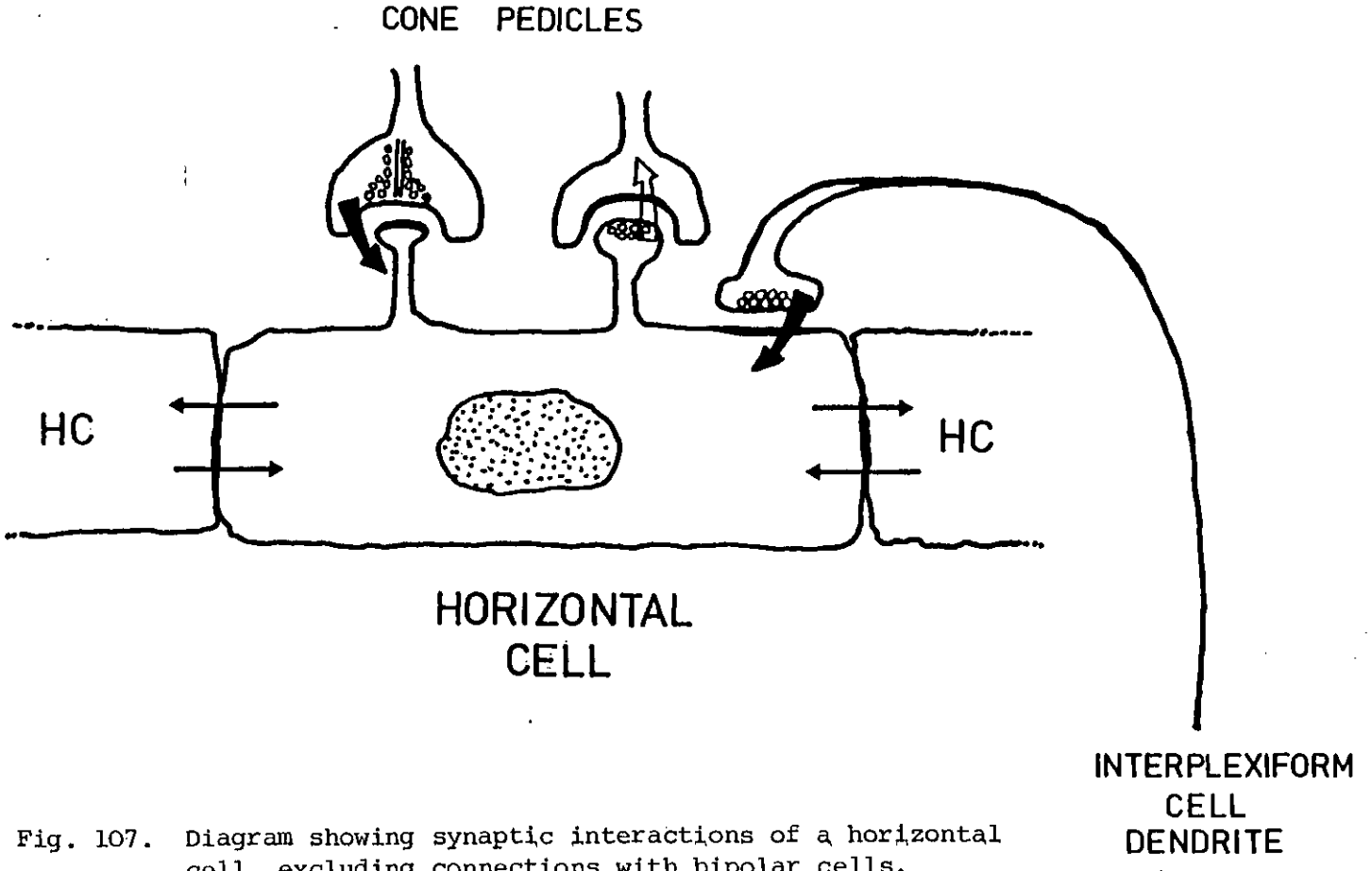

Fig. 107. Diagram showing synaptic interactions of a horizontal cell, excluding connections with bipolar cells.

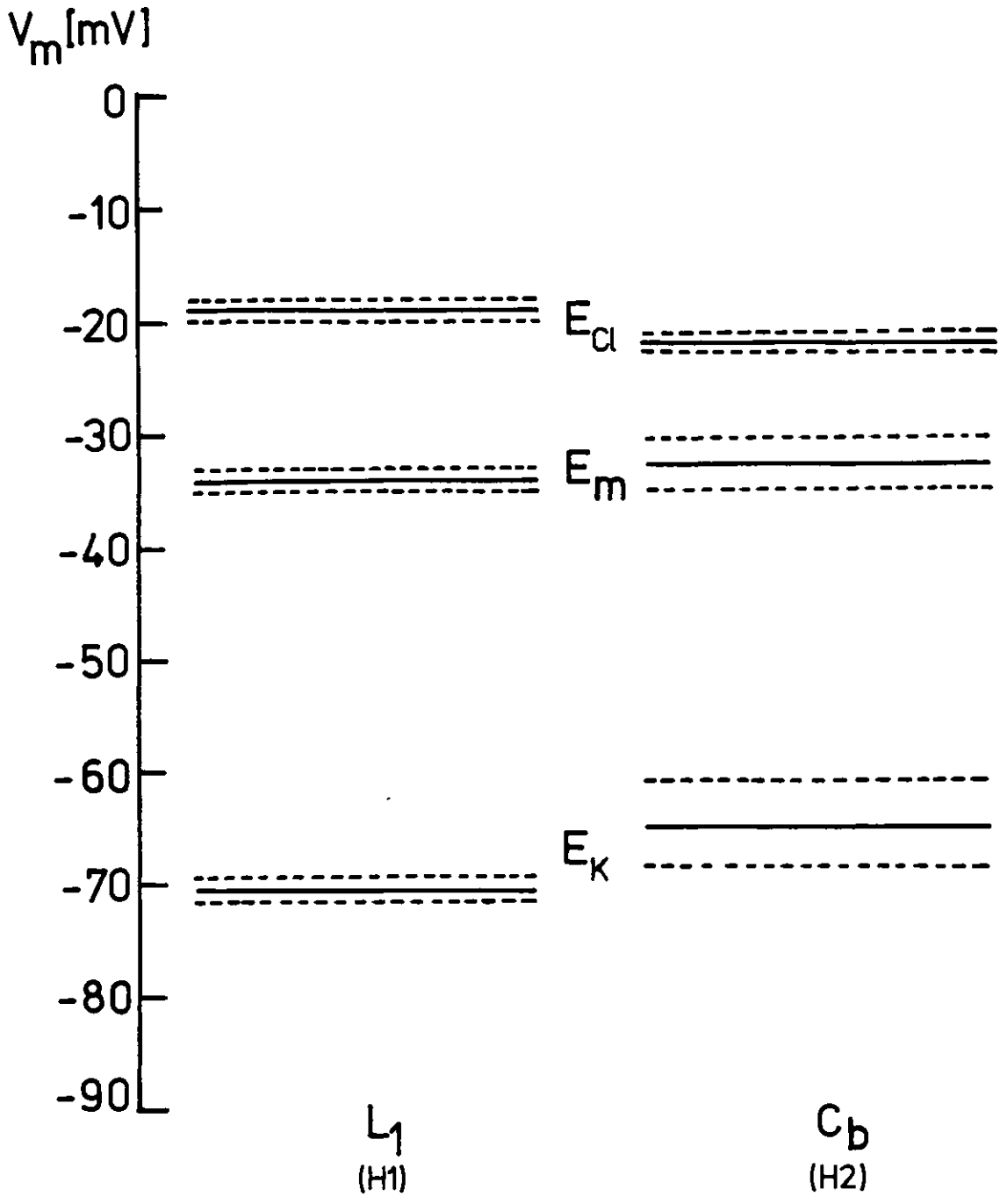

Fig. 108. Summary diagram showing levels of E_m, E_{Cl} and E_K for both L_1- and C_b-type horizontal cells. Heavy lines denote mean values and broken lines the corresponding standard errors.

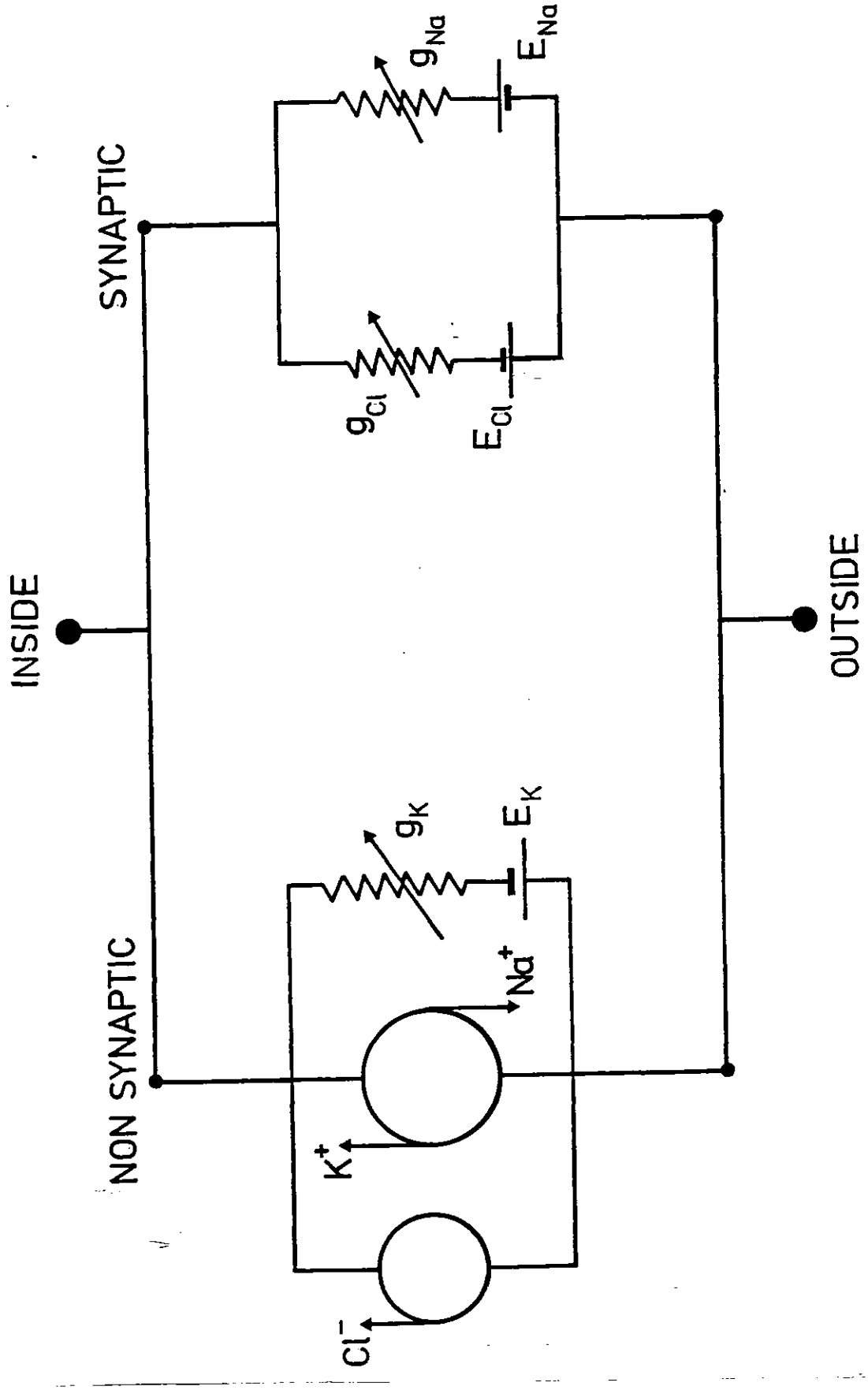

Fig. 109. Electrical model of the horizontal cell membrane showing synaptic and non-synaptic components (see text).

considered to be made up of synaptic and non-synaptic components in accordance with the approach of Eccles (1964). When the synaptic part is eliminated by blocking post-receptoral activity with saturating light stimulation, the horizontal cell membrane potential reaches the maximum level of hyperpolarisation defined by E_K, i.e. the non-synaptic membrane is permeable mainly to K^+ such that $E_m = E_K$. The K^+ permeability (g_K) is voltage-dependent, however, and when the membrane potential hyperpolarises g_K increases, and a_K^i falls, as K^+ move outwards down their electrochemical gradient (but against the electrical potential gradient across the membrane). Werblin (1975) has shown that g_K is also time-dependent. Since the horizontal cells maintain a high level of K^+ (this study) and a low level of Na^+ intracellularly (expected normally, and also observed during the preliminary measurements), metabolic mechanisms must also exist for pumping in K^+ and pumping out Na^+. The simplest mechanism that would achieve this is a coupled Na^+-K^+ ATPase pump, and this is shown incorporated into the non-synaptic membrane.

L_1(H1) type horizontal cells receive at least two kinds of chemical synaptic input: (i) An excitatory (depolarising) input from the dopaminergic interplexiform cells. This has been suggested to be associated with Cl^-. $|E_{Cl}| < |E_m|$, so Cl^- has a depolarising action on the negative membrane potential. There has to be an inwardly directed chloride pump, which maintains a_{Cl}^i at a relatively high level with respect to the equilibrium distribution. This pump has also been incorporated into the non-synaptic membrane, since during saturating light stimulation (synaptic blockage), $|E_{Cl}|$ is still $< |E_m|$. It is not known whether the pumping in of Cl^- is coupled to the pumping out of another anion. The chloride conductance g_{Cl} is increased by dopamine, but it is not certain whether g_{Cl} is also voltage- and time-dependent in the same way as g_K. (ii) An excitatory (depolarising)

input from red-sensitive cones. In accordance with Kaneko & Shimazaki's (1975a,b) results, this synaptic input is shown to be mediated by a Na^+ conductance mechanism.

This model explains the data recorded during the present study, and some of the discrepancies observed by other workers. The real test of the model would involve recording from the horizontal cell intracellularly with ion-sensitive microelectrodes whilst voltage-clamping its membrane potential. Unfortunately this does not appear to be feasible for the isolated retinal preparation, but horizontal cells dissociated from the retina and maintained in a culture medium might provide a suitable preparation.

FURTHER DISCUSSION

Is the non-synaptic permeability change an adequate reason for the light-evoked change in a_K^i ?

Werblin (1975) observed a 15% decrease in resistance of the mudpuppy horizontal cell membrane for each 10mV hyperpolarisation and a similar resistance increase on depolarisation. The resistance of the membrane is directly proportional to the reciprocal of the membrane conductance, $r = \frac{1}{g_m}$. Thus the effects of a change in K^+ conductance, g_K, on the transmembrane K^+ current, I_K, can be predicted by the equation :

$$I_K = \frac{1}{r} (V_m - E_K)$$

where $r = \frac{1}{g_K}$, V_m = membrane potential, V_K = K^+ equilibrium potential. Consider a horizontal cell with E_m = -35mV, E_K = -70mV, hyperpolarising by 20 mV and showing a 15% decrease in resistance per 10 mV hyperpolarisation. The transmembrane K^+ current would change from $I_K(0)$, at the resting membrane potential E_m, to $I_K(20)$, at 20 mV below E_m. Then :

$$I_K(0) = \frac{1}{r} (-35 + 70) = \frac{35}{r} \text{ units}$$

$$I_K(20) = \frac{1}{0.7r} (-55 + 70) = \frac{21.4}{r} \text{ units} < I_K(0)$$

Thus a 15% decrease in resistance per 10mV hyperpolarisation is insufficient to cause an increase in outward K^+ current for a 20mV hyperpolarisation in this range of membrane potential. It would be necessary to have at least a 28.6% decrease in resistance per 10mV hyperpolarisation for the outward K^+ current to increase. Then :

$$I_K(20) = \frac{1}{0.428r} (-55 + 70) = \frac{35.05}{r} \simeq I_K(0)$$

$$I_K(30) = \frac{1}{0.142r} (-65 + 70) = \frac{35.21}{r} > I_K(0)$$

APPENDIX 2

Formulae for series of solutions for calibration of ISMs:

i) Routine Calibrations

For K^+ ISMs

1 mM KCl + 99 mM NaCl

2 mM KCl + 98 mM NaCl

5 mM KCl + 95 mM NaCl

10 mM KCl + 90 mM NaCl

50 mM KCl + 50 mM NaCl

100 mM KCl

For Cl^- ISMs

5 mM NaCl + 195 mM NaGlu

10 mM NaCl + 190 mM NaGlu

20 mM NaCl + 180 mM NaGlu

50 mM NaCl + 150 mM NaGlu

100 mM NaCl + 100 mM NaGlu

200 mM NaCl ('Glu' = glucoronate)

ii) Calibrations to determine selectivity coefficients for K^+ LIX

a) Solutions with varying C_{KCl} and constant C_{NaCl} = 10 mM

1 mM KCl + 10 mM NaCl

5 mM KCl + 10 mM NaCl

10 mM KCl + 10 mM NaCl

50 mM KCl + 10 mM NaCl

100 mM KCl + 10 mM NaCl

500 mM KCl + 10 mM NaCl

1 M KCl + 10 mM NaCl

b) Solutions with varying C_{KCl} and constant C_{NaCl} = 50 mM

1 mM KCl + 50 mM NaCl

5 mM KCl + 50 mM NaCl

10 mM KCl + 50 mM NaCl

50 mM KCl + 50 mM NaCl

100 mM KCl + 50 mM NaCl

500 mM KCl + 50 mM NaCl

1M KCl + 50 mM NaCl

c) Solutions of varying C_{KCl} only

1 mM KCl

5 mM KCl

10 mM KCl

50 mM KCl

100 mM KCl

500 mM KCl

1M KCl

d) Solutions of varying C_{NaCl} only

1 mM NaCl

5 mM NaCl

10 mM NaCl

50 mM NaCl

100 mM NaCl

500 mM NaCl

1M NaCl

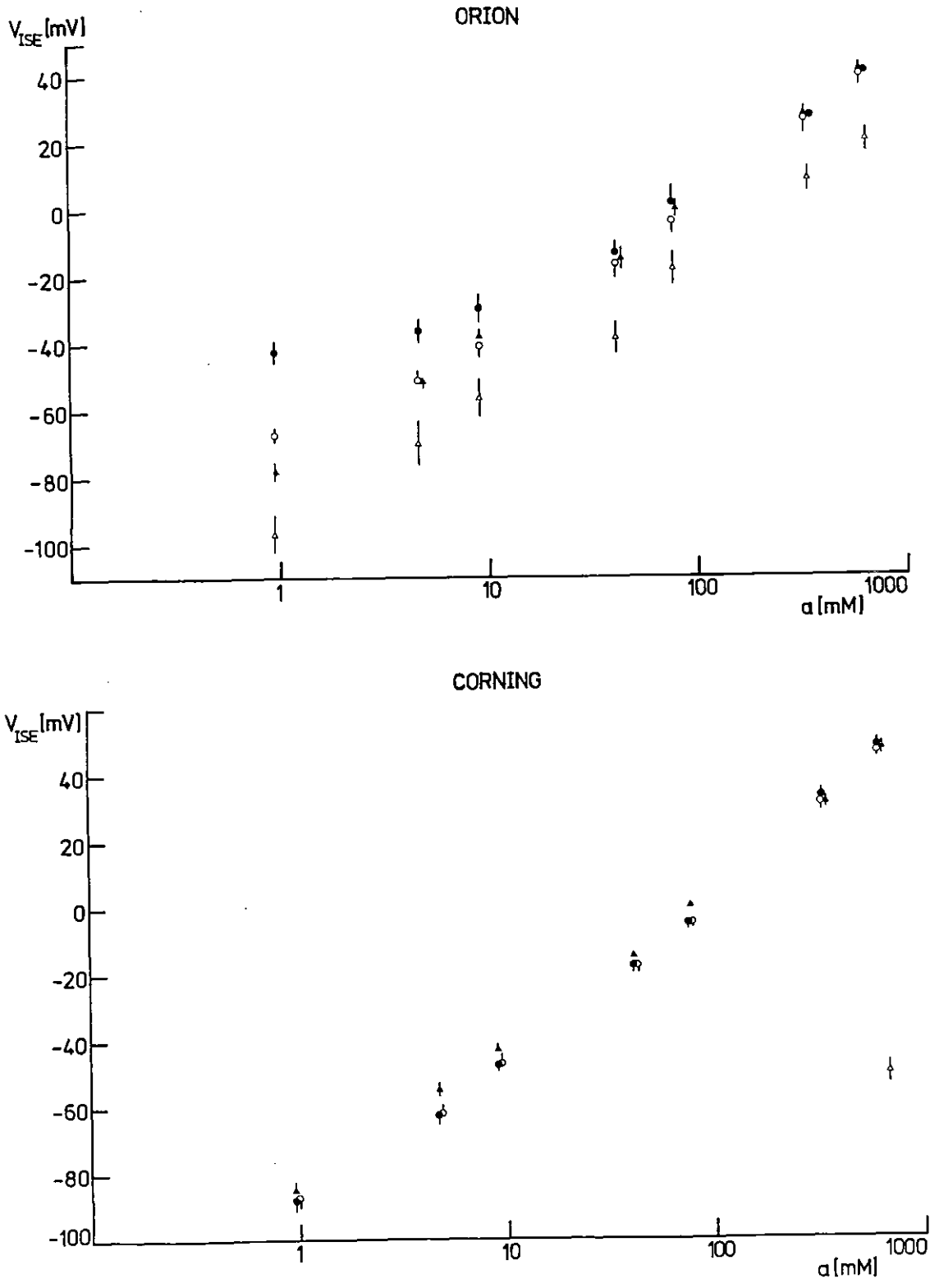

Graphs of calibration curves for Corning and Orion K^+ LIXs. The response of the electrode, V_{ISE}, is plotted against the activity, a, on a log. scale. $a = a_K$ for all series of solutions except pure Na^+, where $a = a_{Na}$. The selectivity coefficient, k_{KNa}, was calculated from these four curves by three methods for each LIX (see text). A fourth method of calculating k_{KNa} from solutions of mixed K^+ and Na^+ of constant total ionic strength by fitting an equation to the calibration curve is described in Appendix 3.

APPENDIX 3

Fitting Nikolsky equation to calibration curve

For a K^+ ISM, the Nikolsky equation may be given by:

$$V_K = V_o + S_{10}\log_{10}(a_K + k_{KNa}a_{Na}) \quad (27)$$

where V_K is the K^+ activity signal, V_o the 'standard electrode potential', S_{10} the slope of the linear region of the calibration curve (mV/tenfold activity change), a_K and a_{Na} the activities of potassium and sodium, and k_{KNa} the selectivity coefficient of the ISM for K^+ against Na^+.

For a certain ISM, S_{10} = 58 mV/decade.

For 100 mM total ionic strength solutions, the activity coefficients for K^+ and Na^+ are $\gamma_K = 0.77$, $\gamma_{Na} = 0.78$ (28)

For the 100 mM KCl solution, eqn. (27) gives:

$$0 = V_o + 58 \log_{10} 77$$

$$\therefore V_o = -109.4 \text{ mV} \quad (29)$$

From equation (27), $k_{KNa} = \dfrac{10^{(V_K - V_o)/58} - a_K}{a_{Na}}$ (30)

Thus k_{KNa} can be calculated for each solution in the calibrating series, except the 100 mM KCl solution by using the following table of values obtained for the ISM. The activity values are obtained from the concentration in the solutions using the activity coefficients (28) and the value of k_{KNa} is obtained for each solution by substituting the value of V_o (29) and values from the table into equation (30).

Solution	V_K(mV)	a_K(mM)	a_{Na}(mM)
100 mM K^+, 0 mM Na^+	0	77	0
50 mM K^+, 50 mM Na^+	-16	38.5	$39 \rightarrow k_{KNa} = 5.90 \times 10^{-2}$
10 mM K^+, 90 mM Na^+	-54	7.7	$70.2 \rightarrow k_{KNa} = 1.89 \times 10^{-2}$
5 mM K^+, 95 mM Na^+	-69	3.85	$74.1 \rightarrow k_{KNa} = 1.52 \times 10^{-2}$
1 mM K^+, 99 mM Na^+	-94	0.77	$77.2 \rightarrow k_{KNa} = 1.39 \times 10^{-2}$

Using these empirically determined values of k_{KNa}, we can compare the actual values of V_K with those predicted from equation (27) for a given value of k_{KNa}. Thus we can find the best value of k_{KNa} which, when substituted in equation (27) will yield points fitting most closely to the real empirical curve. The following table compares empirical and theoretical values in order to find the optimum value of k_{KNa}.

V_K empirical	V_K $k=1.39.10^{-2}$	V_K $k=1.52.10^{-2}$	V_K $k=1.89.10^{-2}$	V_K $k=5.90.10^{-2}$
0	0.0	0.0	0.0	0.0
-16	-17.1	-17.1	-17.0	-16.0
-54	-55.0	-54.7	-54.0	-47.2
-69	-69.5	-69.0	-67.6	-56.4
-94	-94.0	-92.7	-89.2	-67.3

$\therefore$ $k_{KNa} = 1.39 \times 10^{-2}$ gives the best fit of the equation (27) to the empirical data, giving agreement to within ±1mV.

APPENDIX 4

Effect upon E_x of n% increase in a_x^o

The equilibrium potential, E_x, is given by:

$$E_x = 58 \log_{10} \frac{a_x^o}{a_x^i} \qquad \text{(cf. equations 4,22,25)}$$

(where 58mV is the slope factor for a tenfold increase in a_x, a_x^o and a_x^i are extracellular and intracellular activities of x respectively).

When a_x^o changes by n% during an experiment the new value of E_x accounting for this change in a_x^o will be as follows (assuming in this approximation that the a_x^i remains constant):

$$E_x' = 58 \log_{10} \left[(1+\tfrac{n}{100})\ a_x^o/a_x^i \right]$$

$\therefore$ the error in E_x is given by

$$\Delta E_x = E_x' - E_x$$

$$= 58 \left[\log_{10} \frac{(1+n/100)\,a_x^o}{a_x^i} - \log_{10} \frac{a_x^o}{a_x^i} \right]$$

$$= 58 \left[\log_{10} \frac{(1+n/100)\,a_x^o}{a_x^i} \ \frac{a_x^i}{a_x^o} \right]$$

$$= 58 \log_{10}(1 + \tfrac{n}{100}) \qquad (31)$$

Thus, for a 10% increase in a_x^o,

$$|\Delta E_x| = 58 \log_{10} (1.1) = 2.4 \text{ mV}$$

It is concluded that an increase in a_x^o during an experiment of up to about 10% will have only a negligible effect upon the value of E_x and so, as long as the value of a_x^o is monitored during the experiment, the effects of dehydration etc. in this regard are not critical.

APPENDIX 5

Differential Time Response Artefact

Theory

The active barrel of a double-barrelled ISM has a much higher resistance than the reference barrel and thus it has a slower response time. In response to a step voltage change in the external solution a transient response artefact is produced in the ionic activity signal, A-B, where A is the signal from the active barrel and B the signal from the reference barrel. The generation of the transient artefact due to the difference in time response between channels A and B can be explained by the following first order linear approximation. If a votage step V_1 is applied at time t=0, the responses of A (V_A) and of B (V_B) are as in fig. 110 where t_a is the time response of A (time taken to reach final steady level) and t_b is the time response of B to the voltage step. Therefore, the response of the ionic activity signal is given by $V_A(t) - V_B(t)$; fig. 111.

The magnitude of the peak of the transient artefact, V_E (fig. 111) is given by

$$V_E = [V_A - V_B](t = t_b)$$

$$\text{i.e. } V_E = (a-b)t_b = V_1 t_b\left(\frac{1}{t_a} - \frac{1}{t_b}\right)$$

$$\therefore V_E = V_1\left(\frac{t_b}{t_a} - 1\right) \qquad (32)$$

Thus, the amplitude of the transient peak compared with that of V_1 depends on the difference of the ratio of the time responses of A and B from unity. When the time responses are equal, $t_a = t_b$, then $V_E = 0$, and when the time responses are considerably different, $t_a >> t_b$ then $V_E = V_1$. The time duration of the transient depends on the response time of channel A since it persists for time t_a (fig. 111).

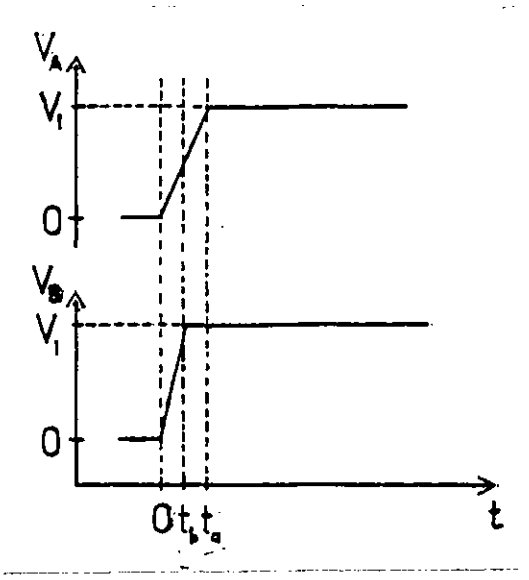

Fig. 110. Schematic representation of responses of active (V_A) and reference (V_B) barrels of a double barrelled ISM to a voltage step of magnitude V_1 applied at time t = 0.

$$V_A(t) = \begin{cases} 0, & t \leq 0 \\ at, & 0 < t \leq t_a \quad \text{where } a = V_1/t_a \\ V_1, & t > t_a \end{cases}$$

$$V_B(t) = \begin{cases} 0, & t \leq 0 \\ bt, & 0 < t \leq t_b \quad \text{where } b = V_1/t_b \\ V_1, & t > t_b \end{cases}$$

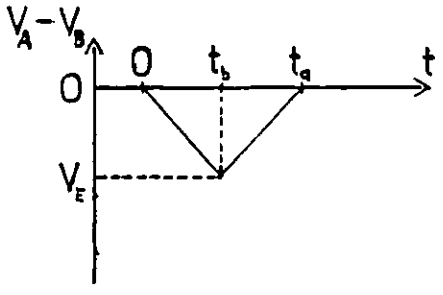

Fig. 111. Schematic representation of transient deflection in ionic activity signal, $V_A - V_B$, due to voltage step V_1 applied at t = 0 and difference between time responses of A and B.

$$V_A - V_B \ (t) = \begin{cases} 0, & t \leq 0 \\ (a-b)t, & 0 < t \leq t_b \\ at - V_1, & t_b < t \leq t_a \\ 0, & t > t_a \end{cases}$$

As t_a is usually quite a short time (a fraction of a second - few seconds), the transient artefact does not interfere with steady state measurements of ionic activity on a much longer time scale. The production of the transient merely needs to be taken into account so that it is recognised for what it is when it appears. Filling the reference barrel with a high resistance organic solution (Thomas & Cohen, 1981) should eliminate this artefact by equalising the resistances and time responses of the two barrels.

Experiment

In order to compare the time responses of the two barrels of a Cl^- ISM, a simple experiment described in fig. 112 caption was performed. As expected, the reference barrel ('B') responds to a square wave electrical pulse much faster than the active barrel ('A') (Fig. 113). Thus, 'A-B' would appear as a transient signal with a polarity opposite to that recorded by 'B'. This is referred to as the 'differential time response artefact'.

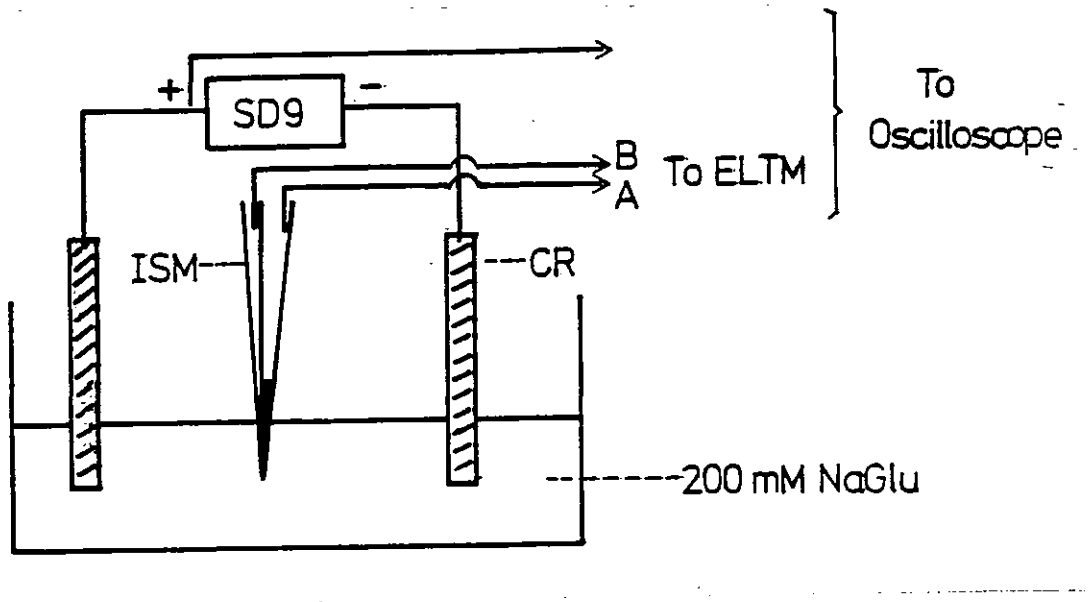

Fig. 112. A simple experimental arrangement to compare the response times of the two barrels, A and B, of a Cl^- ISM. An electrical pulse from a Grass SD9 stimulator is applied to a solution of 200 mM sodium glucoronate via two carbon rod electrodes, CR. The responses of A and B, at the electrometer (ELTM) output, and the stimulator output are displayed on a storage oscilloscope, CRT.

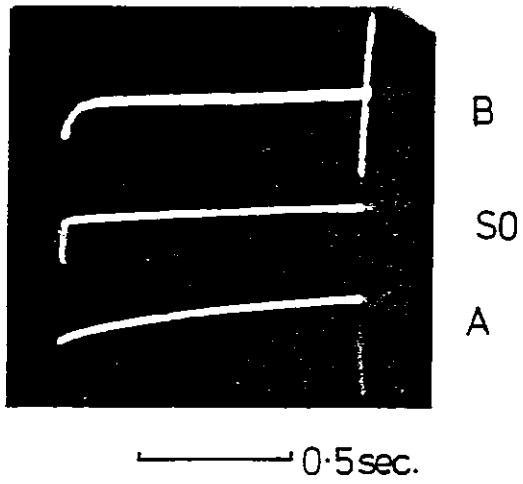

Fig. 113. The photocopy of a polaroid photograph of the oscilloscope screen showing the stimulator output of 20 mV, SO, and the responses of active barrel, A, and the reference barrel 'B' of a Cl^- ISM.

APPENDIX 6

Dependence of ISM Response upon Total Ionic Strength (TIS) in Calibrating Solutions of Constant TIS

The response of an ISM in calibrating solutions is given (from eqn. 16) by:

$$E = E_o + S_{10} \log_{10} (a_x + k_{xy}\, a_y) \qquad (33)$$

For a K^+ ISM;

$$E = E_o + S_{10} \log_{10} (a_K + k_{KNa}\, a_{Na})$$

$$= E_o + S_{10} \log_{10} (\gamma_K C_K + k_{KNa}\gamma_{Na} C_{Na})$$

To compare the ISM response in calibrating solutions of TIS = 100 mM and 200 mM respectively, let γ_K^{100}, γ_{Na}^{100} represent activity coefficients of K^+, Na^+ in 100 mM TIS solutions, and γ_K^{200}, γ_{Na}^{200} represent activity coeffs. in 200 mM TIS solutions. Thus, comparing ISM responses at 3 different values of C_K :

TIS = 100 mM

C_K = 100 mM: $V_K^{100/100} = E_o + S_{10} \log_{10} (100\, \gamma_K^{100})$

C_K = 10 mM: $V_K^{10/100} = E_o + S_{10} \log_{10} (10\gamma_K^{100} + k_{KNa}^{90}\gamma_{Na}^{100})$

C_K = 1 mM: $V_K^{1/100} = E_o + S_{10} \log_{10} (\gamma_K^{100} + k_{KNa}\, 99\gamma_{Na}^{100})$

TIS = 200 mM

C_K = 100 mM: $V_K^{100/200} = E_o + S_{10} \log_{10} (100\gamma_K^{200} + k_{KNa}100\gamma_{Na}^{200})$

C_K = 10 mM: $V_K^{10/200} = E_o + S_{10} \log_{10} (10\gamma_K^{200} + k_{KNa}190\gamma_{Na}^{200})$

C_K = 1 mM: $V_K^{1/200} = E_o + S_{10} \log_{10} (\gamma_K^{200} + k_{KNa}199\gamma_{Na}^{200})$

Putting in values, viz. S_{10} = 58 mV, γ_K^{100} = 0.77, γ_K^{200} = 0.717, γ_{Na}^{100} = 0.78, γ_{Na}^{200} = 0.73, k_{KNa} = 0.01:

$$\Delta V_K^{100} = V_K^{100/100} - V_K^{100/200} = 109.4 - 107.9 = 1.5 \text{ mV}$$

$$\Delta V_K^{10} = V_K^{10/100} - V_K^{10/200} = 53.6 - 54.1 = -0.5 \text{ mV}$$

$$\Delta V_K^{1} = V_K^{1/200} - V_K^{1/200} = 10.9 - 19.5 = -8.6 \text{ mV}$$

$\therefore$ The maximum difference between ISM responses during calibration in solutions with TIS = 100 mM and TIS = 200 mM is less than 9 mV. This occurs at a region of the calibration curve where this max. error would correspond to a difference of <1 mM in aK.

APPENDIX 7

A Comparison of Cyprinid Fish Ringer's Solutions

Chemical (mM)	Reference			
	Kaneko & Shimazaki (1975b) (carp)	Wu & Dowling (1978) (carp)	Kato & Negishi (1978) (carp)	Ishida & Fain (1981) (goldfish)
NaCl	110	80	119.5	120
$NaHCO_3$	-	22.7	22.6	-
KCl	2.5	3.5	3.6	2.5
$MgSO_4.7H_2O$	-	2.4	1.04	1.2
$CaCl_2.2H_2O$	2.2	2.3	1.15	2.2
NaH_2PO_4	-	-	0.4	-
Na_2HPO_4	-	-	0.1	-
Dextrose	10	10	10	10
HEPES	5	10	-	3
pH	7.7	7.35	8.0-8.1	7.8

REFERENCES

Adams, A.J. & Afandor, A.J. (1971) Ganglion cells receptive field organization at different levels of light adaptation. Am. J. Optometry Arch. Acad. Optometry. 48, 889-904.

Adrian, R.H. (1958) The effects of membrane potential and external potassium concentration on the potassium permeability of muscle fibres. J. Physiol. 143, 59P.

Adrian, R.H. (1956) The effect of internal and external potassium concentration on the membrane potential of frog muscle. J. Physiol. (Lond) 133, 631-658.

Agin, D.P. (1969) Electrochemical properties of glass microelectrodes. In "Glass Microelectrodes": M. Lavallee, O.F. Schanne and N.C. Hebert editors. Wiley and Sons; New York, 62-75.

Aickin, C.C. & Thomas, R.C. (1977) An investigation of the ionic mechanism of intracellular pH regulation in mouse soleus muscle fibres. J. Physiol. 273, 295-316.

Ammann, D., Lanter, F., Steiner, R.A., Schulthess, P., Shijo, Y. & Simon, W. (1981) Neutral-carrier-based hydrogen ion selective microelectrode for extra- and intracellular studies. Anal. Chem. 53, 2267-2269.

Arden, G.B. & Ernst, W. (1970) The effect of ions on the photoresponses of pigeon cones. J. Physiol. 211, 311-339.

Arden, G.B. & Low, J.C. (1978) Changes in pigeon cone photocurrent caused by reduction in extracellular calcium activity. J. Physiol. 280, 55-76.

Armstrong, C.M. (1975) Ionic pores, gates and gating currents. Quart. Rev. Biophys. 7, 179-210.

Armstrong, W.McD., Wojtkowski, W. & Bixenman, W.R. (1977) A new solid-state micro-electrode for measuring intracellular chloride activities. Biochim. Biophys. Acta. 465, 165-170.

Armstrong, W.McD. & Garcia-Diaz, J.F. (1980) Ion-selective micro-electrodes: theory and technique. Fed. Proc. 39, 2851-2858.

Ascher, P., Kunze, D. & Neild, T.O. (1976) Chloride distribution in Aplysia neurones. J. Physiol. 256, 441-464.

Bailey, P.L. (1980) Analysis with ion-selective electrodes. 2nd Ed. Heyden-London.

Baker, P.F., Blaustein, M.P., Hodgkin, A.L. & Steinhaedt, R.A. (1969) The influence of calcium on sodium efflux in squid axons. J. Physiol. Lond. 200, 431-458.

Baker, P.F., Hodgkin, A.L. & Shaw, T.I. (1962a) Replacement of the axoplasm of giant nerve fibres with artificial solutions. J. Physiol. 164, 330-354.

Baker, P.F., Hodgkin, A.L. & Shaw, T.I. (1962b) The effects of changes in internal ionic concentrations on the electrical properties of perfused giant axons. J. Physiol. 164, 355-374.

Baker, P.F., Hodgkin, A.L. & Meves, H. (1963) Internal potassium concentration and the action potential of giant axons of Loligo. J. Physiol. 167, 56-57P.

Baker, P.F. & Singh, R. (1981) Mechanisms underlying the net movements of calcium in nerve. In "Calcium and Phosphate Transport across Biomembranes",3-7. Academic Press, London.

Barford, N.C. (1967) Experimental measurements: precision error and truth. Addison Wesley, London.

Bastian, B.L. & Fain, G.L. (1979) Light adaptation in toad rods: requirement for an internal messenger which is not calcium. J. Physiol. 297, 493-520.

Baylor, D.A. & Fuortes, M.G.F. (1970) Electrical responses of single cones in the retina of the turtle. J. Physiol. 207, 77-92.

Baylor, D.A., Fuortes, M.G.F. & O'Bryan, P.M. (1971) Receptive fields of cones in the retina of the turtle. J. Physiol. 214, 265-294.

Baylor, D.A. & Hodgkin, A.L. (1973) Detection and resolution of visual stimuli by turtle photoreceptors. J. Physiol. 234, 163-198.

Baylor, D.A., Lamb, T.D. & Yau, K.W. (1979a) The membrane current of single rod outer segments. J. Physiol. 288, 589-612.

Baylor, D.A., Lamb, T.D. & Yau, K.W. (1979b) Responses of retinal rods to single photons. J. Physiol. 288, 613-634.

Beauchamp, R.D. & Daw, N.W. (1972) Rod and cone input to single goldfish optic nerve fibres. Vison Res. 12, 1201-1212.

Bennett, M.V.L. (1973) Permeability and structure of electrotonic junctions and intracellular movements of tracers. In "Intracellular Staining in Neurobiology" Eds. S.B. Kater & C. Nicholson. Springer, New York, 115-134.

Bernstein, J. (1902) Untersuchungen zur Thermodynamik der bioelectrischen Ströme. Pflüg. Arch. Ges. Physiol. 92, 521-562.

Berridge, M.J. & Schlue, W.R. (1978) Ion-selective electrode studies on the effects of 5-hydroxytryptamine on the intracellular level of potassium in an insect salivary gland. J. Exp. Biol. 72, 203-216.

Bertrand, D., Fourtes, M.G.F. & Pochobradsky, J. (1978) Actions of EGTA and high calcium on the cones in the turtle retina. J. Physiol. 275, 419-437.

Bitensky, M.W., Keirns, J.J. & Wagner, R.C. (1973) In "Biochemistry and Physiology of Visual Pigments". 335-340, Ed. H. Langer, Springer-Verlag, Berlin.

Bitensky, M.W., Mihi, N., Keirns, J.J., Keirns, M., Baraban, J., Freeman, J., Wheeler, M.A., Cacy, J. & Marcus, F.R. (1975) Activation of photoreceptor disk membrane phosphodiesterase by light and ATP. Adv. Cyclic Nucleotide Res. 5, 213-240.

Bolton, T.B., & Vaugan-Jones, R.D. (1977) Continuous direct measurement of intracellular chloride and pH in frog skeletal muscle. J. Physiol. 270, 801-833.

Brown, H.M. (1976) Intracellular Na^+, K^+ and Cl^- activities in Balanus photoreceptors. J. Gen. Physiol. 68, 281-296.

Brown, H.M. & Ottoson, D. (1976) Dual role for potassium in Balanus photoreceptor: Antagonist of calcium and suppression of light-induced current. J. Physiol. 257, 355-378.

Brown, H.M., Ottoson, D. & Rydqvist, B. (1978) Crayfish strech Receptor: An investigation with voltage clamp and ion-sensitive electrodes. J. Physiol. 284, 155-179.

Brown, H.M. & Owen, J.D. (1979) Micro ion-selective electrodes for intracellular ions. Ion-Selective Electrode Rev. 1, 145-186.

Buck, R.P. (1974) Ion selective electrodes, potentiometry and potentiometric titrations. Anal. Chem. 46, 28R-51R.

Burkhardt, D.A. (1977) Response and receptive field organization of cones in perch retinae. J. Neurophysiol. 40, 53-62.

Byzov, A.L. & Trifonov, Yu.A. (1968) The response to electric stimulation of horizontal cells in the carp retina. Vis. Res. 8, 817-822.

Byzov, A.L. & Trifonov, Yu.A. (1981) Ionic mechanisms underlying the non-linearity of horizontal cell membrane. Vis. Res. 21, 1573-1578.

Byzov, A.L., Trifonov, Yu.A., Chailahian, L.M. & Golubtzov, K.W. (1977) Amplification of graded potentials in horizontal cells of the retina. Vision Res. 17, 265-273.

Cajal, S.R. (1893) La retine des vertebres. La Cellule 9, 17-257.

Caldwell, D.C. (1954) An investigation of the intracellular pH of crab muscle fibres by means of micro-glass and micro-tungsten electrodes. J. Physiol. Lond. 126, 169-180.

Cammann, K. (1979) "Working with Ion Selective Electrodes" 2nd ed. Springer-Verlag, Berlin - Heidelberg - New York.

Capovilla, M., Cervetto, L. & Torre, V. (1980) Effects of changing external potassium and chloride concentrations on the photoresponses of Bufo Bufo rods. J. Physiol. 307, 529-551.

Cervetto, L. (1973) Influence of sodium, potassium and chloride ions on the intracellular responses of turtle photoreceptors. Nature 241, 401-403.

Cervetto, L., Pasino, E., Torre, V. (1977) Electrical responses of rods in the retina of Bufo marinus. J. Physiol. 267, 17-51.

Cohen, A.I. (1965) Some electron microscopic observations on inter-receptor contacts in the human and macaque retinae. J. Anat. 99, 595-610.

Coles, J.A. & Tsacopoulos, M. (1977) A method of making fine double-barrelled potassium-sensitive micro-electrodes for intra-cellular recording J. Physiol. 270, 13-14P.

Coles, J.A. & Tsacopoulos, M. (1979) Potassium activity in photoreceptors, glial cells and extracellular space in the drone retina: Changes during photostimulation. J. Physiol. 290, 525-549.

Coombs, J.S., Eccles, J.C. & Fatt, P. (1955) The specific ionic conductances and the ionic movements across the moto-neuronal membrane that produce the inhibitory post-synaptic potential. J. Physiol. 130, 326-373.

Cremer, M. (1906) Uber dreursache der electromotorischen Eigenschafter der Gewebe, Zugleichein Beitrag zur Lehre von den polyphasischen electrolytketten. Z. Bin. 47, 562-608.

Dacheux, R.F. & Miller, R.F. (1976) Photoreceptor-bipolar cell transmission in the perfusedretina eyecup of the mudpuppy. Science 191. 963-964.

Daw, N.W. (1968) Colour-coded ganglion cells in the goldfish retina: Extension of their receptive fields by means of new stimuli. J. Physiol. (Lond) 197, 567-592.

Djamgoz, M.B.A. (1978) Electrophysical, biochemical and anatomical studies of the vertebrate (fish) retina. PhD thesis, Imperial College, London SW7 2BZ.

Djamgoz, M.B.A. & Laming, P.J. (1981) Intracellular measurement of ionic activity. Trends Neurosci. 4, 280-3.

Djamgoz, M.B.A. & Ruddock, K.H. (1978). Effects of local cobalt chloride injection on lateral spread of signals in fish' (roach) retina. Neurosci. Lett. 10, 23-28.

Djamgoz, M.B.A. & Ruddock, K,H. (1979) Adaptation effects in electrical responses recorded from post-receptoral neurones in the isolated fish (roach) retina. Vis. Res. 19, 413-418.

Djamgoz, M.B.A. & Ruddock, K.H. (1980) Evidence for a GABA-ergic feedback loop in the outer plexiform layer of the vertebrate retina. Colour Vis. Deficiencies 5, 45-50.

Djamgoz, M.B.A., Stell, W.K., Chen-An Chin & Lam, D.M,K. (1981) An opiate system in the goldfish retina. Nature 292, 620-623.

Dowling, J.E. (1968) Synaptic organization of the frog retina: An elctron microscopic analysis comparing the retinas of frogs and primates. Proc. R. Soc (B) 170, 205-228.

Dowling, J.E. (1974) The functional organisation of the vertebrate retina. In "Retina Congress" Eds. Pruett, R.C. & Regan, D.J. Appleton-Century-Crofts, New York, 1-17.

Dowling, J.E. (1975) Local circuit neurons in the vertebrate retina. Neurosciences Res. Prog. Bull. 13, 334-343.

Dowling, J.E., Brown, J.E. & Major, D. (1966) Synapses of horizontal cells in rabbit and cat retinas. Science 153, 1639-1641.

Dowling, J.E. & Ehinger, B. (1975) Synaptic organisation of the amine-containing interplexiform cells of the goldfish and cebus monkey retinas. Science 188, 270-273.

Dowling, J.E. & Ehinger, B. (1978) The interplexiform cell system 1. Synapses of the dopaminergic neurones of the goldfish retina. Proc. R. Soc. Lond. B. 201, 7-26.

Dowling, J.E., Ehinger, B. & Hedden, W.L. (1976) The interplexiform cell: a new type of retinal neurone. Invest. Opthal. 15, 916-926.

Dowling, J.E. & Ripps, H. (1977) The proximal negative response and visual adaptation in the skate retina. J. Gen. Physiol. 69, 57-74.

Dowling, J.E. & Werblin, F.S. (1969) Organisation of retina of the mudpuppy, Necturus maculosus - I. Synaptic Structure. J. Neurophysiol. 32, 315-338.

Dufau, E., Acker, H. & Sylvester, D. (1980) Double barrel ion-sensitive microelectrodes with extra thin tip diameters for intracellular measurements. Medical Progress through Technology 7, 35-39.

Eccles, J.C. (1964) "The Physiology of Synapses". Springer-Verlag: Berlin, Göttingen, Heidelberg.

Eisenman, G. (1969) Theory of membrane electrode potentials. Chapter I in "Ion-Selective Electrodes" Ed. R.A. Durst, NBC Spec. Publ. 314, U.S. Gov. Printing Off., Washington DC.

Eisenman, G., Bates, R.G., Mattock, G. & Friedman, S.M. (1966) "The Glass Electrode". Interscience, New York.

Eisenman, G., Rudin, D.O. & Casby, J.V. (1957) Glass electrode for measuring sodium ion. Science N.Y. 126, 831-834.

Ellis, D. (1977) The effects of external cations and ouabain on the intracellular sodium activity of sheep hear Purkinje fibres. J. Physiol. (Lond) 273, 211-240.

Ernst, W. (1979) The internal transmitter of vertebrate photoreceptors. Photobiol. Bull. 1, 128-137.

Fain, G.L. (1975) Interactions of rod and cone signals in the mudpuppy retina. J. Physiol. (Lond) 252, 735-769.

Fain, G.L., Quandt, F.N. & Gerschenfeld, H.M. (1977) Calcium-dependent regenerative responses in rods. Nature 269, 707-710.

Fain, G.L., Quandt, F.N., Bastian, B.L. & Gerschenfeld, H.M. (1978) Contribution of a caesium-sensitive conductance increase to the rod photoresponse. Nature 272, 467-469.

Famiglietti, E.V.Jr., Kaneko, A. & Tachibana, M. (1977) Neuronal architecture of on and off pathways to ganglion cells in carp retina. Science 198, 1267-1269.

Fatt, P. & Falk, G. (1977) Photosensitivity of elctrical conductance of the rod disc membrane. In "Vertebrate Photoreception" H.B. Barlow & P. Fatt Eds. Academic Press, London, 77-95.

Fatt, P. & Ginsborg, B.L. (1958) The ionic requirements for the production of action potentials in crustacean muscle fibres. J. Physiol. (Lond.) 142, 516-543.

Fry, C.H. & Poole-Wilson, P.A. (1981) Effects of acid-base changes on excitation-contraction. Coupling in guinea-pig and rabbit cardiac ventricular muscle. J. Physiol. (Lond) 313, 141-160.

Fuortes, M.G.F. (1976) Interactions and feedbacks in the turtle retina. In "Neural Principles in Vision", Eds. F. Zettler & R.Weiler. Springer, Berlin, 121-130.

Fuortes, M.G.F., Schwartz, E.A. & Simon, E.J. (1973) Colour-dependence of cone responses in the turtle retina. J. Physiol. (Lond) 234, 199-216.

Fuortes, M.G.F. & Simon, E.J. (1974) Interactions leading to horizontal cell responses in the turtle retina. J. Physiol. (Lond) 240, 177-198.

Gardner-Medwin, A.R. (1977) The migration of potassium produced by electric current through brain tissue. J. Physiol. (Lond) 269, 32-33P.

Gerschenfeld, H.M. & Piccolino, M. (1977) Muscarinic antagonists block cone to horizontal cell transmission in turtle retina. Nature 268, 257-258.

Ginsborg, B.L. (1967) Ion movements in junctional transmission. Pharmacol. Rev. 19, 289-316.

Green, R. & Giebisch, G. (1974) Some problems with the antimony microelectrode. In "Ion-Selective Microelectrodes". Berman, H.J. & Hebert, N.C. Eds. Plenum Pr., New York, 43-52.

Hagins, W.A. (1972) The visual process: excitatory mechanisms in the primary receptor cells. Ann. Rev. Biophys. & Bioeng. 1, 131-158.

Hagins, W.A., Penn, R.D. & Yoshikami, S. (1970) Dark current and photocurrent in retinal rods. Biophys. J. 10, 380-412.

Hagins, W.A. & Yoshikami, S. (1977) Intracellular transmission of visual excitation in phtoreceptors: Electrical effects of chelating agents introduced into rods by vesicle fusion. In "Vertebrate Photoreception", Eds. H.B. Barlow & P. Fatt. Academic Pr., London, 97-139.

Hashimoto, Y., Abe, M. & Inskuchi, M., (1980) Identification of the interplexiform cell in the dace retina by dye-injection method. Brain Res. 197, 331-340.

Hashimoto, Y., Kato, A., Inokuchi, M. & Watanabe, K. (1976). Re-examination of horizontal cells in the carp retina with procion yellow electrode. Vison Res. 16, 25-29.

Heinemann, U. & Lux, H.D. (1975) Undershoots following stimulus-induced rises of extracellular potassium concentration in cerebral cortex of cat. Brain Res. 93, 63-76.

Heyer, C.B. & Lux, H.D. (1976) Controls of the delayed outward potassium currents in bursting pace-maker neurones of the snail Helix pomatia. J. Physiol. 262, 349-382.

Hinke, J.A.M. (1959) Glass microelectrodes for measuring intracellular activities of sodium and potassium. Nature, 184, 1257-1258.

Hodgkin, A.L. (1951) The ionic basis of electrical activity in nerve and muscle. Biol. Rev. 26, 339-409.

Hodgkin, A.L. & Horowicz, P. (1957) Effects of K and Cl on the membrane potential of isolated muscle fibres. J. Physiol. Lond. 137, 30P.

Hodgkin, A.L. & Horowicz, P. (1959a) Movements of Na and K in single muscle fibres. J. Physiol. 145, 405-432.

Hodgkin, A.L. & Horowicz, P. (1959b) The influence of potassium and chloride ions on the membrane potential of single muscle fibres. J. Physiol. London. 148, 127-160.

Hodgkin, A.L. & Huxley, A.F. (1952) A quantitative description of membrane current and its application to conduction and excitation in nerve. J. Physiol. Lond. 117, 500-544.

Hodgkin, A.L. & Katz, B. (1949) The effect of sodium ions on the electrical activity of the giant axon of the squid. J. Physiol. Lond. 108, 37-77.

Hodgkin, A.L. & Keynes, R.D. (1955a) Active transport of cations in giant axons from Sepia and Loligo. J. Physiol. Lond. 128, 28-60.

Hodgkin, A.L. & Keynes, R.D. (1955b) The potassium permeability of a giant nerve fibre. J. Physiol. Lond. 128, 61-88.

Ishida, A.T. & Fain, G.L. (1981) D-Aspartate potentiates the effects of L-Glutanate on horizontal cells in goldfish retina. Proc. Nat. Acad. Sci. 78, 5890-5894.

Jack, J.S.B., Noble, D. & Tsien, R.W. (1975) Electric current flow in excitable cells. Clarendon Press, Oxford.

Johnson, D. & Lam, D.M.K. (1981) Regenerative and passive membrane properties of isolated horizontal cells from a teleost retina. Nature 292, 451-454.

Kaneko, A. (1970) Physiological and morphological identification of horizontal, bipolar and amacrine cells in goldfish retina. J. Physiol. Lond. 207, 623-633.

Kaneko, A. (1971) Physiological studies of single retinal cells and their morphological identification. Vision Res. Supp. No. 3, 17-26.

Kaneko, A. (1973) Receptive field organization of bipolar and amacrine cells in the goldfish retina. J. Physiol. Lond. 235, 133-153.

Kaneko, A. & Hashimoto, H. (1967) Recording site of the single cone response determined by an electrode marking technique. Vision Res. 7, 847-851.

Kaneko, A. & Shimazaki, H. (1975a) Synaptic transmission from photoreceptors to bipolar and horizontal cells in the carp retina. Cold Spring Harbour Symp. Quant. Biol. 40, 537-46.

Kaneko, A. & Shimazaki, H. (1975b) Effects of external ions on the synaptic transmission from photoreceptors to horizontal cells in the carp retina. J. Physiol. Lond. 252, 509-522.

Kaneko, A. & Shimazaki, H. (1976) Synaptic transmission from photo-receptors to second order neurons in the carp retina. In "Neural Principles in Vision" Eds. F. Zettler, R. Weiler. Springer, Berlin, 143-157.

Kaneko, A. & Tachibana, M. (1981) Retinal bipolar cells with double colour-opponent receptive fields. Nature 293, 220-223.

Kaneko, A., Famiglietti, E.V. & Tachibana, M.Jr. (1979) Physiological and Morphological Identification of Signal Pathways in the Carp Retina. In "Neurobiology of Chemical Transmission" Ed. M. Otsuka & Z.W. Hall, Wiley, New York.

Kaneko, A. & Yamada, M. (1972) S-potentials in the dark adapted retina of the carp. J. Physiol. Lond 227, 261-273.

Karwoski, C.J. & Proenza, L.M. (1977) Hyperpolarizing on/off responses in mudpuppy retina. Vision Res. 17, 152-153.

Kato, S. & Negishi, K. (1978) Effects of variations in the perfusate on the ERG and discharge of ganglion cells in carp retina. Exp. Eye Res. 26, 363-376.

Kernan, R.P. & MacDermott, M., (1976) Intracellular potassium concentrations and extracellular spaces in rat skeletal muscles immersed in normal, hypotonic and high-K modified Krebs fluid, determined by potassium-selective microelectrodes. J. Physiol. Lond. 263, 158P.

Keynes, R.D. (1963) Chloride in the giant squid axon. J. Physiol. Lond. 169, 690-705.

Khuri, R.N. (1971) Intracellular potassium and the electrochemical properties of striated muscle fibres. Proc. Int. Union. Physiol. Sci. 9, 301.

Khuri, R.N. (1976) Microelectrodes utilizing glass and liquid ion-exchanger sensors. In "Ion and Enzyme Electrodes in Biology and Medicine". Ed. M. Kessler, L.C. Clark Jr., D.W. Lubbers, I.A. Silver & W. Simon. University Park Press, Baltimore, London, Tokyo.

Koryta, J. (1975) Ion-Selective electrodes. Cambridge Univ. Press, Cambridge.

Kotera, K., Satake, N., Honda, M. & Fujimoto, M. (1979) The measurement of intracellular sodium activities in the bullfrog by means of double-barreled sodium liquid ion-exchanger microelectrodes. Memb. Biochem. 2, 323-338.

Kraig, R.P. & Nicholson, C. (1976) Sodium liquid ion-exchanger microelectrode used to measure large extracellular sodium transients. Science NY 194, 725-726.

Kuffler, S.W. (1953) Discharge patterns and functional organization of mammalian retina. J. Neurophysiol. 16, 37-68.

Lamb, T.D. (1976) Spatial properties of horizontal cells responses in the turtle retina. J. Physiol. (Lond) 263, 239-255.

Lasansky, A. (1971) Synaptic organisation of cone cells in the turtle retina. Phil. Trans. Roy. Soc. B., 262, 365-381.

Lasansky, A. (1973) Organization of the outer synaptic layer in the retina of the larval tiger salamander. Phil. Trans. Roy. Soc. B 265, 471-489.

Lasansky, A. (1981) Synaptic action mediating cone responses to annular illumination in the retina of the larval tiger salamadner. J. Physiol. 310, 205-214.

Lavallee, M. & Szabo, G. (1969) The effect of glass surface conductivity phenomena on the tip potential of micropipette electrodes. Chapter 6 in "Glass microelectrodes" Ed. M. Lavallee, O.F. Schanne & N.C. Hebert. John Wiley & Sons Inc., New York, London.

Lederer, W.J., Spindler, A.J. & Eisner, D.A. (1979). Thick slurry bevelling. A new technique for bevelling extremely fine microelectrodes and micropipettes. Pflugers Arch. 381, 287-288.

Lee, C.O. & Armstrong, W.McD. (1974) State and distribution of potassium and sodium ions in frog skeletal muscle. J. Memb. Biol. 15, 331-362.

Lev, A.A. & Buzhinsky, E.P. (1961) On the method for determining the activity of K^+-sensitive glass microelectrodes. Tsitologiya 3, 614-621.

Lewis, S.A., Wills, N.K. & Eaton, D.C. (1978) Basolateral membrane potential of a tight epithelium: Ionic diffusion and electrogenic pumps. J. Membrane Biol. 41, 117-148.

Lewis, S.A. & Wills, N.K. (1980) Resistive artifacts in liquid-ion-exchanger microelectrode estimates of Na^+ activity in eipthelial cells. Biophys. J. 31, 127-138.

Liebman, P.A. & Pugh, E.N.Jr. (1979) The control of phosphodiesterase in rod disk membranes: Kinetics, possible mechanics and significance for vision. Vision Res. 19, 375-382.

Lowenstein, W.R. (1975) Permeable junctions in the synapse. Cold Spring Har. Symp. Quant. Biol. 49-63.

Lux, H.D. (1974) Fast recording ion specific microelectrodes: their use in pharmacological studies in the CNS. Neuropharmac. 13, 509-517.

MacNichol, E.F.Jr. & Svaetichin, G. (1958) Electric responses from the isolated retinas of fishes. American J. Opthalmol. 46, No. 3, Part II, 26-46.

Magalhaes, M.M. (1976) Functional cytoarchitecture of the retina Muller Cell. In "The structure of the eye III". Eds. E. Yamada & S. Mishima, 330-340.

Marban, E., Rink, T.J., Tsien, R.W. & Tsien, R.Y. (1980) Free calcium in heart muscle at rest and during contraction measured with a Ca^{2+}-sensitive micro-electrode. Nature 286, 845-850.

Marc, R.E. (1980) Retinal colour channels and their neurotransmitters. In: "Colour Deficiencies V", Institute of Physics, London.

Marc, R.E. & Sperling, H.G. (1976a) Colour receptor identities of goldfish cones. Science 191, 487-488.

Marc, R.E. & Sperling, H.G. (1976b) The chromatic organization of the goldfish cone mosaic. Vision Res. 16, 1211-1224.

Marks, W.B. (1965) Visial pigments of single golfish cones. J. Physiol. (Lond) 178, 14-32.

Matsuura, T., Miller, W.H. & Tomita, T. (1978) Cone-specific c-wave in the turtle retina. Vision Res. 18, 767-775.

Meech, R.W. (1978) Calcium-dependent potassium activation in nervous tissues. An. Rev. Biophys. and Bioeng. I, 1-18.

Miller, R.F. (1978) Low sodium uncouples electrotonic connections between horizontal cells. Brain Res. 139, 178-182.

Miller, R.F. (1979) The neuronal basis of ganglion cell receptive field organisation and the physiology of amacrine cells. In "The Neurosciences 4th Study Programme", Eds. F.O. Schmitt & F.G. Worden. MIT Press, Cambridge and London, 227-245.

Miller, R.F. & Dacheux, R.F. (1973) Information processing in the retina: Importance of chloride ions. Science 181, 266-268.

Miller, R.F. & Dacheux, R.F. (1975) Chloride-sensitive receptive field mechanisms in the isolated retina eye-cup of the rabbit.

Miller, R.F. & Dacheux, R.F. (1976a) Synaptic organisation and ionic basis of on and off channels in mudpuppy retina I. Intracellular analysis of chloride-sensitive electrogenic properties of receptors, horizontal cells, bipolar cells and amacrine cells. J. Gen. Physiol. 67, 639-659,

Miller, R.F. & Dacheux, R.F. (1976b) Synaptic organization and ionic basis of on and off channels in mudpuppy retina II. Chloride-dependent ganglion cell mechanisms. J. Gen. Physiol. 67, 661-678.

Miller, R.F. & Dacheux, R.F. (1976c) Dendritic and somatic spikes in mudpuppy amacrine cells: Identification and TTX-sensitivity. Brain Res. 104, 157-162.

Missotten, L. (1966) The ultrastructure of the human retina. Arscia. Vitgaven N.V., Brussels.

Mitarai, G., Asano, T. & Miyake, Y. (1974) Identification of five types of S-potential and their corresponding generating sites in the horizontal cells of the carp retina. Jap. J. Ophthalmol. 18, 161-176.

Moody, G.J. & Thomas, J.D.R. (1971) "Selective Ion Sensitive Electrodes". Merrow, Watford.

Morf, W.E., Ammann, D., Bissing, R., Prestch, E. & Simon, W. (1979) In "Progress in Macrocyclic Chemistry", Eds. R.M. Izatt & J.J. Christensen. Vol. 1, Wiley, N.Y., 1-61.

Murakami, M., Ohtsu, K. & Ohtsuka, T. (1972) Effects of chemicals on receptors and horizontal cells in the retina. J. Physiol. Lond. 227, 899-913.

Murakami, M., Ohtsuka, T. & Shimazaki, H. (1975) Effects of aspartate and glutamate on the bipolar cells in the carp retina. Vision Res. 15, 456-458.

Murakami, M. & Shimoda, Y. (1977) Identification of amacrine and ganglion cells in the carp retina. J. Physiol. Lond. 265, 801-818.

Naka, K.I. (1972) The horizontal cells. Vision Res. 12, 573-588.

Naka, K.I. (1977) Functional organization of catfish retina. J. Neurophysiol. 40, 26.

Naka, K.I. & Christensen, B.N. (1981) Direct electrical connections between transient anacrine cells in the catfish retina. Science 214, 462-464.

Naka, K.I. & Rushton, W.H.A. (1966a) S-potentials from colour units in the retina of fish (Cyprinidae). J. Physiol. (Lond) 185, 536-555.

Naka, K.I. & Rushton, W.H.A. (1966b) An attempt to analyse colour reception by electrophysiology. Ibid., 556-586.

Naka, K.I. & Rushton, W.H.A. (1966c) S-potentials from luminosity units in the retina of fish (Cyprinidae). Ibid., 587-599.

Naka, K.I. & Rushton, W.H.A. (1967) Generation and spread of S-potentials in fish (Cyrpinidae). J. Physiol. (Lond) 192, 437-461.

Nastuk, W.L. & Hodgkin, A.L. (1950) The electrical activity of single muscle fibers. J. Cell Comp. Physiol. 35, 39-73.

Neal, M.J. & Iversen, L.L. (1972) Autoradiographic localization of ^{3}H-GABA in rat retina. Nature 235, 217-218.

Neild, T.O. & Thomas, R.C. (1974) Intracellular chloride activity and the effects of acetylcholine in snail neurones. J. Physiol. London 242, 453-470.

Nelson, R. (1973) A comparison of electrical properties of neurones in Necturus retina. J. Neurophysiol. 67, 639-659.

Neher, E. & Lux, H.D. (1973) Rapid changes of potassium concentration at the outer surface of exposed single neurones during membrane current flow. J. Gen. Physiol. 61, 385-399.

Nelson, R., Famiglietti, E.V.Jr. & Kolb, H. (1978) Intracellular staining reveals different levels of stratification for on- and off-center ganglion cells in cat retina. J. Neurophysiol. 41, 472-483.

Nikolsky, B.P. (1937) A theory of the glass electrode. Zh. Fiz. Khim. 10, 495-503.

Norton, F.J. (1944) Organo-silicon films. Gen. Elect. Rev. 47, 6-16.

Norton, A.L., Spekreijse, H., Wolbarsht, M.L. & Wagner, H.G. (1968) Receptive field organization of the S-potential. Science 160, 1021-1022.

Oakley, B. (1977) Potassium and the photoreceptor-dependent pigment epithelial hyperpolarization. J. Gen. Physiol. 70, 405-425.

Oakley, B. & Green, D.G. (1976) Correlation of light-induced changes in retinal extracellular potassium concentration with c-wave of the electroretingoram. J. Neurophysiol. 39, 1117-1133.

Oakley, B., Flaming, D.G. & Brown, K.T. (1979) Effects of the rod receptor potential upon retinal extracellular potassium concentration. J. Gen. Physiol. 74, 713-738.

O'Bryan, P.M. (1973) Properties of depolarising synaptic potential evoked by peripheral illumination in cone of the turtle retina. J. Physiol. Lond. 235, 207-223.

O'Doherty, J., Garcia-Diaz, J.F. & Armstrong, W.McD. (1979) Sodium-selective LIX microelectrodes for intracellular measurements. Science 203, 1349-1351.

Oehme, M., Kessler, M. & Simon, W. (1976) Neutral carrier Ca^{2+} microelectrode. Chimia 30, 204.

Owen, J.D., Brown, H.M. & Saunders, J.H. (1975) Chloride activity in the giant cells of the Aplysia. Biophys. J. 15, 45a.

Parthe, V. (1972) Horizontal bipolar and oligopolar cells in the teleost retina. Vis. Res. 12, 395-406.

Penn, R.D. & Hagins, W.A. (1969) Signal transmission along retinal rods and the origin of the electroretinographic a-wave. Nature 223, 201-203.

Piccolino, M. & Gerschenfeld, H.M. (1977) Lateral interactions in the outer plexiform layer of turtle retinas after atropine block of horizontal cells. Nature 268, 259-260.

Piccolino, M., Neyton, S. & Gerschenfeld, H.M. (1980) Synaptic mechanisms involved in responses of chromaticity horizontal cells of turtle retina. Nature 284, 58-60.

Pinto, L.H., Brown, J.E. & Coles, J.A. (1977) In "Vertebrate Photoreception", Ed. H.B. Barlow & P. Fatt. Mechanism for the generation of the receptor potential of rods of Bufo Marinus, 159-167. Academic Press London.

Plamondon, R., Gagné, S. & Poussart, D. (1976) Low resistance and tip potentials of glass microelectrode: Improvement through a new filling method. Vision Res. 16, 1355-1357.

Pungor, E. & Toth, K. (1969) Selectivity of ion-specific membrane electrodes. Anal. Chim. Acta. 47, 291-297.

Pungor, E. & Toth, K. (1970) Ion-selective membrane electrodes: A review. The Analyst, 95, 625-648.

Reeves, J.P. & Sutko, J.L. (1980) Sodium-calcium exchange activity generates a current in cardiac membrane vesicles. Science 208, 1461-1464.

Rink, T.J. & Tsien, R. (1980) Calcium-selective micro-electrodes with bevelled sub-micron tips containing poly(vinyl-chloride)-gelled neutral-ligand sensor. J. Physiol. Lond. 308, 5-6P.

Rodieck, R.W. (1973). "The Vertebrate Retina". Freeman, San Francisco.

Russel, J.M. (1978) Effects of ammonium and bicarbonate-CO_2 on intracellular chloride levels in Aplysia neurones. Biophys. J. 22, 131-137.

Russel, J.M. (1980) Anion transport mechanisms in neurones. Annals New York Acad. Sci. 341, 510-523.

Sachs, F. & McGarrigle, R. (1980) An almost completely shielded microelectrode. J. Neurosci. Meth. 3, 151-157.

Saito, T., Kondo, H. & Toyoda, J. (1978) Rod and cone signals in the on-centre bipolar cell: their different ionic mechanisms. Vision Res. 18, 591-595.

Saunders, J.H. & Brown, H.M. (1977) Liquid and solid-state Cl^--sensitive microelectrodes: Characteristics and application to intracellular Cl^- activity in Balanus photoreceptor. J. Gen. Physiol. 70, 507.

Scholes, J.H. (1975) Colour receptors, and their synaptic connections in the retina of a cyprinid fish. Phil. Trans. R. Soc. B. 70, 61-118.

Scholes, J.H. (1976) Neuronal connections and cellular arrangement in the fish retina. Neural principles in vision. Ed. F. Zettler & R. Weiler. Springer-Verlag, 63-93.

Scholes, J.H. & Morris, J. (1973) Receptor-bipolar connectivity patterns in fish retina. Nature 241, 52-54.

Schultze, B. (1866) Zur anatomie und physiologie der retina. Arch. Mikr. Anat. 2, 175-286.

Sillman, A.J., Ito. H. & Tomita, T. (1969a) Studies on the mass receptor potential of the isolated frog retina. I. General properties of the response. Vision Res. 9, 143 -1442.

Sillman, A.J., Ito. H. & Tomita, T. (1969b) Studies on the mass receptor potential of the isolated frog retina. II. On the basis of ionic mechanisms. Ibid. 1443-1451.

Sjöstrand, F.S. (1969) The outer plexiform layer and the neural organization of the retina. In "The Retina: Morphology, function and clinical characteristics". UCLA forum in medical sciences 8, eds. B.R. Straatsma, M.O. Hall, R.A. Allen & F. Crescitelli. Univ. Calif. Pr., Berkeley, 63-100.

Somjen, G.G., Rosenthal, M., Cordingley, G., LaManna, J. & Lothman, E. (1976) Potassium neuroglia and oxidative metabolism in central gray matter. Fed. Proc. 38, 1266-1271.

Spekreijse, H. & Norton, A.L. (1970) The dynamic characteristics of colour-coded S-potentials. J. Gen. Physiology 56, No. 1, 1-15.

Steinberg, R.H. & Schmidt, R. (1970) Intracellular responses to light from the cat's pigment epithelium: Origin of the c-wave of the electroretinogram. Nature 227, 728-730.

Steiner, R.A., Oehme, M., Ammann, D. & Simon, W. (1979) Neutral carrier sodium ion-selective microelectrode for intracellular studies. Anal. Chem. 51, 351-353.

Stell, W.K. (1967) The structure and relationships of horizontal cells and photoreceptor-bipolar synaptic complexes in goldfish retina. Am. J. Anat. 121, 401-423.

Stell, W.K. (1972) The morphological organization of the vertebrate retina. Handbook of Sensory Physiol. VII/2, Ed. M.G.F. Fuortes, 111-214.

Stell, W.K. (1975) Horizontal cell axons and axon terminals in goldfish retina. J. Comp. Neurol. 159, 503-520.

Stell, W.K. (1976) Functional polarization of horizontal cell dendrites in goldfish retina. Invest. Opthalmol. 15, 895-908.

Stell, W.K. (1980) Photoreceptor - specific synaptic pathways in goldfish retina: a world of colour, a wealth of connections. Colour Vis. Deficiences, 5, 1-14.

Stell, W.K., Ishida, A.T. & Lightfoot, D.O. (1977) Structural basis for on- and off-center responses in retinal bipolar cells. Science 198, 1269-1271.

Stell, W.K. & Harosi, F. (1976) Cone structure and visual pigment content in the retina of the goldfish. Vison Res. 16, 647-657.

Stell, W.K. & Lightfoot, D.O. (1975) Colour-specific interconnections of cones and horizontal cells in the retina of the goldfish. J. Comp. Neurol. 159, 473-502.

Stell, W.K., Lightfoot, D.O., Wheeler, T.G. & Leeper, H.F. (1975) Goldfish Retina: Functional polarization of cone horizontal cell dendrites and synapses. Science 190, 989-990.

Stell, W.K., Marshak, D., Yamada, T., Brecha, N. & Karten, H. (1980) Trends Neurosci. 3, 292-295.

Suzuki, K., Rohlicek, V. & Frömter, E. (1978) A quasi totally shielded, low capacitance glass microelectrode with suitable amplifiers for high frequency intracellular potential and impedance measurements. Pflüg. Arch. 378, 141-148.

Svaetichin, G. (1953) The cone action potential. Acta. Physiol. Scand. 29, Suppl. 106, 565-600.

Svaetichin, G. & McNichol, E.I.Jr. (1958) Retinal mechanisms for chromatic and achromatic vision. Ann. N.Y. Acad. Sci. 74, 385-404.

Tachibana, M. (1981) Membrane properties of solitary horizontal cells isolated from goldfish retina. J. Physiol. London 321, 141-161.

Tamura, T. & Niwa, H. (1967) Spectral sensitivity and colour vision of fish as indicated by S-potential. Comp. Biochem. Physiol. 22, 745-754.

Thomas, R.C. (1969) Membrane current and intracellular sodium changes in a snail neurone during extrusion of injected sodium. J. Physiol. Lond. 201, 495-514.

Thomas, R.C. (1970) A new design for sodium-sensitive glass microelectrodes. J. Physiol. Lond. 210, 82-83P.

Thomas, R.C. (1972) Iutracellular sodium activity and the sodium pump in snail neurones. J. Physiol. Lond. 220, 55-71.

Thomas, R.C. (1974) Intracellular pH of snail neurones measured with a new pH-sensitive glass microelectrode. J. Physiol. Lond. 238, 159-180.

Thomas, R.C. (1976) Construction and properties of recessed-tip microelectrodes for sodium and chloride ions and pH. In "Ion and Enzyme Electrodes in Biology and Medicine". Ed. M. Kessler et al., Urban and Schwarzenberg, Munich, 141-148.

Thomas, R.C. (1977) The role of bicarbonate, chloride and sodium ions in the regulation of intracellular pH in snail neurones. J. Physiol. Lond. 273, 317-338.

Thomas, R.C. (1978a) Ion-sensitive intracellular microelectrodes: How to make and use them. Acad. Press, London.

Thomas, R.C. (1978b) Comparison of the mechanisms controlling intracellular pH and sodium in snail neurones. Resp. Physiol. 33, 63-73.

Thomas, R.C. & Cohen, J.C. (1981) A liquid ion-exchanger alternative to KCl for filling intracellular reference microelectrodes. Pflügers Arch. 390, 96-98.

Tomita, T. (1965) Electrophysiological study of the mechanisms subserving color coding in the fish retina. Cold Spring Harb. Symp. Quant. Biol., 30, 559-566.

Tomita, T., Kaneko, A., Murakami, M. & Pautler, E.L. (1967) Spectral response curves of single cones in the carp. Vis. Res., 7, 519-531.

Toyoda, J.I. (1973) Membrane resistance changes underlying the bipolar cell response in the carp retina. Vison Res. 13, 283-294.

Toyoda, J.I., Hashimoto, H. & Ohtsu, K. (1973) Bipolar-amacrine transmission in the carp retina. Vision Res. 13, 295-307.

Toyoda, J., Nosaki, H. & Tomita, T. (1969) Light-induced resistance changes in single photoreceptors of Necturus and Gekko. Vis. Res. 9, 453-463.

Trifonov, Yu.A. (1968) Study of synaptic transmission between photoreceptors and horizontal cells by means of electrical stimulation of the retina. Biofizika, 13, 809-817.

Trifonov, Yu.A., Byzov, A.L. & Chailahian, L.M. (1974) Electrical properties of subsynaptic and non-synaptic membranes of horizontal cells in fish retina. Vision Res. 14, 229-241.

Tsien, R.Y. (1980) Liquid sensors for ion-selective microelectrodes. Trends Neurosci. 3, 219-220.

Vaughan-Jones, R.D. (1977) Intracellular chloride activity of quiescent cardiac Purkinje fibres. J. Physiol. 272, 32P.

Vesely, J. et al. (1978) Analysis with ion-selective electrodes. Ed. R.A. chalmers & M. Masson. Ellis Harwood Series in Analytical Chemistry.

Vyskocil, F. & Kriz, N. (1972) Modifications of single and double-barrel potassium specific microelectrodes for physiological experiments. Pflüg. Arch. 337, 265-276.

Vyskocil, F., Kriz, N. & Bures, J. (1972) Potassium-selective microelectrodes used for measuring the extracellular brain potassium during spreading depression and anoxic depolarisation in rats. Brain Res. 39, 255-259.

Wagner, H.G., MacNichol, E.F., Jr. & Wolbarsht, M.L. (1963) Functional basis for 'on'-centre and 'off'-centre receptive fields in the retina. J. Optical Society of America, 53, 66-70.

Walker, J.L. (1971) Ion specific liquid ion-exchanger microelectrodes. Analyt. Chem. 43, 89A-93A.

Walker, J.L. (1976) Ion-selective liquid ion-exchanger microelectrodes. In "Ion and Enzyme Electrodes in Biology and Medicine". Eds. M. Kessler, L.C. Clark Jr., D.W. Lübbers, I.A. Silver, & W. Simon. University Park Press, Baltimore, 116-118.

Walker, J.L. (1979) Ion selective electrode measurements. Meth. Enzymol. 56, 359-368.

Walker, J.L. & Brown, H.M. (1977) Intracellular ionic activity measurements in nerve and muscle. Physiol. Rev. 57, 729-778.

Waloga, G. (1975) Ionic mechanisms for the generation of S-potentials: Horizontal cells in isolated axolotl retina. PhD thesis. Purdue University, West Lafayette, Ind.

Waloga, G. & Pak, W.L. (1976) Horizontal cell potentials: Dependence on external sodium ion concentration. Science 191, 964-966.

Waloga, G. & Pak, W.L. (1978) Ionic mechanism for the generation of horizontal cell potentials in isolated axolotl retina. J. Gen. Physiol. 71, 69-92.

Weast, R.C. Handbook of Chemistry and Physics. The Chemical Rubber Co. 1971-1972.

Werblin, F.S. (1975b) Regenerative hyperpolarisation in rods. J. Physiol. 244 53-81.

Werblin, F.S. (1975a) Anomalous rectification in horizontal cells. J. Physiol. Lond. 244, 639-658.

Werblin, F.S. (1977) Regenerative amacrine cell depolarization and formation of on-off ganglion cell response. J. Physiol. Lond. 264, 767-785.

Werblin, F.S. & Copenhagen, D.R. (1974) Control of retinal sensitivity. III Lateral interactions at the inner plexiform layer. J. Gen. Physiol. 63, 88-110.

Werblin, F.S. & Dowling, J.E. (1969) Organisation of the retina of the mudpuppy Necturus Maculosus: II Intracellular recording. J. Neurophysiol. 32, 339-355.

White, J.F. (1976) Intracellular potassium activities in Amphiuma small intestine. Am. J. Physiol. 231, 1214-1219.

Wills, N.K. & Lewis, S.A. (1980) Intracellular Na^+ activity as a function of Na^+ transport rate across a tight epithelium. Biophys. J. 30, 181-186.

Witkovsky, P. & Dowling, J.E. (1969) Synaptic relationships in the plexiform layers of carp retina. Z. Zellforsch, 100, 60-82.

Woodruff, M.L., Bownds, D., Green, S.H., Morrisey, J.L. & Shedlovsky, A. (1977) Guanosine 3', 5'-cyclic monophosphate and the in vitro physiology of frog photoreceptor membranes. J. Gen. Physiol. 69, 667-679.

Wu, S.M. & Dowling, J.E. (1978) L -'aspartate': evidence for a role in cone photoreceptor synaptic transmission in the carp retina. Proc. Nat. Acad. Sci. 75, 5205-5209.

Yamada, E. & Ishikawa, T. (1965) The fine structure of the horizontal cells in some vertebrate retinae. Cold Spring Harb. Sympos. Quart. Biol. 30, 383-392.

Yoshikami, S. & Hagins, W.A. (1973) Control of the dark current in vertebrate rods and cones. In "Biochemistry and Physiology of Visual Pigments". Ed. H. Langer, Springer, Berlin, 245-255.

Yoshikami, S., George, J.S. & Hagins, W.A. (1980) Light-induced calcium fluxes from outer segment layer of vertebrate retinas. Nature, 286, 395-398.

Zeuthen, T. (1971) A method to fill glass microelectrodes by local heating. Acta Physiol. Scand. 81, 141.

Zeuthen, T. (1981) The application of ion-selective micro-electrodes. Elsevier/N. Holland Biomedical Press. Amsterdam, New York, Oxford.

Zeuthen, T., Hiam, R.C. & Silver, I.A. (1974) Microelectrode recording of ion activity in brain. In "Ion Selective Microelectrodes" 145-156. Eds. H. Berman, and N. Hebert, Plenum, N.Y.

ACKNOWLEDGEMENTS

These studies were carried out whilst on a Science and Engineering Research Council Postgraduate Studentship. I would like to thank Dr. K.H. Ruddock for making this SERC grant available to me and also for giving support and advice. I thank especially Dr. M.B.A. Djamgoz for his friendly and keen supervision of the studies reported in this thesis. I am grateful for the support of family and friends, and colleagues at the Middlesex Hospital which greatly helped to enable the completion of this thesis.

Mrs. Guliz Onkal provided invaluable technical assistance in the laboratory. I am also grateful to the technical staff of the Pure and Applied Biology Department, especially Mr. J. Harmer and Mr. D. Hopkins for their expert help with regard to apparatus and instrumentation. Mr. S. Stammers was helpful in providing a very good photographic service. Drs. R. Sinden and J. Hardie gave an excellent introductory course and useful advice on electron microscopy.

Some of the fish used during this study were donated by Fishery Sections of the Thames and Southern Water Authorities. Mr. P. Morriss and Mr. J. Downing who helped to catch and collect these fish deserve my thanks.

I am grateful to Dr. H.M. Brown for providing the gift of Corning K^+ and Cl^- liquid ion-exchangers (see chapter II.3.i).

I would like to thank the following people for helpful discussions and advice: Dr. C.C. Aickin (University Dept. of Pharmacology, Oxford); Dr. H. Bradford (Imperial College, London); Dr. A.R. Gardner-Medwin (University College, London); Dr. H.M. Gerschenfeld (Ecole Normale Superieure, Paris, France); Dr. R.C. Thomas (Physiology Dept., University of Bristol) and Dr. J.I. Toyoda (University School of Medicine, Sugao, Kawasaki, Japan).

Finally I thank Mrs. P.A. Mill for her skill and patience in typing this thesis, and Miss J.B. Nielsen for helping with the typing.

Reprinted from:

Trends in NeuroSciences

Intracellular measurement of ionic activity

M. B. A. Djamgoz and P. J. Laming

ELSEVIER/NORTH-HOLLAND
BIOMEDICAL PRESS

Reprinted from Trends in NeuroSciences – *November 1981*, Vol. 4, No 11, pp 280–3

Intracellular measurement of ionic activity

M. B. A. Djamgoz and P. J. Laming

The measurement of intracellular ionic activity is crucial to a quantitative understanding of neuronal function. Intracellular ion-sensitive microelectrodes (ISMs) can now be routinely made which are capable of determining the ionic activities of Na^+, K^+, Cl^-, H^+ and Ca^{2+} and of monitoring their changes even in small neurones. This article outlines some of the theoretical and practical aspects underlying the use of ISMs, and provides details of some applications. Interested readers should also consult the recent article by Charles Nicholson on extracellular measurement (TINS *1980, pp. 218–218).*

The ionic basis of electrical activity in the nervous system was first formalized by Bernstein using the electrochemical theories of Nernst. He suggested that in the resting state the potential difference across the nerve membrane could be accounted for by the membrane's selective permeability to potassium ions, and that excitation involved a general increase in membrane permeability to Na^+, K^+ and Cl^- which effectively short circuited this potential. Later, however, Hodgkin, Huxley and Katz showed that during excitation the interior of the nerve becomes transiently positive, due to a selective increase in the membrane's permeability to Na^+.

It is now generally accepted that the signalling ability of excitable cells depends on the transmembrane concentration gradients of Na^+, K^+, Cl^-, Ca^{2+} ions. Each ion has its characteristic equilibrium potential which is expressed by the Nernst equation:

$$E_x = \frac{RT}{Z_x F} \ln \frac{a_x^o}{a_x^i}$$

where E_x is the equilibrium potential for the ion 'x'; R, the universal gas constant; T, the absolute temperature; F, the Faraday constant, a_x^o and a_x^i, the activities* of the ion x on the outside and the inside of the membrane, respectively, and Z_x its valency.

The membrane potential is a function of the Nernstian potential for these four ions, but usually it is dominated by the contribution of a single species. Increasing the membrane permeability to a particular ion displaces the potential towards the equilibrium value for that species.

In order to be able to determine the contribution of a particular ion to the active and passive properties of a particular cell both the intracellular and extracellular concentrations must be determined. Clearly, the most difficult of these measurements is the intracellular one. In the case of the squid giant axon sufficient cytoplasm can be extruded to carry out ion analysis by conventional chemical means (e.g. flame photometry). However, this technique is obviously impractical for small cells in the nervous system. The ISM however allows these measurements to be carried out *in vivo*. The theory and application of this technique have been described in greater detail by several authors[1,7,17,19–21] – what follows is a brief summary of the aspects most pertinent to the general reader.

Classification and construction

ISMs consist of a conventional glass micropipette electrode filled with the appropriate reference solution (Fig. 1) whose tip is plugged with a material which is ion-sensitive/selective. Since the tip can be a micron or less in diameter, it can be used for intracellular recording. ISMs can be classified according to the physical nature of the ion-selective sensor (liquid-state and solid-state ISMs), and the ionic species to which it is primarily sensitive (K^+-sensitive ISM, Cl^--sensitive ISM, etc.). An overall classification is given in Table I.

TABLE I. A classification of intracellular ion-sensitive microelectrodes

Type of ISM sensor	Primary sensitivity	Reference
Liquid state:		
Liquid ion exchanger	K^+, Cl^-, Na^+, Ca^{2+}	1, 3, 7, 17, 20
Neutral ion carrier	K^+, Ca^{2+}, Na^+	1, 7, 8, 13, 17, 19
Solid state:		
Glass membrane	Na^+, H^+, K^+	6, 7, 15, 16, 17
Metal	Cl^-, H^+	7, 10, 14, 17

The liquid sensors for ISMs are water-immiscible[17,19]. They would normally be displaced from the tip of a glass microelectrode by the aqueous reference solution that fills the back of the electrode, since a glass surface is normally hydrophilic. Having pulled a glass micropipette of the desired tip size and shape, the next crucial step is to make its inside wall hydrophobic (water-repellant) by treating it with an organic silicon compound[19]. Not surprisingly, a variety of different silanes and silanizing procedures have been used for this reason, as the subsequent performance of a liquid-state ISM to a great extent will depend on how well it was silanized initially. In general, under-silanization will lead to the filling solution gradually creeping to the tip of the ISM and forming a thin layer of relatively high conductivity thereby shunting some of the ISM electrochemical potential. On the other hand, over-silanization will partially (if not completely) block ISM tips and induce undesirably high electrode resistances. Typically 3% tri-N-butylchlorosilane in chloronaphthalene is used to silanize single-barrel ISMs[17] and the vapour from dimethyl dichlorosilane to silanize the active side of a double-barrel ISM[3,8]. Following the introduction of the silane solution into the microelectrode shafts, the latter are baked at 100°C for 1 h to complete the silanization procedure. A small quantity of the liquid sensor is then injected as far down the shank of the electrode as possible and made to fill 200 μm to a few millimetres from the tip by applying pressure or using

*The activity of an ion, a_x, is related to its concentration C_x, by the relationship $a_x = \gamma_x C_x$, where γ_x is known as the activity coefficient.

the capillary action of a cat's whisker. The rest of the microelectrode is filled with a reference solution (e.g. 0.5 M KCl for K^+- and Cl^--sensitive ISMs) into which the chlorided end of a silver wire is sealed to complete the ISM assembly.

Solid-state ISMs are, in general, more difficult to manufacture than the liquid-state variety, and if a suitable liquid sensor is available for a given ion, the latter type of ISM is almost always preferred. For example, solid-state K^+-sensitive ISMs are now hardly ever used, and there is increasing demand for a suitable Na^+ liquid ion exchanger in preference to using the Na^+-sensitive glass. At present, however, glass membrane ISMs for Na^+ and H^+(pH) remain the best sensors available for these ions. The first step in the manufacture of this type of ISM is to pull a microelectrode from the ion-sensitive glass and seal its tip using a heated microforge element. The sealed glass is lowered into an insulating glass micropipette (aluminosilicate rather than borosilicate glass for improved durability) of similar tip shape and size until the two tips are separated by some 10 μm. The ion-sensitive conical glass membrane is sealed locally onto the inside of the outer glass by applying heat from the outside to a region 50–100 μm above the tip of the inner pipette (Fig. 1b). The electrodes are then filled with the appropriate reference solution (e.g. 0.1 M NaCl + 1 M EDTA for Na^+ ISM; 0.1 M NaCl buffered to pH 6 with 0.1 M citrate buffer for pH ISM)[17]. Finally, a Ag – AgCl wire is sealed into the back of the ISM. This recessed-tip type solid-state ISM was introduced by Thomas[15,16], and has the advantage of ensuring that the ion-sensitive glass membrane comes into contact with the intracellular medium only. This is achieved at the expense of a tip size (1 μm to a few micrometres) and response time (several seconds are required to achieve diffusional equilibrium at the tip of the ISM). An alternative to this is the Hinke-type design in which the ion-sensitive glass membrane cone protrudes from the tip of the insulating glass[11]. The latter type of ISM is faster, but suitable only for recording from relatively large cells since the exposed ion-sensitive component is usually several microns in length.

Metal based ISMs are manufactured in an analogous way. For example, a chlorided silver wire (Ag:AgCl) behaves as a Cl^--sensitive electrode, so a recessed-tip or a protruding-tip type Cl^- ISM can be constructed by sealing a sharpened AG:AgCl wire into the end of a glass micropipette (Fig. 1c)[17]. This type of Cl^- ISM has been used to check results obtained

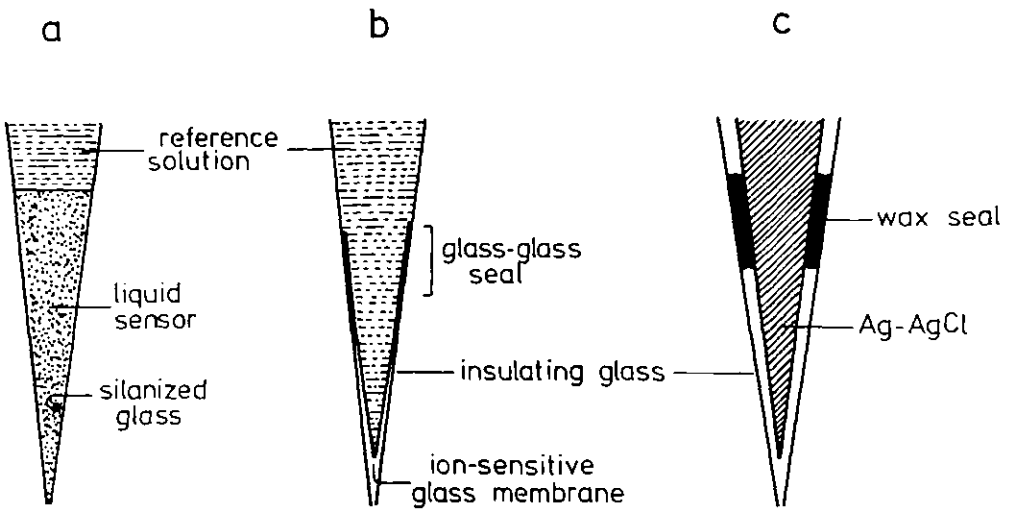

Fig. 1. The tip assembly of three different types of ISM (not drawn to scale). (a) Liquid-state ISM. The length of the liquid sensor column can be 200 μm to several millimetres; the inside wall of the micropipette must be silanized. (b) Solid-state, glass membrane, recessed-tip type ISM; the recess volume is critical and determines the response time of the electrode. (c) Solid-state, metallic surface type ISM. (Modified and redrawn from Thomas[17].)

with liquid ion exchanger type ISMs[14]. The reliability of the antimony-based pH ISM, however, has been doubtful[10].

Operational characteristics

The voltage response V_i of an ISM sensitive primarily to an ion x of valency Z_i, in the presence of a number of interfering ions y of valencies Z_y, is Nernstian and given by the Nikolskii equation:

$$V_i = V_o \pm \frac{RT}{Z_i F} \ln\left[a_i + \sum_y k_{iy}\, a_y \cdot \exp\left(\frac{Z_i}{Z_y}\right)\right]$$

(+ cationic ISM; − anionic ISM) where V_o is a constant reference potential, a_i and a_y are the activities of the primary and interfering ions, respectively, and k_{iy} is the selectivity 'constant' of the ISM for the primary ion over each of the interfering ions. In the simple case of a K^+ ISM for which the main interfering ion is Na^+, the response potential is given by:

$$V_K = V_o + S \log_{10}(a_K + k_{KNa}\, a_{Na})$$

where S is known as the slope constant of the ISM and has a value of approximately 58 mV at 20°C. The selectivity 'constant' k_{iy} of an ISM does not necessarily have a fixed value. It has been shown to depend on the ionic strength of the solution[4] and tip diameter[1]. A number of different methods have been described for the assessment of selectivity constants[2]. The ISM selectivity problem is worst when ionic activity measurements are desired in cells in which the activity of the primary ion is low compared with the activity of the main interfering ions e.g. Na^+ v. K^+, Ca^{2+} v. K^+ and Na^+.

ISMs have electrical resistances in the range $10^9 - 10^{11}\Omega$, due mainly to their ion-sensitive tip components. To record an electrochemical potential correctly one must match the ISM resistance with a high input impedence ($10^{15}\Omega$) electrometer which will draw negligible current from the

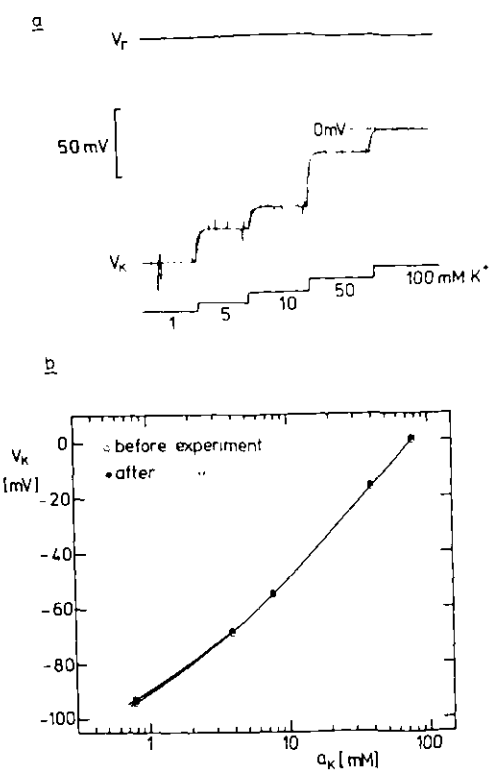

Fig. 2. Calibration traces and graphs for a double barrel K^+ISM. (a) The voltage responses of both the potassium acetate filled reference electrode (V_r) and that for the ISM barrel (V_K) were monitored simultaneously. The calibrating solutions contained 1, 5, 10, 50, 100 mM of K^+ concentration; the ionic strength was kept constant at 100 mM with corresponding amounts of NaCl. V_K for 100 mM K^+ was arbitrarily fixed as 0 mV. (b) The voltage readings, V_K (mM) from (a) plotted against the logarithms of the K^+ activities a_K (mM, γ_K = 0.770. Open circles, calibration values obtained prior to the experiment; full circles, calibration values obtained for the same ISM following the completion of the recording session. The calibration points can be fitted by the Nikolskii equation to within ± 1 mV assuming k_{KNa} equals 1.4×10^{-2}.

ISM. Such high resistance ISMs suffer from external electrical interference pick-ups and require careful electrical shielding of the preparation with a metallic enclosure and of the ISM itself by a signal-driven guard. Furthermore, capacity compensation is often required to improve the response time of the electrodes.

When an ISM impales a cell, the voltage it records is the sum of the transmembrane (resting) potential (E_m) plus the electrochemical potential associated with the ionic activity. To obtain the latter measurement alone, E_m must be recorded independently and subtracted from the ISM potential. With large cells (e.g. snail neurones, barnacle photoreceptors) it is possible to impale the unit under visual control with a second (reference electrode) for the measurement of E_m alone. If this is impossible, double-barrel microelectrodes must be used; one barrel is an ISM whilst the other one is the reference (ion-insensitive) electrode. The ionic activity levels recorded by an ISM will depend to some extent on the nature of the electrolyte filling the reference barrel because of leakage, and because the reference electrode itself can be slightly ion-sensitive depending on the liquid junction potentials. It is therefore, crucial to ensure that the reference electrodes are as ion-insensitive as possible and that any leakage from them are not sensed by the ISMs.

Prior to using an ISM in an experiment, its voltage response is calibrated in a series of standard solutions containing varying amounts of the primary ion detected. The relative merits of various calibration procedures have been discussed elsewhere[17]. The general rule is that the calibration media should resemble, as closely as possible, the intracellular pool of ions from which activity measurements will be made. Fig. 2 illustrates the calibration responses of a double-barrel K^+ ISM in a series of KCl + NaCl solutions (of constant ionic strength 100 mM; activity coefficient 0.770). The reference barrel is filled with 0.5 M lithium acetate and does not respond to the changes in the K^+ activity (Fig. 2a). The potassium signal, V_K, is given by the differential measurement (ISM potential minus reference electrode potential) and this is plotted as a function of the potassium activity in Fig. 2b. At high ionic activity the response of this electrode increases by 56 mV for each 10-fold increase in K^+ activity but it deviates from the straight line predicted by the Nernstian relationship at low K^+ levels – here interference from Na^+ ions becomes significant. Fig. 2b illustrates another important procedure in ISM experiments, namely the necessity to calibrate the ISM before and after a recording session – the two calibrations must not vary by more than a few millivolts.

The following sections provide examples of the vast range of applications for which ISMs have been used in neurobiology.

Vertebrate retinal horizontal cells

Horizontal cells are a type of interneurone in the vertebrate retina. They are driven by the photoreceptor cells (rods and three spectral classes of cone) through chemical synapses and, in response to light generate slow, graded hyperpolarizing and depolarizing electrical responses (S-potentials)[9]. We have started an analysis of horizontal cell ionic mechanisms in the fish (roach, *Rutilus rutilus*) retina using ISMs. Fig. 3a is a chart recording showing the impalement of a red-sensitive L-type unit with a double barrel K^+ liquid ion exchanger ISM. With this type of ISM, the membrane potential (E_m, in this case, −39 mV) and the K^+ signal (upper trace) are recorded simultaneously from the same neurone. In these units, a^i_K had an average value of about 60 mM ($a^o_K \simeq 3.5$ mM), and E_K was consistently more negative than E_m by at least 20 mV. From these measurements, it is deduced that in the dark the L-type horizontal cell membrane is permeable to other ion(s) 'x' with E_x more positive than E_m. One candidate is Cl^-, since in these units E_{Cl} is more positive than E_m by at least 15 mV (Fig. 3b). During synaptic blockage by light stimulation or application of 1–2 mM $CoCl_2$, the membrane potential tends towards E_K, and at saturation $E_m \simeq E_K$ thereby showing that the non-synaptic conductance mechanisms of the horizontal cell membrane is K^+ driven.

Invertebrate photoreceptors

The intracellular K^+, Cl^-, Na^+, Ca^{2+} and H^+ levels have been measured in barnacle photoreceptors by Brown and co-workers[5–7,14,21]. The dark-adapted photoreceptor was found to have a significant chloride permeability such that Cl^- was distributed passively ($E_{Cl} \simeq E_m$). The potassium equilibrium potential was in the range 70–80 mV negative whilst that for sodium was greater than +60 mV. The light-evoked depolarization of the photoreceptor was accompanied by a decrease in the internal pH (a^i_H) and an increase in a^i_{Na}[5,6]. It was suggested that changes in intracellular pH of the photoreceptor induced by light stimulation might modulate its sensitivity.

Molluscan neurones

Several of the neurones in molluses are

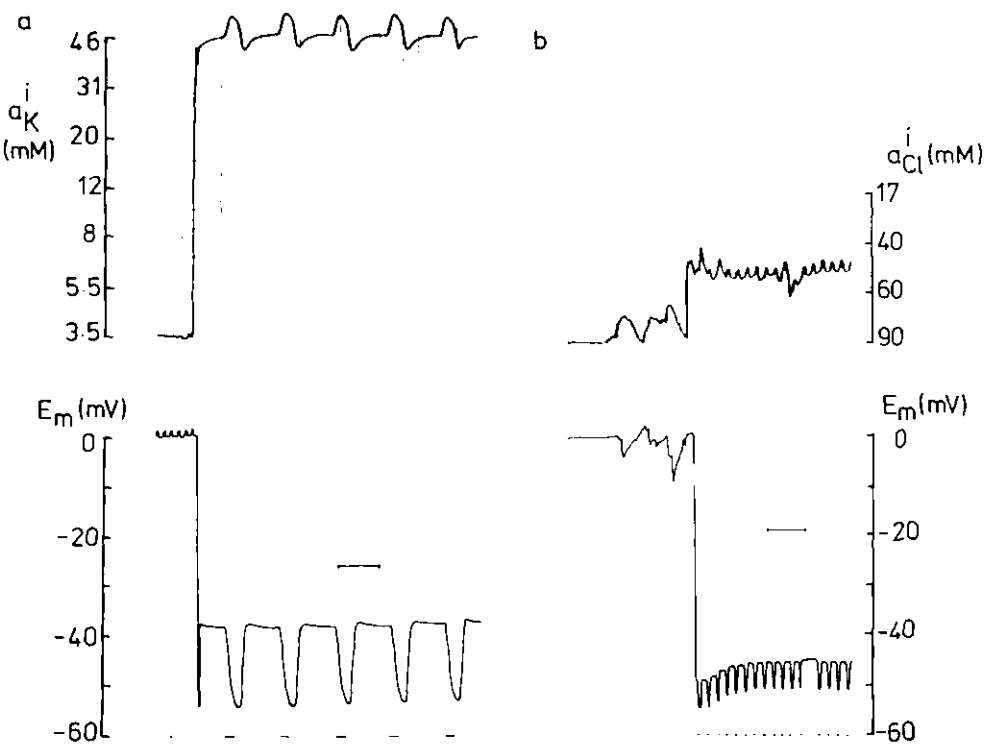

Fig. 3. Intracellular recordings from L-type horizontal cells with double-barrel K^+ ISM (a) and Cl^- ISM (b). Membrane potentials (E_m), and K^+ ISM and Cl^- ISM response voltages were recorded simultaneously. The large negative deflection in each case marks the impalement of the cells upon which light-evoked hyperpolarizing responses were obtained (presentation of the test light stimuli are marked by the dots and short bars below the E_m trace). During the light-evoked changes in V_m, apparent transient changes in V_K and V_{Cl} are seen due to the relatively slow response time of the ISMs. No capacity compensation was possible in these experiments. In all cases, it was found that all voltage readings stabilised within some seconds of cell impalement. The horizontal 'time bars' denote 5 s in (a) and 20 s in (b).

unusually large, and, as a result, have been subject to extensive electrophysiological investigation with ISMs. Perhaps the best known is the correlation between a^i_{Na} and the electrogenic sodium pump made by Thomas in 1969. (He later found, with a sharper microelectrode, that a^i_{Na} was rather lower than previously thought.) The intracellular Cl^- activity in both H and D cells of *Helix aspersa* was found to be about 8.3 mM, giving an E_{Cl} of about −58mV (Ref. 12). The action of acetylcholine on these cells was to increase both the Na^+ and the Cl^- permeabilities. The intracellular pH of snail neurones was found by Thomas to be regulated by a mechanism that involves the simultaneous influx of Na^+ and HCO_3^-, and the efflux of Cl^- and H^+. It was suggested that such a regulation might be mediated by a single membrane carrier with separate transport sites for each of these ions[18].

Acknowledgements

We wish to thank R. C. Thomas and his students for teaching one of us (M.D.) the ISM technique. We also thank him, H. M. Brown, T. Gillett, R. W. Meech and W. R. Schlue for discussions and advice, the SRC for financial support and Guliz Onkal for technical assistance.

Reading list

1 Armstrong, W. McD. and Garcia-Diaz, J. F. (1980) *Fed. Proc. Fed. Am. Soc. Exp. Biol.* 39, 2851–2859
2 Bailey, P. L. (1980) *Analysis with Ion-selective Electrodes*, 2nd edn, Heyden, London
3 Berridge, M. J. and Schlue, W. R. (1978) *J. Exp. Biol.* 72, 203–216
4 Bolton, T. B. and Vaughan-Jones, R. D. (1977) *J. Physiol. (London)* 270, 801–833
5 Brown, H. M. (1976) *J. Gen. Physiol.* 68, 281–296
6 Brown, H. M. and Meech, R. W. (1979) *J. Physiol. (London)* 297, 73–93
7 Brown, H. M. and Owen, J. D. (1979) *Ion-selective Electrode Rev.* 1, 145–186
8 Coles, J. A. and Tsacopoulos, H. (1979) *J. Physiol. (London)* 290, 525–549
9 Djamgoz, M. B. A. and Ruddock, K. H. (1979) *Vision Res.* 19, 413–418
10 Green, R. and Giebisch, G. (1974) in *Ion-selective Microelectrodes* (Berman, H. J. and Herbert, N. C., eds), pp. 43–53, Plenum, New York
11 Hinke, J. A. M. (1959) *Nature (London)* 184, 1257–1258
12 Neild, T. O. and Thomas, R. C. (1974) *J. Physiol. (London)* 242, 453–470
13 O'Doherty, J., Garcia-Diaz, J. F. and Armstrong, W. McD. (1979) *Science* 203, 1349–1351
14 Saunders, J. H. and Brown, H. M. (1977) *J. Gen. Physiol.* 70, 507–530
15 Thomas, R. C. (1970) *J. Physiol. (London)* 210, 82–83P
16 Thomas, R. C. (1974) *J. Physiol. (London)* 238, 159–180
17 Thomas, R. C. (1978) *Ion-sensitive Intracellular Microelectrodes. How to Make and Use Them*, Academic Press, London
18 Thomas, R. C. (1980) in *Current Topics in Membranes and Transport* (Boulpaep, E. L., Bonner, F. and Kleinzellar, A., eds), pp. 23–29, Academic Press, New York
19 Tsien, R. Y. (1980) *Trends NeuroSci.* 3, 219–221
20 Walker, J. L. (1971) *Anal. Chem.* 43, 89–92A
21 Walker, J. L. and Brown, H. M. (1977) *Physiol. Rev.* 57, 729–778

M. B. A. Djamgoz is at the Department of Pure and Applied Biology, and P. J. Laming at the Department of Physics, Imperial College, London SW7 2BB, U.K.